

NONLINEAR PROPAGATION OF INTENSE ELECTROMAGNETIC WAVES IN QUASAR AND PULSAR PLASMAS

A Thesis

Submitted for the Degree of

Doctor of Philosophy

in the Faculty of Science

By

R. T. GANGADHARA




DEPARTMENT OF PHYSICS
INDIAN INSTITUTE OF SCIENCE
BANGALORE - 560 012 (INDIA)

APRIL 1993

DECLARATION

I hereby declare that the work presented in this Thesis is entirely original, and has been carried out by me at the Indian Institute of Astrophysics under the auspices of the Joint Astronomy Programme of the Department of Physics, Indian Institute of Science. I further declare that this has not formed the basis for the award of any degree, diploma, membership, associateship or similar title of any University or Institution.

April 26, 1993



R. T. Gangadhara

Department of Physics
Indian Institute of Science
Bangalore-560 012
INDIA

ACKNOWLEDGMENTS

It is a great pleasure to thank Prof. Vinod Krishan, for her continuous guidance and valuable suggestions throughout the course of investigation. Her balanced and open-minded approach to any problem is an education in itself. I am deeply indebted to her for teaching me the ways and means of scientific research.

I would like to thank Prof. Som Krishan for his kind cooperation and advice especially during first phase of my research work. He introduced me with computer software such as Mathematica, Maple and $\text{V}\text{T}\text{E}\text{X}$. Using these software, I could carry out my computations with high accuracy.

The work presented here has been carried out at the Indian Institute of Astrophysics under the Joint Astronomy Programme of the Indian Institute of Science. My thanks are due to both these Institutes for providing me such an excellent research opportunity. I have greatly benefited from the lecture courses in the Joint Astronomy Programme, and I wish to thank all the lecturers who taught me Astronomy.

During the course of this work, I have benefited by discussions with many people from different Institutions and observatories. I would like to take this opportunity to thank them all, and in particular Prof. Paul J. Wiita, Prof. Padma K. Shukla, Prof. Abhijit Sen and Prof. J. C. Bhattacharyya for illuminating conversations and helpful criticisms.

I thank Prof. Ramanath Cowsik, Director, Indian Institute of Astrophysics for providing excellent research facilities.

It is my earnest duty to thank the authorities of the Indian Institute of Astrophysics and the Indian Institute of Science for their financial support.

The excellent Libraries of the Indian Institute Astrophysics and Indian Institute

of Science have been an invaluable support for my research work. It is a pleasure to thank Ms. A. Vagiswari and other members of the Library staff for their help and cooperation.

I would like to thank Mr. B. A. Varghese, Dr. D. Mohan Rao and Dr. K. E. Rangarajan for providing prompt computational help.

Many thanks to all my friends and colleagues at the Indian Institute of Science and Indian Institute of Astrophysics who have been helpful in many ways during my stay in Bangalore. A special word of thanks to S. Karibasappa, H. S. Jayanna, Monica Velluri, K. M. Hiremath, H. N. Ranganath Rao, R. D. Prabhu, D. Banerjee, S. Sengupta, Eashwar Reddy, Uma Gorti, Annapurni, R. Ramesh, G. Pandey and A. V. Thampan for the good company and the generous help they provided through many years.

My sincere thanks are due to Mr. Mohmood Khon for his help and care in making copies of the Thesis.

I am most grateful to my parents, brothers, wife Sukanya and son Rajesh for their encouragement, and patience throughout the course of this work.

R. T. Gangadhara

CONTENTS

Abstract	viii
List of Publications	xi
Chapter 1	
Introduction	1-19
1.1 Astrophysical Plasmas	1
1.2 Quasars	4
1.2.1 Jets, beams and non-thermal Continuum	7
1.2.2 Absorption and heating in the emission-line regions	9
1.2.3 Polarization	10
1.2.4 Variability	11
1.3 Pulsars	13
<i>REFERENCES</i>	16
Chapter 2	
The Parametric Instability	20-30
2.1 Introduction	20
2.2 General formalism of parametric instability in a plasma	22
<i>REFERENCES</i>	30
Chapter 3	
The role of Compton and Raman scattering in the quasar continuum	31-62
3.1 Introduction	32
3.2 Stimulated Raman and Compton scattering as energy loss mechanisms	34

3.2.1 Lorentz Transformations	35
3.2.2 Stimulated Compton or stimulated Raman scattering?	38
3.2.3 The growth rates of the stimulated Raman and Compton scattering	43
3.2.4 Numerical solution of equation (3.35)	47
3.2.5 Limiting gain and output power	48
3.3 Discussion	51
3.4 Conclusion	62
<i>REFERENCES</i>	63
Chapter 4	
Anomalous absorption of radiation in Astrophysical plasmas	65-102
4.1 introduction	66
4.1.1 Density and temperature structure of broad line region of active galactic nuclei	67
4.1.2 Density and temperature structure of Crab Nebula	68
4.1.3 The radio source	68
4.2 Parametric decay instability (PDI)	69
4.2.1 Decay of a pump wave into an electron plasma wave and an ion-acoustic wave (PDI-I)	73
4.2.2 Decay into a Reactive Quasi-Ion Mode (PDI-II)	83
4.2.3 Decay into a Resistive Quasi-Ion Mode (PDI-III)	86
4.2.4 Oscillating Two-Stream Instability (OTS)	88
4.2.5 Comparisons between PDI-I, II, III and OTS	92
4.3 Formation of 21-cm absorption line in the emission-line region	99
4.4 Conclusion	99
<i>REFERENCES</i>	101

Chapter 5	
Polarization changes of radiation through stimulated Raman scattering	103-131
5.1 Introduction	104
5.2 Stimulated Raman scattering	107
5.3 Stokes parameters	115
5.4 Numerical solution of equation (5.28)	116
5.4.1 In pulsars	116
5.4.2 In quasars	122
5.5 Faraday rotation versus stimulated Raman scattering	125
5.6 Large amplitude electromagnetic waves and the effect of their incoherence on SRS instability	126
5.7 Conclusion	128
<i>REFERENCES</i>	129
Chapter 6	
The modulation of radiation in an electron-positron plasma	132-162
6.1 Introduction	133
6.2 The modulational instability	137
6.3 Large-amplitude em waves in AGN and pulsars and the effect of their incoherence on the modulational instability	146
6.4 Discussion	148
6.4.1 In an AGN	150
6.4.2 In a Pulsar	157
6.5 Conclusion	159
<i>REFERENCES</i>	160

Chapter 7	
Conclusions	163-166
<i>REFERENCES</i>	166
Appendix	167-183
A. Plasma waves	167
B. The Landau damping	170
C. The ponderomotive force	173
D. Collision frequency	177
E. Propagation of electromagnetic waves in an inhomogeneous plasma	180
F. Effect of incoherence in the pump wave on instability.	182
<i>REFERENCES</i>	183
List of Symbols	184

ABSTRACT

This Thesis presents the results of analytical as well as numerical investigations of radiation-plasma interaction instabilities in astrophysical plasmas. It consists of two introductory chapters, four main chapters and one conclusion chapter. The introductory Chapter 1 provides an introduction to astrophysical situations rich with the possibilities of radiation-plasma instabilities. The Chapter 2 describes the parametric plasma instabilities along with the derivation of the general dispersion relation.

The remaining four chapters are concerned with the specific cases of parametric instabilities. Each chapter begins with an introduction, derivation of analytical results followed by numerical results (Figures). The effect of various parameters such as density and temperature of plasma, luminosity, bandwidth, polarization of radiation on plasma instabilities have been studied in detail. The results which are presented in the graphical form and tables are analyzed and discussed in detail. A brief conclusion at the end of each chapter sums up the results. The books and original papers referred to in the text of the Thesis are enlisted alphabetically at the end of each chapter. Although various symbols and abbreviations are defined as and when they occur, for easy reference the list of more often used symbols and abbreviations are listed at the end of the Thesis.

Chapter 3 explains the possible role that the stimulated Raman and Compton scattering play in the continuum emission of a quasar. There are three ways in which an electromagnetic wave can undergo scattering in a plasma: (i) when the

scattering of radiation occurs by a single electron, it is called Compton scattering; (ii) if it occurs by a longitudinal electron plasma mode, it is called stimulated Raman scattering, and (iii) if it occurs by a highly damped electron plasma mode, it is called stimulated Compton scattering. The non-thermal continuum of quasars is believed to be produced through the combined action of synchrotron and inverse Compton processes, which are essentially single-particle processes. Here, we investigate the role of stimulated Raman scattering and stimulated Compton scattering in the generation of continuum radiation from these compact objects. It is shown as an example that the complete spectrum of 3C 273 can be reproduced by suitably combining stimulated Compton scattering and stimulated Raman scattering. The differential contributions of these stimulated scattering processes under different values of the plasma parameters are also calculated.

In Chapter 4, the coherent plasma process such as parametric decay instability has been applied to a homogeneous and unmagnetized plasma. These instabilities cause anomalous absorption of intense electromagnetic radiation under specific conditions of energy and momentum conservation and thus cause anomalous heating of the plasma. The maximum plasma temperatures reached are functions of luminosity of the radio radiation and plasma parameters. It is believed that these processes may be taking place in many astrophysical objects. Here, the conditions in the sources 3C 273, 3C 48 and Crab Nebula are shown to be conducive to the excitation of parametric decay instability. These processes also contribute towards the absorption of 21-cm radiation, which is otherwise mostly attributed to neutral hydrogen regions.

In Chapter 5, the change in polarization of an electromagnetic wave due to stimulated Raman scattering in a plasma is discussed. In this process an electromagnetic wave undergoes coherent scattering off an electron plasma wave. It is found that some of the observed polarization properties such as the rapid temporal variations, sense reversal, rotation of the plane of polarization and change of nature of polarization in the case of pulsars and quasars, could be accounted for through stimulated Raman scattering.

Chapter 6 deals with the modulational instability of a large-amplitude, electromagnetic wave in an electron-positron plasma. The modulational instability excites due to the effect of relativistic mass variation of the plasma particles, harmonic generation, and the non-resonant, finite frequency electrostatic density perturbations, all caused by the large-amplitude radiation field. The radiation from many strong sources such as quasars and pulsars, has been observed to vary over a host of time-scales. It is possible that extremely rapid variations in the non-thermal continuum of quasars as well as in the non-thermal radio radiation from pulsars can be accounted for by the modulational instabilities to which the radiation may be subjected during its propagation out of the emission region.

In Chapter 7, we conclude that coherent plasma processes must be included in the study of generation, absorption, polarization and modulation of electromagnetic radiation in high-energy sources such as quasars and pulsars.

LIST OF PUBLICATIONS

Work presented in this Thesis is based on the following publications.

In Journals

1. Gangadhara, R. T., and Krishan, V., 1990, *Radio wave heating of astrophysical plasmas*, J. Astrophys. Astr., 11, 515.
2. Gangadhara, R. T. & Krishan, V., 1992, *Role of Compton and Raman scattering in the quasar continuum*, Mon. Not. R. astr. Soc., 256, 111.
3. Gangadhara, R. T., Krishan, V. & Shukla, P.K., ¹⁹⁹³1992, *Modulation of radiation in an Electron-Positron plasma*, Mon. Not. R. astr. Soc., 262, 151. (Accepted).
4. Gangadhara, R. T. & Krishan V., 1993, *Polarization changes through stimulated Raman scattering*, Astrophys. J, (Accepted). 415, 505.

In Symposium Proceedings

1. Gangadhara, R. T. & Krishan, V., 1989, *Absorption of Electromagnetic Radiation in Astrophysical Plasmas*. in the IAU Symp.142 on Basic Plasma Processes on the Sun, Bangalore, India, eds. Priest, E. R., & Krishan, V., D. Reidel, Dordrecht, p 519.
2. Gangadhara, R. T. & Krishan, V., 1991, *Parametric Decay Instability in 3C 273*, in the Meeting in Variability of Active Galactic Nuclei, Atlanta, USA, eds. Miller, D., & Wiita, P. J., Cambridge Uni. Press, p 190.
3. Gangadhara, R. T., Krishan, V. & Shukla, P. K., 1991, *Nonlinear Instability of Photons in an Electron-Positron Plasma* in the *Spring College on Plasma Physics*, International Centre for Theoretical Physics, Trieste, Italy.
4. Krishan, V. & Gangadhara, R. T., 1992, *Polarization changes through stimulated Raman scattering*, in the International Conference on Plasma Physics, Innsbruck, Austria, 3, part 1, p 1671.

Chapter 1

INTRODUCTION

1.1 ASTROPHYSICAL PLASMAS

It is generally believed that the Universe is a plasma. Even before the invention of the concept of a plasma, astrophysicists studied its properties. The essential difference between a plasma and a normal gas lies in the fact that it consists of ions and electrons along with the neutral atoms. It is important to note that due to the long range of the Coulomb forces, the mobility of the light electrons, and the existence of several thermal equilibration times, collective properties such as electromagnetic and electrostatic oscillations or waves and instabilities form an integral part of the plasma phenomena.

One of the main problems of astrophysics is the analysis of the radiation of celestial objects in the widest sense of the word. Astrophysical objects such as stars, galaxies, quasars, pulsars, so on and so forth, can only be studied through the analysis and interpretation of their radiation over the entire electromagnetic spectrum. Some information is also obtained from corpuscular radiation (cosmic rays and neutrinos).

In order to understand the workings of celestial objects we must know the radiation mechanisms as well as the state of the emitting system. The detection of sporadic radio-emission from the Sun and particularly in sixties, the discovery of powerful radio-sources (radio-galaxies, quasars, pulsars) brought out the need for efficient radiation mechanisms through which different forms of energy could be converted into electromagnetic waves. Moreover, it became clear that the acceleration of charged particles under cosmic conditions is not a rare phenomenon, but an often encountered process. Here, one requires everything that plasma physics can

offer and more. Especially important are the processes associated with collisionless plasmas in which the electron mean free path is much longer than the characteristic dimensions of the collective phenomena. Such a plasma exhibits its wave nature in an all-encompassing way. The large brightness temperatures in many cosmic objects (especially in the radio-band) are a pointer to the non-thermal radiation processes. Thus, the pursuit of astrophysics through plasma physics promises to be a highly rewarding experience.

The dimensions of astrophysical plasma systems are huge, and their optical thickness can be large. This means that an appreciable part of the energy contained in the plasma can change into electromagnetic radiation of relatively high-frequencies. In a cosmic plasma high-frequency electromagnetic waves can excite an intensive plasma turbulence or, on the contrary, lead to stronger dissipation of the turbulence. The first difference between plasma astrophysics and laboratory plasma physics lies thus in the appreciably stronger interaction with the radiation. The cosmic plasma can be considered to be practically homogeneous: the characteristic lengths over which its parameters change are generally larger than the characteristic lengths of the collective processes. The availability of high spatial and temporal resolution observations has however necessitated the inclusion of inhomogeneities, as for example, in the solar plasmas.

A plasma, by nature is hyperactive. More often than not, it responds violently to external stimuli in an attempt to attain equilibrium. An important feature of electromagnetic wave propagation in an isotropic and unmagnetized plasma, is a cutoff (dielectric function ϵ vanishes) at the plasma frequency; an electromagnetic wave with frequency less than the plasma frequency cannot propagate in the plasma. Since plasma frequency is proportional to the square root of the charged particles density, the density fluctuations in interstellar space create local variations in the velocity and direction of propagation of radio wave propagation. The frequency of

the electromagnetic wave for which its phase velocity vanishes, is called as resonance frequency. The electromagnetic waves at resonance frequency are strongly absorbed in a plasma.

When a plasma is subjected to the electric field of a high-intensity electromagnetic wave, it exhibits a variety of non-linear processes which modify the plasma parameters as well as those of the electromagnetic waves. When the size of the plasma region disturbed by the electromagnetic wave is much larger than the mean free path of an electron, the electron can gain enough energy before suffering collisions with other ions and neutrals. Further the large mass difference between electron and other particles hinder the transfer of energy from electrons to the heavy particles. Thus the electric field of the electromagnetic wave heats the electrons preferentially, as a result of which the dielectric function ϵ and the conductivity σ of the plasma become functions of the electromagnetic wave field and a non-linear relation between the electric field \vec{E} and the current density $\vec{J} = \sigma(\vec{E})\vec{E}$ is set up. In the opposite case, when the size of the disturbed plasma region is much smaller than the mean free path of an electron, the inhomogeneous electric field of the electromagnetic wave exerts a pressure on the electrons, creating compressions and rarefactions. Thus, the dielectric function begins to depend on the electromagnetic wave field and the plasma again becomes a non-linear medium. Summarizing, a collisional plasma becomes non-linear mainly through the dependence of electron temperature on the electromagnetic wave field and a collisionless plasma becomes non-linear mainly through the dependence of electron density on the electromagnetic wave field. In such a non-linear medium an electromagnetic wave undergoes anomalous absorption, anomalous scattering, modulation and polarization change. In this thesis, the role of these non-linear plasma processes in the functioning of quasars and pulsars is investigated.

1.2 QUASARS

The observations made by Seyfert (1943) and Allen et al. (1962) showed the existence of powerful energy sources in the nuclei of galaxies and posed several theoretical problems. The magnitude of the problem became apparent during 1962 and 1963 with the identification of a new class of astronomical objects, the quasi-stellar objects (QSOs). The quasar 3C 273 being one of these objects, turned out to be several orders of magnitude brighter than the brightest known field and cluster galaxies, yet with dimensions comparable to the size of a galactic nucleus rather than the galaxy itself.

Quasars and active galactic nuclei are the most luminous objects in the universe. It is generally believed that they consist of a central engine, perhaps a supermassive ($M = 10^8$ - $10^9 M_\odot$) black hole powered by the accreting matter. Fig. 1.1 shows a schematic representation of a quasar with Schwarzschild radius $R_s = 2GM/c^2 = 2.95 \times 10^{13} M_8 \text{ cm}$, where $M = M_8 \times 10^8 M_\odot$.

The truly remarkable character of 3C 273 became apparent when Schmidt (1963) identified a series of broad emission features with lines of the Balmer series and a line of MgII but at a redshift $z = 0.168$. The total energy output of 3C 273 at cosmological redshift $z = 0.168$ is about $10^{47} \text{ erg sec}^{-1}$. However, the angular size of the object in both the optical and radio regions was estimated to be not more than 0.5 arcsec, corresponding to a linear size of not more than 1 kpc, ($1 \text{ pc} = 3.086 \times 10^{18} \text{ cm}$).

The identification of 3C 273 had led to the recognition of a completely new type of an extragalactic object. Its optical energy output was some 100 times that of a giant galaxy and originated in a region less than 1 pc. The discovery of light variations on a time scale of order of 1 year (Smith & Haffleit 1963; Sandage 1964), led to the conclusion that the source of radiation was confined to a region

of size less than 1 pc. Later with the observations of 3C 48, 3C 196 and 3C 286, it was concluded that these objects were extragalactic, if the observed redshifts were cosmological in origin.

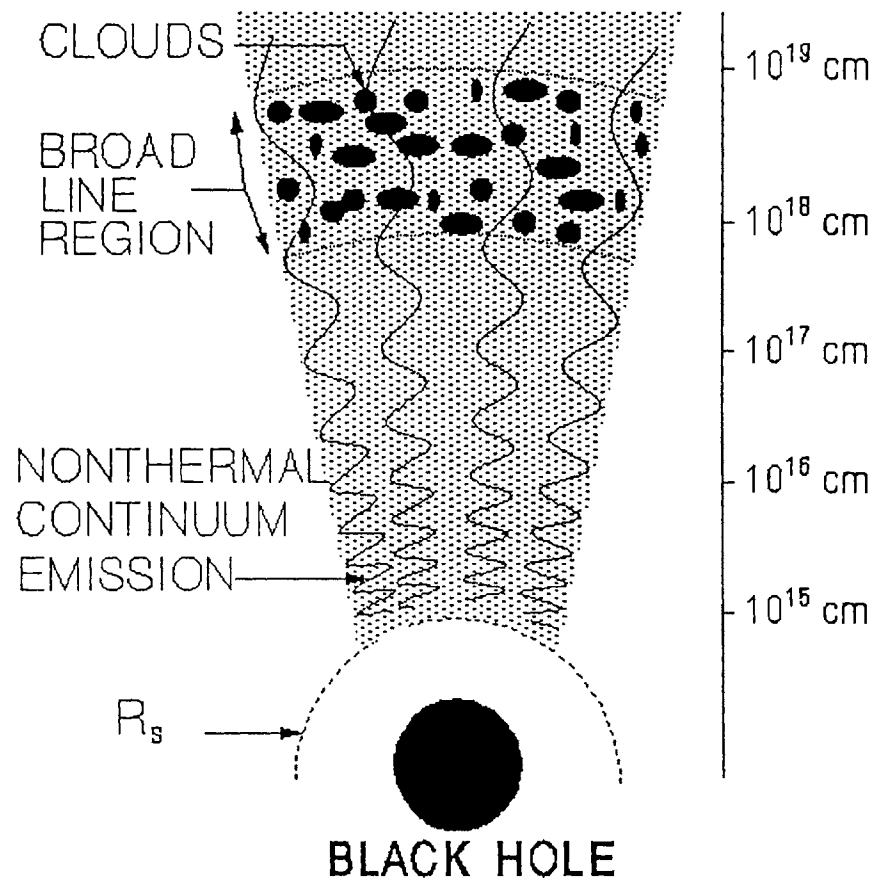


Fig. 1.1 Schematic representation of a quasar.

Alternative explanations for the redshifts, given by Greenstein and Schmidt (1964) include: (1) Doppler effects from a high-velocity star, and (2) gravitational redshift at the surface of a massive object. But both the suggestions were discarded early. The cosmological interpretation of the QSO redshifts was later strongly challenged by Terrel (1964), Hoyle and Burbidge (1966), Arp (1966), and Burbidge et al. (1971). However, the most widely accepted interpretation is that the redshifts of QSO's are due to the expanding Universe. The QSO phenomenon is common

to other types of astronomical objects such as BL Lacs and Seyfert galaxies. The defining characteristics of QSO's are (Wiita 1985):

- (a) stellar appearance,
- (b) strong ultraviolet emission, relative to main-sequence stars, arising as result of non-thermal continuum by synchrotron and Compton processes, with a spectrum of the form $F(\nu) \propto \nu^{-\alpha}$, where $\alpha \approx 1$,
- (c) rapidly varying emission,
- (d) an emission-line spectrum with broad permitted lines (more than 20 Å in the high-redshift QSOs) and in some cases absorption features,
- (e) if we believe large redshifts are due to the expansion of the Universe then the absolute magnitudes for the QSOs range from about $M_v = -23$ to -30 . This shows that QSO's are significantly brighter than the brightest cluster galaxies ($-24 < M_v < -22$).

One can construct a model, consisting of a non-thermal source of small angular size in the nucleus, to explain main features and relationships among QSOs, BL Lacs and Seyfert galaxies. Then, the properties of QSOs, Seyferts and BL Lacs are consistent with the view that common physical processes contribute to the total non-thermal emission.

The study of spectrum of quasars and active galactic nuclei with broad emission-line features provide most valuable information on the physical processes going on around the central engine. The information on temperature, density and abundances of the emitting gas can be obtained by measuring relative strengths and widths of the lines. The shape of the line profile reflects the dynamics of the gas whereas the temporal variations indicate the physical dimensions of the emitting region. The photoionization models, in which clouds or filaments illuminated by a central source of ionizing radiation, have been partly successful in accounting for

the observed strengths of the emission lines (Davidson 1972). The emission lines are commonly separated into “narrow lines” and “broad lines”, whose full widths at half intensities correspond to gas speeds of a few hundred to 1000 km sec⁻¹ and of a few thousands to 20,000 km sec⁻¹, respectively. The emission regions of these lines have varied dimensions and densities. The narrow-line emitting region (NLR) has dimensions of a few hundred to 1000 pc and an electron density of 10⁴ to 10⁶ cm⁻³, while the broad-line emitting region (BLR) has dimensions of 0.01 to 1 pc and an electron density of at least 10¹⁰ cm⁻³. The BLR lies close to the central region of an active galactic nuclei (AGN) and therefore its study has a tremendous diagnostic potential.

1.2.1 Jets, beams and non-thermal continuum

Quasars and active galactic nuclei are usually associated with jets which can reach distances of the order of megaparsecs. The basic idea underlying jet models is that a continuous collimated outflow transports energy from the nucleus to the radio hot spot (Begelman et al. 1984). It is believed that the production and initial collimation of the jets occur on much smaller scales (parsecs) near the central engine. The jets are thought to originate as relativistic particle beams that tap the rotational kinetic energy of the black hole or the accretion disk, and are accelerated by electromagnetic or hydrodynamic mechanisms (e.g., Lovelace 1976; Blandford 1976; Lovelace, Wang and Sulkenen 1987). The radiative deceleration model (Königl 1991) indicates the transformation of ultrarelativistic beams into relativistic jets in extragalactic radio sources. Camenzind (1986 1989) believe that these jets may be produced due to the magnetic sling effect in a rapidly rotating magnetosphere. The collimation of the outflow can be provided by the pinching effect of the toroidal

magnetic field. This would resolve the puzzle that some jets are not freely expanding and an agent is necessary to confine them. Jets carry currents which enhance their stability (Benford 1978).

Collective plasma processes play a major role in the energy dissipation of jets at the hot spots of extragalactic radio sources (Lesch, Appl and Camenzind 1989). The polarization measurements by Röser and Meisenheimer (1987) have proved beyond doubt that the hot spot emission is non-thermal. It is generally agreed that jets provide links between the central activity and the hot spots.

On smaller scales, closer to the active nucleus, beams of accelerated particles are supposed to be streaming through the ambient plasma. The ambient medium is basically a plasma made of protons and electrons. There may be three types of beams with different constituents: (i) electrons and positrons, (ii) electrons and protons, or (iii) a mixture of electrons, positrons and protons. Depending upon the physical conditions and energy density close to the central engine, other particles such as neutrons, pions or anti-protons could be present at the very beginning of the beams but they may not propagating out to large distances. These beams must be relativistic, at least in some objects, as required by the standard model to account for the observed superluminal motions. Recently, the models based upon the conversion of relativistic beam energy into radiation (Baker et al. 1988; Weatherall and Benford 1991) have received much interest. They more or less explain the observed frequency distribution of non-thermal radiation from cosmic sources (for review see Schlickeiser 1986). The most probable processes for the relativistic electron beams to lose energy are: (i) inverse Compton scattering of ambient photon gas, (ii) synchrotron radiation, (iii) non-thermal bremsstrahlung emission (Weatherall and Benford 1991) and (iv) ionization.

The role of stimulated Compton and Raman scattering of soft photons and generation of continuum emission from active galactic nuclei, is discussed in Chapter 3. There are three ways in which an electromagnetic wave can undergo scattering in a plasma: (i) when the scattering of radiation occurs by a single electron, it is called Compton scattering; (ii) if it occurs by a longitudinal electron plasma mode, it is called stimulated Raman scattering, and (iii) if it occurs by a highly damped electron plasma mode, it is called stimulated Compton scattering.

1.2.2 Absorption and heating in the emission-line regions

It has been generally believed that the dominant heating mechanism in the quasar emission-line regions is the absorption of ionizing ultra-violet radiation. Krolik, McKee & Tarter (1978) have demonstrated that in quasars with compact radio sources, the radio frequency (RF) heating can dominate the ultra-violet heating. The RF heating produces a hot corona around each emission-line cloud in the emission-line region. Under extreme conditions, the RF heating may be so strong that cooling by the gas is unable to maintain the thermal balance. Such heating may explain the absence of broad emission lines in BL Lac objects. The most plausible explanation for the absence of broad emission lines is the absence of gas, but this leaves the question of why the gas is missing. For the lack of observable gas in BL Lacs, Krolik and McKee (1978) have proposed that the RF heating is so strong in BL Lac objects that the emission-line gas is ablated and thus heated to high-temperatures. Davidson and Netzer (1979) have reviewed some of the heating processes proposed by several workers, which are (1) ionization by ultra-violet photons, (2) excitation and ionization energetic by non-thermal particles, (3) shock waves dissipation, and (4) free-free (bremsstrahlung) absorption of radio waves.

The coherent plasma process such as parametric decay instability (see Chapter 4) can cause anomalous absorption of strong radio waves and thus lead to heating of the plasma. We believe that this process may be taking place in quasars. It can also contribute to the formation of 21-cm absorption line (Krishan 1988).

1.2.3 Polarization

By assuming a synchrotron origin for the radiation in compact extragalactic radio sources, source models have been readily constructed which explain both the spectral and temporal behavior of intensity (e.g., van der Laan 1966; Blandford & Königl 1979), but polarization does not lend itself to such a straightforward explanation. The problems arise mainly from the observed value of the ratio of circular to linear polarization and the often observed large depolarization factor. It is important to determine whether this depolarization is a geometric effect or the one that results from radiation-plasma interactions. There have only been very preliminary attempts to explain depolarization and microvariability using plasma mechanisms.

The change of polarization of an electromagnetic wave due to its propagation in a magnetized plasma as well as due to an electron scattering is well known. In a magnetized plasma, the Faraday rotation is recognized to be the most common cause of the rotation of the plane of polarization of an electromagnetic wave. In a plasma, the spectral components of radiation of finite band-width travel different path lengths and lead to the depolarization. Any change in the direction of the magnetic field also manifests itself through polarization variation. The strong linear polarization observed in the radio as well as in the optical regions of the spectrum in BL Lacs is believed to originate in the source itself. The fact that optically violently

variables and NGC 1275 show similar polarization characteristics, suggest that BL Lacs, quasars and Seyfert galaxies have a similar source of energy. If so, then the lack of polarization in quasars and Seyfert galaxies can be due to depolarization effects (Stockman 1978). The rotation of the electric vector has been observed in core-jet structure of 3C 454.3 (Cotton et al. 1984) and is interpreted to be due to the propagation of radiation in a medium of varying optical thickness.

It is shown in Chapter 5 that in strong radio radiation sources, the rapid temporal variations, sense reversal, rotation of plane of polarization and change of nature of polarization can be accounted for through stimulated Raman scattering. When an elliptically polarized electromagnetic wave scatters off two electron density fluctuations with a phase difference of π , the scattered electromagnetic wave, will have polarization change, depending upon the ratio of amplitudes of density fluctuations. The polarization changes through stimulated Raman scattering may take place in accretion disks, emission line regions and the intercloud medium of quasars and active galactic nuclei. A comparison between stimulated Raman scattering and the well known process of the Faraday rotation and situations in which stimulated Raman scattering dominates, is discussed in Chapter 5.

1.2.4 Variability

Observations have revealed that many compact radio sources, in addition to the usual long-term variability, possess an intrinsic variability with time-scales less than a day. Heeschen et al. (1987) found, quite unexpectedly, the variations of ~ 1 day at a wavelength of 11 cm in several flat-spectrum sources. Observations of intraday radio variability in compact radio sources and their probable explanations are given by Quirrenbach (1990).

In addition to usual long term variability, the short time (rapid) optical variability has been observed in several quasars and BL Lacs (Smith and Hoffleit 1963; Angione 1969; Shen and Usher 1970; Eachus and Liller 1975; Liller and Liller 1975; Miller 1975, 1977; Heeschen et al. 1987; Webb et al. 1988). Oke (1967) observed 0.25 magnitude change in a day for 3C 279. Bertaud et al. (1973) reported a variation for BL Lacertae of 1.3 magnitude in a day and of 0.7 magnitude in 74 minutes. Racine (1970) detected an optical variability of 0.1 magnitude within a few hours in BL objects.

In principle, several mechanisms can account for radio source variability. One needs detailed information about spectral characteristics, time dependence and polarization behavior to separate intrinsic variability from that arising from propagation effects.

Gravitational microlensing is one of the such possible mechanisms, to explain the observed variability. In the microlensing theory the observed time-scales are related to the relative transverse velocity of either the observer, the lens, or the source by:

$$\Delta t = \frac{1}{v} \left(\frac{M}{M_{\odot}} \right)^{1/2} 5 \times 10^{16} \text{ cm.}$$

To produce short time scales $\Delta t < 1$ day, by a deflector of mass $M = M_{\odot}$ requires transverse velocities v of the order c . Such velocities cannot be due to the deflector but must be attributed to relativistic motions in the source. The lensing magnifies variability but does not to produce.

The rapid variability of BL Lac object 0716+71 has been assumed to be due to a mechanism known as the refractive interstellar scintillation (Heeschen et al. 1987). The arguments against this mechanism come from the wavelength dependence and from the short time-scale of variations. It needs very small scatterers situated close to the Sun (≤ 100 pc).

Intrinsic variability seems to be the most plausible explanation for intraday radio variability. The most dramatic challenge to present-day models of rapid variability is given by the extremely high-brightness temperatures $\sim 10^{18}$ K suggested from the intraday variability. Coherent radiation mechanisms can explain the high-brightness temperatures fairly easily (Benford 1984; Lesch 1991).

We believe a plasma process such as modulational instability may be a potential mechanism for rapid variability in quasars and BL Lacs (see Chapter 6). Low-frequency electrostatic density perturbations are non-linearly excited due to the interaction of a large amplitude electromagnetic wave with a plasma. The superposition of low-frequency oscillation (electrostatic wave) over an high-frequency wave (electromagnetic wave) produce a amplitude-modulated electromagnetic wave.

1.3 PULSARS

Jocelyn Bell and Antony Hewish at Cambridge University discovered clockwise radio pulses and pulsars in the year 1967. Since then pulsars are being (e.g., Cocke, Disney and Taylor 1969; Kanbach et al. 1980; Demianski and Proszynski 1983; Bignami and Caraveo 1988; Lyne, Pritchard and Smith 1988) to delineate the duration, shape, spectrum and polarization of the pulses.

The radio emission is believed to occur from each magnetic pole of a pulsar, with an angular width of the order of 10° . The magnetic axis and the line of sight may be arbitrarily oriented with respect to the rotation axis of the pulsar. The geometry of the pulsar polar cap emission is shown in the Fig. 1.2. The observer sees radiation from the point P, which moves across the arc ST as the pulsar rotates. The zero of the longitude ϕ starts at the meridian through the rotation axis, and position angle ψ is measured with respect to the projected direction of the magnetic

axis.

The radio pulse occurs during a small fraction of the period, corresponding to between 5° and 20° of angular rotation, for most pulsars. Due to the rotation of the pulsar, the beam of radiation sweeps across the line of sight of the observer and it forms a pulse at each rotation, in analogy with the lighthouse. The high-energy plasma particles moving along the curved magnetic field lines emit a beam of radiation. Because of magnetic field, the source of radiation is rigidly attached to the solid surface of the neutron star. The emission occurs at a radial distance of about a few tens of neutron star radius (~ 10 km). High frequency radiation is emitted at lower radius while lower frequency radiation at higher radius of the beam.

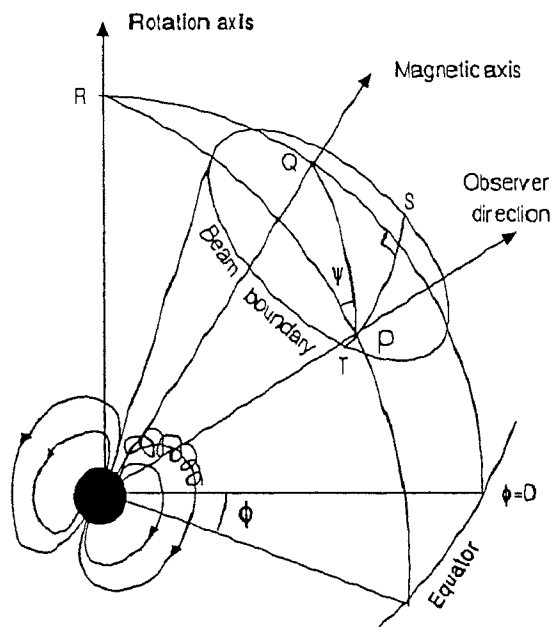


Fig. 1.2 The geometry of pulsar beams.

The intensities of the pulsar radio emission are extremely high and are observed to fluctuate on several time scales. Therefore, the radio radiation cannot be due to thermal emission or incoherent synchrotron emission. It is therefore concluded that the sources of radio emission are coherent. Coherent emission is also implied by the

high-intensity of the radio sources. For the Crab Pulsar the brightness temperature estimated for the radio spectrum exceeds 10^{30} K. Pulsars have power-law spectra $F \sim \nu^{-\alpha}$ at radio frequencies. The spectral index α lies between about 1 and 3, with a low energy cutoff and the flux density F is normally of the order of 1 Jansky, (1 Jansky = 10^{-23} erg cm⁻² sec⁻¹Hz⁻¹).

The individual radio pulses are often observed to be highly variable in intensity as well as in polarization. However, the integrated pulse profile obtained by the superimposition of some 10^3 – 10^4 recorded pulses is stable and a unique characteristic of each pulsar.

The anomalous absorption of radio waves can take place in pulsars also. In Chapter 4 we have shown that the rate of anomalous absorption of radio radiation in Crab Nebula is much higher than that due to collisional absorption rate (Gangadhara and Krishan 1990).

Many pulsars have subpulses or quasi-periodic sequences of subpulses, called as ‘periodic microstructures’. Measurements with time resolutions ≤ 1 msec show subpulse structure with characteristic widths of several percent of the period. But for resolutions $\leq 1\mu$ sec the subpulses of some pulsars exhibit microstructure with widths of the order of $\sim 10^{-3}P$, where P is the period of a pulsar. This fine structure is usually regarded as modulation of the radiation by the noise (Cordes 1983; Lyne & Graham-Smith 1990). In Chapter 6, we discuss the modulational instability of electromagnetic waves and the production of micropulses.

The radio emission from many pulsars shows linear and often circular or elliptical polarization. The integrated pulse profile may have a high-average polarization and the position angle of the linearly polarized component swings monotonically through the integrated pulse by an angle up to 180° . In some cases (e.g., Vela, PSR 0833-45) essentially all the integrated profile is linearly polarized while in others

a circular component is seen near the center of the pulse. The sense of polarization may remain same throughout the pulse or it may reverse (Manchester and Taylor 1977). Roughly, about 20 percent of the integrated profile is circularly polarized. In Chapter 5, we discuss the change of polarization properties, such as sense reversal, rotation of the polarization plane and degree, on extremely short time scales due to the stimulated Raman scattering.

The general dispersion relation for parametric instabilities in a homogeneous unmagnetized plasma is derived in Chapter 2. In appendix, we discuss the concepts such as collision frequency, plasma waves, Landau damping and ponderomotive force in a plasma medium.

References

- Allen, L. R., Anderson, B., Conway, R., Palmer, H. P., Reddish, V. C. & Ronson, B., 1962, *Mon. Not. R. astr. S.*, **124**, 477.
- Angione, R., 1969, *Pub. A. S. P.*, **80**, 339.
- Arp, H. C., 1966, *Science, New York*, **151**, 1214.
- Baker, D. N., Borovsky, J. E., Benford, G., & Eilek, J. A., 1988, *Astrophys. J.*, **326**, 110.
- Begelman, M. C., Blandford, R. D. & Rees, M. J., 1984, *Rev. Mod. Phys.*, **56**, 255.
- Benford, G., 1978, *Mon. Not. R. astr. Soc.*, **183**, 29
- Benford, G., 1984, in *Physics of Energy Transport in AGNs*, NRAO Proceedings, p 185.
- Bertaud, Ch., Wlerick, G., Veron, P., DuMortier, B., Bigay, J., Paturel, G., Dupuy, M. & deSaevsky, P., 1973, *Astr. Astrophys.*, **24**, 357.
- Bignami, G. F. & Caraveo, P. A., 1988, *Astrophys. J.*, **325**, L 5.

- Blandford, R. D., 1976, *Mon. Not. R. astr. S.*, **176**, 465.
- Blandford, R. D., & Königl, A., 1979, *Astrophys. J.*, **232**, 34.
- Burbidge, E. M., Burbidge, G. R., Solomon, P. M. & Strittmatter, P. A., 1971, *Astrophys. J.*, **170**, 233.
- Camenzind, M., 1986, *Astr. Astrophys.*, **156**, 137.
- Camenzind, M., 1989, in *Accretion Disks and Magnetic fields*, ed. G. Belvedere, Kluwer, Dordrecht, p 129.
- Cocke, W. J., Disney, M. J. & Taylor, D. J., 1969, *Nature*, **221**, 525.
- Cordes, J. M., 1983, in proceedings of *Conference No.101, on Positron—Electron pairs in Astrophysics*, eds. M. L. Burns, A. K. Harding & R. Ramaty, American Institute of Physics, p 98.
- Cotton, W. D., Gelzahler, B. J., Marcaide, J. M., Shapiro, I. I., & Sanroma, M., 1984, *Astrophys. J.*, **286**, 503.
- Davidson, K., 1972, *Astrophys. J.*, **171**, 213.
- Davidson, K. & Netzer, H., 1979, *Rev. Mod. Phys.*, **51**, 715.
- Demianski, M. & Proszynski, M., 1983, *Mon. Not. R. astr. Soc.*, **202**, 437.
- Eachus, A. D. & Liller, W., 1975, *Astrophys. J.*, **200**, L 61.
- Gangadhara, R. T., & Krishan, V., 1990, *J. Astrophys. Astr.*, **11**, 515
- Greenstein, J. L. & Schmidt, M., 1964, *Astrophys. J.*, **140**, 1.
- Heeschen, D. S., Krichbanm, T., Schalinski, C. J. & Witzel, A., 1987, *Astron. J.*, **94**, 1493.
- Hoyle, F. & Burbidge, G. R., 1966, *Astrophys. J.*, **144**, 534.
- Kanbach, G., et al., 1980, *Astr. Astrophys.*, **90**, 163.
- Krishan, V., 1988, *Mon. Not. R. astr. Soc.*, **231**, 353.

- Königl, A., 1991, in proceedings of the 7th IAP meeting on *Extragalactic Radio Sources—From Beams to Jets*, ed. J. Roland, H. Sol and G. Pelletier, Cambridge Univ. Press, p 195.
- Krolik, J. & McKee, C. F., 1978, *Astrophys. J. Suppl.*, **37**, 459.
- Krolik, J., McKee, C. F. & Tarter, C. B., 1978, in proceedings of the *Pittsburgh BL Lac Conference*.
- Lesch, H., 1991, in proceedings of the 7th IAP meeting on *Extragalactic Radio Sources—From Beams to Jets*, ed. J. Roland, H. Sol and G. Pelletier, Cambridge Univ. Press, p 78.
- Lesch, H., Appl, S. & Camenzind, M., 1989, *Astr. Astrophys.*, **225**, 341.
- Liller, W. & Liller, M., 1975, *Astrophys. J.*, **199**, L 133.
- Lovelace, R. V. E., 1976, *Nature*, **262**, 649.
- Lovelace, R. V. E., Wang, J. C. L. & Sulknen, M. E., 1987, *Astrophys. J.*, **315**, 504.
- Lyne, A. G. & Graham-Smith, F., 1990, *Pulsar Astronomy*, Cambridge Univ. Press, p 24.
- Lyne, A. G., Pritchard, R. S. & Smith, F. G., 1988, *Mon. Not. R. astr. Soc.*, **233**, 667.
- Manchester, N. R. & Taylor, H., 1977, *Pulsars*, W. H. Freeman and Company, San Francisco, p 49.
- Miller, H. R., 1975, *Astrophys. J.*, **201**, L 109.
- Miller, H. R., 1977, *Astrophys. J.*, **212**, 153.
- Oke, J. B., 1967, *Astrophys. J.*, **147**, 901.
- Quirrenbach, A., 1990, in *Meeting on Variability of Active Galactic Nuclei*, eds. Miller, H.R. & Wiita, P.J., Cambridge Univ. Press, p 165.

- Racine, R., 1970, *Astrophys. J.*, **159**, L 99.
- Röser, H.-J. & Meisenheimer, K., 1987, *Astrophys. J.*, **314**, 70.
- Sandage, A. R., 1964, *Astrophys. J.*, **139**, 416.
- Schlickeiser, R., 1986, in *Cosmic Radiation in Contemporary Astrophysics*, ed. M. M. Shapiro, Reidel, Dordrecht.
- Schmidt, M., 1963, *Nature*, **197**, 1040.
- Seyfert, C. K., 1943, *Astrophys. J.*, **97**, 28.
- Shen, B. S. P. & Usher, P., 1970, *Nature*, **228**, 1070.
- Smith, H. J. & Hoffleit, D., 1963, *Nature*, **198**, 650.
- Stockman, H. S., 1978, in Pittsburgh Conference on BL Lac Objects, ed. Arthur M. Wolfe, p 149.
- Terrel, J., 1964, *Science New York*, **145**, 918.
- van der Laan, H., 1966, *Nature*, **211**, 1131.
- Weatherall, J. C., & Benford, G., 1991, *Astrophys. J.*, **378**, 543.
- Webb, J. R., Smith, A. G., Leacock, R. J., Fitzgibbons, G. L., Gombola, P. P. & Shepard, D.W., 1988, *Astron. J.*, **95**, 374.
- Wiita, P. J., 1985, *Phys. Rep.*, **123**, 117.

Chapter 2

THE PARAMETRIC INSTABILITY

2.1 INTRODUCTION

Parametric excitation has been recognized to be a very important non-linear phenomenon in plasmas. By this mechanism, non-linear mode conversion takes place: electromagnetic waves can be converted into the electrostatic waves and vice versa. These processes through absorption and scattering of electromagnetic and electrostatic waves facilitate heating and acceleration of the plasmas which then become strong emitters of radiation.

Parametric excitation may be defined as an amplification of an amplitude of oscillation due to a periodic modulation of a parameter that characterizes the oscillation. The first systematic investigation was made by Lord Rayleigh in 1883. He studied a stretched string attached to a prong of a tuning fork vibrating in the direction of the string. When the frequency of the tuning fork was twice the natural frequency of the string, vibration of the string was observed to be amplified. This amplification was due to a periodic modulation of the frequency of the string at twice its natural value. Here, the longitudinal vibration of the string induced by the tuning fork modulates the string's tension and hence the frequency of the transverse vibration at the tuning fork frequency. In general if the frequency of an oscillator is modulated weakly with a period T , an amplification of the amplitude of oscillator can take place only when one of the following conditions are satisfied:

$$\Omega T = n\pi, \quad (n = 1, 2, 3, \dots) \quad (2.1)$$

where Ω is the natural frequency of the oscillator.

Parametric excitation has a large variety of applications in physics, in technology and even in everyday life. The phenomenon of parametric excitation may be characterized with the following properties:

- (1) **Matching condition:** Frequencies of the modulation (pump) and the excited oscillations should satisfy a phase-matching condition, such as the one given by equation (2.1).
- (2) **Threshold:** amplification occurs only when the modulation amplitude exceeds a certain critical value so that the growth rate of the wave is larger than its damping rate.
- (3) **Frequency locking:** A resonant amplification of the amplitudes occur only when the frequencies of the excited modes are equal to their natural frequencies or harmonics of natural frequencies. For example, when $n=1$ in equation (2.1) amplification occurs at the frequency π/T , while for $n=2$ at $2\pi/T$ and zero.

Through parametric instability two non-linearly excited waves (a signal and an idler) are exponentially grow at the cost of energy of the modulating (pump) wave due to a mode-coupling interaction. The three-wave interaction is a simple example of a parametric instability. The following frequency and wave number matching conditions have to be satisfied for the resonant coupling of the three waves:

$$\omega_o = \omega_i + \omega_s, \quad \vec{k}_o = \vec{k}_i + \vec{k}_s, \quad (2.2)$$

where the subscripts o , i and s , respectively, denote the pump (\vec{k}_o, ω_o) , idler (\vec{k}_i, ω_i) and signal (\vec{k}_s, ω_s) . Any non-linear medium can support such a three-wave interaction process. When the pump intensity exceeds a threshold value, determined by the damping rates of the idler and the signal, an instability is sets in. In the absence of the pump wave the idler and the signal in general, may exist as small amplitude normal modes of a plasma. If one of them is weakly damped and the

other a highly damped mode or a quasi-mode, the three-wave interaction described above is known as non-linear Landau damping of the pump wave.

It is clear that parametric excitation is an important mode-coupling mechanism. Above threshold, the energy of the pump wave can be efficiently transferred to the idler and signal waves. If these waves are plasma waves, i.e., those that are localized inside the plasma and if the pump energy is supplied by some external devices, then the mode-conversion results in a deposition of the external pump energy into the plasma. If the excited plasma waves subsequently damp, their energy can be converted to thermal energy of the particles. In this way, parametric excitation can act as an efficient mechanism to heat the plasmas.

From a practical point of view, it is important to know the physical processes responsible for absorption and heating, and their efficiencies. One has to estimate the saturation mechanism and the resulting saturation levels of the decay waves (idler and signal) by means of a non-linear treatment of parametric instability. Spatial non-uniformity of the plasma, spectral cascade, particle trapping, and many other effects can act as saturation mechanisms.

2.2 General formalism of parametric instability in a plasma

An unmagnetized plasma supports three types of natural modes, namely

- (1) the electromagnetic wave (\vec{k}_o, ω_o) with the dispersion relation (see equation 2.19):

$$\omega_o^2 = \omega_{pe}^2 + k_o^2 c^2, \quad (2.3)$$

- (2) the high-frequency electron plasma wave (\vec{k}_e, ω_e) with dispersion relation [see section (A) in appendix]:

$$\omega_e^2 = \omega_{pe}^2 + \frac{3}{2} k_e^2 v_e^2 \quad (2.4)$$

and

(3) the low-frequency ion plasma wave (\vec{k}_i, ω_i) with dispersion relation [see section (A) in appendix]:

$$\omega_i = \omega_{pi} \left\{ 1 + \frac{1}{(k\lambda_{De})^2} \right\}^{-1/2}. \quad (2.5)$$

The parameters n_j , m_j , T_j , $\omega_{pj} = (4\pi n_j e^2 / m_j)^{1/2}$, $v_j = (2k_B T_j / m_j)^{1/2}$ and $\lambda_{Dj} = (k_B T_j / 4\pi n_j e^2)^{1/2}$ are density, mass, temperature, plasma frequency (angular), thermal velocity and Debye length of j^{th} species, where $j = e$ for electrons and i for ions. Here, k_B is the Boltzmann constant.

Consider a large amplitude plane polarized electromagnetic pump wave

$$\vec{E}_o = \frac{1}{2} \left(E_o e^{i(\vec{k}_o \cdot \vec{r} - \omega_o t)} \hat{e} + cc \right) \quad (2.6)$$

propagating in a homogeneous plasma, where cc stands for the complex conjugate. In the equilibrium, electrons oscillate with velocity $\vec{v}_o (= e\vec{E}_o / m_e \omega_o < c)$ in the incident electric field \vec{E}_o and the ions form a stationary background. Imagine a propagating density perturbation (\vec{k}, ω) associated with an electrostatic wave disturbing this equilibrium. These electron density fluctuations will be carried about by the oscillating field \vec{E}_o and will lead to currents at $\vec{k}_o \pm \vec{k}$, $\omega_o \pm \omega$. These currents will generate mixed electromagnetic-electrostatic side-band modes at $\vec{k}_o \pm \vec{k}$, $\omega_o \pm \omega$. The side-band modes, in turn, interact with the pump wave field producing a ponderomotive bunching force $\sim \nabla E^2$ [see section (C) in appendix] which amplifies the original density perturbation. Thus, there is a positive feedback system which will lead to an instability of the original density perturbation and the side-band modes (signal and idler) provided the rate of transfer of energy into them exceeds their natural damping rates.

Consider a pair of Maxwell's equations:

$$\nabla \times \vec{E} = -\frac{1}{c} \frac{\partial \vec{B}}{\partial t}, \quad (2.7)$$

$$\nabla \times \vec{B} = \frac{4\pi}{c} \vec{J} + \frac{1}{c} \frac{\partial \vec{E}}{\partial t}. \quad (2.8)$$

Taking curl operator on both sides of equation (2.7) and substituting equation (2.8), we find

$$\nabla \times (\nabla \times \vec{E}) = -\frac{4\pi}{c^2} \frac{\partial \vec{J}}{\partial t} - \frac{1}{c} \frac{\partial^2 \vec{E}}{\partial t^2}. \quad (2.9)$$

Using a standard vector identity, we find

$$(\nabla^2 - \frac{1}{c^2} \frac{\partial^2}{\partial t^2}) \vec{E} = \nabla(\nabla \cdot \vec{E}) + \frac{4\pi}{c^2} \frac{\partial \vec{J}}{\partial t}. \quad (2.10)$$

The current density \vec{J} is defined as

$$\vec{J} = -en_e \vec{u}, \quad (2.11)$$

where \vec{u} is the oscillatory velocity of electrons in the electric field \vec{E} . We obtain \vec{u} from the equation of motion of an electron

$$\frac{\partial \vec{u}}{\partial t} = -\frac{e}{m_e} \vec{E}, \quad (2.12)$$

where $\vec{E} = \vec{E}_o + \vec{E}_\pm$ with

$$\vec{E}_\pm = \frac{1}{2} [E_\pm e^{i(\vec{k}_\pm \cdot \vec{r} - \omega_\pm t)} \hat{e}_\pm + cc] \quad (2.13)$$

are the electric fields of the side-band modes, which are perturbations to the incident radiation field \vec{E}_o , in a plasma.

Substituting \vec{E} into equation (2.12), we get

$$\vec{u} = \vec{u}_o + \vec{u}_\pm = -i \frac{e}{m_e} \left(\frac{\vec{E}_o}{\omega_o} + \frac{\vec{E}_\pm}{\omega_\pm} \right). \quad (2.14)$$

Substituting equation (2.14) into equation (2.11), we get

$$\vec{J} = \vec{J}_o + \vec{J}_\pm = i \frac{e^2}{m_e} n_e \left(\frac{\vec{E}_o}{\omega_o} + \frac{\vec{E}_\pm}{\omega_\pm} \right). \quad (2.15)$$

Let $n_e = n_o + \delta n_e$ be the density of the electron plasma where $\delta n_e = \delta n \exp\{i(\vec{k} \cdot \vec{r} - \omega t)\}$ is the perturbation. Then retaining terms only upto the first order (i.e., neglecting the terms containing $\delta n_e \vec{E}_\pm$), we obtain

$$\vec{J} = i \frac{\omega_{pe}^2}{4\pi\omega_o} \vec{E}_o + i \frac{1}{4\pi} \frac{\omega_{pe}^2}{\omega_\pm} \vec{E}_\pm + i \frac{e^2}{m_e} \frac{\vec{E}_o}{\omega_o} \delta n_e, \quad (2.16)$$

where $\omega < \omega_o$. Now, substituting equation (2.16) into equation (2.10), we get

$$\begin{aligned} (c^2 k_o^2 - \omega_o^2 + \omega_{pe}^2) \vec{E}_o - c^2 \vec{k}_o (\vec{k}_o \cdot \vec{E}_o) + (c^2 k_\pm^2 - \omega_\pm^2 + \omega_{pe}^2) \vec{E}_\pm - c^2 \vec{k}_\pm (\vec{k}_\pm \cdot \vec{E}_\pm) \\ = -\frac{\omega_{pe}^2}{n_o} \delta n_e \vec{E}_o. \end{aligned} \quad (2.17)$$

From the zeroth order terms in equation (2.17), we find

$$(c^2 k_o^2 - \omega_o^2 + \omega_{pe}^2) \vec{E}_o = c^2 \vec{k}_o (\vec{k}_o \cdot \vec{E}_o). \quad (2.18)$$

Since the incident wave is transverse, the right hand side of equation (2.18) is zero.

Therefore, we obtain

$$\omega_o^2 = \omega_{pe}^2 + k_o^2 c^2. \quad (2.19)$$

This is the dispersion relation for an electromagnetic wave propagating in a plasma medium. Equation (2.19) shows that ω_{pe} is the minimum frequency for propagation of an electromagnetic wave in a plasma i.e., k becomes imaginary for $\omega_o < \omega_{pe}$. Hence the condition $\omega_{pe} = \omega_o$ defines the maximum plasma density in which an electromagnetic wave of frequency ω_o can penetrate.

Now, by considering the first order terms in equation (2.17), we get

$$D_\pm \vec{E}_\pm - c^2 \vec{k}_\pm (\vec{k}_\pm \cdot \vec{E}_\pm) = -\frac{\omega_{pe}^2}{n_o} \delta n_e \vec{E}_o, \quad (2.20)$$

where $D_\pm = k_\pm^2 c^2 - \omega_\pm^2 + \omega_{pe}^2$.

To find \vec{E}_\pm we have to invert equation (2.20). Taking scalar product on both sides of equation (2.20) with \vec{k}_\pm , we obtain

$$\vec{k}_\pm \cdot \vec{E}_\pm = \frac{\omega_{pe}^2}{n_o} \frac{(\vec{k}_\pm \cdot \vec{E}_o)}{(\omega_\pm^2 - \omega_{pe}^2)} \delta n_e. \quad (2.21)$$

Taking twice vector product on both sides of equation (2.20) with \vec{k}_\pm , we get

$$k_\pm^2 \vec{E}_\pm - \vec{k}_\pm (\vec{k}_\pm \cdot \vec{E}_\pm) = \frac{\omega_{pe}^2}{n_o} \frac{\delta n_e}{D_\pm} [\vec{k}_\pm (\vec{k}_\pm \cdot \vec{E}_o) - k_\pm^2 \vec{E}_o]. \quad (2.22)$$

Substituting equation (2.21) into equation (2.22), we have

$$\vec{E}_\pm = -\omega_{pe}^2 \frac{\delta n_e}{n_o} \left[\frac{k_\pm^2 \vec{E}_o - \vec{k}_\pm (\vec{k}_\pm \cdot \vec{E}_o)}{k_\pm^2 D_\pm} - \frac{\vec{k}_\pm (\vec{k}_\pm \cdot \vec{E}_o)}{k_\pm^2 \omega_\pm^2 (1 - \omega_{pe}^2 / \omega_\pm^2)} \right]. \quad (2.23)$$

To calculate the low-frequency electron density perturbation $\delta n_e(\vec{k}, \omega)$, produced by the beating of the side-band modes with the pump wave, it is most convenient to introduce the ‘ponderomotive force or the non-linear Lorentz force’, [see section (C) in appendix] given by

$$\vec{F}_\omega = -\nabla \psi_\omega. \quad (2.24)$$

The ponderomotive force depends quadratically on the amplitude and produces a slowly varying longitudinal field, which leads to slow longitudinal motions and modifies the plasma density. The ponderomotive potential (Drake et al. 1974) is given by

$$\begin{aligned} \psi_{e\omega}(\vec{r}, t) &= \frac{e^2}{2m_o} \left\langle \left(\text{Re} \left| \frac{\vec{E}_o}{i\omega} + \frac{\vec{E}_-}{i\omega_-} + \frac{\vec{E}_+}{i\omega_+} \right| \right)^2 \right\rangle_\omega \\ &= \frac{e^2}{m_e \omega_o^2} (\vec{E}_o \cdot \vec{E}_- + \vec{E}_o \cdot \vec{E}_+). \end{aligned} \quad (2.25)$$

The angular bracket $\langle \rangle_\omega$ represents the ω frequency component of an average over the fast time scale $\omega_o \gg \omega$; only linear terms in \vec{E}_\pm are retained. With the inclusion

of the ponderomotive force, as a driving force, the Vlasov equation for the low frequency response of electrons can then be written as

$$\frac{\partial f_e}{\partial t} + \vec{v} \cdot \nabla f_e + \frac{1}{m_e} (e \nabla \varphi - \nabla \psi_{e\omega}) \cdot \frac{\partial f_e}{\partial \vec{v}} = 0, \quad (2.26)$$

where φ is the self-consistent scalar potential associated with the electrostatic waves and $f_e(\vec{r}, \vec{v}, t)$ is the electron distribution function.

Linearizing the equation (2.26) with $f_e(\vec{r}, \vec{v}, t) = f_{e0}(\vec{v}) + \delta f_e(\vec{r}, \vec{v}, t)$, we get

$$\frac{\partial(\delta f_e)}{\partial t} + \vec{v} \cdot \nabla(\delta f_e) + \frac{1}{m_e} (e \nabla \varphi - \nabla \psi_{e\omega}) \cdot \frac{\partial f_{e0}}{\partial \vec{v}} = 0, \quad (2.27)$$

The Fourier transformations of δf_e , $\psi_{e\omega}$ and φ are given by

$$\delta f_e(\vec{k}, \vec{v}, \omega) = \frac{1}{2\pi} \int_{-\infty}^{\infty} \int_{-\infty}^{\infty} \delta f_e(\vec{r}, \vec{v}, t) e^{-i(\vec{k} \cdot \vec{r} - \omega t)} d^3 r dt, \quad (2.28)$$

$$\psi_{e\omega}(\vec{k}, \omega) = \frac{1}{2\pi} \int_{-\infty}^{\infty} \int_{-\infty}^{\infty} \psi_{e\omega}(\vec{r}, t) e^{-i(\vec{k} \cdot \vec{r} - \omega t)} d^3 r dt, \quad (2.29)$$

and

$$\varphi(\vec{k}, \omega) = \frac{1}{2\pi} \int_{-\infty}^{\infty} \int_{-\infty}^{\infty} \varphi(\vec{r}, t) e^{-i(\vec{k} \cdot \vec{r} - \omega t)} d^3 r dt. \quad (2.30)$$

The Fourier transformation of the equation (2.27) gives:

$$\delta f_e(\vec{k}, \vec{v}, \omega) = \frac{1}{m_e} [e\varphi - \psi_{e\omega}] \frac{\vec{k} \cdot \frac{\partial f_{e0}}{\partial \vec{v}}}{(\omega - \vec{k} \cdot \vec{v})}. \quad (2.31)$$

The perturbation in the electron density is given by

$$\delta n_e(\vec{k}, \omega) = \int_{-\infty}^{\infty} n_0 \delta f_e d\vec{v} = \frac{k^2}{4\pi e^2} [e\varphi - \psi_{e\omega}] \chi_e, \quad (2.32)$$

where

$$\chi_e(k, \omega) = \frac{\omega_{pe}^2}{k^2} \int_{-\infty}^{\infty} \frac{\vec{k} \cdot \frac{\partial f_{e0}}{\partial \vec{v}}}{(\omega - \vec{k} \cdot \vec{v})} d\vec{v} \quad (2.33)$$

is the electron susceptibility function. For a Maxwellian plasma

$$f_{eo}(v) = \left(\frac{m_e}{2\pi k_B T_e} \right)^{3/2} \exp(-v^2/v_e^2),$$

therefore, we obtain

$$\chi_e(k, \omega) = \frac{1}{(k\lambda_{De})^2} \left[1 + \frac{\omega}{kv_e} Z(\omega/kv_e) \right], \quad (2.34)$$

where $Z(\xi)$ is the plasma dispersion function (Fried and Conte, 1961):

$$Z(\xi) = \frac{1}{\sqrt{\pi}} \int_{-\infty}^{\infty} \frac{e^{-x^2}}{(x - \xi)} dx. \quad (2.35)$$

Note that χ_e has the following asymptotic forms:

$$\chi_e(k, \omega) = \begin{cases} -\frac{\omega_{pe}^2}{\omega^2} \left(1 + \frac{3}{2} \frac{k^2 v_e^2}{\omega^2} \right) + i \frac{\sqrt{\pi}}{(k\lambda_{De})^2} \frac{\omega}{kv_e} \exp[-\omega^2/(kv_e)^2], & \text{for } \omega \gg kv_e; \\ \frac{1}{(k\lambda_{De})^2} \left(1 + i\sqrt{\pi} \frac{\omega}{kv_e} \right), & \text{for } \omega \ll kv_e, \end{cases} \quad (2.36)$$

To determine $\varphi(\vec{r}, t)$ self consistently we use Poisson equation,

$$\nabla \cdot \vec{E} = 4\pi e(n_i - n_e). \quad (2.37)$$

Using $\vec{E} = -\nabla\varphi$, $n_i = n_o + \delta n_i$ and $n_e = n_o + \delta n_e$ we obtain

$$\nabla^2 \varphi = -4\pi e(\delta n_i - \delta n_e). \quad (2.38)$$

Using Fourier transforming (equation 2.30), equation (2.38) reduces to

$$\varphi(\vec{k}, \omega) = \frac{4\pi e}{k^2} [\delta n_i - \delta n_e], \quad (2.39)$$

where $\delta n_i(\vec{k}, \omega)$ is given by (similar to equation 2.32)

$$\delta n_i(\vec{k}, \omega) = \frac{k^2}{4\pi e^2} [-e\varphi - \psi_{i\omega}] \chi_i, \quad (2.40)$$

and

$$\chi_i(k, \omega) = \frac{\omega_{pi}^2}{k^2} \int_{-\infty}^{\infty} \frac{\vec{k} \cdot \frac{\partial f_{i\alpha}}{\partial \vec{v}}}{(\omega - \vec{k} \cdot \vec{v})} d\vec{v} \quad (2.41)$$

is the ion susceptibility function. For a Maxwellian plasma, we obtain

$$\chi_i(k, \omega) = \frac{1}{(k\lambda_{De})^2} \frac{T_e}{T_i} \left[1 + \frac{\omega}{kv_i} Z(\omega/kv_i) \right]. \quad (2.42)$$

Note that χ_i has the following asymptotic forms:

$$\chi_i(k, \omega) = \begin{cases} -\frac{\omega_{pi}^2}{\omega^2} \left(1 + \frac{3}{2} \frac{kv_i}{\omega} \right) + i \frac{\sqrt{\pi}}{(k\lambda_{De})^2} \frac{T_e}{T_i} \frac{\omega}{kv_i} \exp[-\omega^2/(kv_i)^2], & \text{for } \omega \gg kv_i; \\ \frac{1}{(k\lambda_{De})^2} \frac{T_e}{T_i} \left(1 + i\sqrt{\pi} \frac{\omega}{kv_i} \right), & \text{for } \omega \ll kv_i, \end{cases} \quad (2.43)$$

Substituting $\delta n_e(\vec{k}, \omega)$ from equation (2.32) and $\delta n_i(\vec{k}, \omega)$ from equation (2.40) into equation (2.39), we get

$$\varphi(\vec{k}, \omega) = \frac{\psi_{c\omega}\chi_e}{e\epsilon} \left(1 - \frac{\psi_{i\omega}\chi_i}{\psi_{e\omega}\chi_e} \right), \quad (2.44)$$

where $\epsilon(\vec{k}, \omega) = 1 + \chi_e(\vec{k}, \omega) + \chi_i(\vec{k}, \omega)$ is the plasma dielectric function. Substituting equation (2.44) into equation (2.32), we get

$$\delta n_e(\vec{k}, \omega) = -\frac{k^2}{4\pi m_e \omega_o^2} \frac{[1 + \chi_i + (m_e/m_i)\chi_i]\chi_e}{\epsilon} (\vec{E}_o \cdot \vec{E}_- + \vec{E}_o \cdot \vec{E}_+). \quad (2.45)$$

Now, substituting \vec{E}_- and \vec{E}_+ , from equation (2.23) into equation (2.45), we obtain

$$\frac{1 + \chi_i + \chi_e}{\chi_e[1 + \chi_i + (m_e/m_i)\chi_i]} = k^2 \left[\frac{|\vec{k}_- \times \vec{v}_o|^2}{k_-^2 D_-} - \frac{|\vec{k}_- \cdot \vec{v}_o|^2}{k_-^2 \omega_-^2 (1 - \omega_{pe}^2/\omega_-^2)} + \frac{|\vec{k}_+ \times \vec{v}_o|^2}{k_+^2 D_+} - \frac{|\vec{k}_+ \cdot \vec{v}_o|^2}{k_+^2 \omega_+^2 (1 - \omega_{pe}^2/\omega_+^2)} \right], \quad (2.46)$$

where $\vec{v}_o = e\vec{E}_o/m_e\omega_o$ is the quiver velocity of electrons in the field \vec{E}_o .

The dispersion relation (2.46) describe the parametric instability, excited by a large amplitude electromagnetic wave (\vec{k}_o, ω_o) in a plasma. This dispersion relation

describe the parametric coupling of a low frequency electrostatic mode at (\vec{k}, ω) and two high frequency mixed electrostatic–electromagnetic side band modes at $(\vec{k}_o \pm \vec{k}, \omega_o \pm \omega)$. The $\vec{k}_\pm \times \vec{v}_o$ terms in equation (2.46) arise from the electromagnetic components of the side–band modes and $\vec{k}_\pm \cdot \vec{v}_o$ terms from the electrostatic components. Note that equation (2.46) reduces to equation (I-20) (Liu and Kaw 1976) for $m_e/m_i \approx 0$. This equation is used to study the parametric phenomena in astrophysical plasmas.

References

- Drake, J. F., Kaw, P. K., Lee, Y. C., Schmidt, G., Liu, C. S. & Rosenbluth, M. V.,
1974, *Phy. Fluids.*, **17**, 778
- Fried, D., & Conte, S. D., *The Plasma Dispersion Function*, (Academic Press,
New York, 1961)
- Liu, C. S. & Kaw, P. K., 1976, *Advances in plasma physics*, eds. Simon, A. &
Thompson, B., **6**, 83
- Lord Rayleigh, 1883, *Phil. Mag.*, **15**, 229

Chapter 3

THE ROLE OF COMPTON AND RAMAN SCATTERING IN THE QUASAR CONTINUUM

In this chapter, the possible role that stimulated Raman and Compton scattering can play in the continuum emission of a quasar is explored. There are three ways in which an electromagnetic wave can undergo scattering in a plasma: (i) when the scattering of radiation occurs by a single electron, it is called Compton Scattering; (ii) if it occurs by a longitudinal electron plasma mode, it is called stimulated Raman scattering (SRS); and (iii) if it occurs by a highly damped electron plasma mode, it is called stimulated Compton scattering (SCS). The nonthermal continuum of quasars is believed to be produced through the combined action of synchrotron and inverse Compton processes, which are essentially single particle processes. As an example, it is shown that the complete spectrum of 3C 273 can be reproduced by a suitable combination of stimulated Compton scattering and stimulated Raman scattering processes. It is shown that the observed spectral breaks in the blue region could be due to the change of emission process from stimulated Raman scattering and stimulated Compton scattering. The differential contributions of these stimulated scattering processes for different values of the plasma parameters are also calculated.

3.1 INTRODUCTION

One of the most challenging problems in the area of active galactic nuclei (AGN) is the mechanism of continuum emission. In the broadest sense, the important issues are (1) mechanisms responsible for the radiation, (2) the kinematics and the spatial distribution of the continuum emitting regions, and (3) the connection of the continuum emission to the central engine. A surprisingly large number of plausible explanations for the origin of this continuum have involved incoherent radiation mechanisms. The most common is synchrotron self-Compton emission from nonthermal electrons, which seems to work rather well from the infrared (IR) to ultraviolet (UV), particularly for blazars (e.g., Stein and O'Dell 1985; Stein 1988). But the Comptonized, self-absorbed thermal cyclotron radiation from a mildly relativistic electron beam also appears to be able to fit that part of the spectrum (e.g., Begelman 1988). The magnetized accretion disc of a massive black hole acts as an electric dynamo producing two oppositely directed beams of ultrarelativistic particles (Lovelace, 1976). The physics of relativistic jets on submilliarcsecond scales ($\sim 10^{15}$ cm to 10^{19} cm) is discussed by Rees (1984). He concluded that the power emerges mainly as directed Poynting flux, rather than primarily as particle kinetic energy. Melia and Königl (1989) studied the radiative deceleration of ultrarelativistic jets in AGN. The inverse Compton scattering of ambient radiation by a cold relativistic jet in the case of blazars has been studied by Begelman and Sikora (1987).

The generation (Blandford and Payne 1982; Wiita, Kapahi and Saikia 1982) and stability of extremely sharp electron beams in the quasar environment has been

discussed by Lesch, Schlickeiser and Crusius (1988). Baker, Borovsky, Benford and Eilek (1988) have constructed a model of the inner portions of astrophysical jets in which a relativistic electron beam is injected from the central engine into the jet plasma. This beam drives electrostatic plasma wave turbulence, which leads to the collective emission of electromagnetic waves. The coherent scattering of relativistic electron beam from concentrations of electrostatic plasma waves (cavitons) produce emission over extremely broad-band (Benford 1992).

The collective plasma processes have been shown to play significant role in the absorption (Krishan 1987; Krishan 1988b; Beal 1990; Gangadhara and Krishan 1990) and spectral modification of the radiation through its interaction with the plasma in the accretion disc and the emission-line region (Krishan 1988a). A sequence of plasma processes, which account for the energy gain and loss of the electron beam, has been discussed by Krishan (1983, 1985), and Krishan and Wiita (1986, 1990). This Chapter, illustrates the scattering of the incident electromagnetic wave (pump) off the electron plasma wave in the two regimes, namely stimulated Raman scattering and stimulated Compton scattering, and estimate the contribution of these processes in the generation of the complete spectrum, from radio to X-rays, in quasars. The special features, like the threshold of the pump, the growth rate of the instability, and the angular and spectral distribution of scattered power, are studied under various conditions of electron density and temperature. Using power-law spatial variations of density, Lorentz factor, temperature, and the spectrum of the pump, one can reproduce the spectrum of 3C 273 (Gangadhara and Krishan 1992). The inclusion of stimulated Raman scattering (SRS) and stimulated Compton scattering (SCS) seems to be essential to account for spectral breaks in the observed non-thermal continuum emission of quasars.

3.2 STIMULATED RAMAN AND COMPTON SCATTERING AS ENERGY LOSS MECHANISMS

Consider a standard model consisting of a black hole of mass $M = 10^8 M_\odot$ surrounded by a relativistic plasma which extends to a few times Schwarzschild radius R_s , ($R_s = 2GM/c^2$) and produces the nonthermal continuum (Wiita 1985). The non-thermal polarized low-frequency electromagnetic wave (soft photon) is considered as a pump which drives parametric instabilities. This soft photon field may be identified with cyclotron or synchrotron radiation (Stein 1988, Krishan and Wiita 1990). Our model consists of a relativistic electron beam which propagates radially outwards and interacts with the soft photon field and produces radiation at higher frequencies. The scattering of soft photons off the electron plasma wave, the collective mode of the relativistic electron beam, can be studied more easily in the rest frame of the electrons, as is done in the study of the inverse Compton scattering.

Consider a relativistic electron beam (REB) moving radially outward from a central engine. Assume that, in the laboratory frame, the direction of propagation of REB is in the positive z -axis, and there exists a randomly moving radiation field in the path (see Fig. 3.1).

In the REB frame, electrons will be at rest and radiation field will get confined to a cone of angular width $\sim 1/\gamma$, because of Lorentz transformation of angles, where γ is the relativistic Lorentz factor. The radiation beam will be in the direction of negative z' axis. This beamed radiation is intense and can excite stimulated scattering instabilities in the electron beam plasma. Here, we assume that massive ions form a neutralizing background.

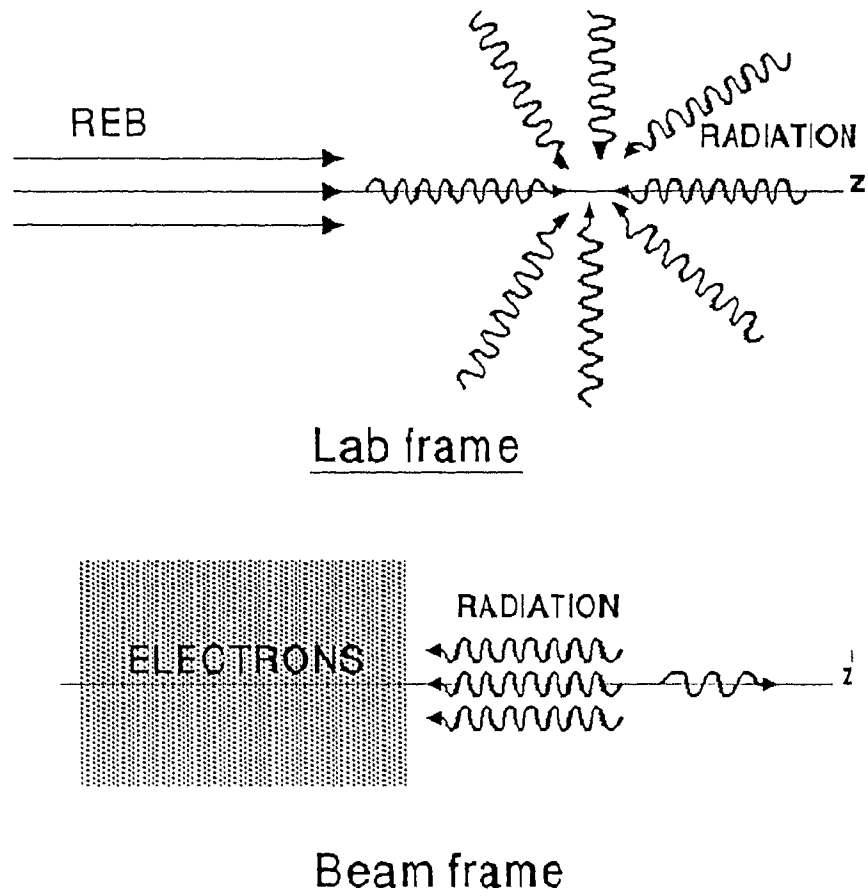


Fig. 3.1 Interaction of electromagnetic radiation with relativistic electron beam in quasars.

3.2.1 Lorentz Transformations

Since it is much simpler to do the non-relativistic calculations in the beam frame, we compute growth rates and the scattered flux in the beam frame and then transfer these quantities to the laboratory frame.

Consider a linearly polarized electromagnetic wave with electric field

$$\vec{E}_i = \frac{1}{2} [E_i \exp\{i(\vec{k}_i \cdot \vec{r} - \omega_i t)\} \hat{e}_i + cc], \quad (3.1)$$

undergoes scattering from a relativistic electron beam moving in the z-direction, in the laboratory frame, where cc stands for complex conjugate. We use primes on

the quantities in the beam frame to distinguish them from the quantities (without primes) in the laboratory frame. The invariance of the phase of an electromagnetic wave gives:

$$\vec{k}'_i \cdot \vec{r}' - \omega'_i t' = \vec{k}_i \cdot \vec{r} - \omega_i t, \quad (3.2)$$

where time t' and the components \vec{r}' have the following Lorentz transformations:

$$x' = x, \quad y' = y, \quad z' = \gamma(z - v_b t), \quad t' = \gamma\left(t - \frac{v_b}{c^2} z\right). \quad (3.3)$$

Here, v_b and $\gamma = 1/\sqrt{1 - v_b^2/c^2}$ are the relativistic electron beam velocity and Lorentz factor, respectively. The equation (3.2) implies that:

$$k'_x = k_x, \quad k'_y = k_y, \quad (3.4)$$

$$k'_z = \gamma\left(k_z - \frac{v_b}{c^2} \omega_i\right) \quad (3.5)$$

and

$$\omega'_i = \gamma(\omega_i - k_z v_b). \quad (3.6)$$

The Lorentz transformation of electric field \vec{E}_i and magnetic field \vec{B}_i to beam frame is given by

$$\vec{E}'_{i\parallel} = \vec{E}_{i\parallel}, \quad \vec{E}'_{i\perp} = \gamma\left[\vec{E}_{i\perp} + \frac{\vec{v}_b}{c} \times \vec{B}_i\right], \quad (3.7)$$

$$\vec{B}'_{i\parallel} = \vec{B}_{i\parallel}, \quad \vec{B}'_{i\perp} = \gamma\left[\vec{B}_{i\perp} - \frac{\vec{v}_b}{c} \times \vec{E}_i\right], \quad (3.8)$$

where the parallel and perpendicular components of \vec{E}_i and \vec{B}_i refer to along and perpendicular to \hat{z} . Taking $\vec{E}_{i\parallel} = 0$, the angle α between the magnetic field of the incident radiation \vec{B}_i and \hat{z} can be transformed to the beam frame and is given by:

$$\sin(\alpha') = \frac{\sin(\alpha) - v_b/c}{1 - (v_b/c)\sin(\alpha)}. \quad (3.9)$$

The tips of \vec{E}_i' and \vec{B}_i' lie in a disc of angular width $\approx 2/\gamma$ perpendicular to the beam velocity.

In addition to these quantities, we need the transformation of the plasma frequency, ω_{pe} , the beam thermal speed v_e , and the growth rate Γ .

Since a Lorentz contraction increases both the density and the effective mass by a factor γ , the plasma frequency $\omega_{pe} (= 4\pi n_e e^2/m_e)^{1/2}$ (where e is the electron charge, n_e the beam density and m_e the electron mass) is frame-invariant.

The thermal speed v_e in the beam frame can be expressed in terms of the energy spread of the beam in the laboratory frame as follows. From the definition of γ , we have

$$v_b = c \left(1 - \frac{1}{\gamma^2} \right)^{1/2} \quad (3.10)$$

The velocity spread δv_b in the laboratory frame can be expressed in terms of the spread in γ ,

$$\delta v_b \approx c \frac{\delta \gamma}{\gamma^3} \quad \text{for} \quad \gamma \gg 1. \quad (3.11)$$

Now, using the Lorentz transformation of velocity

$$v_z = \frac{v'_z + v_b}{1 + v_b v'_z/c^2}, \quad (3.12)$$

we obtain

$$\begin{aligned} \delta v_b = \delta v_z &= \frac{\delta v'_z}{\gamma^2 (1 + v_b v'_z/c^2)^2} \\ &\approx \frac{1}{\gamma^2} \delta v'_z = \frac{v_e}{\gamma^2}, \end{aligned} \quad (3.13)$$

because $v'_z = 0$. Hence from equation (3.13), the thermal speed in the beam frame is obtained:

$$v_e = c \frac{\delta \gamma}{\gamma}. \quad (3.14)$$

We now consider the transformation of the growth rate Γ . If a wave with slowly varying amplitude $A'(z', t')$ grows in time and space at a temporal growth rate Γ'

in the beam frame, then A' satisfies the following equation:

$$\frac{\partial A'}{\partial t'} + v'_g \frac{\partial A'}{\partial z'} = \Gamma' A', \quad (3.15)$$

where v'_g is the group velocity in the beam frame. Using the Lorentz transformation we get from equation (3.15):

$$\frac{\partial A'}{\partial t} + \frac{v'_g + v_b}{1 + v_b v'_g / c^2} \frac{\partial A'}{\partial z} = \frac{\Gamma'}{\gamma(1 + v_b v'_g / c^2)} A'. \quad (3.16)$$

The amplitude A in the laboratory frame is linearly proportional to A' . Hence the equation (3.16) gives the Lorentz transformation of the group velocity as well as the growth rate, i.e.,

$$v_g = \frac{v'_g + v_b}{1 + v_b v'_g / c^2}, \quad (3.17)$$

$$\Gamma = \frac{\Gamma'}{\gamma(1 + v_b v'_g / c^2)} \approx \frac{\Gamma'}{2\gamma}, \quad (3.18)$$

for $v_b \approx v'_g \approx c$.

3.2.2 Stimulated Compton or stimulated Raman scattering?

In the equilibrium, electrons oscillate with velocity v'_i in the pump field \vec{E}'_i . Assume that in a plasma the propagating density perturbation (\vec{k}', ω') associated with an electron plasma wave disturbs this equilibrium. This electron density perturbation combined with the oscillatory velocity v_i of the electrons produce currents at $(\vec{k}'_i \pm \vec{k}', \omega'_i \pm \omega')$. These currents will generate mixed electromagnetic-electrostatic side-band modes at $(\vec{k}'_i \pm \vec{k}', \omega'_i \pm \omega')$. The side-band modes, in turn, interact with the pump wave field, producing a ponderomotive bunching force $\sim \nabla E'^2$ which amplifies the original density perturbation. Thus, there is a positive feedback system which leads to instability, called parametric instability, of the original density perturbation and the side-band modes, provided the rate of transfer of energy into them exceeds their natural damping rates.

We consider a special case of parametric instability in which the high-frequency side-band modes are predominantly electromagnetic, so we essentially have the problem of stimulated scattering where a pump (electromagnetic) wave excites an electron plasma wave (\vec{k}'_e, ω'_e) and two new electromagnetic waves at shifted frequencies: the stokes mode (\vec{k}'_s, ω'_s) and the anti-stokes mode ($\vec{k}'_{as}, \omega'_{as}$). The instability is excited resonantly only when the following phase matching conditions are satisfied

$$\omega'_i = \omega'_s + \omega'_e, \quad (3.19)$$

$$\vec{k}'_i = \vec{k}'_s + \vec{k}'_e, \quad (3.20)$$

$$\omega'_i + \omega'_e = \omega'_{as} \quad (3.21)$$

and

$$\vec{k}'_i + \vec{k}'_e = \vec{k}'_{as}. \quad (3.22)$$

Fig. 3.2 shows the frequency spectrum of the stimulated scattering of electromagnetic radiation into sideband modes.

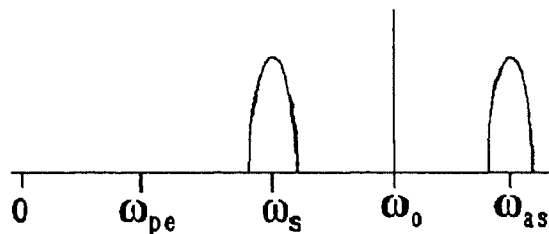


Fig. 3.2 Frequency spectrum of stimulated scattering.

Each of the excited modes satisfies its own linear dispersion relation in the plasma medium. The dispersion relation of the electron plasma wave in the beam frame (a stationary plasma) is [Hasegawa 1978; see section (A) in appendix]:

$$1 - \frac{\omega_{pe}^2}{k_e'^2} \int_{-\infty}^{\infty} \frac{\partial f_e / \partial v}{v - (\omega'_e + i0) / k_e'} dv = 0, \quad (3.23)$$

where $f_e(v)$ is assumed to be the Maxwellian velocity distribution function of the electrons in the beam frame and ϵ is the small imaginary part of frequency of the electrostatic perturbation. If we solve equation (3.23) for ω'_e , we have

$$\omega'_e \approx \omega_{pe} \quad \text{for } k'_e \lambda'_{De} \ll 0.4; \quad (3.24)$$

$$\omega'_e \approx k'_e v_e [1 - i\epsilon(1)] \quad \text{for } k'_e \lambda'_{De} \geq 0.4, \quad (3.25)$$

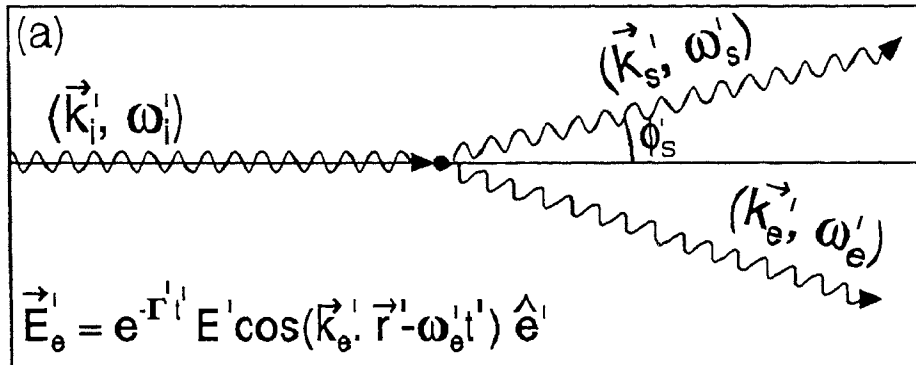
where $v_e = [(2/n'_e) \int_{-\infty}^{\infty} v^2 f_e dv]^{1/2}$ and $\lambda'_{De} = (k_B T_e / 4\pi n'_e e^2)^{1/2}$ are the thermal speed and Debye length of the electron plasma, respectively ($k_B =$ Boltzman constant). Equation (3.25) indicates that if $k'_e \lambda'_{De}$ is larger than or equal to 0.4 then the electron plasma mode loses its wave nature because of its large Landau damping.

The dispersion relation of an electromagnetic wave in a plasma is

$$\omega'^2 = \omega_{pe}^2 + k'^2 c^2. \quad (3.26)$$

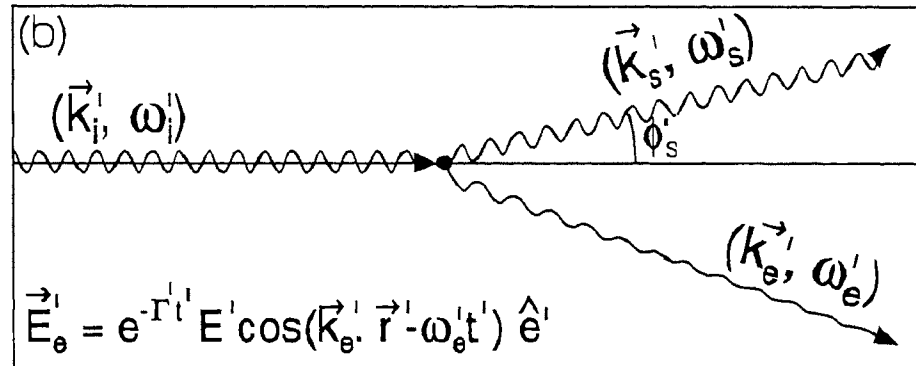
The pump wave, the stokes mode and the anti-stokes mode satisfy the dispersion relation (3.26) in the plasma medium. If the pump wave undergoes backscattering, i.e., $\vec{k}'_i = -\vec{k}'_s$ and for $(\omega'_i, \omega'_s) \gg \omega_{pe}$ so that $\omega'_i = k'_i c$, $\omega'_s = k'_s c$, $k'_i \approx k'_s$, we get $k'_e \approx 2k'_s$. Hence for a given quality of a beam, if ω'_s is increased by increasing pump frequency ω'_i , k'_e which may be initially smaller than $0.4/\lambda'_{De}$ becomes larger than $0.4/\lambda'_{De}$ at some value of ω'_s . Now, we know that for $k'_e \lambda'_{De} \geq 0.4$, the electron plasma wave suffers strong Landau damping. Thus, there are two distinct scattering processes: (i) the scattering of an electromagnetic wave off a weakly damped electron plasma wave known as the stimulated Raman scattering (see Fig. 3.3a) and (ii) the scattering by a damped electron plasma wave known as stimulated Compton scattering (see Fig. 3.3b). Hence, there exists a critical frequency of the scattered wave above which the scattering occurs through stimulated Compton process and below which through stimulated Raman process.

STIMULATED RAMAN SCATTERING ($k_e \lambda_{De} \ll 1$)



\vec{E}_e^i is the electric field of a weakly damped electron plasma wave

STIMULATED COMPTON SCATTERING ($k_e \lambda_{De} \geq 1$)



\vec{E}_e^i is the electric field of a highly damped electron plasma wave

COMPTON SCATTERING ($k_e \lambda_{De} \gg 1$)

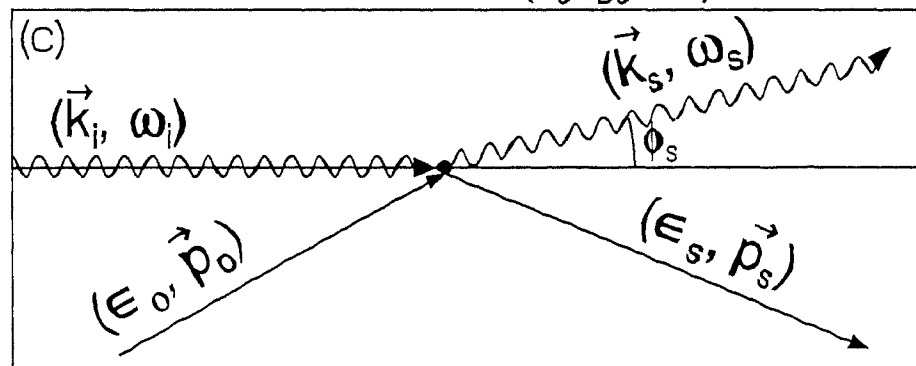


Fig. 3.3 The scattering of an electromagnetic wave (\vec{k}_i, ω_i) in a plasma medium.

If $\omega_i \gg \omega_{pe}$ or $k'\lambda'_{De} \gg 1$ then the electron plasma wave vanishes. In this case, incident photon undergoes Compton scattering from a relativistic electron with energy ϵ_0 and momentum \vec{p}_0 (see Fig. 3.3c).

Consider the transformation of the scattered frequency (see equation 3.6)

$$\omega_s = \gamma(\omega'_s + k'_s v_b). \quad (3.27)$$

For $v_b \approx c$ and $\omega'_s = k'_s c$, we get

$$\omega_s \approx 2\gamma\omega'_s \quad (3.28)$$

We define the critical frequency $\omega_{cr} = \omega_s$ of the scattered wave corresponding to $k'_e \lambda'_{De} = 0.4$, where $\lambda'_{De} = \sqrt{2}v_e/\omega_{pe}$ is the Debye length.

Using the expressions

$$k'_e = 2k'_s \quad (3.29)$$

and

$$k'_e = \frac{0.4}{\sqrt{2}} \frac{\omega_{pe}}{v_e}, \quad (3.30)$$

we get

$$k'_s = \frac{0.2}{\sqrt{2}} \frac{\omega_{pe}}{v_e}. \quad (3.31)$$

Therefore, we have

$$\omega'_s = ck'_s = \frac{0.2}{\sqrt{2}} \frac{c}{v_e} \omega_{pe}. \quad (3.32)$$

Substituting equation (3.32) into equation (3.28), we get

$$\omega_{cr} = 0.2\sqrt{2}\gamma \frac{c}{v_e} \omega_{pe}, \quad (3.33)$$

Now, using equation (3.14), we obtain

$$\omega_{cr} = 0.2\sqrt{2}\gamma\omega_{pe} \frac{\gamma}{\delta\gamma}. \quad (3.34)$$

Thus the critical frequency depends on the relative spread $\delta\gamma/\gamma$ of the beam energy observed in the laboratory frame, as well as the beam density n_e and the Lorentz factor γ .

3.2.3 The growth rates of the stimulated Raman and Compton scattering

The general plasma dispersion relation (see equation 2.46) to describe parametric instability excited in a plasma medium by a large amplitude coherent electromagnetic wave, has been derived in section (2.2). If the excited side-band modes are predominantly electromagnetic then by treating ions as a stationary backgrounds, it reduces to

$$1 + \frac{1}{\chi'_e(k', \omega')} = k'^2 \left[\frac{|\vec{k}'_- \times \vec{v}'_i|^2}{k'^2_- D_-} + \frac{|\vec{k}'_+ \times \vec{v}'_i|^2}{k'^2_+ D_+} \right], \quad (3.35)$$

where $v'_i = eE'_i/m'_e\omega'_i$ is the quiver velocity of electrons, $\omega'_\pm = \omega'_i \pm \omega'$, $\vec{k}'_\pm = \vec{k}'_i \pm \vec{k}'$ and

$$\begin{aligned} D_\pm &= c^2 k'^2_\pm - \omega'^2_\pm + \omega_{pe}^2 \\ &= c^2 k'^2 \pm 2\vec{k}' \cdot \vec{k}'_i c^2 \mp 2\omega'\omega'_i - \omega'^2. \end{aligned} \quad (3.36)$$

For the three-wave stimulated Raman scattering process, in equation (3.35) ω' and \vec{k}' become the angular frequency and the wave vector of the electron plasma wave (ω'_e, \vec{k}'_e). The electron susceptibility function is given by (Fried and Conte, 1961):

$$\chi'_e(k', \omega') = \frac{1}{(k'\lambda'_{De})^2} \left[1 + \frac{\omega'}{k'v_e} Z(\omega'/k'v_e) \right], \quad (3.37)$$

where

$$Z(\omega'/k'v_e) = \frac{1}{\sqrt{\pi}} \int_{-\infty}^{\infty} \frac{e^{-x^2}}{x - (\omega'/k'v_e)} dx \quad (3.38)$$

is the plasma dispersion function. The $\chi'_e(k', \omega')$ has the following asymptotic forms:

$$\chi'_e(k', \omega') = \begin{cases} -\frac{\omega_{pe}^2}{\omega'^2} \left(1 + \frac{3}{2} \frac{k'^2 v_e^2}{\omega'^2} \right) + i \frac{\sqrt{\pi}}{(k'\lambda'_{De})^2} \exp[-\omega'^2/(k'v_e)^2], & \text{for } \omega' \gg k'v_e; \\ \frac{1}{(k'\lambda'_{De})^2} \left(1 + i\sqrt{\pi} \frac{\omega'}{k'v_e} \right), & \text{for } \omega' \ll k'v_e. \end{cases} \quad (3.39)$$

If we use the dispersion relations for ω'_i (which satisfies equation 3.26) and ω'_e (which satisfies equation 3.23), the resonant conditions (3.19), (3.20), (3.21) and (3.22) can be plotted in a (k, ω) diagram. In Figs. 3.4 and 3.5, the arrows show the direction

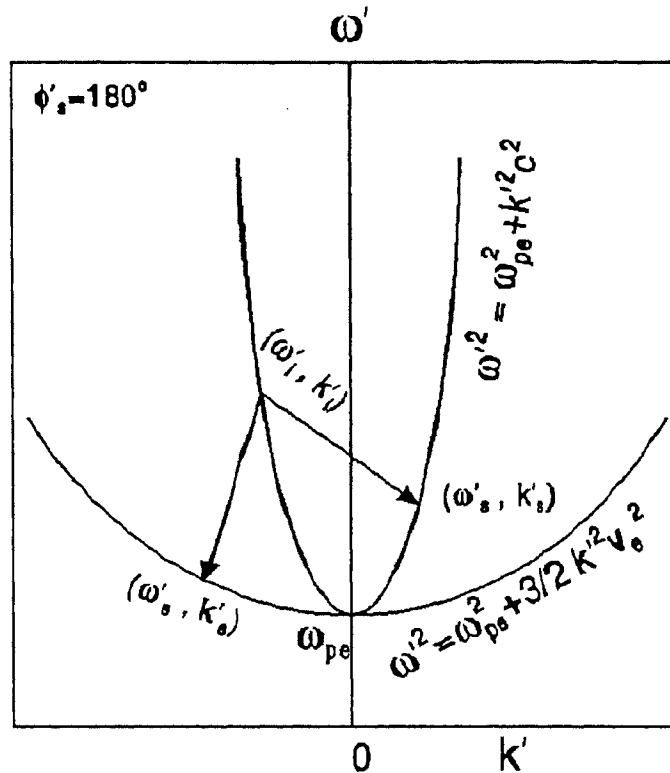


Fig. 3.4 Dispersion diagram of the electromagnetic wave and the plasma wave in the beam frame. Arrows indicate the direction of decay of the incident wave (ω'_i, \vec{k}'_i) into the stokes mode (ω'_s, \vec{k}'_s) and electron plasma mode (ω'_e, \vec{k}'_e) during the backscattering of incident wave. Since $(\omega'_{as}, \vec{k}'_{as})$ does not fall on the dispersion curve of the electromagnetic wave, the anti-stokes mode is not excited in the backscattering of the incident wave.

in which energy and momentum transfer from one mode into the other. In the case of backscattering, $[\phi'_s = \cos^{-1}(\hat{k}'_i \cdot \hat{k}'_s) = 180^\circ]$, $D_- \approx 0$ and $D_+ \neq 0$, therefore, Fig. 3.4 shows that the stokes mode is excited but the anti-stokes mode is not. But in the case of right angle scattering ($\phi'_s = 90^\circ$) both $D_- \approx 0$ and $D_+ \approx 0$ and hence both the modes are excited as indicated by Fig. 3.5. The anti-stokes mode is not excited for $\omega' \ll (c^2 \vec{k}'_i \cdot \vec{k}'_e / \omega'_i)$ and it is excited only the \vec{k}'_e is very small or if \vec{k}'_e is nearly perpendicular to \vec{k}'_i .

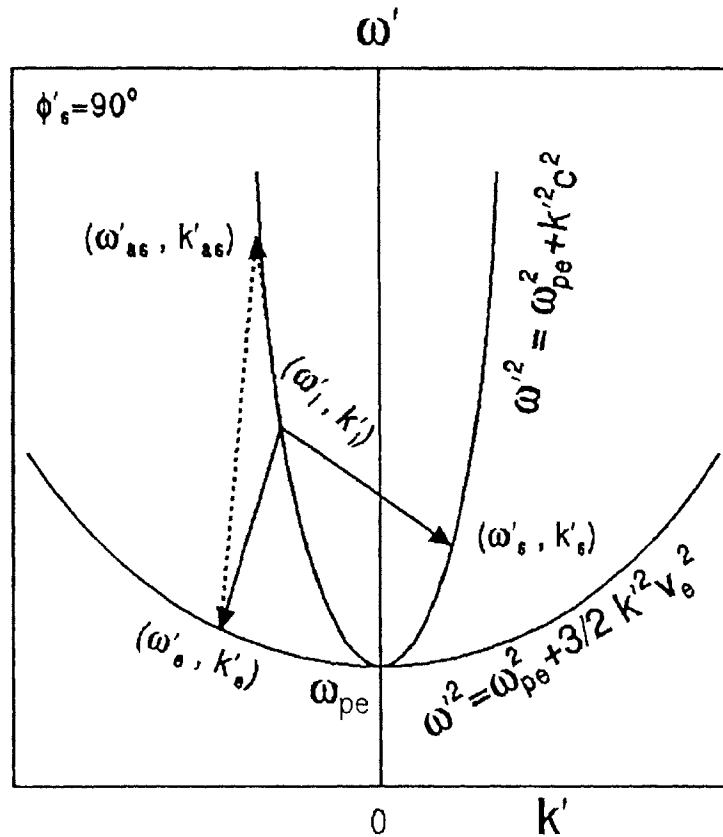


Fig. 3.5 Dispersion diagram showing the right angle scattering of incident wave (ω'_i, \vec{k}'_i) . In this case, both stokes mode (ω'_s, \vec{k}'_s) and anti-stokes mode $(\omega'_{as}, \vec{k}'_{as})$ are excited. The arrows on the solid lines show the decay of incident wave into electron plasma mode (ω'_e, \vec{k}'_e) and stokes mode (ω'_s, \vec{k}'_s) and the arrows on the broken lines arrows show the production anti-stokes mode.

When $\omega' \gg k'_e v_e$, the electron plasma mode is well defined and weakly damped. In this case using $\omega' = \omega'_e + i\Gamma'_{SRS}$ and the asymptotic form of χ'_e , we find from equation (3.35), with $D_+ \neq 0$ (Drake et al. 1974; Liu and Kaw 1976),

$$\Gamma'_{SRS} = -\frac{1}{2}(\Gamma'_e + \Gamma'_s) \pm \frac{1}{2} \left[(\Gamma'_e - \Gamma'_s)^2 + 4 \frac{v_e'^2}{c^2} \sin^2(\psi'_s) \cos^2(\theta'_e) \omega'_i \omega'_{pe} \right]^{\frac{1}{2}}. \quad (3.40)$$

This is the expression for the growth rate of the stimulated Raman scattering of an electromagnetic wave in a plasma. Here we have introduced $\Gamma'_s = (\omega'_{pe}/\omega'_s)^2 \nu'_{ei}/2$ to denote the collisional damping rate of the scattered electromagnetic wave (ω'_s, \vec{k}'_s) .

In equation (3.40), Γ'_e is the damping rate of electron plasma mode,

$$\Gamma'_e = \frac{\sqrt{\pi}}{2} \frac{\omega_{pe}}{(k'\lambda'_{De})^3} \exp \left[-\frac{1}{(k'\lambda'_{De})^2} - \frac{3}{2} \right] + \nu'_{ei}. \quad (3.41)$$

Here, we have introduced $\nu'_{ei} = 4\pi n'_e e^4 \ln \Lambda / m_e'^2 v_e^3$ and $\ln \Lambda \approx 10$ is the Coulomb logarithm [see sections (A) and (D) in appendix], to denote the collisional damping rate of electron plasma mode, where v_e is the electron thermal velocity.

In equation (3.40), θ'_e is the angle between \vec{k}'_i and \vec{k}'_e , and ψ'_s the angle between \vec{E}'_i and \vec{E}'_s . The growth rate is a maximum when the scattered wave has the same polarization as the incident wave ($\psi'_s = 0$).

The threshold condition for SRS can be obtained by setting $\Gamma'_{SRS} = 0$ in equation (3.40)

$$\left(\frac{v'_i}{c} \right)^2 = \frac{\Gamma'_e \Gamma'_s}{\omega'_i \omega_{pe} \sin^2(\psi'_s) \cos^2(\theta'_e)}. \quad (3.42)$$

Using flux $S' = c |\vec{E}'_i|^2 / 8\pi$ and $v_i = c |\vec{E}'_i| / m'_e \omega'_i$, we get

$$S' = \frac{c}{8\pi} \left(\frac{m'_e \omega'_i v'_i}{e} \right)^2 \quad (3.43)$$

Now, from equations (3.42) and (3.43), we obtain the threshold flux required for the excitation of SRS

$$S_{thr} = \frac{c^3}{8\pi} \left(\frac{m'_e}{e} \right)^2 \frac{\omega'_i}{\omega_{pe}} \frac{\Gamma'_e \Gamma'_s}{\sin^2(\psi'_s) \cos^2(\theta'_e)}. \quad (3.44)$$

We now look for electron plasma modes with frequency $\omega' \approx k'_e v_e$. In this region, the large argument expansion of electron susceptibility is not valid. Here $k'_e \lambda'_{De} \geq 0.4$, hence the electron plasma mode in this domain is heavily Landau damped. The growth rate for SCS derived from equation (3.35) is given by:

$$\Gamma'_{SCS} = -2 \frac{v_i'^2}{c^2} \sin^2(\psi'_s) \cos^2(\theta'_e) \omega'_i \text{Im} \left(\frac{\chi'_e}{1 + \chi'_e} \right) - \Gamma'_s. \quad (3.45)$$

The threshold for SCS can be obtained by setting $\Gamma'_{SCS} = 0$.

3.2.4 Numerical solution of equation (3.35)

When $\omega'_e \approx \omega_{pe} \leq k'_e v_e$ or $k'_e \lambda'_{De} \approx 0.4$, it is not possible to expand $\chi'_e(\omega', k')$ into an asymptotic series. Therefore, using $\omega' = \omega'_e + i\Gamma'$, we numerically solve equation (3.35) including all the damping effects. If we separate the real and imaginary parts of equation (3.35) we get two coupled equations. To find ω'_e and Γ' , we solve these two equations with the plasma dispersion function (see equation 3.38) and its relation with the error function. We have to find the value of k'_e such that it satisfies equations (3.19), (3.20), (3.21), (3.22), (3.23) and $D_- \approx 0$.

We assume a power-law spatial variation along the path of the beam for electron density n_e , Lorentz factor γ , pump frequency ν'_i and pump flux f_{ν_i} , to calculate the growth rate Γ' and the scattered flux f_{ν_s} [equation (3.63)]. We find the following power laws give a fairly good agreement with the observed spectrum in the case of 3C 273. The density of relativistic electron beam follows the power-law given by:

$$n_e = n_o \left(\frac{r}{r_o} \right)^{-3.2}, \quad (3.46)$$

where $n_o = 9.24 \times 10^{17} \text{ cm}^{-3}$ and $r_o = 10R_s$ for a black hole of mass $M = 10^8 M_\odot$. In the beam frame, an electron density is given by $n'_e = n_e/\gamma$. The frequency and flux of the soft photon field are assumed to follow the power laws given by:

$$\nu_i = \nu_o \left(\frac{r}{r_o} \right)^{-1}, \quad (3.47)$$

where $\nu_o = 4 \times 10^{10} \text{ Hz}$ and

$$f_{\nu_i} = f_o \left(\frac{\nu_i}{\nu_o} \right)^{-0.1}, \quad (3.48)$$

where $f_o = 7.1 \times 10^{-25} \text{ erg cm}^{-2} \text{ sec}^{-1} \text{ Hz}^{-1}$. Thus we study the scattering of this low-frequency ($\nu_i = \omega_i/2\pi$) wave with the beam electrons through the processes SRS and SCS. Here we find that even though $\omega_i < \omega_{pe}$, $\omega'_i > \omega_{pe}$ for $\hat{k}'_i = -\hat{z}'$.

Therefore it suffices to take $\omega_i \leq \omega_{pe}$ for $\gamma > 1$ for the present calculations. The radiation field which is isotropic in the laboratory frame becomes beamed in a direction opposite to beam velocity in the beam frame. In the beam frame, the component of flux vector of the pump drawn antiparallel ($-\hat{z}'$) to beam velocity becomes much stronger than the perpendicular component. The tips of electric field \vec{E}'_i and magnetic field \vec{B}'_i lie in a ring of angular width $\approx 1/\gamma$ perpendicular to the beam velocity. Any anisotropy in the radiation field in the laboratory frame becomes magnified in the beam frame. The power-law for the Lorentz factor is assumed to be:

$$\gamma = \gamma_o \left(\frac{r}{r_o} \right)^{-1.2}, \quad (3.49)$$

where $\gamma_o = 3 \times 10^3$. We observe that in the beam frame the plasma expands uniformly with the density proportional to r^{-2} . The spread in energy of the beam $\Delta\gamma/\gamma$ is assumed to remain constant throughout its path. Also, we assume the scattered radiation has the same polarization as the incident radiation ($\psi'_s = 0$).

3.2.5 Limiting gain and output power

The scattered radiation fields \vec{E}'_s and \vec{B}'_s become large as the instability progresses. At the critical frequency (see equation 3.34) the Lorentz force $\vec{v}'_i \times \vec{B}'_s$ begins to act on the electrons. The associated electric potential traps the beam electrons which results in an increase in their thermal spread. The trapping potential ϕ'_t , due to the Lorentz force $\vec{v}'_i \times \vec{B}'_s$, in the beam frame, is obtained from

$$\left| \frac{\partial \phi'_t}{\partial z'} \right| = |k'_e \phi'_t| \approx \frac{1}{c} |v'_i B'_s| \quad (3.50)$$

so that

$$\phi'_t = \frac{1}{k'_e} \frac{|v'_i|}{c} |B'_s|. \quad (3.51)$$

The effective thermal speed v_e^{eff} due to the trapping potential is

$$v_e^{eff} = (2e\phi'_t/m_e)^{1/2}. \quad (3.52)$$

The growth rate of the instability reaches a maximum ($\Gamma' = \Gamma'_m$) at the critical frequency (equation 3.34) when $k'_e = \omega_{pe}/v_e^{eff}$ (see Fig. 3.7) because for $v_e^{eff} \geq \omega_{pe}/k'_e$ Landau damping begins to play a dominant role and the gain changes from Raman to Compton. The scattered radiation magnetic field, at the critical frequency, is found by substituting for $v_e^{eff} \approx \omega_{pe}/k'_e$ in equation (3.52) and using equation (3.51):

$$B'_{sm} = \left(\frac{m_e}{2e}\right) \frac{c}{v'_i} \frac{\omega_{pe}^2}{k'_e}. \quad (3.53)$$

The growth of the scattered radiation magnetic field B'_s is governed by the equation:

$$\frac{dB'_s}{dt'} = \Gamma' B'_s, \quad (3.54)$$

where Γ' is the growth rate in the beam frame. Integrating equation (3.54), we get

$$B'_s(t') = C_1 \exp[\Gamma' t']. \quad (3.55)$$

The flux vector of the scattered radiation in the beam frame is

$$\vec{S}' = \frac{c}{4\pi} (\vec{E}'_s \times \vec{B}'_s). \quad (3.56)$$

At $\Gamma' = \Gamma'_m$, $B'_s = B'_{sm}$. We find the flux emitted during the characteristic time $t' = 1/\Gamma'_m$, chosen as the saturation time for instability. Using equation (3.55), equation (3.56) can be written as:

$$\vec{S}' = \frac{c}{4\pi} B'^2_{sm} \exp \left[2 \left(\frac{\Gamma'}{\Gamma'_m} - 1 \right) \right] \hat{k}'_s. \quad (3.57)$$

To transfer flux to the laboratory frame, first we resolve \vec{E}'_s and \vec{B}'_s into components $\vec{E}'_{s\parallel}$ and $\vec{B}'_{s\parallel}$ parallel, and $\vec{B}'_{s\perp}$ and $\vec{E}'_{s\perp}$, perpendicular to \hat{z}' . Now, the flux in the laboratory frame is given by:

$$\vec{S}_{\parallel} = \frac{c}{4\pi} \gamma^2 \left[\left(1 + \frac{v_b^2}{c^2}\right) \frac{B'_{s\perp} E'_{s\perp}}{v_b} + \frac{E'^2_{s\perp} + B'^2_{s\perp}}{c} \right] \vec{v}_b \quad (3.58)$$

$$\vec{S}_{\perp} = -\frac{c}{4\pi} \gamma \left[\left(\frac{E'_{s\perp}}{B'_{s\perp}} + \frac{v_b}{c}\right) B'_{s\parallel} \vec{B}'_{s\perp} + \left(\frac{B'_{s\perp}}{E'_{s\perp}} + \frac{v_b}{c}\right) E'_{s\parallel} \vec{E}'_{s\perp} \right] \quad (3.59)$$

Taking \vec{E}'_s , \vec{E}'_i along \hat{x}' , the components of \vec{E}'_s and \vec{B}'_s are given by:

$$\begin{aligned} \vec{B}'_{s\perp} &= -B'_s \cos(\phi'_s) \hat{y}', & \vec{E}'_{s\perp} &= E'_s \hat{x}', \\ \vec{B}'_{s\parallel} &= -B'_s \sin(\phi'_s) \hat{z}', & \vec{E}'_{s\parallel} &= 0, \end{aligned} \quad (3.60)$$

where $\phi'_s = \cos^{-1}(\hat{k}'_i \cdot \hat{k}'_s)$. Now, the components of the flux vector in the laboratory frame are given by:

$$\vec{S}_{\parallel} = \frac{c}{4\pi} \gamma^2 B'^2_{sm} \exp \left\{ 2 \left(\frac{\Gamma'}{\Gamma'_m} - 1 \right) \right\} \left[\left\{ 1 + \cos^2(\phi'_s) \right\} \frac{v_b}{c} - \left(1 + \frac{v_b^2}{c^2} \right) \cos(\phi'_s) \right] \hat{z}', \quad (3.61)$$

$$\vec{S}_{\perp} = \frac{c}{4\pi} \gamma B'^2_{sm} \exp \left\{ 2 \left(\frac{\Gamma'}{\Gamma'_m} - 1 \right) \right\} \left[1 - \frac{v_b}{c} \cos(\phi'_s) \right] \sin(\phi'_s) \hat{y}'. \quad (3.62)$$

If the pump field strength is increased it produces a spread in the beam velocity due to radiation pressure, consequently it decreases the scattered power even though the growth rate increases. The component \vec{S}_{\parallel} is much stronger than \vec{S}_{\perp} because it is proportional to γ^2 , while the latter is proportional to γ . The scattered radiation gains its energy from the relativistic electron beam. Consequently, the electron beam gets decelerated due to the interaction with the pump. The emitted radiation is beamed and confined to a cone of angular radius $\approx 1/\gamma$. The scattered radiation flux, at the observer, is given by:

$$f_{\nu_s} = \frac{1}{2} \left(\frac{R_b}{R_e} \right)^2 \frac{S}{\nu_s}, \quad (3.63)$$

where $S = [S_{\parallel}^2 + S_{\perp}^2]^{1/2}$, $\Delta\theta$ the angular radius of the beam, $R_b = r \tan(\Delta\theta)$ the radius of the beam at a distance of $r \geq 10R_s$ from the central engine and $R_e = 7.9 \times 10^8$ pc is the distance between quasar 3C 273 and the Earth. Using the observed value of the flux of 3C 273 at 10^{18} Hz, we fix $\Delta\theta = 0.0065^\circ$. We calculate the scattered flux at other frequencies using the spatial variation of plasma parameters as discussed earlier. Thus R_b increases as r increases for constant $\Delta\theta$ at all frequencies.

3.3 DISCUSSION

Figs. 3.4 and 3.5 show the conditions for SRS and SCS.

The quantity $k'_e \lambda'_{De}$ is related to the frequency of the incident radiation via phase matching conditions:

$$k'_e \lambda'_{De} \approx 2 \frac{\lambda'_{De}}{c} \sqrt{4\pi^2 \nu_i'^2 - \omega_{pe}^2}. \quad (3.64)$$

In Fig. 3.6, we have plotted $k'_e \lambda'_{De}$ [equation (3.64)] as a function of the frequency ν_i of the incident radiation. For plasma parameters indicated on the figure, we find that in the range $\nu_i \geq \omega_{pe}/\pi$, $k'_e \lambda'_{De} \leq 0.4$. In this regime, electrons show the collective behavior and the excited electron mode is weakly damped, because its phase velocity is much larger than the thermal velocity of the electrons. Here the scattering of the electromagnetic radiation off the electron plasma mode occurs due to SRS.

For $\nu_i \gg \omega_{pe}/\pi$, we find $k'_e \lambda'_{De} > 0.4$. Therefore the phase velocity of the electron plasma mode becomes comparable to the thermal velocity of the electrons. This leads to large Landau damping and hence the electrons lose their collective behavior. In this case, scattering of the electromagnetic radiation occurs due to a highly damped electron plasma mode and this process is called the SCS process.

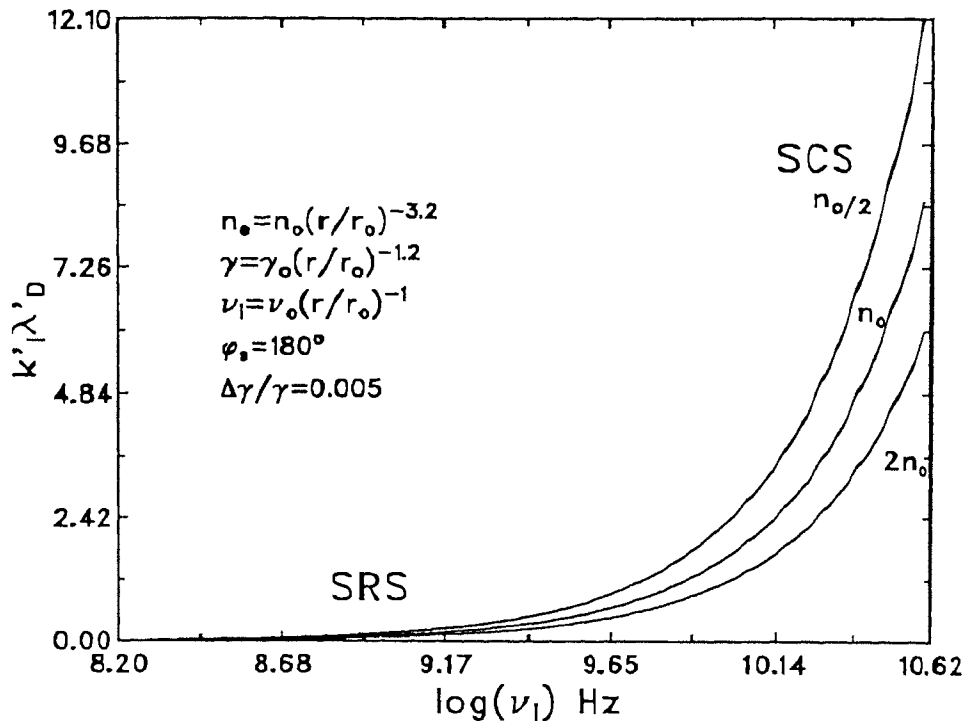


Fig. 3.6 The quantity $k'_e \lambda'_{De}$ versus the frequency of the incident wave ν_i for three different densities. At $k'_e \lambda'_{De} \leq 0.4$, SRS occurs and at $k'_e \lambda'_{De} > 0.4$, SCS occurs. The constants are: $\gamma_o = 3 \times 10^3$, $n_o = 9.24 \times 10^{17} \text{ cm}^{-3}$, $\nu_o = 4 \times 10^{10} \text{ Hz}$.

There are three curves in Fig. 3.6 for three values of initial electron density: n_o , $n_o/2$ and $2n_o$. At higher density ($2n_o$), since $k'_e \lambda'_{De}$ approaches 0.4 at higher ν_i ($= 10^{9.65} \text{ Hz}$), SRS extends to higher frequencies, while at lower density ($n_o/2$), $k'_e \lambda'_{De}$ approaches 0.4 at a lower ν_i ($= 10^{9.2} \text{ Hz}$), and SRS occurs over a smaller range of incident frequencies.

Fig. 3.7 shows the growth rate as a function of the frequency ν_s of the backscattered radiation for three different values of initial density: n_o , $n_o/2$ and $2n_o$, using the power law variations of the parameters given on the figure. First, consider the curve labelled with n_o : in the range $10^{10} \leq \nu_s \leq 10^{13.85} \text{ Hz}$, the growth rate of the backscattered electromagnetic radiation increases with ν_s and reaches a maximum at $\nu_s = 10^{13.85} \text{ Hz}$. As ν_s is further increased, electron plasma mode experiences a

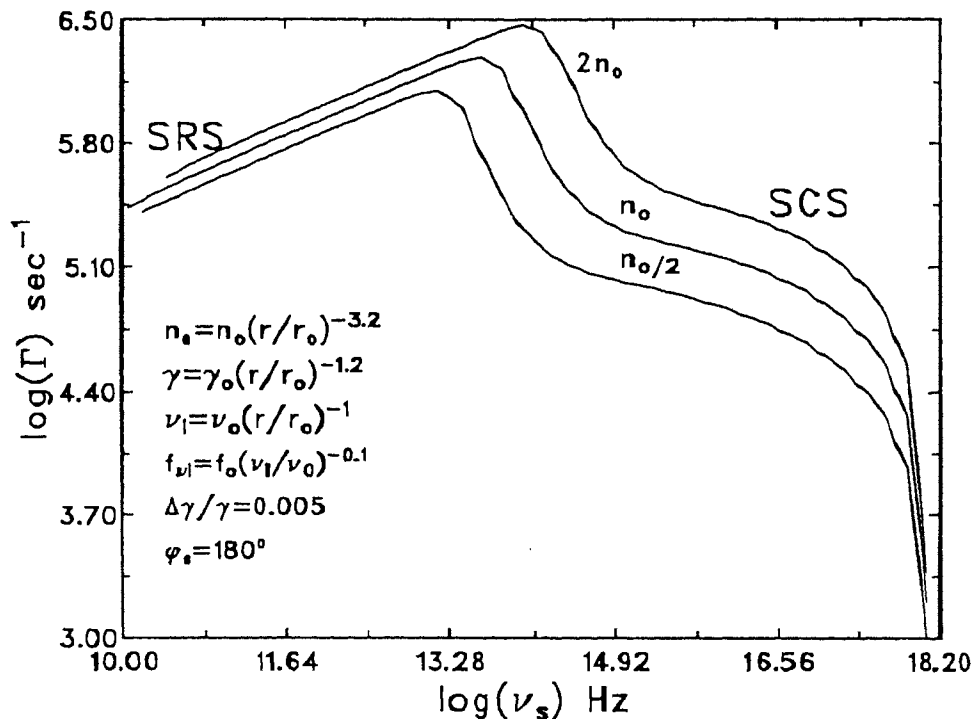


Fig. 3.7 Growth rate Γ versus scattered wave frequency ν_s at three different values of electron density in the laboratory frame. At maxima, the scattering process changes from SRS to SCS. The constants are: $\gamma_o = 3 \times 10^3$, $n_o = 9.24 \times 10^{17} \text{ cm}^{-3}$, $\nu_o = 4 \times 10^{10} \text{ Hz}$ and $f_o = 7.1 \times 10^{-25} \text{ erg cm}^{-2} \text{ sec}^{-1} \text{ Hz}^{-1}$.

large Landau damping in the range $\nu_s \geq 10^{13.85} \text{ Hz}$ and hence the growth rate decreases rapidly with ν_s . For $\nu_s > 10^{17} \text{ Hz}$, which occurs rather in the high-density region, the collisional damping rate of the electron plasma mode becomes large, resulting in a sharp decrease in the growth rate. The frequency of the scattered radiation corresponding to the maximum growth rate, the critical frequency ν_{cr} acquires higher values with an increase in density. The scattered radiation of frequency below ν_{cr} is produced due to the SRS and above ν_{cr} due to SCS.

Fig. 3.8 shows the variation of the growth rate as a function of the incident radiation frequency ν_i for three values of the initial density: n_o , $n_o/2$ and $2n_o$. The variation is found to be qualitatively similar to that shown for Fig. 3.7. However,

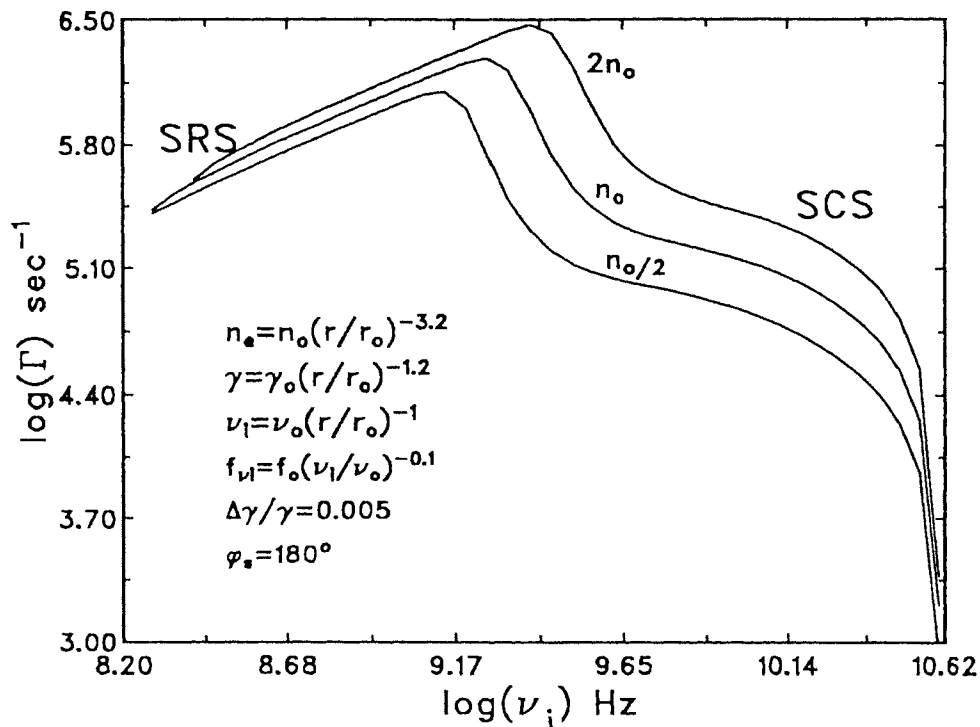


Fig. 3.8 Growth rate Γ versus incident wave frequency ν_i at three different values of electron density in the laboratory frame. At maxima, the scattering process changes from SRS to SCS. The constants are as in Fig. 3.7.

one must note that the bandwidth of the incident radiation ($10^{8.25}\text{Hz} < \nu_i < 10^{10.85}\text{Hz}$) is much narrower.

Fig. 3.9 shows the variation of the growth rate of the backscattered radiation as a function its frequency ν_s for three different values of the energy spread $\Delta\gamma/\gamma = 0.0035, 0.005$ and 0.01 . First consider the curve labeled with $\Delta\gamma/\gamma = 0.005$. In the range $10^{10} \leq \nu_s \leq 10^{13.85}\text{Hz}$, the growth rate increases with frequency due to the increase of pump strength and weak damping, and reaches a maximum at $\nu_s = 10^{13.85}\text{Hz}$. In the range $\nu_s > 10^{13.85}\text{Hz}$, the electron plasma mode experiences a large Landau damping and hence the growth rate decreases. For $\nu_s > 10^{17}\text{Hz}$, due to the large electron density, the collision damping rate becomes large, consequently the growth rate decreases rapidly.

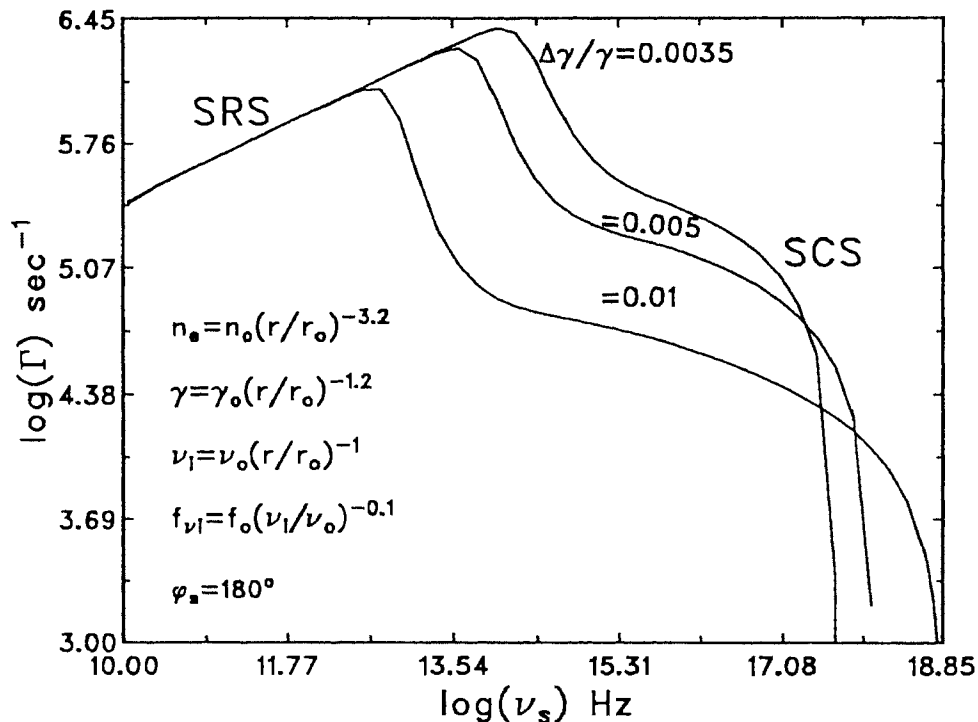


Fig. 3.9 Growth rate Γ versus scattered wave frequency ν_s at three different values of $\Delta\gamma/\gamma$. At maxima, the scattering process changes from SRS to SCS. The constants are as in Fig. 3.7.

At a lower value of $\Delta\gamma/\gamma$ ($=0.0035$), the Landau damping begins to act at a higher frequency, therefore the growth rate peaks at a higher frequency. On the other hand, if $\Delta\gamma/\gamma$ is large ($=0.01$), then Landau damping begins to act at a lower frequency and hence the growth rate peaks at a lower frequency. Hence the critical frequency ν_{cr} shifts to a higher frequency when $\Delta\gamma/\gamma$ is small. Since the collision frequency decreases with the increase of $\Delta\gamma/\gamma$, the growth rate becomes non-zero even up to much higher frequency, i.e., up to $\nu_s > 10^{18}$ Hz. Note that the bandwidth ($10^{8.3}$ Hz $< \nu_i < 10^{10.9}$ Hz) of the incident radiation is much narrower.

Fig. 3.10 shows the growth rate as a function of scattering angle ϕ_s at four different frequencies: $\nu_s = 10^{12}$, 10^{14} , 10^{16} and 10^{17} Hz. Here ϕ_s is the angle between \vec{k}_i and \vec{k}_s . The instability is excited in the range $10^\circ < \phi'_s \leq 180^\circ$, but not in the range $0^\circ \leq \phi'_s < 10^\circ$ because in the latter range k'_e becomes imaginary for the

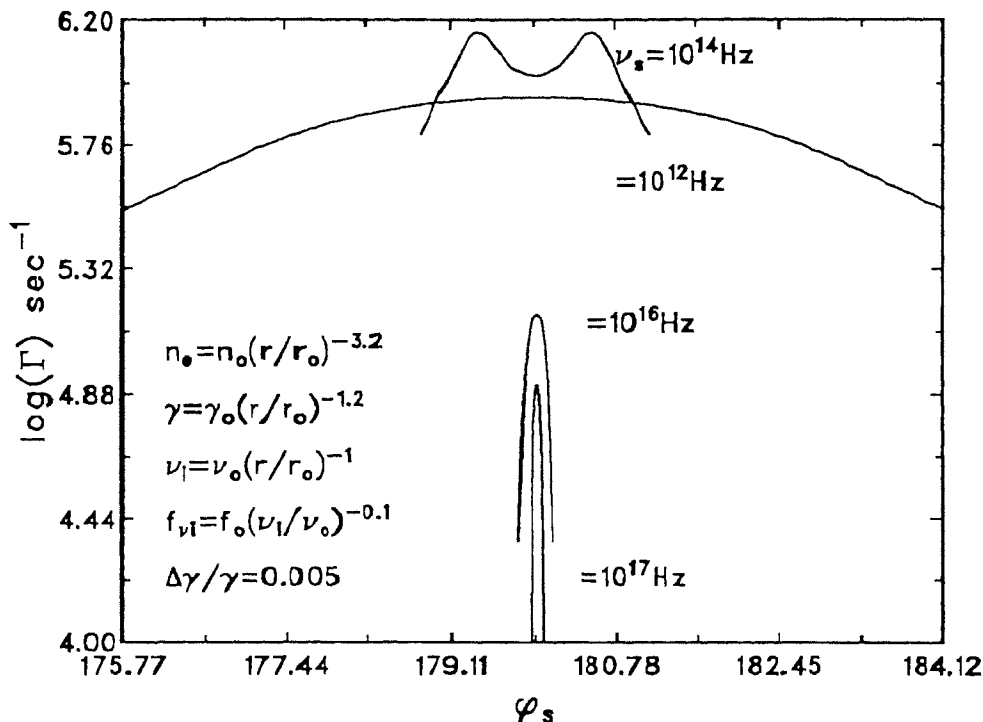


Fig. 3.10 The angular dependence of the growth rate Γ at four values of scattered radiation frequency ν_s in the laboratory frame. The angle ϕ_s is the angle between \vec{k}_i and \vec{k}_s . The constants are as in Fig. 3.7.

plasma parameters given on figure. Due to the Lorentz transformation of ϕ'_s given by:

$$\cos(\phi_s) = \frac{\cos(\phi'_s) + v_b/c}{1 + (v_b/c) \cos(\phi'_s)}, \quad (3.65)$$

ϕ_s , in the laboratory frame, is confined to a narrow angle about the beam axis. The backscattering, ($\phi'_s = 180^\circ$) corresponds to $\theta'_e = 0$, and the growth rate becomes maximum, (see equation 3.40). For $\phi'_s < 180^\circ$, θ'_e increases and hence the growth decreases. At $\nu_s = 10^{14}$ Hz, which is close to the critical frequency, the growth rate peaks at $\phi_s = 179.2^\circ$ and $k'_e \lambda'_{De}$ approaches 0.4. The growth rate peaks for backscattering at all frequencies except when $\nu_s = 10^{14}$ Hz. The strange behavior of the growth rate at $\nu_s = 10^{14}$ Hz reflects the transition in the scattering process.

In Fig. 3.11, the theoretical spectra of the backscattered and the incident radiations are plotted (continuous curves). For comparison we have also shown observed

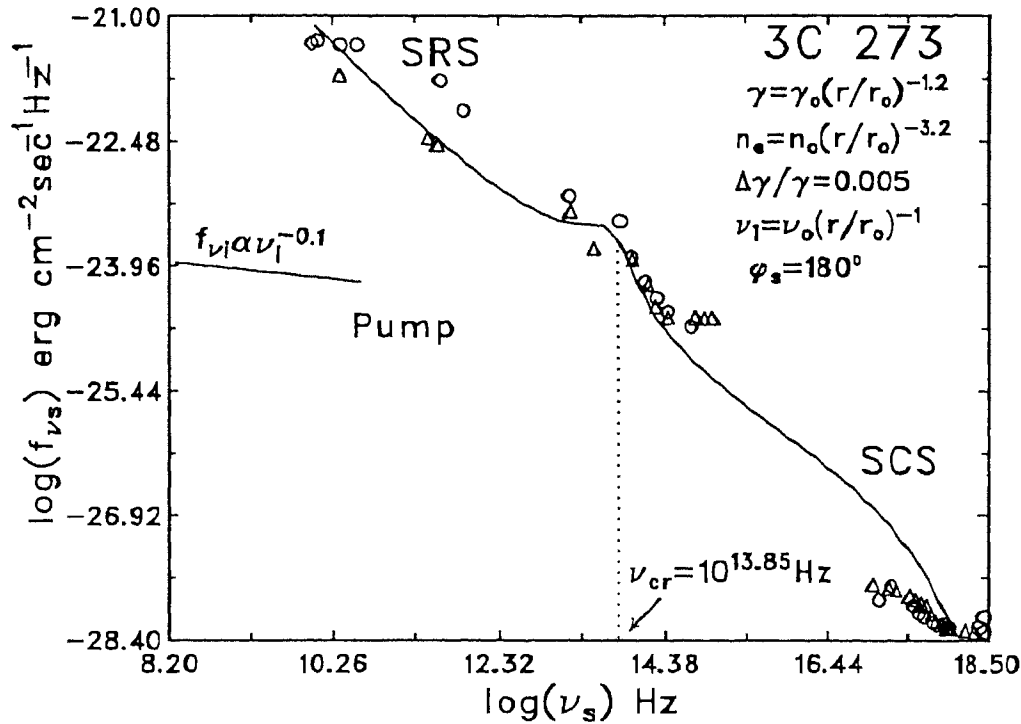


Fig. 3.11 The spectrum of the quasar 3C 273. The solid lines represent the calculated spectrum and the spectrum of the pump wave. The observed points, \circ (February, 1984) and \triangle (February, 1986) by Courvoisier et al. (1987), are also plotted. The constants are as in Fig. 3.7.

points (open circles represent spectrum of 3C 273, when flare activity was occurring during 1984 February and open triangles represent its normal spectrum observed during 1986 February) from the quasi-simultaneous multifrequency observations of Courvoisier et al. (1987). At the critical frequency $\nu_s = 10^{13.85}$ Hz, there is a break in the spectrum due to the change of scattering process from SRS to SCS. The SRS process contributes in the lower frequency part of the spectrum ($\nu_s \leq 10^{13.85}$) Hz, while SCS contributes in the higher energy part. The slope of the spectrum in the SRS region is -0.8 and in the SCS region it is -0.7 . The hard X-ray part of the spectrum is steep, due to collisional damping of electron plasma wave and decreasing growth rate, and the slope of this part is -1.5 . The bump in the spectrum is produced at the transition ($k'_e \lambda'_{De} = 0.4$) between the SRS and SCS regions.

The dependence of the spectrum on the electron beam density is shown in Fig. 3.12, where we have chosen three different values for initial density: n_o , $2n_o$ and $n_o/2$. The region of higher density and lower scattered frequency, corresponds to a weakly damped electron plasma mode and a higher scattered flux f_{ν_s} . The scattered radiation gains its energy from electrons of the relativistic electron beam. Therefore, the scattered flux at higher density is large in comparison with flux generated due to the scattering by a damped electron plasma mode at lower density. Note that at higher density, the SRS region extends to even higher frequencies while at lower density, SCS extends to lower frequencies. However, the entire spectrum can be produced by either SRS or SCS by choosing the density appropriately but without

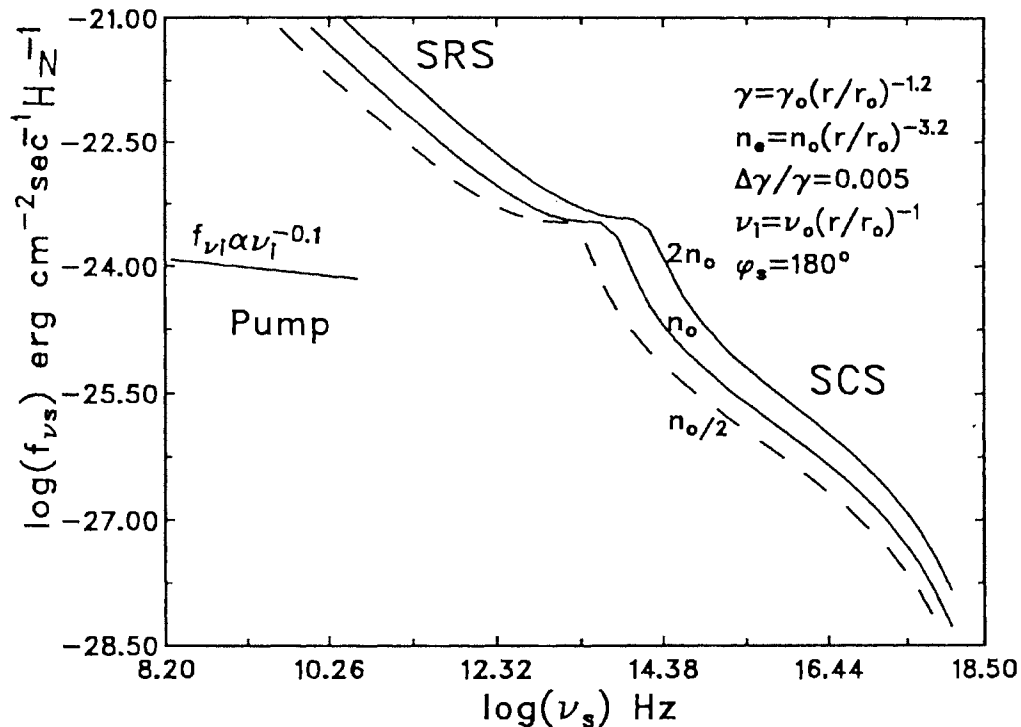


Fig. 3.12 The spectrum of the scattered radiation at three different densities: n_o , $2n_o$ and $n_o/2$. The SRS occurs at lower frequencies and SCS occurs at higher frequencies. In the transition region between the two there is a bump on each curve which shifts towards higher frequencies with an increase in density. The constants are as in Fig. 3.7.

any break in the spectrum. Hence the transition region (bump) between SRS and SCS moves to higher frequencies with an increasing density.

The effect of change in the energy spread $\Delta\gamma/\gamma$ on the spectrum is shown in Fig. 3.13 for various values of $\Delta\gamma/\gamma$, (0.0035, 0.005 and 0.01). The bump between SRS and SCS regions moves towards higher frequencies side with the decrease of $\Delta\gamma/\gamma$, because the damping parameter ($k'_e\lambda'_{De}$) depends on $\Delta\gamma/\gamma$. Though the scattered flux increases with an increase in $\Delta\gamma/\gamma$, the critical frequency decreases. At a lower value of the energy spread, the entire spectrum can be produced by SRS whereas at higher value of the energy spread, the entire spectrum can be produced by SCS. Hence the transition region (bump) between SRS and SCS moves to higher

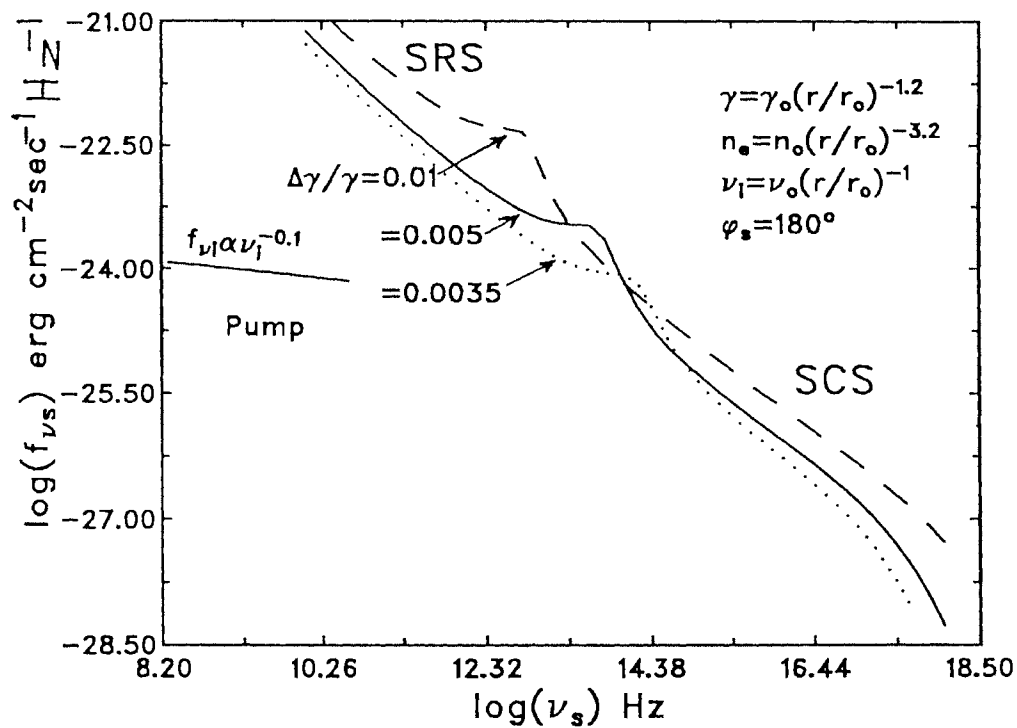


Fig. 3.13 The spectrum of the scattered radiation at three different values of $\Delta\gamma/\gamma$. The SRS occurs at lower frequencies and SCS occurs at higher frequencies. In the transition region between the two there is a bump on each curve which shifts towards higher frequencies with a decrease in $\Delta\gamma/\gamma$. The constants are as in Fig. 3.7.

frequencies with a decrease in the energy spread.

The dependence of the entire spectrum of the scattered radiation on the scattering angle is shown Fig. 3.14 for three different values of the scattering angle $\phi'_s = 180^\circ, 120^\circ$ and 90° . The critical frequency shifts towards lower frequency with decreasing ϕ'_s . The scattered flux as well as the highest scattered frequency decreases with the decrease of ϕ'_s ; see equations (3.6), (3.61) and (3.62).

Fig. 3.15 shows the beamed emission of scattered radiation. As the scattering angle ϕ'_s is varied from 10° to 180° the emitted flux in the laboratory frame remained confined to a cone of angular radius $\approx 1/\gamma$ about the beam axis.

Fig. 3.16 shows the angular distribution of the scattered flux $f_s = \nu_s f_{\nu_s}$. The angular distribution of the scattered flux broadens as the frequency decreases. The flux is higher and narrower at higher frequencies.

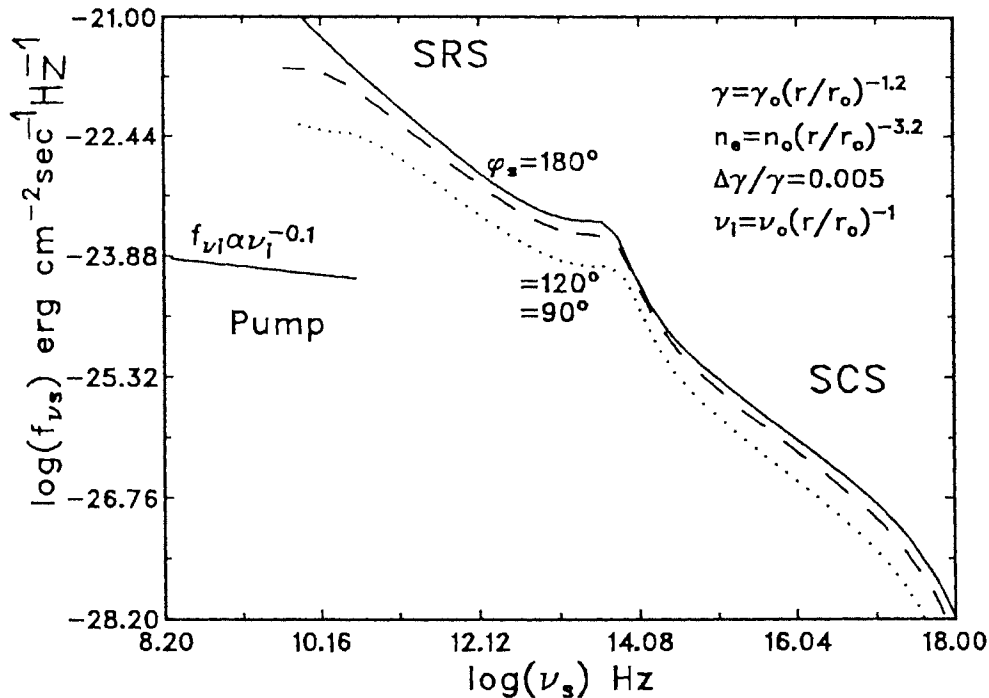


Fig. 3.14 The spectrum of the scattered radiation at three values of scattering angle ϕ_s . The high-frequency end of the spectrum terminates at lower frequency as the scattering angle ϕ_s decreases from 180° to 90° . The constants are as in Fig. 3.7.

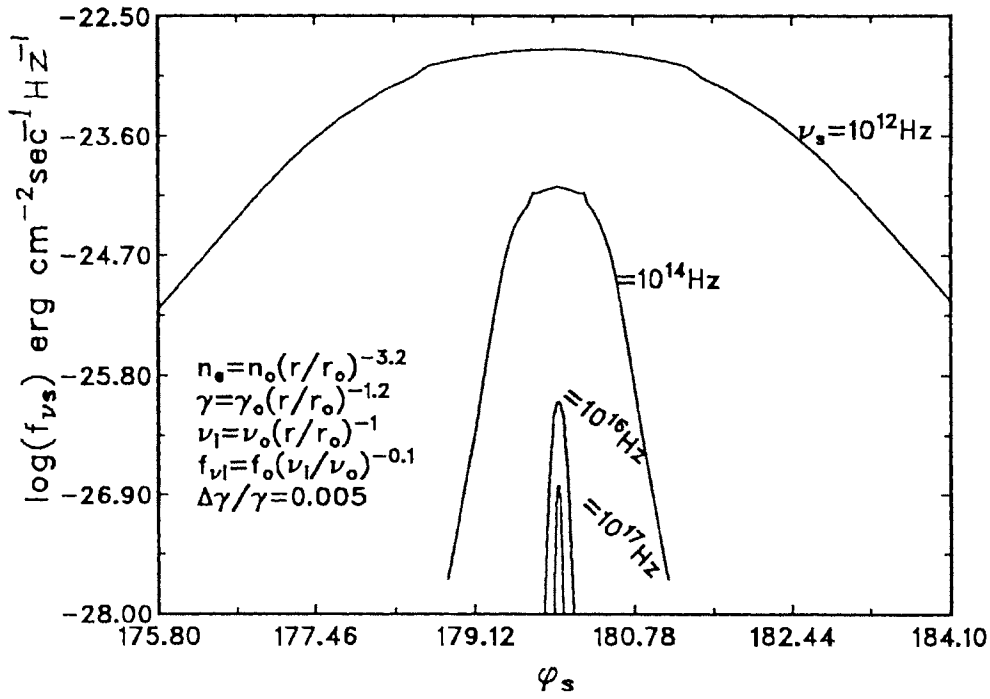


Fig. 3.15 The angular distribution of the scattered radiation flux f_{ν_s} at four scattered radiation frequencies in the laboratory frame. The constants are as in Fig. 3.7.

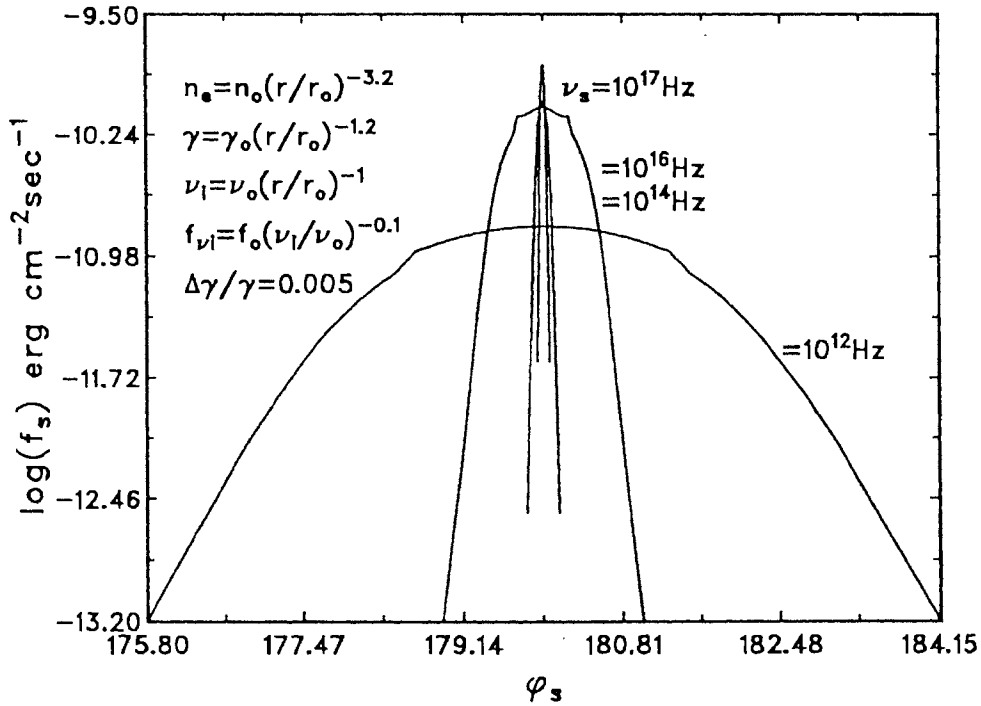


Fig. 3.16 The angular distribution of the scattered radiation flux $f_s = \nu_s f_{\nu_s}$ in the laboratory frame. The constants are as in Fig. 3.7.

3.4 CONCLUSIONS

The conclusions of this chapter can be summarized as follows.

- (i) Compared to Compton scattering, Raman scattering is a faster process.
- (ii) At higher plasma density n_e and lower energy spread $\Delta\gamma/\gamma$, Raman scattering can produce the entire continuum radiation right from radio to X-rays.
- (iii) Similarly, at lower density and higher energy spread $\Delta\gamma/\gamma$, Compton scattering can produce the entire continuum radiation right from radio to X-rays.
- (iv) For the parameters chosen here, the transition region between SRS and SCS lies where the bump is observed for 3C 273. Thus, we suggest the change of scattering process as one of the possible causes for the spectral break observed in the most of the quasars and AGN.
- (v) Raman scattering occurs in a region of density greater than or equal to one quarter of the critical density ($\omega'_i \geq 2\omega_{pe}$).
- (vi) An electron beam gets decelerated much faster due to Raman scattering than due to Compton scattering.
- (vii) The beamed, stimulated Raman or Compton emission can be detected at a small angle to the electron beam axis. The higher frequency radiation is produced in a narrower angular region around the electron beam axis than the lower frequency radiation.
- (viii) As we see, the scattering processes also bring about the polarization changes, which we have studied in Chapter 5.

References

- Beal, J. H., 1990, in *Physical processes in hot cosmic plasmas*, eds. W. Brinkmann et al., Kluwer, Dordrecht, p 341.
- Begelman, M. C., & Sikora, M., 1987, *Astrophys. J.*, **322**, 650.
- Begelman, M. C., 1988, in *Active Galactic Nuclei*, eds. H. R Miller & P.J Wiita, Springer Verlag, Heidelberg, p 202.
- Baker, D. N., Borovsky, J. E., Benford, G., & Eilek, J. A., 1988, *Astrophys. J.*, **326**, 110.
- Benford, G., 1992, *Astrophys. J.*, **391**, L 59.
- Blandford, R. D., & Payne, P. G., 1982, *Mon. Not. R. astr. S.*, **199**, 883.
- Courvoisier, T. J. -L., Turner, M. J. L., Robson, E. I, Gear, W. K., Staubert, R., Blecha, A., Bouchet, P., Falomo, R., Valtonen, M., & Teräsanta, H., 1987, *Astr. Astrophys.*, **176**, 197.
- Drake, J. F., Kaw, P. K., Lee, Y. C., Schmidt, G., Liu, C.S. & Rosenbluth, M. N., 1974, *Phy. Fluids.*, **17**, 778.
- Fried, D., & Conte, S. D., 1961, *The Plasma Dispersion Function*, Academic Press, New York.
- Gangadhara, R. T., & Krishan, V., 1990, *J. Astrophys. Astr.*, **11**, 515.
- Gangadhara, R.T. & Krishan, V., 1992, *Mon. Not. R. astr. Soc.*, **256**, 111.
- Hasegawa, A., 1978, *Bell System Tech. J.*, **57**, 3069.
- Krishan, V., 1983, *Astrophys. Lett.*, **23**, 133.
- Krishan, V., 1985, *Astrophys. Space Sci.*, **115**, 119.

- Krishan, V., 1987, *Mon. Not. R. astr. Soc.*, **226**, 629.
- Krishan, V., 1988a, *Mon. Not. R. astr. Soc.*, **230**, 183.
- Krishan, V., 1988b, *Mon. Not. R. astr. Soc.*, **231**, 353.
- Krishan, V., & Wiita, P. J., 1986, in IAU symp. No.199 on *Quasars*, Eds. G. Swarup & V. K. Kapahi, Reidel, Dordrecht, p 419.
- Krishan, V., & Wiita, P. J., 1990, *Mon. Not. R. astr. S.*, **246**, 597.
- Lesch, H., Schlickeiser, R., & Crusius, A., 1988, *Astr. Astrophysics.*, **200**, L 9.
- Liu, C. S. & Kaw, P. K., 1976, *Advances in plasma physics*, eds. A. Simon, & B. Thompson, **6**, 83.
- Lovelace, R. V. E., 1976, *Nature*, **262**, 649.
- Melia, F., & Königl, A., 1989, *Astrophys. J.*, **340**, 162.
- Rees, M. J., 1984, in IAU Symposium 110 on *VLBI and Compact Radio Sources*, ed. R. Fanti Kellermann, & G. Setti, Reidel, Dordrecht, p 207.
- Stein, W. A., 1988, in *Active Galactic Nuclei*, Eds. H. R Miller & P. J. Wiita, Springer Verlag, Heidelberg, p 202.
- Stein, W. A., & O'Dell, S. L., 1985, in *Astrophysics of Active Galaxies and Quasi-Stellar objects*, Eds. J. S Miller University Science Books, Mill Valley, p 381.
- Wiita, P. J., 1985, *Phy. Repts*, **123**, 117.
- Wiita, P. J., Kapahi, V. K., & Saikia, D. J., 1982, *Bull. Astr. Soc. India*, **10**, 304.

Chapter 4

ANOMALOUS ABSORPTION OF RADIATION IN ASTROPHYSICAL PLASMAS

In this Chapter, coherent plasma processes such as parametric decay instabilities (PDI) have been studied in a homogeneous and unmagnetized plasma. These instabilities cause anomalous absorption of intense electromagnetic radiation under specific conditions of energy and momentum conservation and thus cause anomalous heating of the plasma. The maximum plasma temperatures reached are functions of luminosity of the radio radiation and plasma parameters. It is believed that these processes may be taking place in many astrophysical objects. Here, the conditions in the sources 3C 273, 3C 48 and Crab Nebula are shown to be conducive to the excitation of parametric decay instabilities. These processes also contribute towards the absorption of 21-cm radiation.

4.1 INTRODUCTION

One of the fundamental processes in the interaction of intense electromagnetic radiation, of frequency close to the electron plasma frequency, with fully ionized plasmas is the parametric excitation of two new waves. If both the excited modes are purely electrostatic, they are eventually absorbed in the plasma due to collisional and Landau (wave-particle interaction) dampings. In a plasma, waves and the particles exchange energy. If the phase velocity v_p of a wave lies in the region of positive velocity gradient of the particle velocity distribution, i.e., if $\partial f/\partial v > 0$ for $v = v_p$, the waves gain energy from the particles. If, on the other hand, $\partial f/\partial v < 0$ for $v = v_p$, the waves lose energy to the particles and are said to suffer Landau damping [see section (B) in appendix]. When the wave dissipates, its energy gets converted into thermal energy of particles. The incident electromagnetic radiation is anomalously absorbed in the plasma at a rate which is much larger than the collisional absorption rate [see section (D) in appendix].

Quasars, Seyfert galaxies and pulsars are among the most luminous objects in the universe, emitting strongly at radio frequencies. Krolik, McKee and Tarter (1978) have shown that the radio frequency waves can heat the plasma through free-free absorption process. Here we study parametric decay instabilities in 3C 273, 3C 48 and the Crab Nebula and calculate the anomalous absorption rate of their radio radiation in the surrounding plasma. The excitation of parametric decay instabilities in the emission-line regions of quasar was first discussed by Krishan (1987) and then by Gangadhara and Krishan (1989, 1990, 1991), to include the new effects associated with strong and broad pump in the three astrophysical objects mentioned above.

4.1.1 Density and temperature structure of broad line region of active galactic nuclei

The emission line regions of Active Galactic Nuclei (AGN) are commonly separated into a 'narrow line region' (NLR) and a 'broad line region' (BLR). These regions consist of photoionized 'clouds' moving with large velocities, usually assumed to be embedded in a hot dilute medium providing confinement. It has been recognized for a long time that the intense thermal and/or non-thermal ultra-violet and X-ray radiation emitted by AGN is responsible for heating and ionizing the line-emitting regions. The density structure of the BLR is closely related to the ionization structure (Kwan and Krolik, 1981). The density deduced in the models has gradually increased from 10^7 cm^{-3} up to 10^{11} cm^{-3} , a value which is now commonly assumed. The absence of broad components in the forbidden lines is interpreted as due to collisional de-excitation, so that the electron density must be greater than 10^7 cm^{-3} . On the other hand the presence of the broad semi-forbidden CIII] $\lambda 1909$ line which starts being de-excited at $n_e > 10^9 \text{ cm}^{-3}$ implies $n_e < 10^{10} \text{ cm}^{-3}$. Larger densities are however, indicated by some line intensities like those of FeII. The high-ionization zone (HII), facing the central source of ionizing radiation, emits what we call the high-ionization lines (HIL) L_α , NV, CIV, HeII, CIII], etc. The temperature of HII zone varies between about 15,000 K and 25,000 K according to the values of the density and of the ionization parameter. The BLR has a dimension of 0.01–1 parsec, and clouds have electron densities 10^9 – 10^{10} cm^{-3} and temperatures 1.5×10^4 – 2.5×10^4 K (Collin-Souffrin and Lasota 1988). The BLR is very close to the active nucleus and therefore is an important diagnostic of the central region of AGN.

Davidson and Netzer (1979) have reviewed some of the heating processes proposed by several workers, which are (1) ionization by ultra-violet photons, (2) ex-

citations and ionizations by energetic non-thermal particles via , (3) shock waves dissipation, and (4) free-free (bremsstrahlung) absorption of radio waves. Here, we propose the absorption of radio waves and hence the heating of line-emitting regions due to collective plasma processes such as parametric decay instability driven by intense radio radiation.

4.1.2 The density and the temperature structure of the Crab Nebula

Ginzburg and Ozernoy (1966) considered the simplest plasma mechanism in which radio-wave emission Crab Nebula occurs at frequencies $\nu \sim \nu_{pe}$, where $\nu_{pe} = \omega_{pe}/2\pi$ is the plasma frequency. This means that the following inequality is assumed to hold

$$\omega \sim \omega_{pe} \gg \omega_{II} = \frac{eH}{m_e c} = 1.76 \times 10^7 \text{ Hz},$$

and hence it should be sufficient to analyze only in isotropic plasma. Plasma waves of frequency ω_{pe} change into transverse waves as a result of ‘interaction’ between the normal waves in the inhomogeneous medium and scattering on concentration fluctuations (Ginzberg and Zheleznyakov 1959; Wild, Smerd and Weiss 1963; Zheleznyakov 1964; Ginzburg 1964).

For the ‘compact’ Crab radio source whose radius does not exceed $r \sim 10^{15}$ cm (see Hewish and Okoye 1965) the observed frequency band lies between 2.5×10^7 and 4×10^7 Hz (Hewish and Okoye 1965; Andrew, Branson and Wills 1964) which for $\nu \sim \nu_{pe}$ correspond to a electron density $n \sim 10^7 - 10^8 \text{ cm}^{-3}$, with $T_e \sim 10^4 - 10^6$ K.

4.1.3 The radio source

Most of the radio emission in quasars is believed to originate in accretion disks and also in regions interior to BLR. The radio flux f_ν at 1400 MHz in 3C 273 is 46.4 Jansky and in 3C 48 it is 15.63 Jansky (Lang 1980). The redshift of 3C 273

is $z = 0.158$ and that of 3C 48 is $z = 0.367$. We find the distance ‘ d ’ between an observer and a quasar using the Hubble distance-redshift relation $d = 5000z$ Mpc. The luminosity of 3C 48 and that of 3C 273 at 1400 MHz, determined by using the relation $L_\nu = 4\pi d^2 f_\nu$, are 5.95×10^{34} erg sec $^{-1}$ Hz $^{-1}$ and 3.28×10^{34} erg sec $^{-1}$ Hz $^{-1}$, respectively.

The total luminosity of the Crab Nebula is 10^{38} erg sec $^{-1}$, twelve percent of which is in the radio band (Lyne and Graham-Smith 1990).

4.2 PARAMETRIC DECAY INSTABILITY (PDI)

Consider a large amplitude plane polarized electromagnetic pump wave

$$\vec{E}_o = \frac{1}{2} \left(E_o e^{i(\vec{k}_o \cdot \vec{r} - \omega_o t)} \hat{e} + cc \right) \quad (4.1)$$

propagating in a homogeneous plasma, where cc is the complex conjugate. In a plasma medium electromagnetic wave (\vec{k}_o, ω_o) satisfies the usual non-relativistic dispersion relation,

$$\omega_o^2 = \omega_{pe}^2 + k_o^2 c^2, \quad (4.2)$$

when the oscillation velocity $v_o (= eE_o/m_e \omega_o)$ of electrons is much smaller than the velocity of light c .

The incident electromagnetic wave (pump) with frequency close to the electron plasma frequency, resonantly excites a high-frequency electron plasma wave (\vec{k}_e, ω_e) and a low-frequency ion plasma wave (\vec{k}_i, ω_i) , (see Fig. 4.1), when the following frequency and wave number matching conditions are satisfied:

$$\omega_o = \omega_e + \omega_i, \quad \vec{k}_o = \vec{k}_e + \vec{k}_i, \quad (4.3)$$

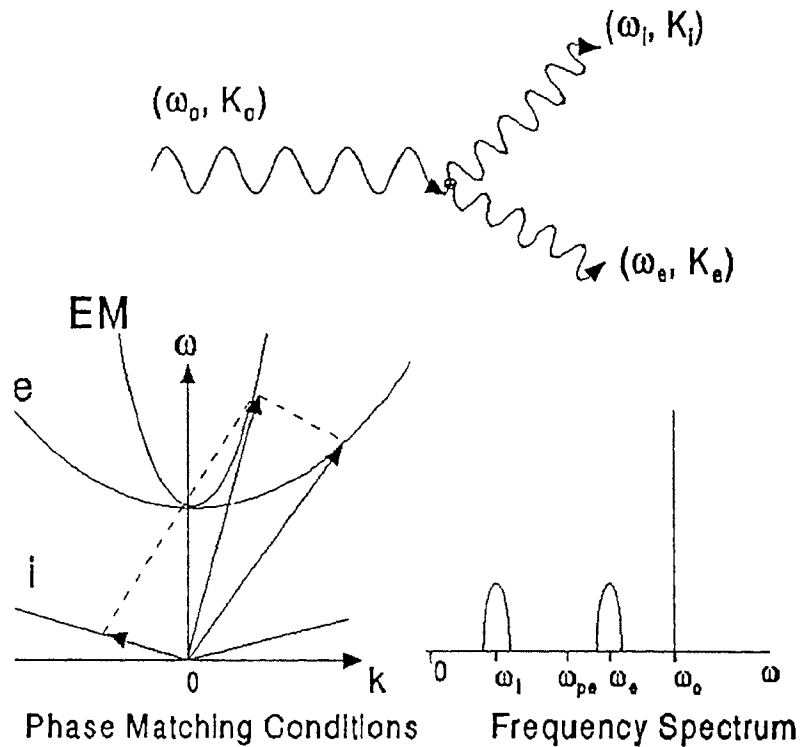


Fig. 4.1 Parametric decay instability.

where

$$\omega_e^2 = \omega_{pe}^2 + \frac{3}{2}k^2v_e^2 \quad (4.4)$$

and

$$\omega_i^2 = \frac{\omega_{pi}^2}{1 + (k\lambda_{De})^{-2}} \quad (4.5)$$

are the resonant dispersion relations of the electron plasma wave and the ion plasma wave, respectively [see section (A) in appendix]. The parameters $\omega_{pj} = (4\pi n_j e^2/m_j)^{1/2}$, $v_j = (2k_B T_j/m_j)^{1/2}$ and $\lambda_{Dj} = (k_B T_j/4\pi n_j e^2)^{1/2}$ are the plasma angular frequency, thermal velocity and Debye length of species j ($=e$ for electrons and i for ions), respectively. Here k_B is the Boltzmann constant. The density, mass and temperature of the species j are n_j , m_j and T_j , respectively.

For $\omega_o \approx \omega_{pe}$, equation (4.2) shows that $k_o \approx 0$, and from equation (4.3) we

have $\vec{k}_e \approx -\vec{k}_i$. When $k\lambda_{De} \ll 1$, from equations (4.4) and (4.5), we find

$$\omega_e \approx \omega_{pe} \left(1 + \frac{3}{4} \frac{k^2 v_e^2}{\omega_{pe}^2} \right) \quad (4.6)$$

and

$$\omega_i \approx \omega_{pi} k \lambda_{De}. \quad (4.7)$$

Substituting equations (4.5) and (4.6) into the frequency matching condition $\omega_o = \omega_e + \omega_i$, we get:

$$(k\lambda_{De})^2 + \frac{2}{3} \left(\frac{\omega_{pi}}{\omega_{pe}} \right) (k\lambda_{De}) - \frac{2}{3} \left(\frac{\omega_o}{\omega_{pe}} - 1 \right) = 0, \quad (4.8)$$

where we have used $v_e = \sqrt{2}\omega_{pe}\lambda_{De}$. Now, solving equation (4.8) for wave number $|\vec{k}_e| \approx |\vec{k}_i| = k$, we obtain:

$$k = \frac{1}{\lambda_{De}} \left[\pm \frac{1}{3} \left\{ \left(\frac{\omega_{pi}}{\omega_{pe}} \right)^2 + 6 \left(\frac{\omega_o}{\omega_{pe}} - 1 \right) \right\}^{1/2} - \frac{1}{3} \frac{\omega_{pi}}{\omega_{pe}} \right]. \quad (4.9)$$

The plasma dispersion relation describing the non-relativistic theory of parametric instabilities of linearly polarized pumps [see section (2.2)] is given by:

$$\frac{1 + \chi_i + \chi_e}{\chi_e [1 + \chi_i + (m_e/m_i)\chi_i]} = k^2 \left[\frac{|\vec{k}_- \times \vec{v}_o|^2}{k_-^2 D_-} - \frac{|\vec{k}_- \cdot \vec{v}_o|^2}{k_-^2 \omega_-^2 (1 - \omega_{pe}^2/\omega_-^2)} + \frac{|\vec{k}_+ \times \vec{v}_o|^2}{k_+^2 D_+} - \frac{|\vec{k}_+ \cdot \vec{v}_o|^2}{k_+^2 \omega_+^2 (1 - \omega_{pe}^2/\omega_+^2)} \right], \quad (4.10)$$

where $v_o = eE_o/m_e\omega_o$ is the quiver velocity of electrons in the field \vec{E}_o .

If the pump wave frequency $\omega_o \approx \omega_{pe}$ then $1 - \omega_{pe}^2/\omega_{\pm}^2 \approx 0$ and hence the $\vec{k}_{\pm} \cdot \vec{v}_o$ terms dominate on the right hand side of equation (4.10), where $\omega_{\pm} = \omega_o \pm \omega$ and $\vec{k}_{\pm} = \vec{k}_o \pm \vec{k}$. Therefore, the excited side-band modes must be predominantly electrostatic. Neglecting the terms containing $\vec{k}_{\pm} \times \vec{v}_o$ and m_e/m_i in equation (4.10), we obtain the following dispersion relation for parametric decay instability:

$$\frac{1}{\chi_e(\vec{k}, \omega)} + \frac{1}{\chi_i(\vec{k}, \omega) + 1} = -(\vec{k} \cdot \vec{v}_o)^2 \left[\frac{1}{\omega_-^2 (1 - \omega_{pe}^2/\omega_-^2)} + \frac{1}{\omega_+^2 (1 - \omega_{pe}^2/\omega_+^2)} \right], \quad (4.11)$$

where ω and \vec{k} are the angular frequency and wavenumber of the low frequency side-band mode. Here χ_e and χ_i are the susceptibility functions of electron and ion plasmas and their asymptotic expansions are given by (Liu and Kaw 1976; Fried and Conte, 1961):

$$\chi_e(k, \omega) = \begin{cases} -\frac{\omega_{pe}^2}{\omega^2} \left(1 + \frac{3}{2} \frac{k^2 v_e^2}{\omega^2}\right) + i \frac{\sqrt{\pi}}{(k\lambda_{De})^2} \frac{\omega}{kv_e} \exp[-\omega^2/(kv_e)^2], & \text{for } \omega \gg kv_e; \\ \frac{1}{(k\lambda_{De})^2} \left(1 + i\sqrt{\pi} \frac{\omega}{kv_e}\right), & \text{for } \omega \ll kv_e, \end{cases} \quad (4.12)$$

$$\chi_i(k, \omega) = \begin{cases} -\frac{\omega_{pi}^2}{\omega^2} \left(1 + \frac{3}{2} \frac{k^2 v_i^2}{\omega^2}\right) + i \frac{\sqrt{\pi}}{(k\lambda_{De})^2} \frac{T_e}{T_i} \frac{\omega}{kv_i} \exp[-\omega^2/(kv_i)^2], & \text{for } \omega \gg kv_i; \\ \frac{1}{(k\lambda_{De})^2} \frac{T_e}{T_i} \left(1 + i\sqrt{\pi} \frac{\omega}{kv_i}\right), & \text{for } \omega \ll kv_i. \end{cases} \quad (4.13)$$

For $k\lambda_{De} \ll 1$, $\omega_i = \omega_{pi} k\lambda_{De} = kc_s$, where $c_s = \lambda_{De} \omega_{pi} = [k_B T_e / m_i]^{1/2}$ is the ion-acoustic velocity. In equation (4.11), we neglect the term containing $(1 - \omega_{pe}^2 / \omega_+^2)$ as the mode (\vec{k}_+, ω_+) is off resonant. If we include the thermal and damping effects then ω_{pe}^2 is replaced by ω_e^2 and the condition $\omega_-^2 (1 - \omega_{pe}^2 / \omega_-^2) \approx 0$ tells us that (\vec{k}_-, ω_-) is the electron plasma mode with frequency $(\omega_o - \omega)$. Therefore, we have

$$\begin{aligned} (\omega_- - i\Gamma_e)^2 - \omega_e^2 &= (\omega_o - \omega - i\Gamma_e)^2 - \omega_e^2 \\ &\approx (\omega_o - \omega)^2 - i2\Gamma_e(\omega_o - \omega) - \omega_e^2 \\ &\approx (\omega_o - \omega + \omega_e)(\omega_o - \omega - \omega_e) - i2\Gamma_e(\omega_o - \omega) \\ &\approx 2\omega_e(\Delta - \omega) - i2\Gamma_e\omega_e \\ &\approx -2\omega_e(\omega - \Delta + i\Gamma_e), \end{aligned} \quad (4.14)$$

where $\Delta = \omega_o - \omega_e$ is the frequency mismatch, $\omega \ll \omega_e$ and $\omega_o \approx \omega_e$ has been used. Here Γ_e is the damping rate of electron plasma wave

$$\Gamma_e = \frac{\sqrt{\pi}}{2} \frac{\omega_{pe}}{(k\lambda_{De})^3} \exp\left[-\frac{1}{2(k\lambda_{De})^2} - \frac{3}{2}\right] + \nu_{ei}, \quad (4.15)$$

where $\nu_{ei} = 4\pi n_e e^4 \ln \Lambda / m_e^2 v_e^3$ is the collision frequency of the electrons, and $\ln \Lambda \approx 10$ is the Coulomb logarithm [see sections (A) and (D) in appendix].

If the pump is strong enough, then the normal side-band modes get modified and no more remain linear. An intense pump can cause amplitude dependent shift in the real and imaginary parts of the normal mode frequencies. For $\omega_o > \omega_e$, PDI occurs due to the parametric decay of a pump wave into an electron and an ion modes. Depending on the pump strength and the ratio T_e/T_i , it can occur through three different routes: PDI-I, PDI-II, PDI-III, discussed below. However, when $\omega_o < \omega_e$, purely growing (zero frequency) ion density fluctuations will arise from the noise level. As it grows in amplitude, so also does the associated electron plasma wave. This case of parametric instability is called the ‘oscillating two stream instability’ (OTS).

4.2.1 Decay of a pump wave into an electron plasma wave and an ion-acoustic wave (PDI-I)

In this case, radiation energy gets transferred to the electrostatic side-band modes: the electron plasma wave and the ion-acoustic wave, consequently their amplitudes grow exponentially in time. To derive an expression for the growth rate we use the asymptotic forms for χ_e and χ_i corresponding to $kv_e \gg \omega \geq kv_i$:

$$\chi_e = \frac{1}{(k\lambda_{De})^2} \left(1 + i\sqrt{\pi} \frac{\omega}{kv_e} \right) \quad (4.16)$$

and

$$\begin{aligned} \chi_i &= -\frac{\omega_{pi}^2}{\omega^2} + i \operatorname{Im}(\chi_i) \\ &= -\frac{\omega_{pi}^2}{\omega^2} + i \frac{\sqrt{\pi}}{(k\lambda_{De})^2} \left(\frac{T_e}{T_i} \right) \left(\frac{\omega}{kv_i} \right) \exp[-\omega^2/(kv_i)^2]. \end{aligned} \quad (4.17)$$

Using equations (4.14), (4.16) and (4.17) we write equation (4.11) as

$$\left[(k\lambda_{De})^2 \left(1 - i\sqrt{\pi} \frac{\omega}{kv_e} \right) + \frac{1}{1 - (\omega_{pi}^2/\omega^2) + i \operatorname{Im}(\chi_i)} \right] = \frac{(\vec{k} \cdot \vec{v}_o)^2}{2\omega_e(\omega - \Delta + i\Gamma_e)}, \quad (4.18)$$

Since $\omega \ll \omega_{pi}$, we obtain

$$\frac{(k\lambda_{De})^2(1 - i\sqrt{\pi}\omega/kv_e)\{(\omega_{pi}/\omega)^2 - i\text{Im}(\chi_i)\} - 1}{(\omega_{pi}/\omega)^2 - i\text{Im}(\chi_i)} = \frac{(\vec{k}\cdot\vec{v}_o)^2}{2\omega_e(\omega - \Delta + i\Gamma_e)}. \quad (4.19)$$

Taking $(\omega_{pi}/\omega)^2 - i\text{Im}(\chi_i) \approx (\omega_{pi}/\omega)^2$ in the denominator on the left hand side of equation (4.19), we obtain

$$\begin{aligned} (k\lambda_{De})^2 \left[\left(\frac{\omega_{pi}}{\omega} \right)^2 - i\text{Im}(\chi_i) - i\sqrt{\pi} \left(\frac{\omega}{kv_e} \right) \left(\frac{\omega_{pi}}{\omega} \right)^2 - \sqrt{\pi} \left(\frac{\omega}{kv_e} \right) \text{Im}(\chi_i) \right] - 1 \\ = \frac{(\vec{k}\cdot\vec{v}_o)^2}{2\omega_e(\omega - \Delta + i\Gamma_e)} \left(\frac{\omega_{pi}}{\omega} \right)^2. \end{aligned} \quad (4.20)$$

Multiplying both sides by ω^2 , we get

$$\begin{aligned} (k\lambda_{De})^2 \left[\omega_{pi}^2 - i\omega^2 \text{Im}(\chi_i) - i\sqrt{\pi} \left(\frac{\omega}{kv_e} \right) \omega_{pi}^2 - \sqrt{\pi} \left(\frac{\omega^3}{kv_e} \right) \text{Im}(\chi_i) \right] - \omega^2 \\ = \frac{(\vec{k}\cdot\vec{v}_o)^2}{2\omega_e(\omega - \Delta + i\Gamma_e)} \omega_{pi}^2. \end{aligned} \quad (4.21)$$

Neglecting the term containing ω^3 , we get

$$\omega^2 - k^2 c_s^2 + i\omega(k\lambda_{De})^2 \left\{ \sqrt{\pi} \left(\frac{\omega_{pi}^2}{kv_e} \right) + \omega \text{Im}(\chi_i) \right\} = -\frac{(\vec{k}\cdot\vec{v}_o)^2}{2\omega_e(\omega - \Delta + i\Gamma_e)} \omega_{pi}^2. \quad (4.22)$$

In equation (4.22), we define

$$\frac{1}{2}(k\lambda_{De})^2 \left\{ \sqrt{\pi} \left(\frac{\omega_{pi}^2}{kv_e} \right) + \omega \text{Im}(\chi_i) \right\} = \Gamma_L \quad (4.23)$$

as the ion Landau damping rate. Now, substituting for $\text{Im}(\chi_i)$ from equation (4.17) into equation (4.23), we get

$$\begin{aligned} \Gamma_L &= \frac{1}{2}(k\lambda_{De})^2 \left[\sqrt{\pi} \frac{\omega_{pi}^2}{kv_e} + \frac{\sqrt{\pi}}{(k\lambda_{De})^2} \left(\frac{T_e}{T_i} \right) \left(\frac{\omega^2}{kv_i} \right) \exp\{-\omega^2/(kv_i)^2\} \right] \\ &= \frac{\sqrt{\pi}}{2} \left[k \frac{c_s^2}{v_e} + \left(\frac{T_e}{T_i} \right) \left(\frac{\omega^2}{kv_i} \right) \exp\{-\omega^2/(kv_i)^2\} \right]. \end{aligned} \quad (4.24)$$

Substituting $\omega = \omega_{pi}k\lambda_{De}$, we get

$$\Gamma_L = \frac{\sqrt{\pi}}{2}kc_s \left[\frac{c_s}{v_e} + \left(\frac{T_e}{T_i} \right) \left(\frac{c_s}{v_i} \right) \exp\{-c_s^2/v_i^2\} \right]. \quad (4.25)$$

If the ion temperature T_i is not too small compared to T_e then

$$c_s = \left(\frac{k_B T_e + 3k_B T_i}{m_i} \right)^{1/2} \quad (4.26)$$

Consider the ratios:

$$\frac{c_s}{v_i} = \left(\frac{k_B T_e + 3k_B T_i}{m_i} \right)^{1/2} \left(\frac{m_i}{2k_B T_i} \right)^{1/2} = \frac{1}{\sqrt{2}} \left(3 + \frac{T_e}{T_i} \right)^{1/2} \approx \frac{1}{\sqrt{2}} \left(\frac{T_e}{T_i} \right)^{1/2}, \quad (4.27)$$

$$\frac{c_s}{v_e} = \left(\frac{k_B T_e + 3k_B T_i}{m_i} \right)^{1/2} \left(\frac{m_e}{2k_B T_e} \right)^{1/2} \approx \frac{1}{\sqrt{2}} \left(\frac{m_e}{m_i} \right)^{1/2} \quad (4.28)$$

Substituting the equations (4.27) and (4.28) into the equation (4.25), we get

$$\Gamma_L = \left(\frac{\pi}{8} \right)^{1/2} kc_s \left[\left(\frac{m_e}{m_i} \right)^{1/2} + \left(\frac{T_e}{T_i} \right)^{3/2} \exp \left\{ -\frac{1}{2} \left(3 + \frac{T_e}{T_i} \right) \right\} \right]. \quad (4.29)$$

Let $\Gamma_i = \Gamma_L + \nu_{ie}$ be the total damping rate of the ion-acoustic wave, where ν_{ie} is the ion collision frequency, given by $\nu_{ie} = 4\pi n_e e^4 \ln \Lambda / m_i^2 v_i^3$.

Now, from equation (4.22), we obtain:

$$(\omega^2 + i2\Gamma_i\omega - k^2c_s^2)(\omega - \Delta + i\Gamma_e) + \frac{(\vec{k} \cdot \vec{v}_o)^2}{2\omega_e} \omega_{pi}^2 = 0. \quad (4.30)$$

Let $\omega = kc_s + i\gamma_1$, $\gamma_1 \ll kc_s$, where γ_1 is the growth rate of the instability, then $\omega^2 \approx k^2c_s^2 + i2kc_s\gamma_1$. Using these expressions for ω and ω^2 , in equation (4.30), we obtain

$$(kc_s + i\Gamma_i)\gamma_1^2 + [(\Gamma_e + \Gamma_i)kc_s + i(kc_s - \Delta)(\Gamma_i - kc_s) - \Gamma_e\Gamma_i]\gamma_1 - i(kc_s - \Delta)kc_s\Gamma_i + kc_s\Gamma_e\Gamma_i - \frac{(\vec{k} \cdot \vec{v}_o)^2}{2\omega_e} \omega_{pi}^2 = 0. \quad (4.31)$$

Since $\Gamma_i \approx (\pi/8)^{1/2} k c_s (m_e/m_i)^{1/2}$, we take $(k c_s + i\Gamma_i) \approx k c_s$. We know from the frequency matching condition $\omega_o - \omega_e = \omega_i$. Therefore, we take $\Delta = \omega_o - \omega_e \approx k c_s$. Using these approximations, in the equation (4.31), we obtain

$$\gamma_1^2 + (\Gamma_e + \Gamma_i)\gamma_1 + \Gamma_e\Gamma_i - \frac{(\vec{k}\cdot\vec{v}_o)^2}{4k c_s \omega_e} \omega_{pi}^2 = 0. \quad (4.32)$$

Solving equation (4.32), we get the growth rate γ_1 of the growing mode:

$$\begin{aligned} \gamma_1 &= -\frac{(\Gamma_e + \Gamma_i)}{2} + \frac{1}{2} \left[\frac{(\vec{k}\cdot\vec{v}_o)^2}{k c_s \omega_e} \omega_{pi}^2 + (\Gamma_e + \Gamma_i)^2 - 4\Gamma_e\Gamma_i \right]^{1/2} \\ &= -\frac{(\Gamma_e + \Gamma_i)}{2} + \left[\frac{(\vec{k}\cdot\vec{v}_o)^2}{4k c_s} \left(\frac{m_e}{m_i} \right)^{1/2} \omega_{pi} + \frac{(\Gamma_e - \Gamma_i)^2}{4} \right]^{1/2} \end{aligned} \quad (4.33)$$

The threshold condition, obtained by setting γ_1 equal to zero in equation (4.33), is given by

$$\frac{(\vec{k}\cdot\vec{v}_o)^2}{4k c_s} \omega_{pi} \left(\frac{m_e}{m_i} \right)^{1/2} = \Gamma_e\Gamma_i. \quad (4.34)$$

We assume $\vec{k} \parallel \vec{E}_o$ (the electric field of pump wave), $n_i = n_e$ in the hydrogen plasma and $\omega_o = 1.01\omega_{pe}$. Though we have chosen initially a single value of the frequency $\omega_o = 1.01\omega_{pe}$, as the instability sets up plasma temperatures T_e and T_i go up due to the damping of excited electrostatic waves and so do ω_e and ω_i . Since $\omega_o = \omega_e + \omega_i$, the resonant pump frequency should also increase. Therefore, a band of pump frequencies satisfies the resonance condition. An inhomogeneity in plasma density will also admit a broad pump. Therefore, we assume that in the maximum band width $\delta\omega \approx \omega_o$ the resonant condition of the parametric decay instability is satisfied. Since γ_1 is the growth rate due to a monochromatic pump at ω_o , the actual growth rate γ'_1 due to the broad pump with spectral width $\delta\omega \gg \gamma_1$ is given by (Kruer 1988)

$$\gamma'_1 = \frac{1}{\delta\omega} \gamma_1^2. \quad (4.35)$$

Hence due to a broad pump the growth rate of PDI is decreased by a factor of $\delta\omega/\gamma_1$. The coherence condition is satisfied for $\delta\omega \leq \gamma_1$. Since the resonance condition for the instability is satisfied for the fraction of the band width, i.e., for $\delta\omega \leq \gamma_1$ only a portion of the total luminosity is useful for the excitation of the instability.

The threshold is higher for an incoherent pump because the incoherency effectively amounts to having more collisions in the system. A partially polarized pump again offers only a part of its luminosity for the excitation of PDI.

We introduce a decay parameter D , defined from equations (4.34), as

$$D = \frac{\int_{\nu_1}^{\nu_2} L_\nu d\nu}{4\pi R^2 n_e c} P(\lambda_{De}, k), \quad (4.36)$$

where the function

$$P(\lambda_{De}, k) = \frac{k\omega_{pi}}{2c_s(m_e m_i)^{1/2} \Gamma_e \Gamma_i} \quad (4.37)$$

expresses the effect of plasma parameters on the instability. The integration over the luminosity has to be computed over the band-width $\nu_2 - \nu_1 = \delta\omega/2\pi$. The variation of the function P with respect to T_e for different densities is shown in Fig. 4.2. The bending of curves at $k\lambda_{De} \ll 1$ is due to collisional damping. But when $k\lambda_{De} \approx 0.4$, Landau damping operates which is a strong function of T_e but not of n_e . The strength of P describes if the conditions in the plasma are favorable for PDI to occur. For small pump, PDI is favored at large P . PDI occur for $D > 1$ and switches off for $D \leq 1$. The variation of D with respect to temperature T_e is shown in Fig. 4.3. When $D \gg 1$, the ion-acoustic mode loses its linearity and the instability falls in to one or the other of the three cases discussed in the following sections.

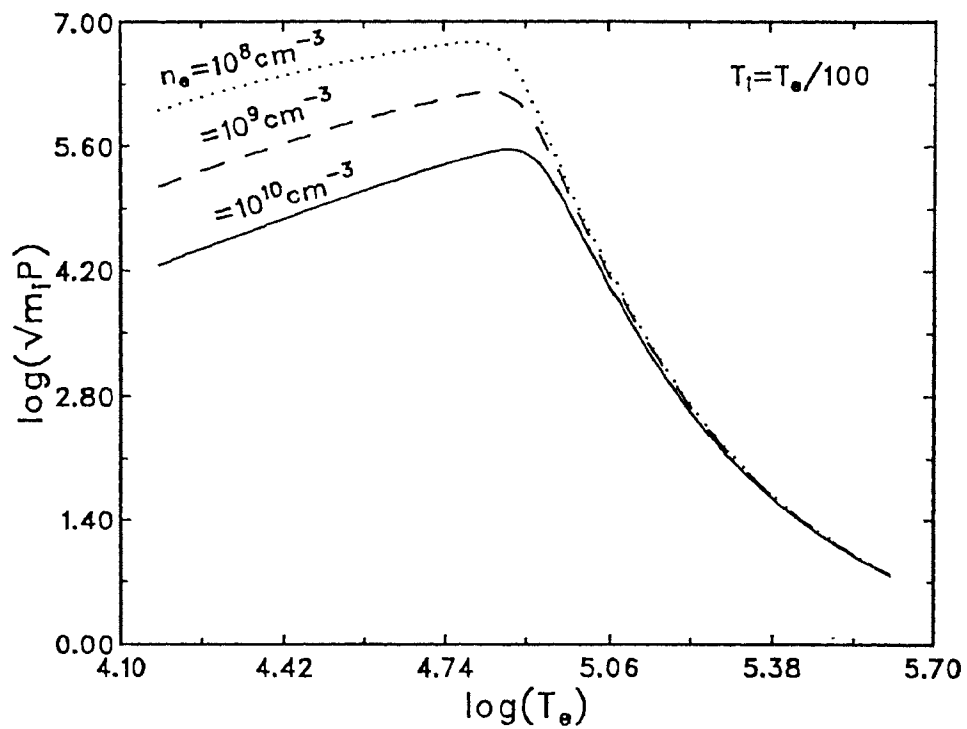


Fig. 4.2 Variation of $\sqrt{m_i}P$ with electron temperature T_e for different electron densities.

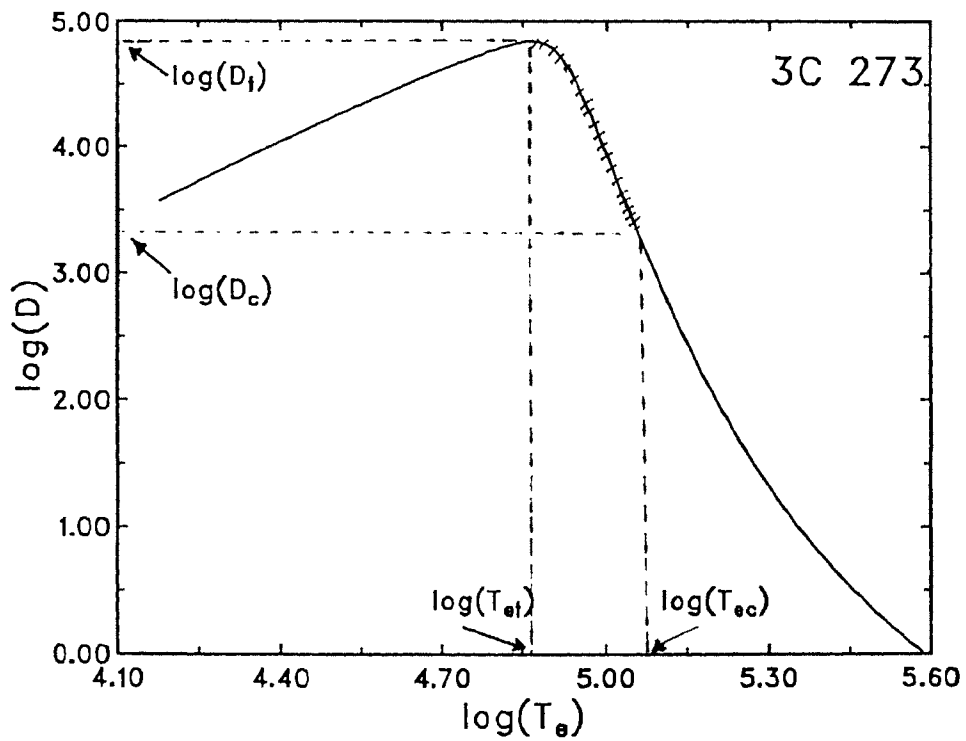


Fig. 4.3 Decay parameter D vs T_e in the 3C 273.

Similar to electrostatic waves, electromagnetic waves also experience collisional damping in the plasma medium. If ν_o is the collisional damping rate of electromagnetic wave, then rate of energy loss from the electromagnetic wave ($\nu_o E_o^2/8\pi$) must balance the rate at which the oscillatory energy of electrons is randomized by the electron-ion scattering, i.e., $(\nu_o E_o^2/8\pi) = (\nu_{ei} m_e v_o^2/2)$. Since $v_o = eE_o/m_o\omega_o$, this power balance gives

$$\nu_o = \left(\frac{\omega_{pe}}{\omega_o} \right)^2 \nu_{ei}, \quad (4.38)$$

where $\nu_{ei} \approx \nu_e$ is the electron-ion collision frequency. The dependence of ν_o on electron temperature T_e is shown in Fig. 4.5.

The energy density $E_o^2/8\pi$ of the pump and the luminosity L ($= L_{41} \times 10^{41}$ erg sec⁻¹) of the source are related by

$$\frac{E_o^2}{8\pi} = \frac{L}{4\pi R^2 c}, \quad (4.39)$$

where R ($= r_{pc} 3.086 \times 10^{18}$ cm) is the distance between the radio source and the plasma. Therefore, the oscillation velocity of electrons in the pump field, is given by

$$v_o = \frac{eE_o}{m_e\omega_o} = \frac{e}{m_e} \left(\frac{2L}{R^2 c} \right)^{1/2} \frac{1}{\omega_o}. \quad (4.40)$$

The average values of different parameters in the resonant interaction region of radio waves in the different sources, determined from observations, are listed in the Table 4.1.

Electrons being lighter generally heat up before the ions and since the electron-ion collision time is much larger than the excitation time of PDI, the inequality in temperature will remain during the instability. The ion temperature T_i and ω_o used for each case of PDI, are given in Table 4.2.

Table 4.1 Observed parameters in the resonant interacting region.

Source	n_e (cm^{-3})	minimum T_e (K)	r (pc)	ω_o (rad/sec)	L_{41} ($\delta\omega = \omega_o$)
3C 273	10^{10}	1.5×10^4	0.05	8.8×10^9	4.59×10^2
3C 48	10^{10}	1.5×10^4	0.05	8.8×10^9	4.59×10^2
Crab Nebula	10^7	1.0×10^4	0.03	1.8×10^8	1.24×10^{-4}

Table 4.2 Model Parameters.

Type of Instability	minimum T_i (K)	ω_o (rad/sec)
PDI-I	$T_e/100$	$1.01\omega_{pe}$
PDI-II	$T_e/100$	$1.01\omega_{pe}$
PDI-III	$10 \times T_e$	$1.01\omega_{pe}$
OTS	$T_e/100$	$(\omega_e + \omega_{pe})/2$

We solve the equation (4.30) numerically for real and imaginary parts of ω , and exhibit the results of PDI-I in Fig. 4.4. At $\log T_e \approx 10^5$ K, instability is well excited. If temperature goes up, due to Landau damping, growth rate falls exponentially. If $T_e > 10^{5.3}$ K then $\omega_{r1} \approx kc_s$ and $\gamma_1 \ll \omega_{r1}$.

Fig. 4.5 shows the growth rate γ_1 due to a monochromatic pump and γ'_1 due to a broad pump of width ($\delta\omega = \omega_o$) as a function of T_e . It shows both γ_1 and γ'_1 are well above the collisional damping rate ν_o of electromagnetic wave. Therefore, the radiation with frequency ω_o close to ω_{pe} gets absorbed more efficiently due to PDI-I rather than due to collisional absorption in a plasma medium. For $T_e > 10^{5.3}$ K growth rate decreases due to large Landau damping.

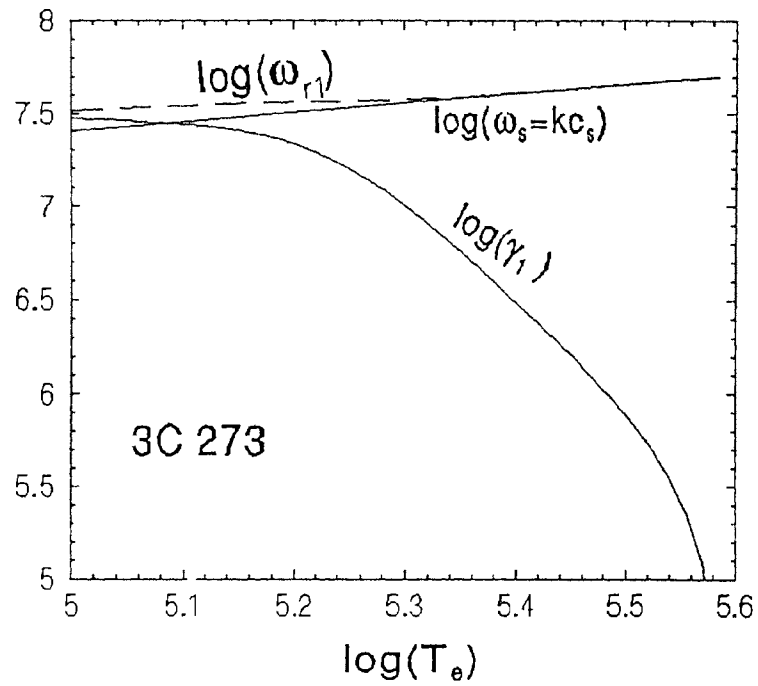


Fig. 4.4 Variation of frequency $\omega_{r1} \approx \omega_s$ and growth rate γ_1 with T_e in 3C 273.

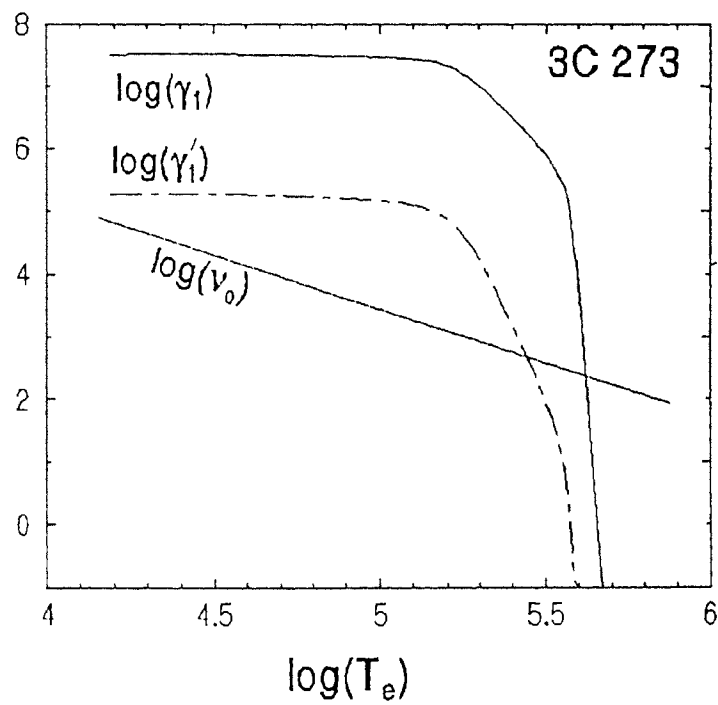


Fig. 4.5 Variation of γ_1 , γ_1' and ν_o with T_e in 3C 273.

The dependence of growth rates γ_1 and γ'_1 on pump strength is shown in Fig. 4.6. It shows that near the threshold, γ_1 is proportional to L_{41} while γ'_1 is proportional to $L_{41}^{1/2}$. At well above the threshold both γ_1 and γ'_1 are proportional to $L_{41}^{1/2}$. If the pump is slightly above the threshold, then both γ_1 and γ'_1 dominate over the collisional damping rate ν_o .

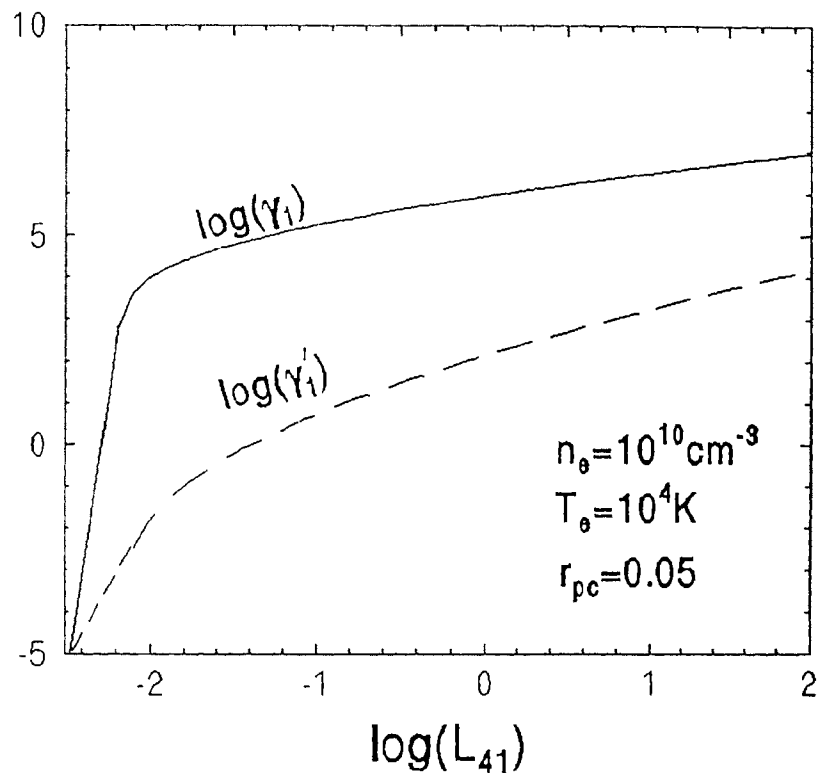


Fig. 4.6 Variation of γ_1 and γ'_1 as functions of luminosity L_{41}

The threshold value of the luminosity is a strong function of electron temperature T_e , as indicated by Fig. 4.7. At lower temperature ($T_e < 10^{4.5}$ K) collisional damping exceeds Landau damping while at higher temperature ($T_e > 10^{5.1}$ K) Landau damping becomes larger than collisional damping. But in the range $10^{4.5} < T_e < 10^{5.1}$ K both collisional and Landau damping are small and therefore lower threshold luminosity is needed.

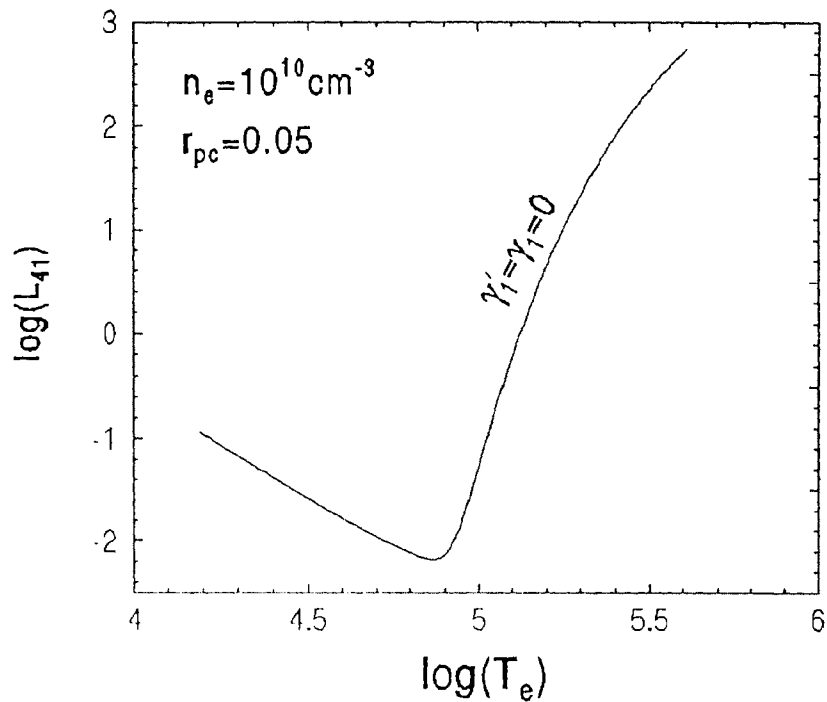


Fig. 4.7 Variation of threshold luminosity with T_e .

4.2.2 Decay into a Reactive Quasi-Ion Mode (PDI-II)

For large pump strengths and low temperatures, the ion mode loses its linearity. Its frequency ω_{r2} becomes higher than the ion-acoustic frequency ($\omega_s = kc_s$). Since its growth is higher than ω_{r2} , this mode is known as reactive quasi-ion mode.

We solve equation (4.30) to evaluate frequency ω_{r2} and growth rate γ_2 of the reactive quasi-ion mode. The variations of ω_{r2} and γ_2 with respect to T_e are shown in the Fig. 4.8.

Fig. 4.9 shows that both γ_2 and γ_2' are much higher than ν_o in 3C 273. Fig. 4.10 shows the variation of γ_2 and γ_2' as functions of L_{41} . It shows both γ_2 and γ_2' are proportional to $L_{41}^{1/2}$. The threshold luminosity required for the excitation of reactive quasi-ion mode as a function of electron temperature T_e is shown in Fig. 4.11.

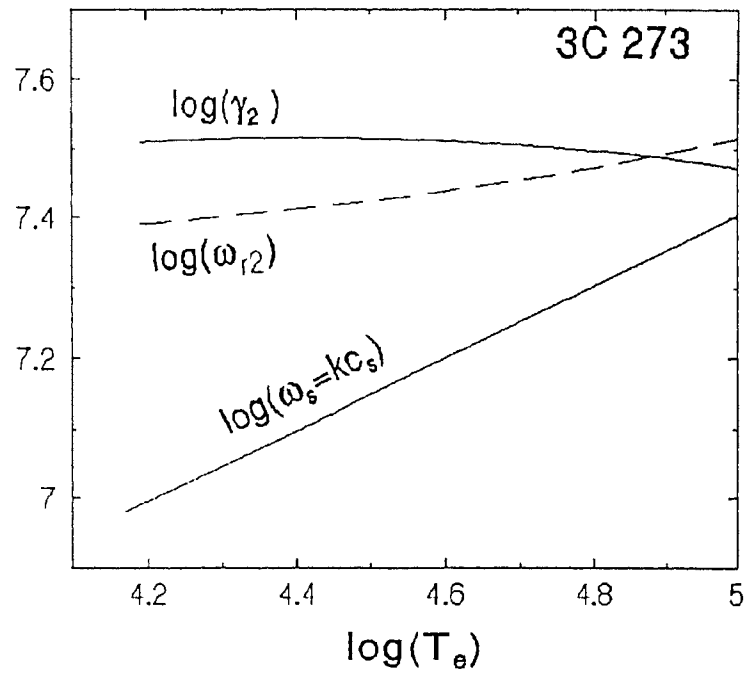


Fig. 4.8 Variation of ω_{r2} and γ_2 of the reactive quasi-ion mode with T_e in 3C 273.

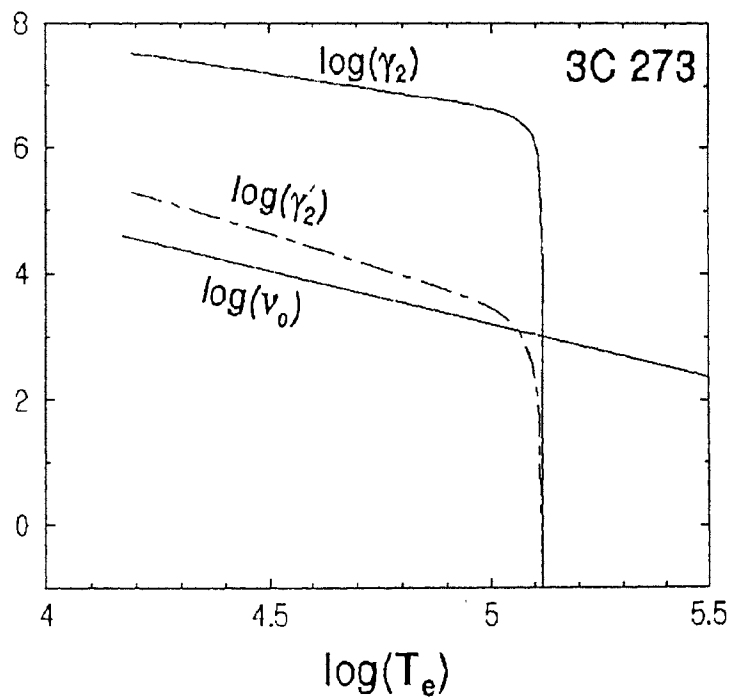


Fig. 4.9 Variation of γ_2 , γ'_2 of the reactive quasi-ion mode and ν_0 with T_e in 3C 273.

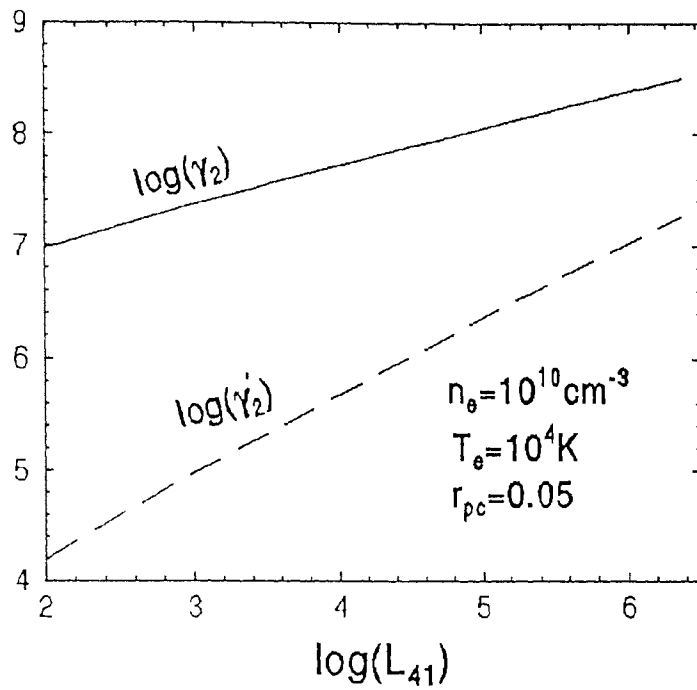


Fig. 4.10 Variation of γ_2 and γ'_2 of the reactive quasi-ion mode with L_{41} .

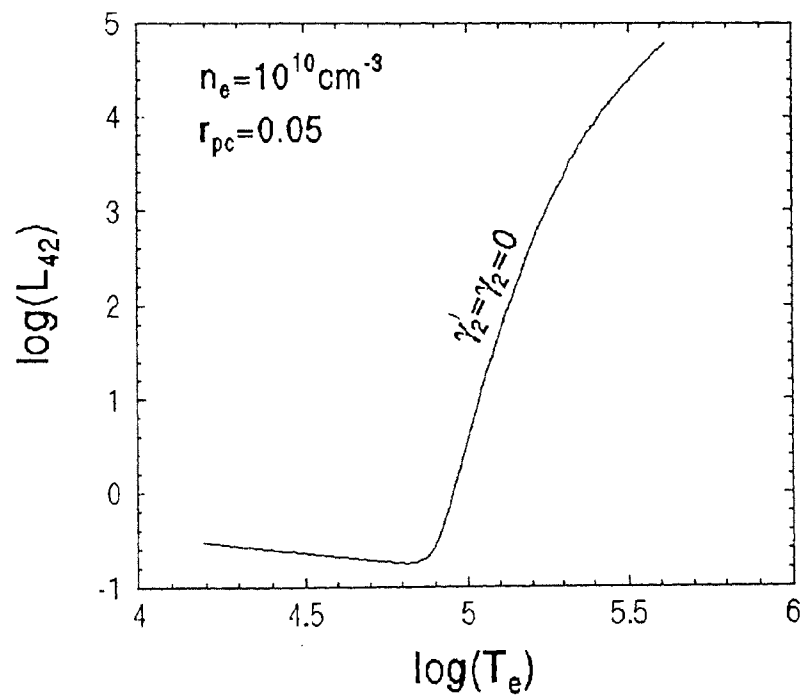


Fig. 4.11 Variation of threshold L_{41} of the reactive quasi-ion mode with T_e .

4.2.3 Decay into a Resistive Quasi-Ion Mode (PDI-III)

When $T_i \approx T_e$, the phase velocity of the ion-acoustic mode (c_s) becomes comparable to the thermal velocity (v_e) of the ions. Therefore, the beat mode (i.e., the ion mode) of a pump wave and an electron plasma mode undergoes the non-linear Landau damping [see section (B) in appendix] over the thermal ions. This ion mode is highly damped and weakly excited compared to the other three cases.

Neglecting the term containing $\omega_+(1 - \omega_{pe}^2/\omega_+^2)$ in equation (4.11), we obtain

$$\omega_-^2 - \omega_e^2 = -(\vec{k} \cdot \vec{v}_o)^2 \left[\frac{\chi_e(\chi_i + 1)}{\epsilon} \right], \quad (4.41)$$

where $\epsilon = 1 + \chi_i + \chi_e$.

Since $\omega/k \approx v_i$, we can not use the asymptotic forms of χ_i . Using equation (4.14) we write equation (4.41) as

$$\omega_- \Delta + i\Gamma_e = \frac{(\vec{k} \cdot \vec{v}_o)^2}{2\omega_e} \left[\frac{\chi_e(\chi_i + 1)}{\epsilon} \right] \bigg|_{\frac{\omega}{k} = \frac{\Delta}{k}}, \quad (4.42)$$

Using $\omega_o = \omega_{r3} + \gamma_{i3}$, separating the real and imaginary parts of equation (4.42), we obtain

$$\omega_{r3} = \frac{(\vec{k} \cdot \vec{v}_o)^2}{2\omega_e} \operatorname{Re} \left[\frac{\chi_e(\chi_i + 1)}{\epsilon} \right] \bigg|_{\frac{\omega}{k} = \frac{\Delta}{k}} + \Delta \quad (4.43)$$

and

$$\gamma_3 = \frac{(\vec{k} \cdot \vec{v}_o)^2}{2\omega_e} \operatorname{Im} \left[\frac{\chi_e(\chi_i + 1)}{\epsilon} \right] \bigg|_{\frac{\omega}{k} = \frac{\Delta}{k}} - \Gamma_e. \quad (4.44)$$

We numerically evaluate ω_{r3} and γ_3 and find $\omega_{r3} = \omega_s$. Fig. 4.12 shows the dependence of γ_3 and γ'_3 on electron temperature T_e for 3C 273. Fig. 4.13 shows the variation of γ_3 and γ'_3 with respect to luminosity L_{41} of the radio source. The threshold luminosity required for the excitation of resistive quasi-ion mode is plotted as function of T_e in Fig. 4.14.

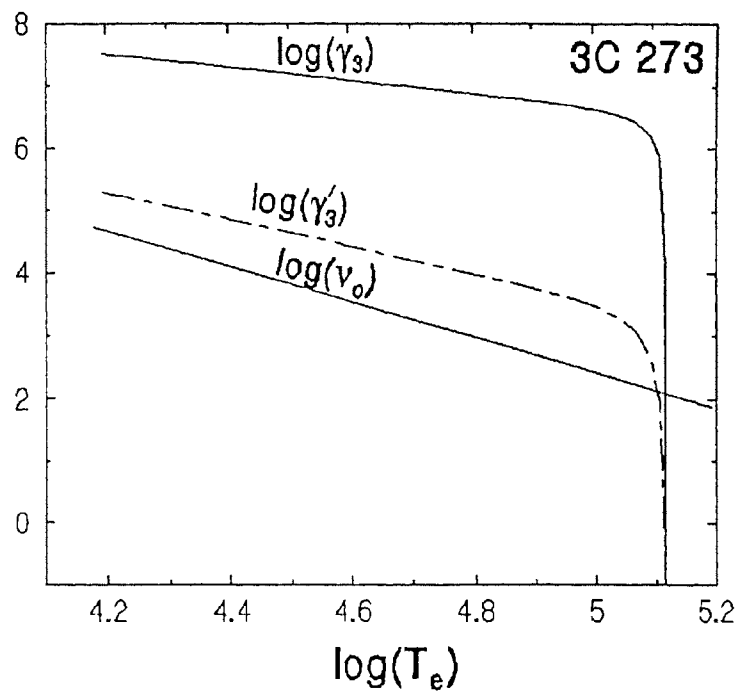


Fig. 4.12 Variation of γ_3 and γ'_3 of the resistive quasi-ion mode with T_e in 3C 273.

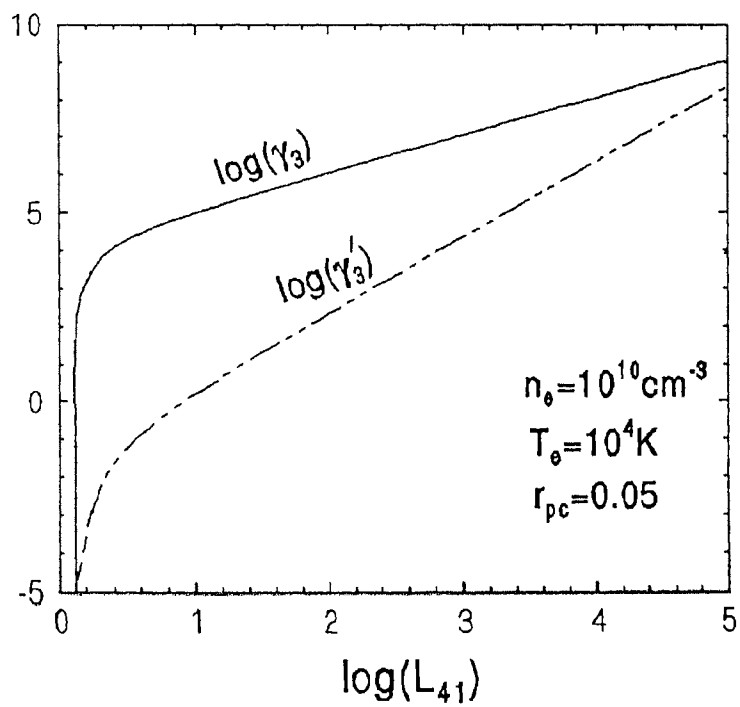


Fig. 4.13 Variation of γ_3 and γ'_3 with with L_{41} .

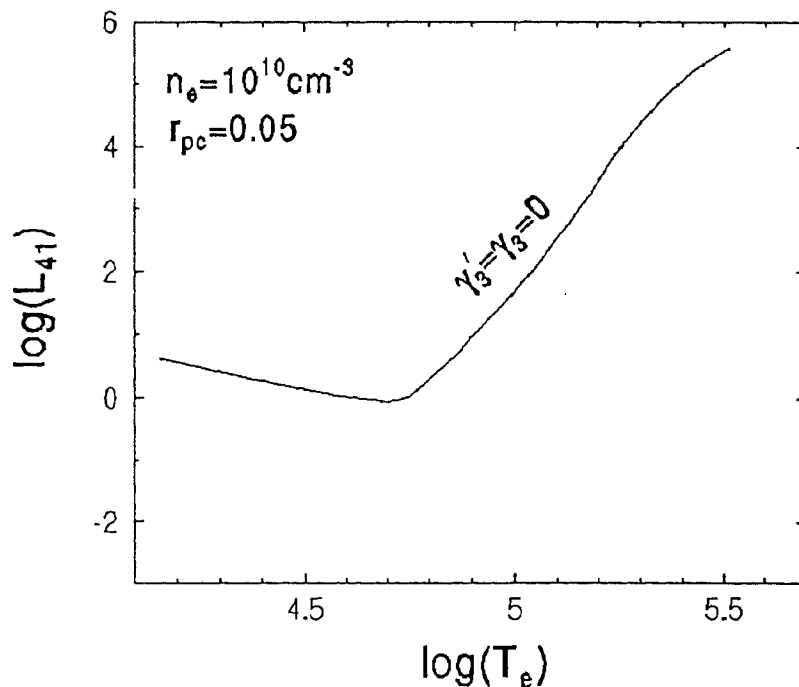


Fig. 4.14 Variation of threshold L_{41} with with T_e .

4.2.4 Oscillating Two-Stream Instability (OTS)

This instability excites when an intense electromagnetic pump of frequency less than or equal to the frequency of an electron plasma wave, interacts with the plasma. Here $\omega_{pe} < \omega_o \leq \omega_e$. The pump electromagnetic wave (ω_o, \vec{k}_o) couples with a high-frequency wave (ω_e, \vec{k}_e) and a non-oscillatory ion mode $(0, \vec{k}_i)$. We find that $\vec{k}_e \approx -\vec{k}_i = \vec{k}$. In this case the thermal ion density fluctuations of zero frequency grow along with an electron plasma mode. Since these static ion density fluctuations do not qualify for a normal mode of the plasma, we can not include OTS in the class of parametric decay instabilities. However, it has been considered as a special case of the parametric instability.

Here both the terms with $\omega_{\pm}^2(1 - \omega_{pe}^2/\omega_{\pm}^2)$ in equation (4.11) are resonant.

Similar to the equation (4.14), we obtain

$$\begin{aligned}
\omega_+^2 \left(1 - \frac{\omega_e^2}{\omega_+^2}\right) &= \omega_+^2 - \omega_e^2 \\
&\approx (\omega_o + \omega + i\Gamma_e)^2 - \omega_e^2 \\
&\approx (\omega_o + \omega - \omega_e)(\omega_o + \omega + \omega_e) + i2\Gamma_e(\omega_o + \omega) \\
&\approx 2\omega_e(\Delta + \omega + i\Gamma_e).
\end{aligned} \tag{4.45}$$

For $\omega = 0 + i\gamma_{ors}$, from equations (4.14) and (4.45), we get:

$$\omega_-^2 \left(1 - \frac{\omega_e^2}{\omega_-^2}\right) = 2\omega_e\{\Delta - i(\Gamma_e + \Gamma_{ors})\} \tag{4.46}$$

and

$$\omega_+^2 \left(1 - \frac{\omega_e^2}{\omega_+^2}\right) = 2\omega_e\{\Delta + i(\Gamma_e + \Gamma_{ors})\}. \tag{4.47}$$

Substituting equations (4.46) and (4.47) into equation (4.11), we get

$$\frac{1}{\chi_e} + \frac{1}{\chi_i + 1} = -\frac{(\vec{k} \cdot \vec{v}_o)^2}{2\omega_e} \frac{\Delta}{\Delta^2 + (\Gamma_e + \gamma_{ors})^2}. \tag{4.48}$$

Consider the asymptotic expansions of χ_e and χ_i :

$$\chi_e \approx \frac{1}{(k\lambda_{De})^2} \left(1 + i\sqrt{\pi} \frac{\omega}{kv_e}\right) = \frac{1}{(k\lambda_{De})^2} \left(1 - \sqrt{\pi} \frac{\gamma_{ors}}{kv_e}\right), \tag{4.49}$$

$$\chi_i \approx \frac{1}{(k\lambda_{De})^2} \frac{T_e}{T_i} \left(1 + i\sqrt{\pi} \frac{\omega}{kv_i}\right) = \frac{1}{(k\lambda_{De})^2} \frac{T_e}{T_i} \left(1 - \sqrt{\pi} \frac{\gamma_{ors}}{kv_i}\right). \tag{4.50}$$

Substituting the equations (4.49) and (4.50) into the equation (4.48), we obtain

$$\frac{1}{1 - \sqrt{\pi}\gamma_{ors}/kv_e} + \frac{1}{(1 - \sqrt{\pi}\gamma_{ors}/kv_i)T_e/T_i + (k\lambda_{De})^2} = -\frac{1}{2\omega_e} \frac{(\vec{k} \cdot \vec{v}_o)^2 (k\lambda_{De})^{-2} \Delta}{\{(\gamma_{ors} + \Gamma_e)^2 + \Delta^2\}}. \tag{4.51}$$

If we simplify equation (4.51) for γ_{ors} , we get

$$a_1\gamma_{ors}^3 + a_2\gamma_{ors}^2 + a_3\gamma_{ors} + a_4 = 0, \tag{4.52}$$

where

$$\begin{aligned}
a_1 &= \frac{\sqrt{\pi}}{kv_e} + \frac{\sqrt{\pi} T_e}{kv_i T_i}, \\
a_2 &= 2\Gamma_e a_1 - (k\lambda_{De})^2 - \frac{T_e}{T_i} - \frac{(\vec{k}\cdot\vec{v}_o)^2}{2\omega_e(k\lambda_{De})^2} \frac{\pi\Delta}{v_e v_i k^2} \frac{T_e}{T_i} - 1, \\
a_3 &= a_1(\Gamma_e^2 + \Delta^2) - 2\left(1 + (k\lambda_{De})^2 + \frac{T_e}{T_i}\right)\Gamma_e + \\
&\quad \frac{\sqrt{\pi}(\vec{k}\cdot\vec{v}_o)^2\Delta}{2\omega_e(k\lambda_{De})^2} \left\{ \left(\frac{1}{kv_e} + \frac{1}{kvi}\right) \frac{T_e}{T_i} + \frac{(k\lambda_{De})^2}{kv_e} \right\}
\end{aligned}$$

and

$$a_4 = -\left(1 + (k\lambda_{De})^2 + \frac{T_e}{T_i}\right)(\Gamma_e^2 + \Delta^2) - \frac{(\vec{k}\cdot\vec{v}_o)^2\Delta}{2\omega_e(k\lambda_{De})^2} \left((k\lambda_{De})^2 + \frac{T_e}{T_i}\right).$$

For $k\lambda_{De} \approx 0.4$, equation (4.52) gives

$$\gamma_{ors} = \pm i \left[\frac{(\vec{k}\cdot\vec{v}_o)^2\Delta}{2\omega_e(k\lambda_{De})^2} \left\{ 1 + \frac{1}{(k\lambda_{De})^2 + T_e/T_i} \right\}^{-1} + \Delta^2 \right]^{1/2} - \Gamma_e. \quad (4.53)$$

The γ_{ors} is real only when $\Delta = \omega_o - \omega_e \leq 0$, i.e., $\omega_o \leq \omega_e$. The expression $\gamma_{ors} = 0$ gives $\Delta = \Delta_{thr}$, while $\partial\gamma_{ors}/\partial\Delta = 0$ gives $\Delta = \Delta_{max}$ corresponding to a maximum growth rate. Now, $\Delta_{thr} = \Delta_{max}$ gives the minimum pump strength at which instability occurs

$$\left(\frac{v_o}{v_e}\right)^2 = \left\{ 1 + \frac{1}{(k\lambda_{De})^2 + T_e/T_i} \right\} \frac{\Gamma_e}{\omega_e}. \quad (4.54)$$

We solve equation (4.52), using $k = 8.75 \text{ cm}^{-1}$ for 3C 273, where k has been determined using the condition $k \geq \sqrt{2/3}(k_o c/v_e)$, obtained from $\omega_{pe} < \omega_o \leq \omega_e$ and the values of parameters given in the Tables 4.1 and 4.2. One of the three roots represents a growing ion density fluctuation while other two represent damped modes. Using $\Delta = \Delta_{max}$, γ_{ors} and γ'_{ors} are plotted as a function of T_e in Fig. 4.15 for 3C 273. Note that the γ_{ors} and γ'_{ors} are much larger than the collisional absorption rate ν_o of the electromagnetic wave.

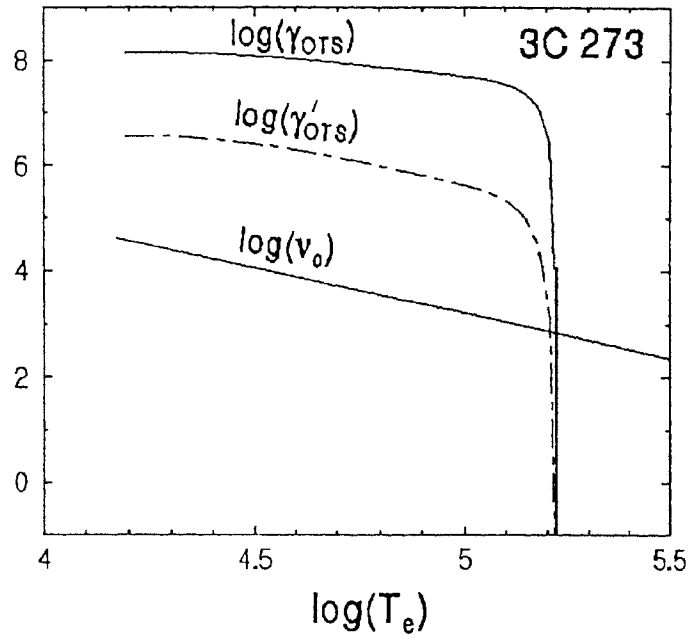


Fig. 4.15 Variation of γ_{ORS} and γ'_{ORS} with T_e in 3C 273.

Fig. 4.16 shows the dependence of γ_{ORS} and γ'_{ORS} on the luminosity of the source.

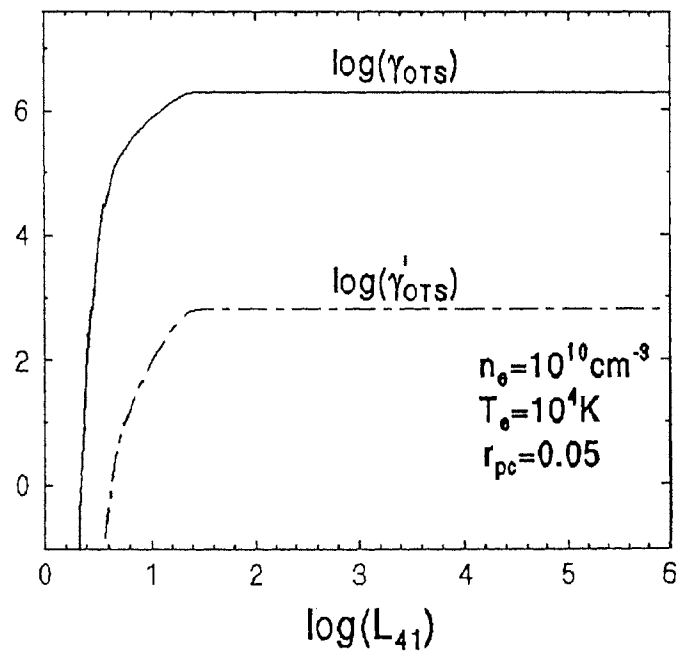


Fig. 4.16 Variation of γ_{ORS} and γ'_{ORS} with L_{41} .

Fig. 4.17 shows the variation of threshold luminosity with T_e .

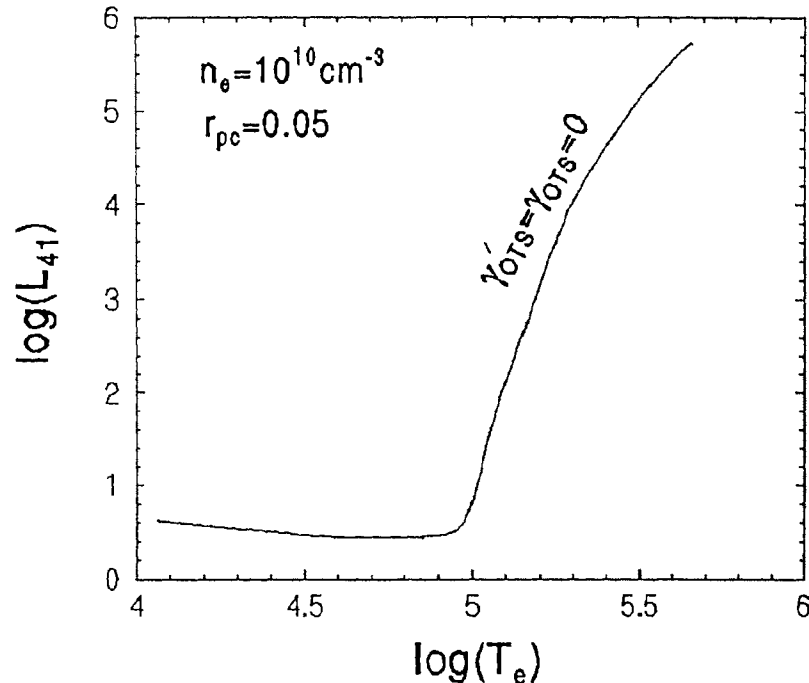


Fig. 4.17 Variation of threshold L_{41} with T_e .

4.2.5 Comparisons between PDI-I, II, III and OTS

Fig. 4.18 shows the frequencies and growth rates of ion-acoustic and reactive quasi-ion modes as functions of T_e . Here we define $T_e = T_{ec}$ and correspondingly $D = D_c$ (Fig. 4.3) at the point where γ_1 crosses ω_s . At this point the ion-acoustic mode loses its linearity. For $T_e < T_{ec}$ the imaginary part of ω crosses its real part at $T_e = T_{et}$ and $D = D_t$ (Fig. 4.3). In Fig. 4.18 the range $T_e > T_{ec}$ represents the region of PDI-I while $T_e < T_{et}$ represents the region of PDI-II. The range $T_{et} \leq T_e \leq T_{ec}$ and $D_t \geq D \geq D_c$ represents the transition region in which the reactive quasi-ion mode changes into an ion-acoustic mode or vice versa (i.e., PDI-I to PDI-II or vice versa). Figs. 4.3 and 4.18 shows for 3C 273, $T_{ec} = 10^{5.1}$ K, $T_{et} = 10^{4.9}$ K, $D_c = 10^{3.2}$ and $D_t = 10^{4.8}$. Under the coherent pump approximation, the variation of growth

rates $\gamma_1, \gamma_2, \gamma_3$ and γ_{OTS} with respect to T_e are shown in Figs. 4.19 for 3C 273, 4.21 for 3C 48 and 4.23 for Crab Nebula. Similarly, using a broad pump of width $\delta\omega = \omega_o$, the variation of growth rate $\gamma'_1, \gamma'_2, \gamma'_3$ and γ'_{OTS} with respect to T_e are shown in Figs. 4.20 for 3C 273, 4.22 for 3C 48 and 4.24 for Crab Nebula. Even if we include a band width of order $\delta\omega = \omega_o$, growth rates are higher than ν_o for 3c 273 and 3C 48. Since the luminosity is low in Crab Nebula, growth rates with broad pump lie below ν_o .

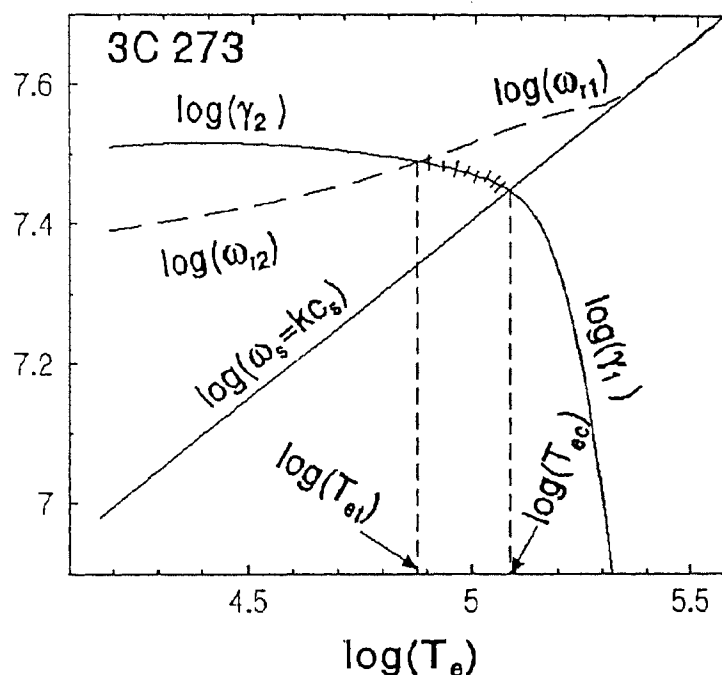


Fig. 4.18 Variation of real parts of the frequencies of the low frequency daughter mode ω_s, ω_{rj} and its growth rates γ_j ($j=1,2$) vs T_e in the 3C 273.

The variation of growth rates $\gamma_1, \gamma_2, \gamma_3$ and γ_{OTS} with respect to the luminosity of the pump are shown in the Fig. 4.25. Similarly, the variation of growth rate $\gamma'_1, \gamma'_2, \gamma'_3$ and γ'_{OTS} with the luminosity of a broad pump are shown in Fig. 4.26 The reactive quasi-ion mode is not excited in the Crab Nebula because radio luminosity is too low to cross the threshold luminosity $L_{41} = 1.1 \times 10^{-2}$, calculated using the parameters given in the Table 4.1 and 4.2.

The dependence of growth rates γ_1 , γ_2 , γ_3 and γ_{OTS} on monochromatic pump strength are shown in the Fig. 4.25. Similarly, Fig. 4.26 shows the variation of γ'_1 , γ'_2 , γ'_3 and γ'_{OTS} with respect to the strength of a broad pump. Fig. 4.27 shows the dependence of threshold luminosity on electron temperature T_e for all cases of PDI together with OTS. At $T_e < 10^{4.5}$ K the collisional damping operates and as the temperature goes up Landau damping takes over for $T_e > 10^{5.1}$ K. But in the range $10^{4.5}$ K $< T_e < 10^{5.1}$ K both collisional and Landau damping are small and therefore lower threshold luminosity is needed. Value of threshold luminosity required for the excitation of PDI-I is small compared to other three cases, see Fig. 4.27. The cross marked regions in Figs. 4.18, 4.19, 4.20, 4.21, and 4.22 represent transitions from PDI-I to PDI-II.

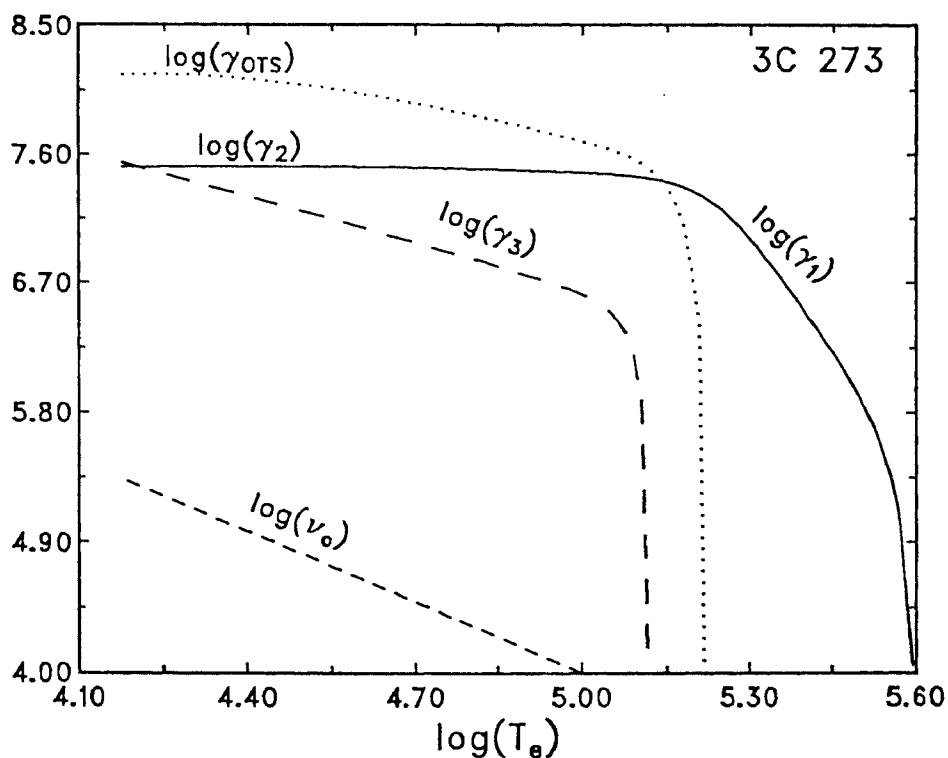


Fig. 4.19 Variation of growth rates γ_j ($j=1,2,3$ & OTS) vs T_e for a monochromatic pump at $\omega_o = 1.01\omega_{pe}$ in the 3C 273.

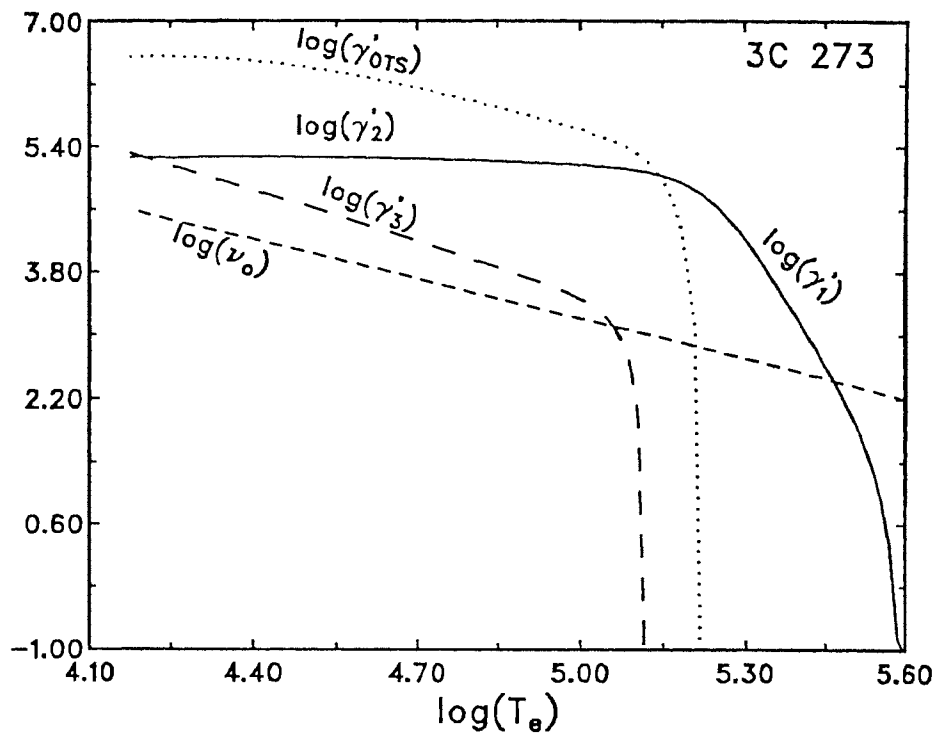


Fig. 4.20 Variation of γ'_j ($j=1,2,3$ & OTS) vs T_e using a broad pump in the 3C 273.

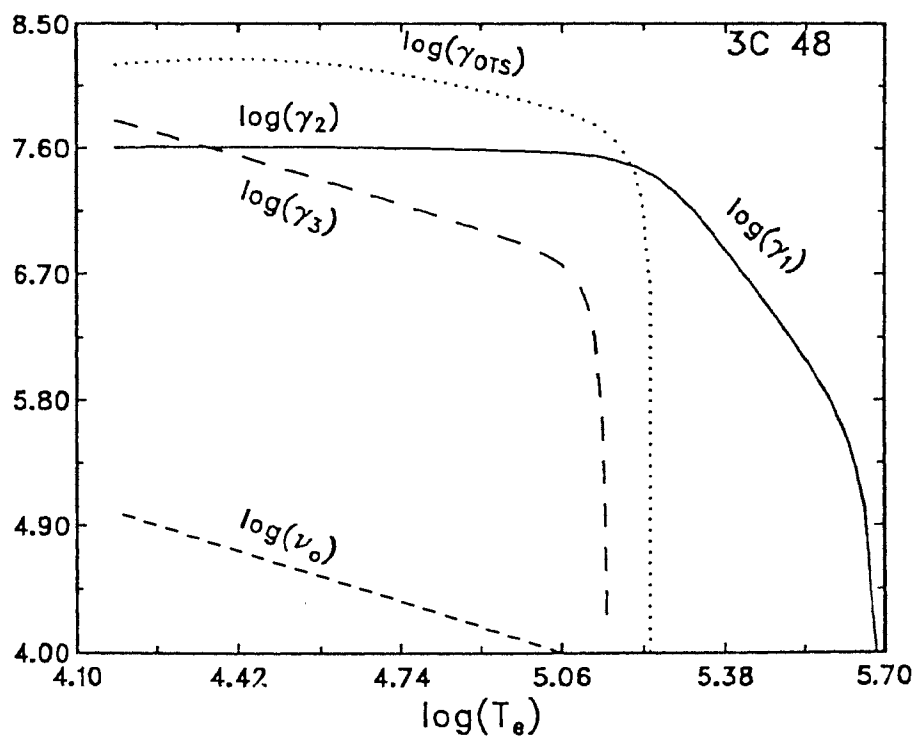


Fig. 4.21 Variation of growth rates γ_j ($j=1,2,3$ & OTS) vs T_e for a monochromatic pump at $\omega_o = 1.01\omega_{pe}$ in the 3C 48.

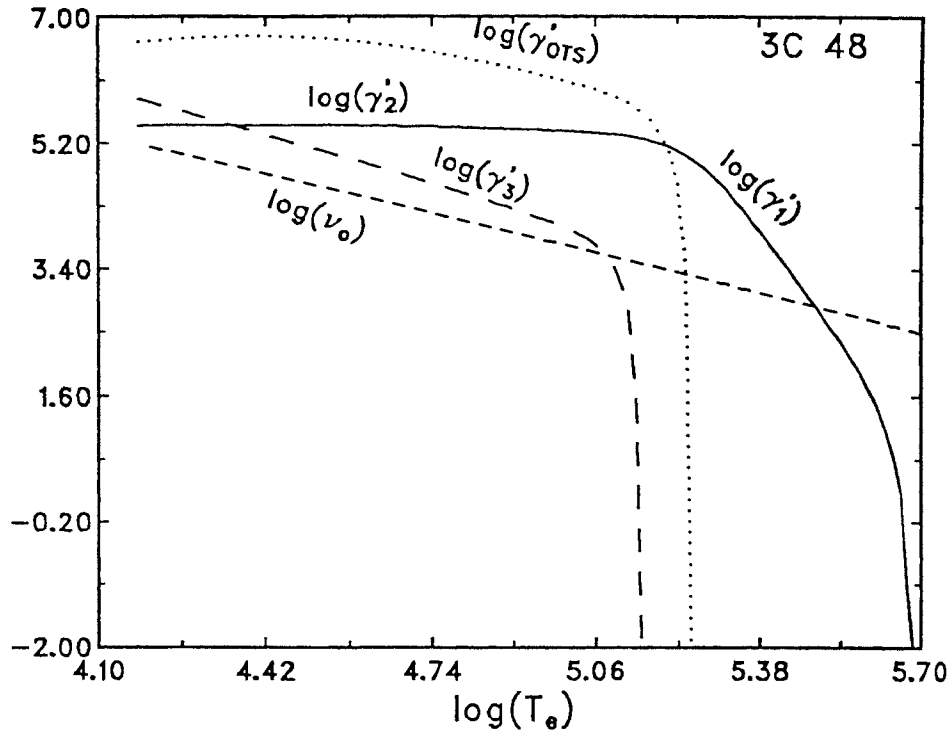


Fig. 4.22 Variation of γ'_j ($j=1,2,3$ & OTS) vs T_e using a broad pump of width $\Delta\omega = \omega_0$ in the 3C 48.

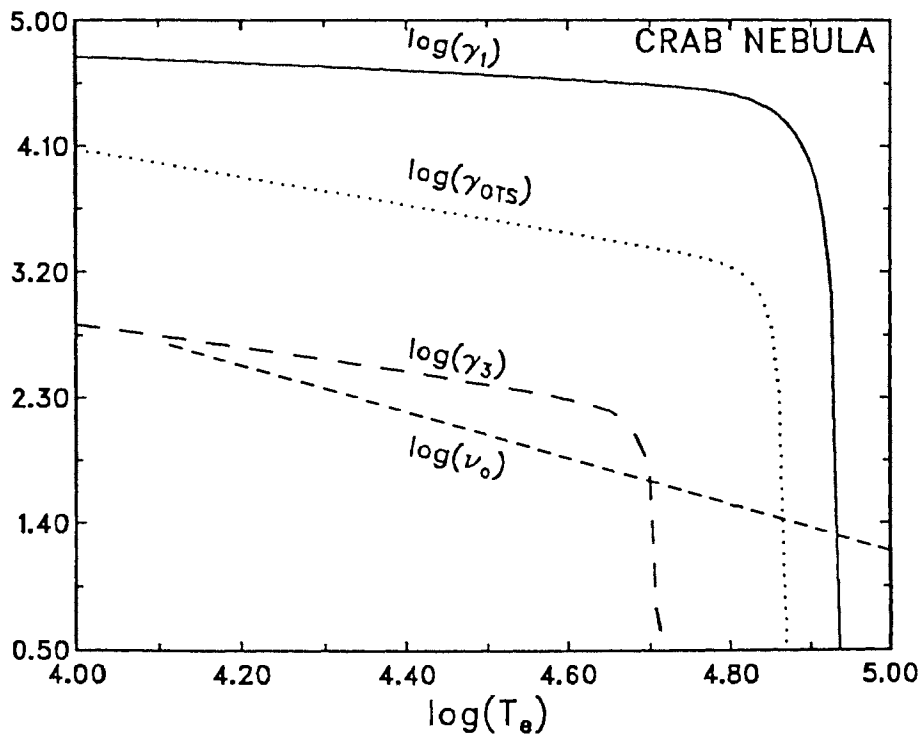


Fig. 4.23 Variation of growth rates γ_j ($j=1,3$ & OTS) vs T_e for a monochromatic pump at $\Delta\omega = 1.01\omega_{pe}$ in the Crab Nebula.

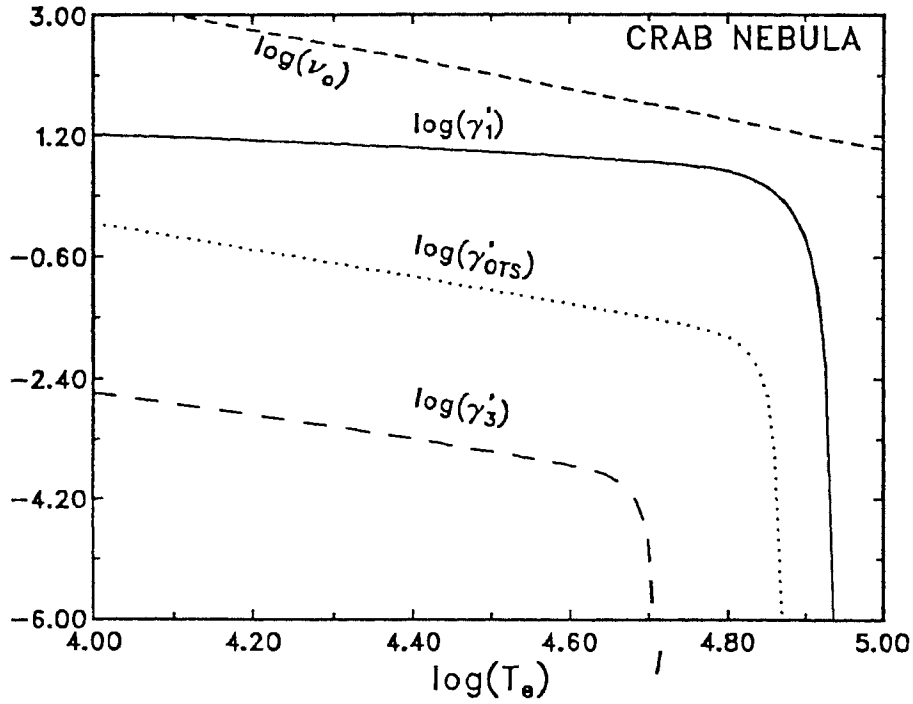


Fig. 4.24 Variation of γ_j ($j=1,3$ & OTS) vs T_e using a broad pump of width $\Delta\omega = \omega_{pe}$ in the Crab Nebula. Note that PDI-II is not excited and also collisional absorption is dominant.

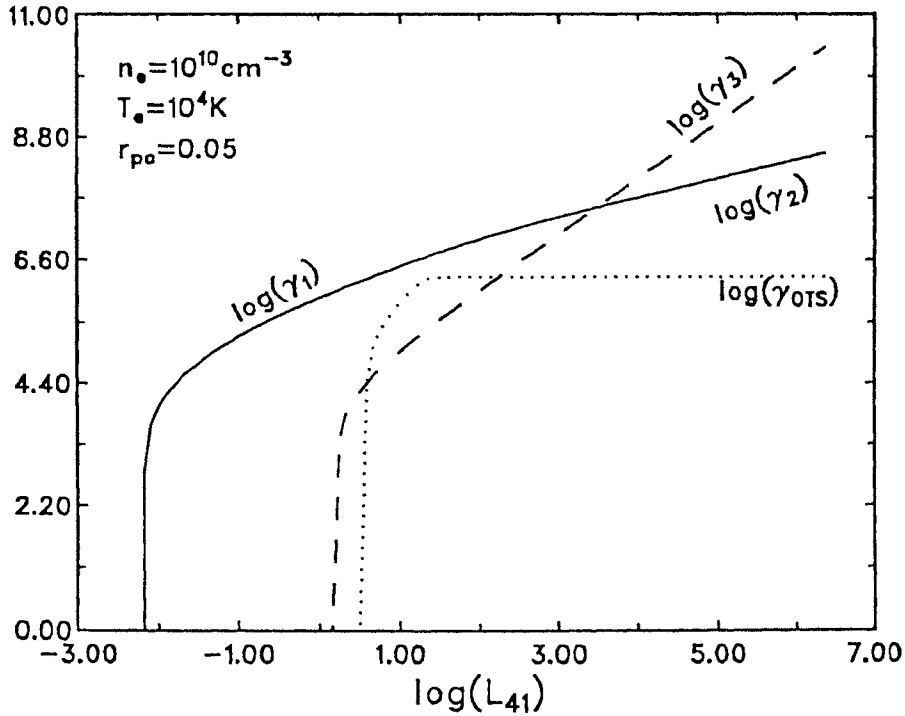


Fig. 4.25 Variation of growth rates γ_j ($j=1,2,3$ & OTS) vs pump luminosity L_{41} at $\omega_o = 1.01\omega_{pe}$.

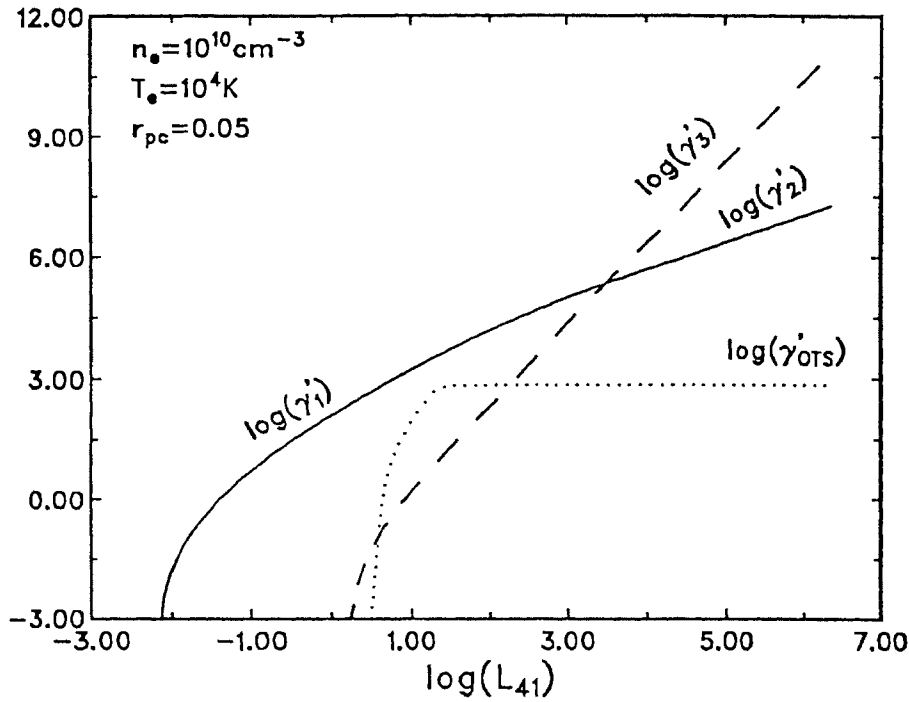


Fig. 4.26 Variation of γ'_j ($j=1,2,3$ & OTS) vs luminosity L_{41} of broad pump of width $\Delta\omega = \omega_o$.

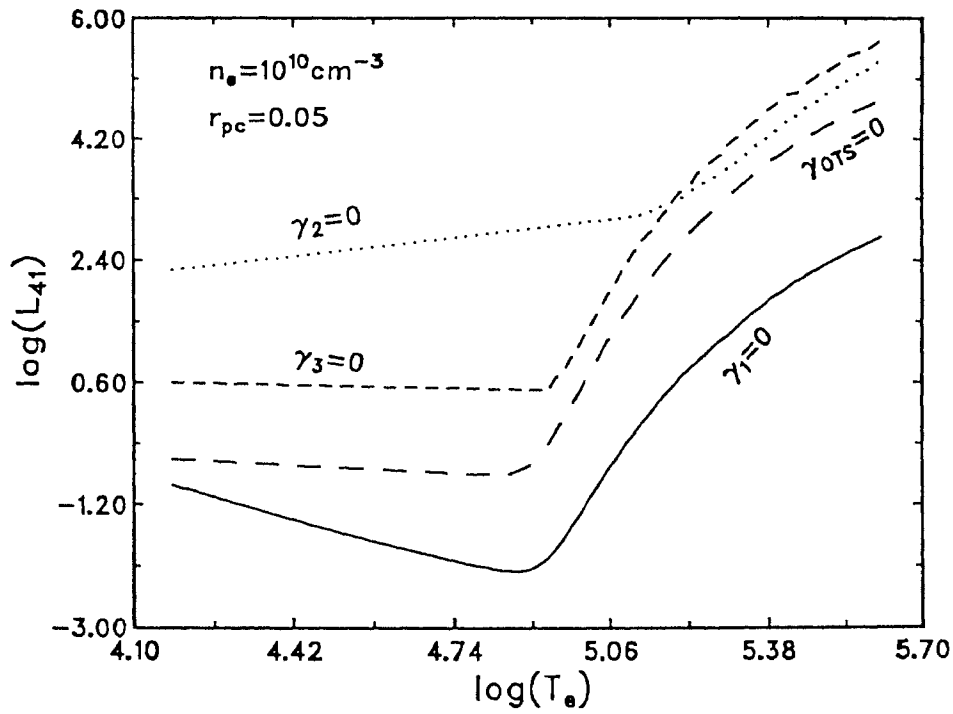


Fig. 4.27 Variation of threshold luminosity L_{41} vs T_e for the plasma parameters given in the figure. [Fluctuations in curves $\gamma_2 = 0$ & $\gamma_3 = 0$ are due to numerical effects].

4.3 FORMATION OF 21-CM ABSORPTION LINE IN THE EMISSION-LINE REGION

The 21-cm absorption line has been observed from several QSO systems. It is believed to originate in the neutral hydrogen clouds in the vicinity of the QSO. This absorption line can also originate when the radiation of frequency 1420 MHz (21-cm) drives the PDI in the plasma having electron plasma frequency close to 1420 MHz. This effect was first considered by Krishan(1988). This process has a line character in principle since it occurs only when a frequency matching condition is satisfied. The presence of 21-cm absorption line indicates that the electron density in the emission-line region must be $\sim 2.5 \times 10^{10} \text{ cm}^{-3}$, which falls within the range of the inferred densities for these regions. The 21-cm radiation luminosities in 3C 273 and 3C 48 are sufficient to drive PDI.

For comparison, the standard expression (Krishan 1988) for absorption rate for the spin flip transition is given by

$$K(\omega) = 2.58 \times 10^{-15} \frac{f(\omega)N}{T_K} \text{ cm}^{-1}, \quad (4.55)$$

where T_K is the temperature which characterizes the population distribution between the two atomic states, $f(\omega)$ is the line shape function normalized to unity and N is the number of hydrogen atoms/cm³. Using standard values of the different parameters we find absorption rate due to PDI in the ionized region is much larger than the absorption rate for the spin flip transition in the neutral hydrogen region.

4.4 CONCLUSION

- (i) An incident electromagnetic pump wave drives purely electrostatic oscillations at two frequencies close to ω_{pe} and ω_{pi} .
- (ii) A parametric amplification occurs for drive frequencies $\omega_o \geq \omega_{pe}$ and for driver amplitude exceeding a certain critical threshold.

- (iii) The growth rate of the instability is maximum for $\vec{k} \parallel \vec{E}_o$ and zero for $\vec{k} \perp \vec{E}_o$.
- (iv) For circularly polarized pumps the general picture remains unchanged, since growth rates are again determined by the component of \vec{E}_o parallel to \vec{k} .
- (v) The absorption rate of an electromagnetic wave depends on the ratio (L_{41}/r_{pc}^2) and it is much larger than the free-free absorption rate ν_o .
- (vi) Electron and ion temperatures increase by orders of magnitudes for moderate radio luminosities.

Compared to all other processes reviewed by Davidson and Netzer (1979), PDI is a faster process. The excited Langmuir wave will heat the plasma when it undergoes Landau damping. Apart from damping it can undergo many other processes: $\omega_e + \omega_e \rightarrow \omega'_o$, $\omega_e \rightarrow \omega'_e + \omega'_i$, etc. In the first process, two electron plasma waves combine together to produce an electromagnetic wave. In the second case, it drives PDI, and produce electron and ion-acoustic wave. Therefore, the incident electromagnetic energy can heat the plasma medium, as well as get reprocessed to other frequencies.

The growth rates indicate the rates at which the plasma medium and the radio radiation try to attain equilibrium with each other. The threshold condition (see equation (4.21) and Fig. 4.6) ensures those values of plasma parameters like density and temperature for which the fast process of PDI does not occur and the equilibrium is reached. Decay instability may be the mechanism for the formation of hot lower density corona adjoining each photoionized dense region. The dip in the spectrum of 3C 273 at 5.0×10^9 Hz (Cowsik and Lee, 1982) may be due to the anomalous absorption of radio waves through PDI. Since PDI is an efficient process, it must be included while accounting for the observed value of the radio luminosity which is less than that obtained by extrapolation from the high-frequency part of the spectrum.

References

- Andrew, B. H., Branson, N. J., & Wills, D., 1964, *Nature*, **203**, 171
- Collin-Souffrin, S. & Lasota, J. P., 1988, *Publ. astr. Soc. Pacific*, **100**, 1041
- Cowsik, R. & Lee, Y. C., 1982, *Proc. R. Soc. London Ser. A* **383**, 409
- Davidson, K., & Netzer, H., 1979, *Rev. Mod. Phys.*, **51**, 715
- Fried, D., & Conte, S. D., 1961, *The Plasma Dispersion Function*, (Academic Press, New York)
- Gangadhara, R. T., & Krishan, V., 1989, in *IAU Symp. 142: on Basic Plasma Processes on the Sun*, eds. E. R. Priest & Vinod Krishan, D. Reidel, Dordrecht, p 519
- Gangadhara, R. T., & Krishan, V., 1990, *J. Astrophys. Astr.*, **11**, 515
- Gangadhara, R. T., & Krishan, V., 1991, in *Meeting on Variability of Active Galactic Nuclei*, eds. D. Miller, & P. J. Wiita, Cambridge Univ. Press, p 190
- Ginzburg, V. L. & Zheleznyakov, V. V., 1959, Paris Symposium on *Radio Astronomy* (Stanford, California, Stanford University Press), p 574.
- Ginzburg, V. L., 1964, *The propagation of electromagnetic waves in Plasmas*, (London: Pergman Press).
- Ginzburg, V. L. & Ozernoy, L. M., 1966, *Astrophys. J.*, **144**, 599
- Hewish, A., & Okoye, S. E., 1965, *Nature*, **207**, 59.
- Krishan, V., 1987, *Mon. Not. R. astr. Soc.*, **226**, 629
- Krishan, V., 1988, *Mon. Not. R. astr. Soc.*, **231**, 353
- Krolik, J. H., McKee, C.F. & Tarter, C. B., 1978, in *BL Lacertae Objects*, ed. A. Wolfe, Univ. Pittsburgh, p 277
- Kruer, W. L., 1988, *The Physics of Laser-Plasma interactions*, Addison-Wesley, New York, p 70
- Kwan, J., & Krolik, J. H., 1981, *Astrophys. J.*, **278**, 558

- Lang, K. R., 1980, *Astrophysical formulae*, Springer-Verlag, Berlin, p 195.
- Liu, C. S., & Kaw, P. K., 1976, *Advances in Plasma Phys.*, ed. Simon, A., & Thompson, W. B., (Interscience New York), **6**, 83
- Lyne, A. G. & Graham-Smith, F., 1990, *Pulsar Astronomy*, (Cambridge Univ. Press), p 127.
- Wild, J. P., Smerd, S. F. & Weiss, A. A., 1963, *Ann. Rev. Astr. and Astrophys.*, **1**, 291.
- Zheleznyakov, V. V., 1964, *Radio wave emission from the Sun and Planets*, (Moscow: Nauka Publishing House).

Chapter 5

POLARIZATION CHANGES OF RADIATION THROUGH STIMULATED RAMAN SCATTERING

In this Chapter, change in the polarization of electromagnetic waves due to the stimulated Raman scattering in a plasma is studied. In this process an electromagnetic wave undergoes coherent scattering off an electron plasma wave. It is found that some of the observed polarization properties such as the rapid temporal variations, sense reversal, rotation of the plane of polarization and change of nature of polarization in the case of pulsars and quasars, could be accounted for through stimulated Raman scattering.

5.1 INTRODUCTION

By assuming a synchrotron origin for the radiation in compact extragalactic radio sources, source models are readily constructed which explain both the spectral and temporal behavior of intensity (e.g., van der Laan 1966; Blandford & Königl 1979), but polarization does not lend itself to such a straightforward explanation. The problems arise mainly from the observed ratio of circular to linear polarization; also, depolarization by a factor of 10 or more is often observed. It is important to determine whether this depolarization is a geometric effect or results from radiation-plasma interactions. There have only been very preliminary attempts to explain depolarization and microvariability using plasma mechanisms.

The change in polarization of an electromagnetic wave due to its propagation in a magnetized plasma as well as due to an electron scattering is well known. In a magnetized plasma, the Faraday rotation is recognized to be the most common cause of the rotation of the plane of polarization of an electromagnetic wave. In a plasma, the spectral components of radiation of finite band-width travel different path lengths and lead to depolarization. Any change in the direction of the magnetic field also manifests itself through polarization variation. The strong linear polarization observed in the radio as well as in the optical regions of the spectrum in the BL Lacertae objects is believed to originate in the source itself. The fact that optically violently variables and NGC 1275 show similar polarization characteristics, suggests that BL Lacs, quasars and Seyfert galaxies have a similar source of energy. If so, then the lack of polarization in quasars and Seyfert galaxies could be due to depolarization effects (Stockman 1978). The rotation of the electric vector has been observed in core-jet structure of 3C 454.3 (Cotton et al. 1984) and is interpreted to be due to the propagation of radiation in a medium of varying optical thickness.

A powerful collective emission occurs when relativistic electron beams with density ~ 1 per cent of the background plasma density, scatter off coherently from concentrations of electrostatic plasma waves (cavitons) (Benford 1992). The polarization of the emitted radiation depends on the orientation and the shape of cavitons. Assuming the usual power-law spectrum for electron energies, polarization features are found to mimic synchrotron radiation (Baker et al. 1988; Weatherall and Benford 1991).

In pulsars, the ambient magnetic field determines the orientation of the polarization ellipse, but with an ambiguity of $\pi/2$: the instantaneous angle often attains bimodal distribution with modes separated by $\sim \pi/2$. Modes are actually elliptically polarized such that one angle correlates with one sense of circular polarization, the orthogonal angle correlates with the other sense. Several pulsars exhibit one or more reversals of the sense of polarization through the profile. The appearance of strong circular polarization (some times > 50 per cent) implies conversion of the elliptically produced radiation some-where along the propagation path. Apart from the appearance of circular polarization, however, pulsar magnetospheres do not appear to be magnetoactive (no generalized Faraday rotation is evident) (Cordes 1983). For pulsars in which the integrated profile is highly polarized, essentially all subpulses must like wise be highly polarized and have stable polarization characteristics. However, many pulsars have rather weakly polarized integrated profiles. Three possible reasons for low polarization, apart from the Faraday rotation, electron scattering and magnetic field orientations, are that (Manchester & Taylor 1977) the subpulses at a given longitude may (1) be themselves weakly polarized; (2) be divisible into groups with orthogonal polarization; or (3) have randomly varying position angles and sense of circular polarization.

Collective plasma processes have been shown to play significant roles in the absorption and spectral modification of the radiation through its interaction with the plasma in the accretion disc and the emission line regions (Beal 1990; Krishan & Wiita 1990; Benford 1992; Gangadhara & Krishan 1990, 1992; Krishan & Gangadhara 1992). This chapter shows that in strong radio sources the rapid temporal variations, sense reversal of rotation of electric field, rotation of plane of polarization and change of nature of polarization in the case of quasars and pulsars, may be accounted for through stimulated Raman scattering (SRS). In this process, an intense electromagnetic wave scatters off an electron plasma wave resulting in the scattered electromagnetic wave. The physics of SRS in a plasma has been explained in many papers and books (e.g., Drake et al. 1974; Liu & Kaw 1976; Hasegawa 1978; Kruer 1988). The role of stimulated Compton and Raman scattering in the quasar continuum has been shown by Gangadhara & Krishan (1992). Polarization changes through SRS may take place in accretion disks, the emission line regions and the intercloud medium of active galactic nuclei and also in the emission region of pulsars (Gangadhara and Krishan 1993). In section 5.2, we derive the dispersion relation describing the SRS of an electromagnetic wave. In section 5.3, the polarization states of the incident and the scattered electromagnetic waves have been defined with stokes parameters. In section 5.4, we numerically solve the dispersion relation to find the value of the growth rate of the SRS instability (see Fig. 5.2). In section 5.5, we make a comparison between SRS and the well known process of the Faraday rotation. We investigate the condition under which (e.g., in Fig. 5.5, growth rate $\Gamma \approx 10^{-5} \text{ sec}^{-1}$) SRS dominates over the Faraday rotation. The effect of incoherence in the electromagnetic waves on SRS instability is discussed in section 5.6.

5.2 STIMULATED RAMAN SCATTERING

We begin with a model consisting of a pulsar with non-thermal component of radiation interacting with the plasma in the emission region at a distance $r = 100R_{NS} = 10^8$ cm (Neutron star radius $R_{NS} \approx 10$ km). In the case of a quasar, we consider a black hole surrounded by a plasma which extends to a few parsecs. The non-thermal continuum is considered as a pump which drives SRS. Here, we consider an electron-ion plasma with uniform and isotropic distribution of temperature and density, and assume that it is at rest with respect to the source of radiation.

Consider a large amplitude elliptically polarized electromagnetic wave,

$$\vec{E}_i = \epsilon_i [\cos(\vec{k}_i \cdot \vec{r} - \omega_i t) \hat{e}_1 + \alpha_i \cos(\vec{k}_i \cdot \vec{r} - \omega_i t + \delta_i) \hat{e}_2], \quad (5.1)$$

propagating in a plasma with density n_0 and temperature T_e .

We can think of \vec{E}_i as the superposition of two linearly polarized waves: $\vec{E}_{i1} = \epsilon_i \cos(\vec{k}_i \cdot \vec{r} - \omega_i t) \hat{e}_1$ and $\vec{E}_{i2} = \alpha_i \epsilon_i \cos(\vec{k}_i \cdot \vec{r} - \omega_i t + \delta_i) \hat{e}_2$. Let

$$\delta n_{e1} = \delta n_1 \cos(\vec{k} \cdot \vec{r} - \omega t) \quad (5.2)$$

and

$$\delta n_{e2} = \delta n_2 \cos(\vec{k} \cdot \vec{r} - \omega t + \delta_e), \quad (5.3)$$

be the density perturbations in a plasma with equilibrium density n_0 . Assume that δn_{e1} couples with \vec{E}_{i1} and δn_{e2} couples with \vec{E}_{i2} . The coupling between the radiation and the density perturbations is non-linear because of the ponderomotive force ($\propto \nabla E_{i1}^2$ and $\propto \nabla E_{i2}^2$). Consequently, density perturbations grow up and lead to currents at $(\vec{k}_i \pm \vec{k}, \omega_i \pm \omega)$. These currents will generate mixed electromagnetic-electrostatic side-band modes at $(\vec{k}_i \pm \vec{k}, \omega_i \pm \omega)$. The side-band modes, in turn,

interact with the incident wave field, producing a ponderomotive force which amplifies the original density perturbation. Thus, there is a positive feedback system which leads to an instability.

The electric field \vec{E}_s of the electromagnetic wave scattered through an angle ϕ_s with respect to \vec{k}_i can be written as

$$\vec{E}_s = \varepsilon_s [\cos(\vec{k}_s \cdot \vec{r} - \omega_s t) \hat{e}'_1 + \alpha_s \cos(\vec{k}_s \cdot \vec{r} - \omega_s t + \delta_s) \hat{e}'_2]. \quad (5.4)$$

Fig. 5.1 shows the directions of \vec{k}_i and \vec{k}_s in the orthogonal coordinate systems $(\hat{e}_1, \hat{e}_2, \hat{e}_3)$ and $(\hat{e}'_1, \hat{e}'_2, \hat{e}'_3)$. The coordinate system $(\hat{e}'_1, \hat{e}'_2, \hat{e}'_3)$ is rotated through an angle ϕ_s about an axis parallel to \hat{e}_2 . Here, $\vec{k}_i \parallel \hat{e}_3$, $\vec{k}_s \parallel \hat{e}'_3$ and $\hat{e}'_2 \parallel \hat{e}_2$.

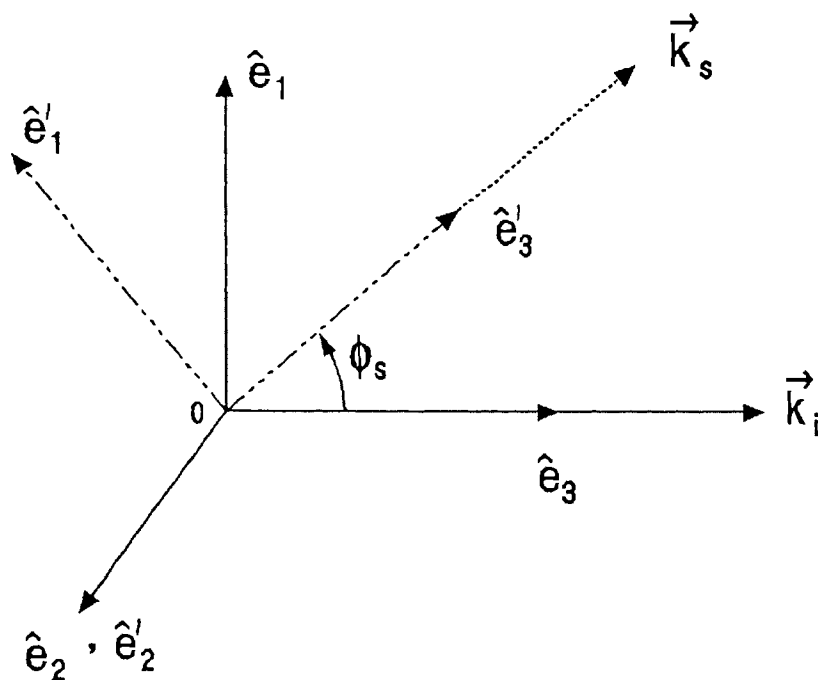


Fig. 5.1 The wave vectors and the electric fields of the incident and the scattered radiation.

The unit vectors are related by

$$\hat{e}'_1 = \cos(\phi_s)\hat{e}_1 - \sin(\phi_s)\hat{e}_3, \quad \hat{e}'_2 = \hat{e}_2, \quad \hat{e}'_3 = \sin(\phi_s)\hat{e}_1 + \cos(\phi_s)\hat{e}_3. \quad (5.5)$$

The scattered wave in the coordinate system $(\hat{e}_1, \hat{e}_2, \hat{e}_3)$ is given by

$$\vec{E}_s = \epsilon_s [\cos(\vec{k}_s \cdot \vec{r} - \omega_s t) \{ \cos(\phi_s)\hat{e}_1 - \sin(\phi_s)\hat{e}_3 \} + \alpha_s \cos(\vec{k}_s \cdot \vec{r} - \omega_s t + \delta_s)\hat{e}_2]. \quad (5.6)$$

The wave equation for the scattered the electromagnetic wave is given by

$$\left(\nabla^2 - \frac{1}{c^2} \frac{\partial^2}{\partial t^2} \right) \vec{E}_s = \frac{4\pi}{c^2} \frac{\partial \vec{J}}{\partial t}, \quad (5.7)$$

where c is the velocity of light and \vec{J} is the current density. The components of the current density are $J_1 = -en_{e1}u_{e1} = -e(n_0 + \delta n_{e1})u_{e1}$, $J_2 = -en_{e2}u_{e2} = -e(n_0 + \delta n_{e2})u_{e2}$ and $J_3 = -en_0u_{e3}$, where u_{e1} , u_{e2} and u_{e3} are the components of the oscillation velocity \vec{u}_e of electrons in the radiation fields \vec{E}_i and \vec{E}_s . We obtain \vec{u}_e from the equation:

$$\frac{\partial \vec{u}_e}{\partial t} = -\frac{e}{m_0} [\vec{E}_i + \vec{E}_s], \quad (5.8)$$

where e and m_0 are the charge and the rest mass of an electron.

In SRS, the scattered radiation consists of the stokes mode (\vec{k}_-, ω_-) and the anti-stokes mode (\vec{k}_+, ω_+) with electric fields

$$\vec{E}_\pm = \epsilon_\pm [\cos(\vec{k}_\pm \cdot \vec{r} - \omega_\pm t) \{ \cos(\phi_\pm)\hat{e}_1 - \sin(\phi_\pm)\hat{e}_3 \} + \alpha_\pm \cos(\vec{k}_\pm \cdot \vec{r} - \omega_\pm t + \delta_\pm)\hat{e}_2]. \quad (5.9)$$

Now, separating the components of equation (5.7), we have

$$D_\pm E_{\pm 1} = -\frac{2\pi e^2}{m_0} \epsilon_i \delta n_1 \left[\frac{\omega_-}{\omega_i} \cos(\vec{k}_- \cdot \vec{r} - \omega_- t) + \frac{\omega_+}{\omega_i} \cos(\vec{k}_+ \cdot \vec{r} - \omega_+ t) \right] \quad (5.10)$$

and

$$D_\pm E_{\pm 2} = -\frac{2\pi e^2}{m_0} \alpha_i \epsilon_i \delta n_2 \left[\frac{\omega_-}{\omega_i} \cos(\vec{k}_- \cdot \vec{r} - \omega_- t + \delta_i - \delta_e) + \frac{\omega_+}{\omega_i} \cos(\vec{k}_+ \cdot \vec{r} - \omega_+ t + \delta_i + \delta_e) \right], \quad (5.11)$$

and

$$D_{\pm}E_{\pm 3} = 0, \quad (5.12)$$

where $E_{\pm 1} = \varepsilon_{\pm} \cos(\phi_{\pm}) \cos(\vec{k}_{\pm} \cdot \vec{r} - \omega_{\pm}t)$, $E_{\pm 2} = \alpha_{\pm} \varepsilon_{\pm} \cos(\vec{k}_{\pm} \cdot \vec{r} - \omega_{\pm}t + \delta_{\pm})$, $E_{\pm 3} = -\varepsilon_{\pm} \sin(\phi_{\pm}) \cos(\vec{k}_{\pm} \cdot \vec{r} - \omega_{\pm}t)$, $\omega_{\pm} = \omega_i \pm \omega$, $\vec{k}_{\pm} = \vec{k}_i \pm \vec{k}$ and $D_{\pm} = k_{\pm}^2 c^2 - \omega_{\pm}^2 + \omega_{pe}^2$. Here, $\omega_{pe} = (4\pi n_0 e^2 / m_0)^{1/2}$ is the plasma frequency. Equation (5.12) restricts the value of ϕ_{\pm} to 0 or π for $\varepsilon_{\pm} \neq 0$ and $D_{\pm} \neq 0$.

Expressions $D_{\pm} = 0$ are the dispersion relations for the stokes mode (\vec{k}_-, ω_-) and the anti-stokes mode (\vec{k}_+, ω_+) , when the following resonant conditions are satisfied:

$$\begin{aligned} \omega_i - \omega &= \omega_-, & \vec{k}_i - \vec{k} &= \vec{k}_-, \\ \omega_i + \omega &= \omega_+, & \vec{k}_i + \vec{k} &= \vec{k}_+. \end{aligned} \quad (5.13)$$

Multiplying equation (5.10) on both sides by $\cos(\vec{k}_i \cdot \vec{r} - \omega_i t)$ and neglecting the terms containing $(2\vec{k}_i, 2\omega_i)$ as being non-resonant, we get

$$D_{\pm} \varepsilon_{\pm} \cos(\phi_{\pm}) = -\frac{4\pi e^2}{m_0} \varepsilon_i \delta n_1. \quad (5.14)$$

Similarly, if we multiply equation (5.11) by $\cos(\vec{k}_i \cdot \vec{r} - \omega_i t + \delta_i)$, we obtain

$$D_{\pm} \alpha_{\pm} \varepsilon_{\pm} \cos[\vec{k} \cdot \vec{r} - \omega t \pm (\delta_{\pm} - \delta_i)] = -\frac{4\pi e^2}{m_0} \alpha_i \varepsilon_i \delta n_2 \cos(\vec{k} \cdot \vec{r} - \omega t + \delta_e). \quad (5.15)$$

Similar to equations (5.13), it gives following conditions between the phases

$$\delta_{\pm} = \delta_i \pm \delta_e. \quad (5.16)$$

Dividing equation (5.15) by equation (5.14), we have

$$\alpha_{\pm} = \alpha_i \frac{\delta n_2}{\delta n_1} \cos(\phi_{\pm}) = \alpha_i R \cos(\phi_{\pm}), \quad (5.17)$$

where $R = \delta n_2 / \delta n_1$. The value of R is related to \vec{E}_i : δn_{e1} couples with \vec{E}_{i1} and δn_{e2} couples with \vec{E}_{i2} . In the linear theory, it is not possible to determine R , but one expects that it may not differ too much from the value of α_i .

If we multiply equation (5.14) by ε_i and equation (5.15) by $\alpha_i\varepsilon_i$, and subtract, we find

$$(\alpha_i\alpha_{\pm} - \cos\phi_{\pm})\varepsilon_{\pm} = \frac{4\pi e^2}{m_0}\varepsilon_i(1 - \alpha_i^2 R)\frac{\delta n_i}{D_{\pm}}. \quad (5.18)$$

Now, we have to determine the electron density perturbations δn_1 and δn_2 . Here, we neglect the ions response because of their larger mass compared to that of the electrons. With the inclusion of the ponderomotive force, as a driving force, the Vlasov equation for the low frequency response of electrons can then be written as

$$\frac{\partial f}{\partial t} + \vec{v}\cdot\nabla f + \frac{1}{m_0}(e\nabla\phi - \nabla\psi)\cdot\frac{\partial f}{\partial\vec{v}} = 0, \quad (5.19)$$

where $\phi(\vec{r}, t)$ is the scalar potential associated with the electrostatic waves, $f(\vec{r}, \vec{v}, t)$, is the particle distribution function and $\psi(\vec{r}, t)$ is the ponderomotive potential.

Linearizing equation (5.19) with $f(\vec{r}, \vec{v}, t) = f_0(\vec{v}) + \delta f_{e1}(\vec{r}, \vec{v}, t) + \delta f_{e2}(\vec{r}, \vec{v}, t)$, we get

$$\frac{\partial(\delta f_{e1})}{\partial t} + \frac{\partial(\delta f_{e2})}{\partial t} + \vec{v}\cdot\nabla(\delta f_{e1}) + \vec{v}\cdot\nabla(\delta f_{e2}) + \frac{1}{m_0}(e\nabla\phi - \nabla\psi)\cdot\frac{\partial f_0}{\partial\vec{v}} = 0, \quad (5.20)$$

where $\delta f_{e1} = \delta f_1 \cos(\vec{k}\cdot\vec{r} - \omega t)$ and $\delta f_{e2} = \delta f_2 \cos(\vec{k}\cdot\vec{r} - \omega t + \delta_e)$. The ponderomotive force of the radiation field is given by $\vec{F}_{\omega} = -\nabla\psi$. It depends quadratically on the amplitude and leads to a slowly varying longitudinal field, corresponding physically to radiation pressure, which leads to slow longitudinal motions and modifies the density. The ponderomotive potential is given by:

$$\begin{aligned} \psi &= \frac{e^2}{2m_0} \left\langle \left(\operatorname{Re} \left[\frac{\vec{E}_i}{i\omega_i} + \frac{\vec{E}_-}{i\omega_-} + \frac{\vec{E}_+}{i\omega_+} \right] \right)^2 \right\rangle_{\omega} \\ &= \frac{e^2}{2m_0\omega_i^2} [\varepsilon_i\varepsilon_- \cos(\phi_-) \cos(\vec{k}\cdot\vec{r} - \omega t) + \alpha_i\alpha_- \varepsilon_i\varepsilon_- \cos(\vec{k}\cdot\vec{r} - \omega t + \delta_i - \delta_-) + \\ &\quad \varepsilon_i\varepsilon_+ \cos(\phi_+) \cos(\vec{k}\cdot\vec{r} - \omega t) + \alpha_i\alpha_+ \varepsilon_i\varepsilon_+ \cos(\vec{k}\cdot\vec{r} - \omega t + \delta_+ - \delta_i)]. \end{aligned} \quad (5.21)$$

The angular bracket $\langle \rangle_{\omega}$ represents the ω frequency component of an average over the fast time scale ($\omega_i \gg \omega$).

To determine ϕ self-consistently we use Poisson equation, which gives

$$\phi = -\frac{4\pi e}{k^2}(\delta n_{e1} + \delta n_{e2}). \quad (5.22)$$

Now, substituting the expressions for δf_{e1} , δf_{e2} , δn_{e1} , δn_{e2} , ϕ and ψ into equation (5.20), we have

$$\begin{aligned} & \delta f_2 + \mu \delta f_1 + \frac{4\pi e^2}{m_0 k^2} \left[\delta n_2 + \mu \delta n_1 + \frac{k^2}{8\pi m_0 \omega_i^2} \left\{ \varepsilon_i \varepsilon_- \cos(\phi_-) \mu + \varepsilon_i \varepsilon_+ \cos(\phi_+) \mu + \right. \right. \\ & \left. \left. \alpha_i \alpha_- \varepsilon_i \varepsilon_- \frac{\sin(\vec{k} \cdot \vec{r} - \omega t + \delta_i - \delta_-)}{\sin(\vec{k} \cdot \vec{r} - \omega t + \delta_e)} + \alpha_i \alpha_+ \varepsilon_i \varepsilon_+ \frac{\sin(\vec{k} \cdot \vec{r} - \omega t + \delta_+ - \delta_i)}{\sin(\vec{k} \cdot \vec{r} - \omega t + \delta_e)} \right\} \right] \times \\ & \frac{\vec{k} \cdot \frac{\partial f_0}{\partial \vec{v}}}{(\omega - \vec{k} \cdot \vec{v})} = 0, \end{aligned} \quad (5.23)$$

where $\mu = \sin(\vec{k} \cdot \vec{r} - \omega t) / \sin(\vec{k} \cdot \vec{r} - \omega t + \delta_e)$.

Equation (5.23) shows that $\delta_{\pm} = \delta_i \pm \delta_e$ and $\delta_e = 0$ or π . We obtain, for $\delta_e = \pi$,

$$\delta f_2 - \delta f_1 = -\frac{4\pi e^2}{m_0 k^2} \left[\delta n_2 - \delta n_1 + \frac{k^2}{8\pi m_0 \omega_i^2} A \right] \frac{\vec{k} \cdot \frac{\partial f_0}{\partial \vec{v}}}{(\omega - \vec{k} \cdot \vec{v})}, \quad (5.24)$$

where $A = (\alpha_i \alpha_- - \cos \phi_-) \varepsilon_i \varepsilon_- + (\alpha_i \alpha_+ - \cos \phi_+) \varepsilon_i \varepsilon_+$. The difference in the density perturbations ($\delta n_2 - \delta n_1$) is given by

$$\begin{aligned} \delta n_2 - \delta n_1 &= \int_{-\infty}^{\infty} n_0 (\delta f_2 - \delta f_1) d\vec{v} \\ &= - \left[\delta n_2 - \delta n_1 + \frac{k^2}{8\pi m_0 \omega_i^2} A \right] \chi_e, \end{aligned} \quad (5.25)$$

where

$$\chi_e = \frac{\omega_{pe}^2}{k^2} \int_{-\infty}^{\infty} \frac{\vec{k} \cdot \frac{\partial f_0}{\partial \vec{v}}}{(\omega - \vec{k} \cdot \vec{v})} d\vec{v}, \quad (5.26)$$

is the electron susceptibility function (Liu and Kaw 1976; Fried and Conte 1961).

Since $R = \delta n_2 / \delta n_1$, from equation (5.25) we have

$$\left(1 + \frac{1}{\chi_e} \right) (1 - R) \delta n_1 = \frac{k^2}{8\pi m_0 \omega_i^2} A. \quad (5.27)$$

Substituting equation (5.27) for δn_1 into equation (5.18), we obtain

$$\left(1 + \frac{1}{\chi_e}\right)(1 - R) = \frac{v_0^2 k^2 (1 - R\alpha_i^2)}{2(1 + \alpha_i^2)} \left(\frac{1}{D_-} + \frac{1}{D_+}\right), \quad (5.28)$$

where $v_0 = e\epsilon_i\sqrt{1 + \alpha_i^2}/m_0\omega_i$ is the quiver velocity of electrons in the field of incident electromagnetic wave. The energy density of the incident field and the luminosity L of the source are related by

$$\frac{1}{8\pi}\epsilon_i^2(1 + \alpha_i^2) = \frac{L}{4\pi r^2 c}, \quad (5.29)$$

where r is the distance between source of radiation and plasma. Therefore, the quiver velocity of electrons is given by

$$v_0 = \frac{e}{m_0} \left(\frac{2L}{r^2 c}\right)^{1/2} \frac{1}{\omega_i}. \quad (5.30)$$

Equation (5.28) is the plasma dispersion relation describing the SRS of elliptically polarized electromagnetic wave. The SRS instability resonantly excites only when the frequency and wave number matching conditions (see equation 5.13) are satisfied. The simplest stimulated scattering process is the one involving only one high-frequency sideband, i.e., the stokes component (\vec{k}_-, ω_-) . Thus, we consider a case where $D_- \approx 0$ and $D_+ \neq 0$, i.e., the anti-stokes component (\vec{k}_+, ω_+) is non-resonant. This approximation is justified as long as $\omega \ll (c^2 \vec{k}_i \cdot \vec{k}/\omega_i)$; it breaks down for very small \vec{k} (i.e., for long wavelength electrostatic perturbations) or if \vec{k} is nearly perpendicular to \vec{k}_i .

The value of k is approximately $2k_i$, corresponding to backward scattering ($\phi_- = \pi$) and for forward scattering ($\phi_- = 0$) it is approximately ω_{pe}/c . Thus, the growth rate of the instability attains its maximum value for backscatter. For the case of backscattering, $D_-(\vec{k}_-, \omega_-) \approx 2\omega_i(\omega - c^2 \vec{k}_i \cdot \vec{k}/\omega_i + c^2 k^2/2\omega_i) \approx 0$ for $\omega_i \gg \omega$. The dispersion relation for primarily backscatter is, therefore,

$$\left(1 + \frac{1}{\chi_e}\right)(1 - R) = \frac{1}{4} \frac{v_0^2 k^2}{\omega_i(\omega - \Delta)} \frac{(1 - R\alpha_i^2)}{(1 + \alpha_i^2)}, \quad (5.31)$$

where

$$\Delta = \vec{k} \cdot \vec{v}_g - \frac{k^2 c^2}{2\omega_i} \quad (5.32)$$

with $\vec{v}_g = \vec{k}_i c^2 / \omega_i$. From the equation (5.31), we can derive the threshold and the growth rate for the SRS instability. For $\omega^2 \approx \omega_c^2 = \omega_{pe}^2 + (3/2)k^2 v_T^2$, the natural frequency of the plasma wave and $\omega_-^2 \approx \omega_{pe}^2 + c^2(\vec{k}_i - \vec{k})^2$, equation (5.31) can be written as

$$(\omega - \omega_e + i\Gamma_e)(\omega - \omega_c + i\Gamma_-)(1 - R) = -\frac{v_0^2 k^2 \omega_{pe}}{8\omega_i} \frac{(1 - R\alpha_i^2)}{(1 + \alpha_i^2)}, \quad (5.33)$$

where

$$\Gamma_e = \frac{\sqrt{\pi}}{2} \frac{\omega_{pe}}{(k\lambda_{De})^3} \exp\left[-\frac{1}{2(k\lambda_{De})^2} - \frac{3}{2}\right] + \nu_e \quad (5.34)$$

is the damping rate of the electron plasma wave, $\nu_e = 3.632n_e \ln \Lambda / T_e^{3/2}$ is the electron collision frequency and Coulomb logarithm $\ln \Lambda \approx 10$. Here, $\Gamma = \omega_{pe}^2 \nu_e / 2\omega^2$ is the collisional damping rate of the scattered electromagnetic wave. Setting $\omega = \omega_c + i\Gamma$, and solving equation (5.33) for the growth rate Γ , we find

$$\Gamma = -\frac{1}{2}(\Gamma_e + \Gamma_-) \pm \frac{1}{2} \sqrt{(\Gamma_e - \Gamma_-)^2 + \frac{v_0^2 k^2 \omega_{pe}}{2\omega_i(1 + \alpha_i^2)} \frac{(1 - R\alpha_i^2)}{(1 - R)}}. \quad (5.35)$$

Setting $\Gamma = 0$, we obtain the threshold condition for the excitation of Raman scattering;

$$\left(\frac{v_0}{c}\right)_{thr} = 2 \frac{\Gamma_e \Gamma_- (1 + \alpha_i^2)(1 - R)}{\omega_i \omega_{pe} (1 - R\alpha_i^2)}. \quad (5.36)$$

The growth rate just above the threshold is given by

$$\Gamma = \frac{v_0^2 k^2 \omega_{pe}}{8(\omega_i - \omega_{pe})\Gamma_e} \frac{(1 - R\alpha_i^2)}{(1 + \alpha_i^2)(1 - R)}, \quad (5.37)$$

which is proportional to E_i^2 . The maximum growth rate attainable for $\omega_{pe} > \Gamma > \Gamma_e$, on the other hand, is

$$\Gamma = \frac{v_0 k}{2} \sqrt{\frac{\omega_{pe}}{2(\omega_i - \omega_{pe})} \frac{(1 - R\alpha_i^2)}{(1 + \alpha_i^2)(1 - R)}}. \quad (5.38)$$

For $k \approx 2k_i$, equation (5.38) becomes

$$\Gamma = \frac{c\epsilon_i}{m_0c} \sqrt{\frac{\omega_{pe}(1 - R\alpha_i^2)}{2\omega_i(1 - R)}}. \quad (5.39)$$

We note that backscatter by plasma wave is possible only if $2k_i\lambda_{De} \ll 1$. For $k_i\lambda_{De}$ not too small, the stimulated Compton backward scattering due to the non-linear Landau damping of the beat mode by resonant electrons becomes important.

5.3 STOKES PARAMETERS

The polarization state of the incident radiation changes due to the stimulated Raman scattering in a plasma (see equations 5.1, 5.9, 5.16, with $\delta_e = 0$ or π). The stokes parameters for the incident and scattered electromagnetic waves (Rybicki & Lightman 1979) are:

$$I_j = \frac{c}{8\pi}(1 + \alpha_j^2)\epsilon_j^2 = \frac{c}{8\pi}\epsilon_j^2, \quad (5.40)$$

$$Q_j = \frac{(1 - \alpha_j^2)}{(1 + \alpha_j^2)}I_j, \quad (5.41)$$

$$U_j = \frac{2\alpha_j}{(1 + \alpha_j^2)}I_j \cos(\delta_j), \quad (5.42)$$

and

$$V_j = -\frac{2\alpha_j}{(1 + \alpha_j^2)}I_j \sin(\delta_j). \quad (5.43)$$

The sense of rotation of the electric field is given by

$$\sin(2\beta_j) = \frac{V_j}{I_j} = -\frac{2\alpha_j}{(1 + \alpha_j^2)}\sin(\delta_j). \quad (5.44)$$

The magnitudes of the principle axes of the ellipse are

$$a_j = I_j|\cos(\beta_j)| \quad \text{and} \quad b_j = I_j|\sin(\beta_j)|. \quad (5.45)$$

The orientation of the major axis of the ellipse relative to \hat{e}_1 axis, is given by

$$\tan(2\chi_j) = \frac{U_j}{Q_j} = \frac{2\alpha_j}{(1 - \alpha_j^2)} \cos(\delta_j). \quad (5.46)$$

Here, $j = i$ for incident and $-$ for scattered electromagnetic waves.

We use the relations $\delta_e = \pi$, $\delta_- = \delta_i - \delta_e$ and $\alpha_- = \alpha_i R$ to compute the stokes parameters for the scattered wave.

5.4 NUMERICAL SOLUTION OF EQUATION (5.28)

For a strongly damped electron plasma wave with $k_l \lambda_{De} \approx 0.4$, it is not possible to expand $\chi_e(\omega, k)$ in to an asymptotic series. The regime $k_l \lambda_{De} \approx 0.4$ corresponds to the transition region between SRS and stimulated Compton scattering (SCS) (Gangadhara & Krishan 1992). Therefore, using $\omega = \omega_e + i\Gamma$, we numerically solve equation (5.28) including all the damping effects.

5.4.1 In pulsars

The typical values of the plasma and radiation parameters at a distance $r = 100R_{NS} = 10^8$ cm, (Neutron star radius $R_{NS} \approx 10$ km), in a pulsar are electron density $n_e = n_8 \times 10^8$ cm $^{-3}$, temperature $T_e = T_5 \times 10^5$ K and luminosity $L = L_{30} \times 10^{30}$ erg/sec in the band $\Delta\nu < \nu = 600$ MHz (Gangadhara, Krishan & Shukla 1992).

Fig. 5.2 shows the e-folding time $t_e = 1/\Gamma$ as a function of ω_i/ω_{pe} at the different values of electron temperature T_e ($= 10^5, 5 \times 10^5, 10^6$, and 7.5×10^6 K) for forward SRS of the incident wave. The frequency of the scattered electromagnetic wave is $\omega_- = \omega_i + \omega_e$. One recalls that at high temperatures an electron plasma wave experiences a small collisional damping but large Landau damping. The rather fast rise in t_e is obtained in the SCS regime ($k_e \lambda_{De} \geq 0.4$). The points indicated by

C correspond to $k_e \lambda_{De} \approx 0.4$ and represent the change of scattering process from Raman to Compton.

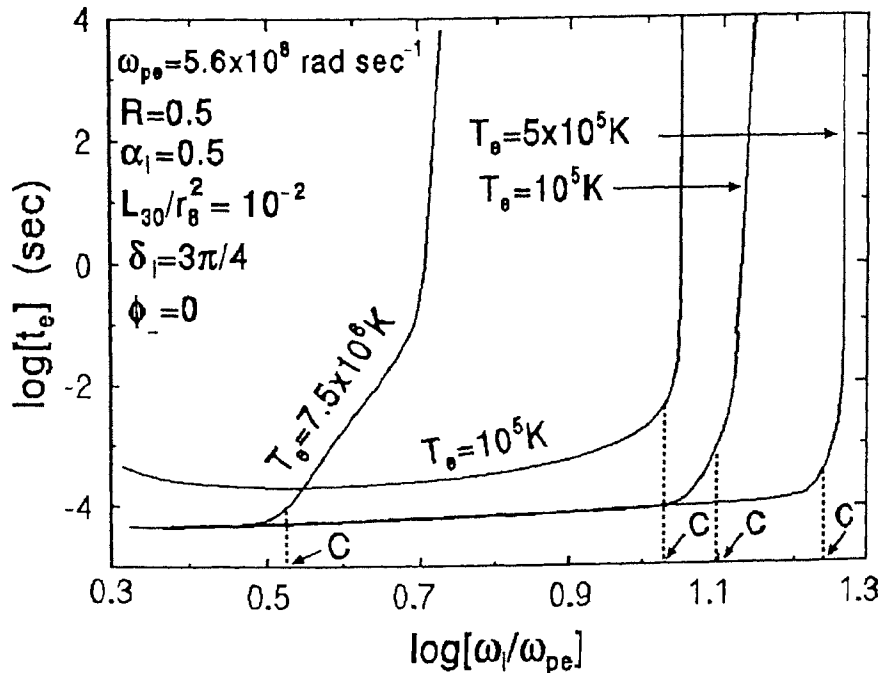


Fig. 5.2 The e-folding time $t_e = 1/\Gamma$ versus the normalized frequency (ω_i/ω_{pe}) . The points C represent the transition between SRS and SCS, where $k_l \lambda_{De} \approx 0.4$. At lower values of (ω_i/ω_{pe}) SRS occurs while at higher values SCS occurs.

We know from the observations of pulsar PSR 1133+16 by Cordes (1983) that flux $I_i = 10^{-20} \text{ erg cm}^{-2} \text{ sec}^{-1} \text{ Hz}^{-1}$ at the radio frequency $\nu_i = 600 \text{ MHz}$. To find the relation between the incident flux I_i and the scattered flux I_- we use condition for conservation of wave-energy within the systems of waves, the Manley-Rowe relation (Weiland & Wilhelmsson 1977), given by

$$\frac{I_i}{\omega_i} = \frac{I_-}{\omega_-}. \quad (5.47)$$

It gives

$$I_- = \left(1 - \frac{\omega}{\omega_i}\right) I_i. \quad (5.48)$$

For $\omega \approx \omega_{pe}$ and $\omega_i = 2.5\omega_{pe}$, we get $I_- = 0.6I_i$.

The sense of rotation and the orientation of the ellipses of the incident and the forward scattered electromagnetic waves are shown in Fig. 5.3.

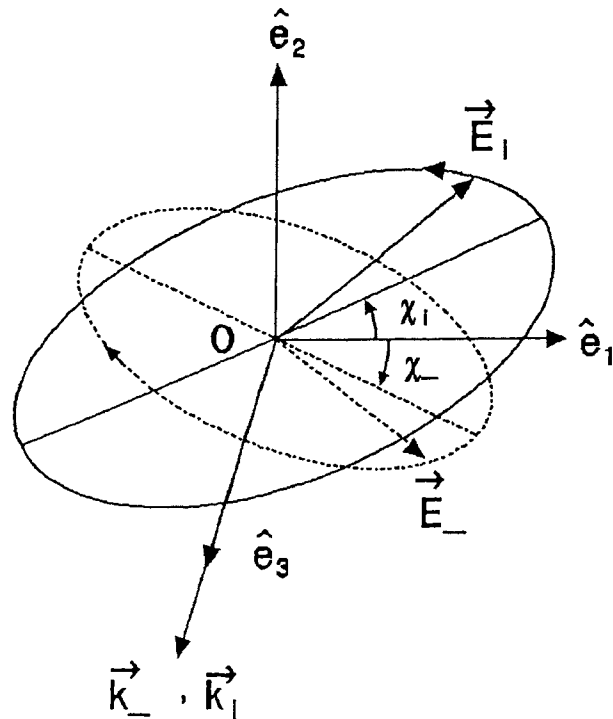


Fig. 5.3 The ellipses of the electric fields of the incident and forward scattered electromagnetic waves.

In Table 5.1, the values of stokes parameters for the incident and the forward scattered electromagnetic waves in a pulsar PSR 1133+16 are listed. It shows that: (1) a linearly polarized incident electromagnetic wave ($\delta_i = \pi, \alpha_i = 0.5$) scatters into another linearly polarized electromagnetic wave with its plane of polarization rotated through an angle χ_s with respect to \hat{e}_1 axis (see Fig. 5.3); (2) a elliptically polarized incident wave with counterclockwise sense ($\delta_i = 3\pi/4, \alpha_i = 1$) scatters into (i) a linearly polarized wave when $R = 0$, (ii) elliptically polarized waves with clockwise sense with major axis rotated thorough an angle χ_s when $R = 0.4, 0.8 \& 1.2$; (3) a circularly polarized incident wave with counterclockwise sense

TABLE 5.1

STOKES PARAMETERS OF THE INCIDENT AND FORWARD SCATTERED EM WAVES
FOR PSR 1133+16

Parameters (erg cm ⁻² sec ⁻¹ Hz ⁻¹)	Incident wave $\delta_i = \pi, \alpha_i = 0.5$		Scattered wave $\delta_- = 0$		
		R=0	R=0.4	R=0.8	R=1.2
I	1.0000E-20	6.0000E-21	6.0000E-21	6.0000E-21	6.0000E-21
Q	6.0000E-21	6.0000E-21	5.5385E-21	4.3448E-21	2.8235E-21
U	-8.0000E-21	0.0	2.3077E-21	4.1379E-21	5.2941E-21
V	0.0	0.0	0.0	0.0	0.0
χ (rad)	-0.4636	0.0	0.1974	0.3805	0.5404
a	1.0000E-20	6.0000E-21	6.0000E-21	6.0000E-21	6.0000E-21
b	0.0	0.0	0.0	0.0	0.0
Sense of rotation
Nature	linear	linear	linear	linear	linear

Parameters (erg cm ⁻² sec ⁻¹ Hz ⁻¹)	Incident wave $\delta_i = 3\pi/4, \alpha_i = 1$		Scattered wave $\delta_- = -\pi/4$		
		R=0	R=0.4	R=0.8	R=1.2
I	1.0000E-20	6.0000E-21	6.0000E-21	6.0000E-21	6.0000E-21
Q	0.0	6.0000E-21	4.3448E-21	1.3171E-21	-1.0820E-21
U	-7.0711E-21	0.0	2.9260E-21	4.1392E-21	4.1731E-21
V	-7.0711E-21	0.0	2.9260E-21	4.1392E-21	4.1731E-21
χ (rad)	...	0.0	0.2963	0.6314	-0.6586
a	9.239E-21	6.0000E-21	5.8064E-21	5.5705E-21	5.5618E-21
b	3.8268E-21	0.0	1.5118E-21	2.2291E-21	2.2510E-21
Sense of rotation	counter-clockwise	...	clockwise	clockwise	clockwise
Nature	elliptical	linear	elliptical	elliptical	elliptical

Parameters (erg cm ⁻² sec ⁻¹ Hz ⁻¹)	Incident wave $\delta_i = \pi/2, \alpha_i = 1$		Scattered wave $\delta_- = -\pi/2$		
		R=0	R=0.4	R=0.8	R=1
I	1.0000E-20	6.0000E-21	6.0000E-21	6.0000E-21	6.0000E-21
Q	0.0	6.0000E-21	4.3448E-21	1.3171E-21	0.0
U	0.0	0.0	0.0	0.0	0.0
V	-1.0000E-20	0.0	4.1379E-21	5.8536E-21	6.0000E-21
χ (rad)	...	0.0	2.9170E-17	1.3613E-16	...
a	7.0711E-21	6.0000E-21	5.5709E-21	4.6852E-21	4.2426E-21
b	7.0711E-21	0.0	2.2283E-21	3.7482E-21	4.2426E-21
Sense of rotation	counter-clockwise	...	clockwise	clockwise	clockwise
Nature	circular	linear	elliptical	elliptical	circular

($\delta_i = \pi/2$, $\alpha_i = 1$) scatters into (i) linearly polarized wave when $R = 0$, (ii) an elliptically polarized wave with clockwise sense when $R = 0.4$ & 0.8 , (iii) circularly polarized wave with clockwise sense when $R = 1$.

Similar to the Table 5.1, the stokes parameters of the incident and backward scattered electromagnetic waves in PSR 1133+16 are listed in Table 5.2. In the case of backward SRS sense reversal does not occur.

Fig. 5.4 shows χ_- as a function of the e-folding time t_e , for different values of α_i in the case of forward scattering of the elliptically polarized radio wave \vec{E}_i , in the emission region of a pulsar. Here, R is varied between 0 and 1. For R close to 1, one observes $t_e \leq 10^{-4}$ sec. The rotational angle χ_- reaches a maximum when the growth rate attains its maximum. It is seen that a reversal in the sense of polarization can take place in a time scale lying between micro to milliseconds.

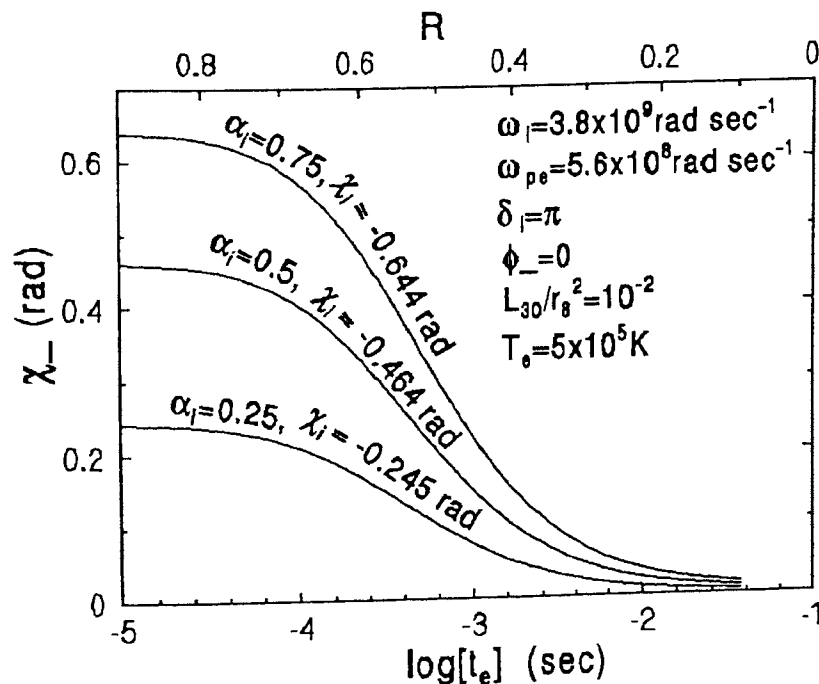


Fig. 5.4 The orientation angle χ_- of the scattered radiation versus the e-folding time t_e for the SRS scattering of radio wave in a pulsar.

TABLE 5.2

STOKES PARAMETERS OF THE INCIDENT AND BACKWARD SCATTERED DEM WAVES
FOR PSR 1133+16

Parameters ($\text{erg cm}^{-2}\text{sec}^{-1}\text{Hz}^{-1}$)	Incident wave $\delta_i = \pi, \alpha_i = 0.5$		Scattered wave $\delta_- = 0$		
		R=0	R=0.4	R=0.8	R=1.2
I	1.0000E-20	6.0000E-21	6.0000E-21	6.0000E-21	6.0000E-21
Q	6.0000E-21	6.0000E-21	5.5385E-21	4.3448E-21	2.8235E-21
U	-8.0000E-21	0.0	-2.3077E-21	-4.1379E-21	-5.2941E-21
V	0.0	0.0	0.0	0.0	0.0
χ (rad)	-0.4636	0.0	-0.1974	-0.38051	-0.54042
a	1.0000E-20	6.0000E-21	6.0000E-21	6.0000E-21	6.0000E-21
b	0.0	0.0	0.0	0.0	0.0
Sense of rotation
Nature	linear	linear	linear	linear	linear

Parameters ($\text{erg cm}^{-2}\text{sec}^{-1}\text{Hz}^{-1}$)	Incident wave $\delta_i = 3\pi/4, \alpha_i = 1$		Scattered wave $\delta_- = -\pi/4$		
		R=0	R=0.4	R=0.8	R=1.2
I	1.0000E-20	6.0000E-21	6.0000E-21	6.0000E-21	6.0000E-21
Q	0.0	6.0000E-21	4.3448E-21	1.3171E-21	-1.0820E-21
U	-7.0711E-21	0.0	-2.9260E-21	-4.1392E-21	-4.1731E-21
V	-7.0711E-21	0.0	-2.9260E-21	-4.1392E-21	-4.1731E-21
χ (rad)	-0.7854	0.0	-0.2963	-0.6314	0.6586
a	9.2388E-21	6.0000E-21	5.8064E-21	5.5705E-21	5.5618E-21
b	3.8268E-21	0.0	1.5118E-21	2.2291E-21	2.2510E-21
Sense of rotation	counter- clockwise	...	counter- clockwise	counter- clockwise	counter- clockwise
Nature	elliptical	linear	elliptical	elliptical	elliptical

Parameters ($\text{erg cm}^{-2}\text{sec}^{-1}\text{Hz}^{-1}$)	Incident wave $\delta_i = \pi/2, \alpha_i = 1$		Scattered wave $\delta_- = -\pi/2$		
		R=0	R=0.4	R=0.8	R=1
I	1.0000E-20	6.0000E-21	6.0000E-21	6.0000E-21	6.0000E-21
Q	0.0	6.0000E-21	4.3448E-21	1.3171E-21	0.0
U	0.0	0.0	0.0	0.0	0.0
V	-1.0000E-20	0.0	-4.1379E-21	-5.8537E-21	-6.0000E-21
χ (rad)	...	0.0	-2.9170E-17	-1.3612E-16	...
a	7.0711E-21	6.0000E-21	5.5709E-21	4.6852E-21	4.2426E-21
b	7.0711E-21	0.0	2.2283E-21	3.7482E-21	4.2426E-21
Sense of rotation	counter- clockwise	...	counter- clockwise	counter- clockwise	counter- clockwise
Nature	circular	linear	elliptical	elliptical	circular

5.4.2 In quasars

The typical values of the plasma and radiation parameters in the broad-line region, at a distance $r = r_{pc} \times 3.086 \times 10^{18}$ cm from the central engine of a quasar are (Krishan & Wiita 1990; Gangadhara & Krishan 1990) electron density $n_e = n_9 \times 10^9 \text{ cm}^{-3}$, temperature $T_e = T_5 \times 10^5$ K and luminosity $L = L_{42} \times 10^{42}$ erg/sec in the radio band $\Delta\omega \approx \omega_{pe}$.

Fig. 5.5 shows χ_- as a function of the e-folding time t_e , for different values of α_i for forward scattering of the elliptically polarized radio wave \vec{E}_i in a quasar. The rotational angle χ_- reaches a maximum when the growth rate attains its maximum. Similarly, Fig. 5.6 shows χ_- as a function of the e-folding time t_e , at different values of α_i for forward scattering of the elliptically polarized optical wave \vec{E}_i in a quasar.

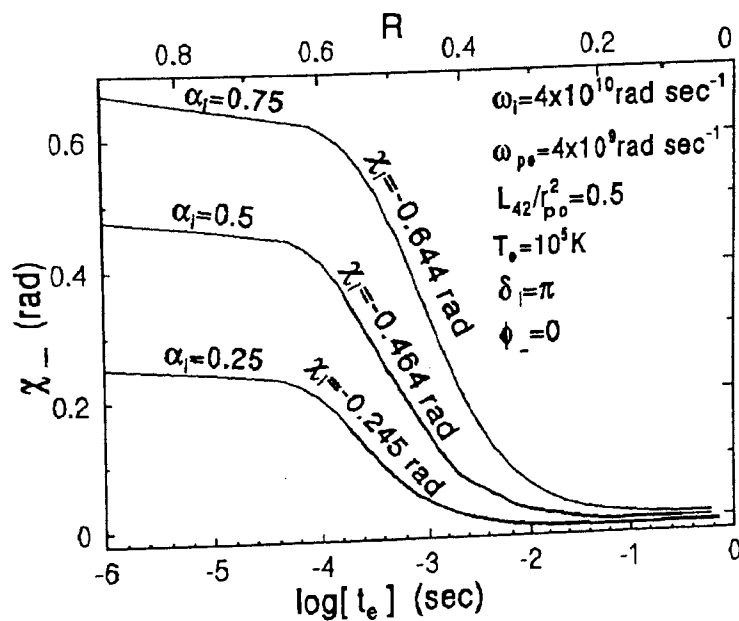


Fig. 5.5 The orientation angle χ_- of the scattered radiation versus the e-folding time t_e for the SRS scattering of a radio wave in a quasar.

We know from the multifrequency observations of 3C 273 by Courvoisier et al. (1987) that $I_i = 4.2266 \times 10^{-22} \text{erg cm}^{-2} \text{sec}^{-1} \text{Hz}^{-1}$ at the radio frequency $\nu_i = 6.366 \times 10^9 \text{Hz}$. For $\omega \approx \omega_{pe}$ and $\omega_i = 2.5\omega_{pe}$, we obtain from equation (5.48) that $I_- = 2.5360 \times 10^{-22} \text{erg cm}^{-2} \text{sec}^{-1} \text{Hz}^{-1}$.

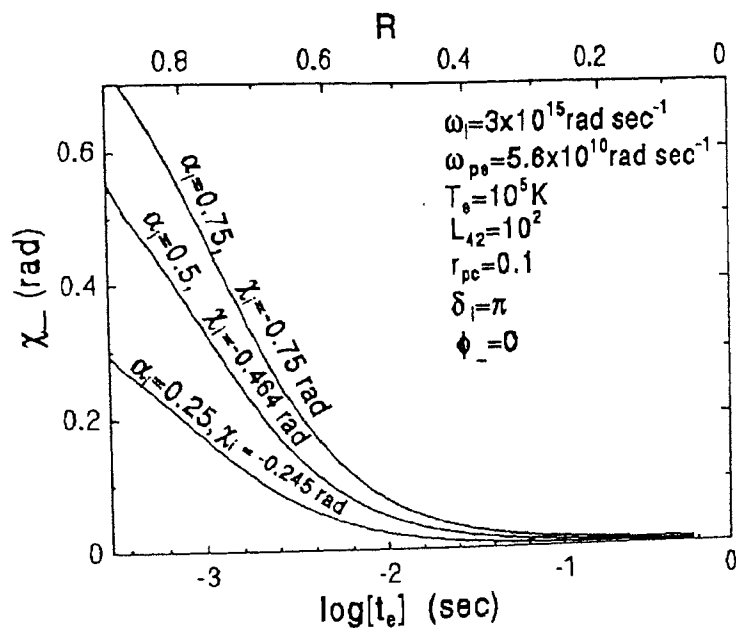


Fig. 5.6 The orientation angle χ_- of the scattered radiation versus the e-folding time t_e for the SRS scattering of optical wave in a quasar.

Similar to Table 5.1, in Table 5.3 the values of stokes parameters for the incident and the forward scattered electromagnetic waves in a quasar 3C 273 are listed. It has been observed that the variability in polarization of non-thermal radiation varies over the time scales between a second to a day.

TABLE 5.3

STOKES PARAMETERS OF THE INCIDENT AND FORWARD SCATTERED EM WAVES
FOR 3C 273

Parameters (erg cm ⁻² sec ⁻¹ Hz ⁻¹)	Incident wave $\delta_i = \pi, \alpha_i = 0.5$			Scattered wave $\delta_- = 0$	
		R=0	R=0.4	R=0.8	R=1.2
I	4.2266E-22	2.5360E-22	2.5360E-22	2.5360E-22	2.5360E-22
Q	2.5360E-22	2.5360E-22	2.3410E-22	1.8364E-22	1.1934E-22
U	-3.3813E-22	0.0	9.7537E-23	1.7490E-22	2.2376E-22
V	0.0	0.0	0.0	0.0	0.0
χ (rad)	-0.4636	0.0	0.1974	0.3805	0.5404
a	4.2266E-22	2.5360E-22	2.5360E-22	2.5360E-22	2.5360E-22
b	0.0	0.0	0.0	0.0	0.0
Sense of rotation
Nature	linear	linear	linear	linear	linear

Parameters (erg cm ⁻² sec ⁻¹ Hz ⁻¹)	Incident wave $\delta_i = 3\pi/4, \alpha_i = 1$			Scattered wave $\delta_- = -\pi/4$	
		R=0	R=0.4	R=0.8	R=1.2
I	4.2266E-22	2.5360E-22	2.5360E-22	2.5360E-22	2.5360E-22
Q	0.0	2.5360E-22	1.8364E-22	5.5667E-23	-4.5730E-23
U	-2.9887E-22	0.0	1.2367E-22	1.7495E-22	1.7640E-22
V	-2.9887E-22	0.0	1.2367E-22	1.7495E-22	1.7638E-22
χ (rad)	-0.7854	0.0	0.2963	0.6314	-0.6586
a	3.9049E-22	2.5360E-22	2.4541E-22	2.3544E-22	2.3507E-22
b	1.6174E-22	0.0	6.3896E-23	9.4217E-23	9.5139E-23
Sense of rotation	counter-clockwise	...	clockwise	clockwise	clockwise
Nature	elliptical	linear	elliptical	elliptical	elliptical

Parameters (erg cm ⁻² sec ⁻¹ Hz ⁻¹)	Incident wave $\delta_i = \pi/2, \alpha_i = 1$			Scattered wave $\delta_- = -\pi/2$	
		R=0	R=0.4	R=0.8	R=1
I	4.2266E-22	2.5360E-22	2.5360E-22	2.5360E-22	2.5360E-22
Q	0.0	2.5359E-22	1.8364E-22	5.5667E-23	0.0
U	0.0	0.0	0.0	0.0	0.0
V	-4.2266E-22	0.0	1.7489E-22	2.47410E-22	2.5360E-22
χ (rad)	0.0	2.9170E-17	1.3612E-16	...
a	2.9886E-22	2.5359E-22	2.3545E-22	1.9802E-22	1.7932E-22
b	2.9886E-22	0.0	9.4183E-23	1.5842E-22	1.7932E-22
Sense of rotation	counter-clockwise	...	clockwise	clockwise	clockwise
Nature	circular	linear	elliptical	elliptical	circular

5.5 FARADAY ROTATION VERSUS STIMULATED RAMAN SCATTERING

Here, we make a comparison between the rotations of the plane of polarization produced by Faraday rotation and forward SRS, using the typical plasma and radiation parameters for a quasar. A linearly polarized electromagnetic wave which is incident on a plasma, will be Faraday rotated through Ω_F rad, where Ω_F is given by (Lang 1974)

$$\Omega_F = \frac{2.36 \times 10^4}{\nu^2} \int_0^L n_e H \cos(\theta) dl \quad \text{rad}, \quad (5.49)$$

after traversing a thickness, L , of the plasma. Here, H is the magnetic field and θ is the angle between the line of sight and the direction of the magnetic field. For $n_e = n_9 \times 10^9 \text{ cm}^{-3}$, $H = H_{-3} \times 10^{-3} \text{ G}$ and $\nu = \nu_9 \times 10^9 \text{ Hz}$ in the broad-line region of quasar, we get

$$\Omega_F = 2.36 \times 10^{-8} \frac{n_9 H_{-3} L}{\nu_9^2} \quad \text{rad}. \quad (5.50)$$

Consider the point $\log[t_e] = -5$ sec and $\chi_- = 0.65$ rad in Fig. 5.5 on the curve with $\alpha_i = 0.75$ and $\chi_i = -0.644$ rad. The angle through which the plane of polarization rotated due to SRS is given by $\Omega_{\text{SRS}} = \chi_- - \chi_i = 1.294$ rad during the time $t_e = 10^{-5}$ sec. To compare Ω_F and Ω_{SRS} we need to convert t_e into the light travel distance $L = ct_e = 3 \times 10^5$ cm. Now, for $n_9 = 5$, $H_{-3} = 1$, and $\nu_9 = 6.366$ (Fig. 5.5) we get $\Omega_F = 8.735 \times 10^{-4}$ rad, much smaller than Ω_{SRS} .

5.6 LARGE AMPLITUDE ELECTROMAGNETIC WAVES AND THE EFFECT OF THEIR INCOHERENCE ON SRS INSTABILITY

We derived the above results assuming the incident field to be monochromatic. In reality, however, some amount of incoherence is always present. It has been shown by Tamour (1973) and Thomson et al. (1974) that the effect of finite bandwidth $\Delta\omega_i$ of the incident field on the instability can be taken care of by replacing the damping rate of the sidebands Γ_L by $(\Gamma_L + 2\xi) \approx (\Gamma_L + \Delta\omega_i)$ where ξ is the number of phase jumps per unit time. This happens because Γ_L is a measure of the duration of time an electron is allowed to oscillate with the driving field before being knocked out of phase by a collision. The same effect results when the driving field suffers a phase shift and the two effects are additive. Thus replacing Γ_L by $\Gamma_L + \Delta\omega_i$ certainly raises the threshold for the instability.

If Γ is the growth rate due to a monochromatic pump at ω_i , then the actual growth rate Γ' due to the broad pump with a spectral width $\Delta\omega_i \gg \Gamma$ is given by (Kruer 1988)

$$\Gamma' = \frac{1}{\Delta\omega_i} \Gamma^2. \quad (5.51)$$

Thus, the reduction in the growth rate due to the finite bandwidth may be compensated to some extent by the large luminosity radiation believed to be generated by coherent emission processes. Hence, the presence of incoherence through finite band width in the radiation field effectively increases the damping rates and the thresholds, and therefore reduces the growth rate (t_e increases) of SRS instability.

Several coherent processes like (i) emission from bunches of relativistic electron beams (Ruderman & Sutherland 1975), (ii) curvature radiation (Gil & Snakowski 1990a, 1990b; Asséo, Pellat & Sol 1980) and (iii) parallel acceleration mechanism (Melrose 1978) have been proposed for the radio emission from pulsars. On the other hand, the role of the coherent emission processes for the generation of continuum

emission of the quasar was emphasized long back (Burbidge & Burbidge 1967) and has now begun to receive the attention it deserves (Lesch & Pohl 1992; Krishan & Wiita 1990; Weatherall & Benford 1991; Baker et al. 1988; Gangadhara & Krishan 1992).

Baker et al. (1988) constructed a model of the inner portions of astrophysical jets, in which a relativistic electron beam is injected from the central engine into the jet plasma. This beam drives electrostatic plasma wave turbulence, which lead to the collective emission of electromagnetic waves. Weatherall and Benford (1991) describe the scattering of charged particles from an intense localized electrostatic fields (cavitons) associated with plasma turbulence. These cavitons arise from a process known as plasma collapse (Zakharov 1972), in which electrostatic energy accumulates in localized wave packets. When the beam is ultra-relativistic, the emitted radiation is enhanced by relativistic beaming along the direction of propagation. In the same spirit, in this paper, we have studied the scattering of coherent electromagnetic radiation by electron density fluctuations or Langmuir waves of different phases in order to explain the polarization changes.

Analysis of the data by University of Michigan (Aller, Aller and Hughes 1991) in the cm-wavelength regime showed both flux and linear polarization variability, and in addition polarization frequently exhibited position angle swings and large changes in percentage of polarization. To explain these observational results one incorporates shock models with special geometries. While SRS, without invoking many constraints, can explain these results.

Sillanpää, Nilsson and Takalo (1991) observed rotation of polarization position angle linearly 55° in five hours, in all five colors, in the optical regime. This is the fastest ever observed position angle swing at optical regions in OJ 287 or blazar. It is difficult to explain this observed position angle swing with shocks in jet model.

5.7 CONCLUSION

Usually, when one talks about polarization change, one is referring to the same wave. SRS however brings about change of frequency but when the frequency of the incident wave is much higher than the plasma frequency, the scattered wave frequency differs very little from the incident wave frequency.

The value of R can be determined only by the non-linear calculations. However, one can easily expect that the value of R may be close to the value of α_i .

Similar to the frequency and wave number matching conditions (see equation 5.13) we found conditions between the phases δ_i, δ_{\pm} and δ_e (see equation 5.16) in the process of three-wave interaction.

Through SRS the clockwise polarized radiation can change into counterclockwise polarized radiation and vice versa. In addition, circularly polarized wave can change into a linearly polarized, a circularly polarized or an elliptically polarized wave or vice versa, depending upon the value of R . The plane of polarization gets rotated through an angle $(\chi_- - \chi_i)$. Compared to the Faraday rotation the SRS is a faster process.

A direct measurement of the growth rate cannot be done by a remote observer. The e-folding time represents a characteristic time during which a significant change in the degree of polarization, sense and rotation of plane of polarization takes place. Therefore, the observed variability time should be of the order of or a few times the e-folding time.

The features like a large change in rotation of polarization plane, sense reversal and extremely rapid temporal changes would help to explain many observations, for which, the existing mechanisms prove to be inadequate. Because of the very strong dependence of rotation angle on plasma parameters via the growth rate, in an inhomogeneous plasma medium the depolarization is a natural outcome. A

strong magnetic field can also affect the process: we intend to study this in detail in later work. We believe that the plasma process such as the SRS may be a potential mechanism for the polarization variability in pulsars and quasars.

References

- Aller, M. F., Aller, H. D. & Hughes, P. A., 1991, in *Extragalactic Radio Sources—From Beams to Jets*, 7th IAP Meeting, ed. Roland, J., Sol, H. & Pelletier, G., (Cambridge Univ. Press), p 167.
- Assó, E., Pellat, R. & Sol, H., 1980, *Pulsars*, IAU Symp. No. 95, eds. Sieber, W. & Wielebinski, R., (Reidel, Dordrecht), p 111.
- Baker, D. N., Borovsky, J. E., Benford, G. & Eilek, J. A., 1988, *Astrophys. J.*, **326**, 110.
- Beal, J. H., 1990, in *Physical Processes in Hot Cosmic Plasmas*, ed. Brinkmann, W., et al., (Kluwer Academic publications), p 341.
- Benford, G., 1992, *Astrophys. J.*, **391**, L 59.
- Blandford, R. D. & Königl, A., 1979, *Astrophys. J.*, **232**, 34.
- Burbidge, G. R. & Burbidge, E. M., 1967, *Quasi-Stellar-Objects*, (Freeman, San Francisco).
- Cordes, J. M. 1983, in *Positron-Electron pairs in Astrophysics*, ed. Burns, M. L., Harding, A. K. & Ramaty, R., (AIP Conf. Proc. No. 101), p 98.
- Cotton, W. D., Gelzahler, B. J., Marcaide, J. M., Shapiro, I. I. & Sanroma, M. 1984, *Astrophys. J.*, **286**, 503.
- Courvoisier, T. J. -L., et al. 1987, *Astr. Astrophys.*, **176**, 197.
- Drake, J. F., Kaw, P. K., Lee, Y. C., Schmidt, G., Liu, C. S. & Rosenbluth, M. N. 1974, *Phys. Fluids*, **17**, 778.

- Fried, D. & Conte, S. D., 1961, *The Plasma Dispersion Function*, (Academic Press, New York).
- Gangadhara, R. T. & Krishan, V. 1990, *J. Astrophys. Astron.*, **11**, 515.
- Gangadhara, R. T. & Krishan, V. 1992, *Mon. Not. R. astr. S.*, **256**, 111.
- Gangadhara, R. T. Krishan, V. & Shukla, P. K. 1992, Modulation of radiation in an Electron–Positron plasma, *Mon. Not. R. astr. S.*, in press.
- Gangadhara, R. T. & Krishan, V., 1993, Polarization changes through stimulated Raman scattering, *Astrophys. J.*, (Submitted).
- Gil, J. A. & Snakowski, J. K., 1990a, *Astr. Astrophys.*, **234**, 237.
- Gil, J. A. & Snakowski, J. K., 1990b, *Astr. Astrophys.*, **234**, 269.
- Hasegawa, A., 1978, *Bell System Tech. J.*, **57**, 3069.
- Krishan, V. & Wiita, P. J. 1990, *Mon. Not. R. astr. S.*, 246, 597.
- Krishan, V. & Gangadhara, R. T., 1992, in *International Conference on Plasma Physics*, ed. Bethe, K., & Thomas, G., Austria, part 1, 1761.
- Kruer, W. L. 1988, *The Physics of Laser-Plasma interactions*, (Addison-Wesley, New York), p 70.
- Lang, K. R. 1974, *Astrophysical Formulae*, (Springer–Verlag), p 57.
- Lesch, H. & Pohl, M., 1992, *Astr. Astrophys.*, **254**, 29.
- Liu, C. S. & Kaw, P. K. 1976, *Advances in Plasma Phys.*, ed. Simon, A. & Thompson, W. B., (Interscience New York), **6**, p 83.
- Manchester, R. N., & Taylor, J. H. 1977, *Pulsars*, (W. H. Freeman and Company, San Francisco), p 49.
- Melrose, D. B., 1978, *Astrophys. J.*, **225**, 557.
- Ruderman, M. & Sutherland, P., 1975, *Astrophys. J.*, **196**, 51.

- Rybicki, G. B. & Lightman, A. P. 1979, *Radiative Processes in Astrophysics*, (A Wiley-Interscience Publication), p 62.
- Sillanpää, A., Nilsson, K. & Takalo, L. O., 1991, in *Extragalactic Radio Sources - From Beams to Jets, 7th IAP Meeting*, ed. Roland, J., Sol, H. & Pelletier, G., (Cambridge Univ. Press), p 174.
- Stockman, H. S. 1978, in *Pittsburgh Conference on BL Lac Objects*, ed. Arthur M. Wolfe, p 149.
- Tamour, S., 1973, *Phys. Fluids*, **16**, 1169.
- Thomson, J. J., Kruer, W. L., Bodner, S. E. & DeGroot J., 1974, *Phys. Fluids*, **17**, 849.
- van der Laan, H., 1966, *Nature*, **211**, 1131.
- Weatherall, J. C. & Benford, G., 1991, *Astrophys. J.*, **378**, 543.
- Weiland, J. & Wilhelmsson, H., 1977, *Coherent Non-Linear Interaction of Waves in Plasmas*, (Pergamon press), p 60.
- Zakharov, V. E., 1972, *Sov. Phys. JETP*, **35**, 908.

Chapter 6

THE MODULATION OF RADIATION IN AN ELECTRON-POSITRON PLASMA

This chapter illustrates, the modulational instability of a large-amplitude electromagnetic wave propagating in an electron-positron plasma. The effects such as relativistic mass variation of the plasma particles and the non-resonant, finite frequency electrostatic density perturbations, caused by the large-amplitude radiation field, are taken into account. The radiation from many strong sources such as AGN and pulsars, has been observed to vary over a host of time-scales. It is possible that extremely rapid variations in the non-thermal continuum of AGN as well as in the non-thermal radio radiation from pulsars can be accounted for by the modulational instabilities to which radiation may be subjected during its propagation out of the emission region.

6.1 INTRODUCTION

The observations of active galactic nuclei (AGN) in all bands of the electromagnetic spectrum have been reviewed by Wiita (1985). He concentrated on quasars, radio galaxies, Seyfert galaxies, and BL Lacertae objects, with an emphasis placed on the energy production efficiency, compactness and variability. Observations have revealed that many compact radio sources have, in addition to the usual long-term variability, an intrinsic variability with time-scales less than a day. Heeschen et al. (1987) found, quite unexpectedly, the variations of ~ 1 day at a wavelength of 11 cm in several flat-spectrum sources. Observations of intraday radio variability in compact radio sources and their probable explanation are given by Quirrenbach (1990).

Generally, the time-scale of the amplitude variation is associated with the size of the emitting region, such that shorter time scales are associated with smaller regions. (Time-scales refer to the e-folding time or the doubling time of the amplitude). However, variations observed for durations smaller than, for example, the doubling time may not, when extrapolated to actual doubling time, provide a meaningful limit on the physical size of the emitting region.

Optical variations in blazars on time-scales ranging from a few minutes to decades are well established (e.g. Webb et al. 1988). In several instances, day-to-day changes of more than 1 mag have been observed to occur (Smith and Hoffeit 1963; Angione 1969; Shen and Usher 1970; Eachus and Liller 1975; Liller and Liller 1975; Miller 1975, 1977). For example, Oke (1967) observed a 0.25 mag change in 1 day for 3C 279; Bertaud et al. (1973) reported a variation for BL Lacertae of

1.3 mag in a day and of 0.7 mag in 74 minutes. Racine (1970) detected optical variability of 0.1 mag within a few hours in BL objects.

OJ 287 is the only AGN for which claims have been made (Kiplinger 1974; Folsom et al. 1976; Smith et al. 1985) for the existence of periodicity P less than a day. Visvanathan and Elliot (1973) reported the detection of $P = 39.2$ minutes in the optical band, which was later confirmed by Frolich (1973). Carrasco, Dultzin-Hacyan and Cruz-Gonzalez (1985) reported the existence of $P = 23.0$ and 40.0 minutes in OJ 287. This object's long history of variability, the evidence of variability with time-scales of 1 day or less and the possibility that such variability may be periodic conspire to make this object a prime candidate for the investigation of microvariability.

There are several mechanisms which can account for the radio variability and the spectral characteristics of AGN. Details of the time dependence and the polarization behavior of the flux are needed to separate the intrinsic variability from the propagation effects.

One might expect that the rapid optical variability of blazars could be explained by gravitational microlensing. However, the comparatively large size of nuclei of AGN in the radio regime tends to smear out such variations, unless the Einstein radii of the microlenses are large. The lensing by massive stars ($M \leq 100M_{\odot}$) could account for variations in the cm. regime, but apparent transverse velocities of the order of $\sim 40c$, much higher than observed in superluminal sources, are required to produce time scales of ~ 1 day. Moreover, the amplitude of the variations is expected to increase with frequency; this clear contradiction with the observed behavior of quasar 0917+624 seems to rule out the microlensing as a possible explanation for

rapid variability (Quirrenbach 1990).

Another more plausible mechanism for intraday radio variability is refractive interstellar scintillation (RISS). The wavelength dependence and short time-scale of variations, however, argue against this explanation; very small scatterers must be present close to the Sun (≤ 100 pc) if this is the mechanism. Heeschen et al. (1987) speculated that unusual filaments associated with the galactic loop III could be responsible for an enhanced scattering in high-declination sources, but the statistics of intraday variations in (Quirrenbach 1990) samples with $60^\circ \leq \delta \leq 90^\circ$ and with $35^\circ \leq \delta \leq 50^\circ$, respectively, are consistent with each other, indicating that the observed effects do not depend on celestial coordinates. Polarization variations and possible correlations with optical variability present further difficulties for the RISS hypothesis. Intrinsic variability seems therefore to be the most plausible explanation for the intraday variability.

Effects such as the absorption, the spectral modification, and the change in polarization of intense radiation propagating through plasma in AGN, have been explained with a sequence of plasma processes and have been shown to be much faster than single-particle processes (e.g. Krishan and Wiita 1986, 1990; Krishan 1988; Beal 1990; Gangadhara and Krishan 1990; Benford 1992).

The radio flux of pulsars fluctuate over the time scales $1\mu\text{s}$ to 1 yr. Observations for pulsars PSR 1133+16 at 600 MHz and PSR 1944+17 at 1.4 GHz, made by Cordes (1983), showed a pulse sequence, with a broad range of quasi-periodic and intermittent structures, which is weakly frequency dependent. Intrapulse fluctuations include narrow spikes and micropulses with durations from $1\mu\text{s}$ to a few *ms* which also show quasi-periodicities of 0.1 to a few *ms*. Broader features and

subpulses ($\Delta t \approx 1\text{--}100$ ms) sometimes appear as envelopes of micropulses and as modulations of amorphous noise-like structures. One may conclude that a large number of independent emitters contribute to the signal in a resolution time of $1\text{--}10$ μs , so even the narrow micropulses may be incoherent composites of many coherent emissions.

The observational data (Gil 1986; Smirnova et al. 1986; Smirnova 1988) strongly support the hypothesis that pulsar micropulses are a temporal phenomenon and can be interpreted within the amplitude-modulation mechanism (Rickett 1975). As discussed by Chain and Kennel (1983) and others (Mofiz, de Angelis and Forlani 1985), modulational instability provides a natural mechanism for amplitude modulation. According to pulsar models (Ruderman and Sutherland 1975; Arons and Scharlemann 1979), the pulsar magnetosphere is composed of secondary electrons and positrons.

This chapter explains the modulational instability of a large amplitude linearly polarized electromagnetic (EM) wave propagating in an electron-positron plasma. We take into account the combined effects of relativistic mass variation of plasma particles and the finite-frequency electrostatic density perturbations which are created by the ponderomotive force of the EM wave. We show that the modulational instability is a possible mechanism for the short-time intrinsic variability of compact radio sources. In addition to accounting for the extremely short time variability, this mechanism could prove to be a valuable diagnostic for the source region. In contrast, the other mechanisms, such as refractive interstellar scintillation and microlensing, depend on the very specific conditions far away from the source of the radiation.

6.2 THE MODULATIONAL INSTABILITY

An electron-positron plasma is found in the early universe (Rees 1983), in active galactic nuclei (Miller and Wiita 1987), in pulsar atmospheres (Goldreich and Julian 1969) and in the Van Allen Belt (Voronov et al. 1986). The collective plasma effects in an electron-positron plasma are of significant interest (e.g. Lominadze, Machabelli and Usov 1983; Shukla et al. 1986). Lately, the processes of non-linear wave conversion (Gedalin, Lominadze and Stenflo 1985) and self-modulation of EM waves have attracted a great deal of attention (Chain and Kennel 1983; Shukla 1985; Mofiz, de Angelis and Forlani 1985; Kates and Kaup 1989; Tajima and Taniuti 1990).

In an AGN, the electron-positron plasma exists at a distance of about $r \geq 10R_{Sh}$ from the central engine (Lightman 1983), where $R_{Sh} = 2GM/c^2$ is the Schwarzschild radius. In pulsars, the plasma exists at a distance of about $r \geq 100R_{N_s}$ from the neutron star (Cordes 1983), where $R_{N_s} \sim 10$ km is the neutron-star radius. In the present model, the electron-positron plasma is considered to be uniform and at rest with respect to the source of radiation.

Let us consider the non-linear propagation of a large-amplitude, linearly polarized EM wave with an electric vector

$$\vec{E}_o = E_o \cos(\vec{k}_o \cdot \vec{r} - \omega_o t) \hat{e} \quad (6.1)$$

through an electron-positron plasma. The EM wave can cause such non-linear effects as charged particle mass modulation and the excitation of forced electrostatic density perturbations. The non-linear processes occur on a time scale slower than the radiation oscillation period and are responsible for the spatio-temporal modulation of the EM wave packet. The charged particle mass modulation arises from relativistic mass variation in the EM fields, whereas the electrostatic den-

sity perturbations are due to the parametric coupling of EM wave and plasma via ponderomotive force. Thus a constant-amplitude EM wave interacting with small amplitude non-resonant perturbations will generate upper ($\vec{k}_o + \vec{k}, \omega_o + \omega$) and lower ($\vec{k}_o - \vec{k}, \omega_o - \omega$) EM sidebands. The non-linear processes, as described above, provide the possibility of coupling sidebands with the original pump. A low-frequency non-linear force will result, which in turn, will reinforce the low-frequency perturbations, thereby lending support to the amplitude modulation of the radiation.

The non-linear interaction of a large-amplitude, plane polarized EM wave with an electron-positron plasma is governed by

$$\frac{\partial \rho}{\partial t} + \nabla \cdot \vec{J} = 0, \quad (6.2)$$

$$m_j \left(\frac{\partial}{\partial t} + \vec{v}_j \cdot \nabla \right) (\Gamma_j \vec{v}_j) = q_j \left(\vec{E} + \frac{1}{c} \vec{v}_j \times \vec{B} \right) - \frac{\gamma_j T_j}{n_j} \nabla n_j, \quad (6.3)$$

$$\nabla \cdot \vec{E} = 4\pi \rho, \quad (6.4)$$

$$\nabla \times \vec{E} = -\frac{1}{c} \frac{\partial \vec{B}}{\partial t} \quad (6.5)$$

and

$$\nabla \times \vec{B} = \frac{4\pi}{c} \vec{J} + \frac{1}{c} \frac{\partial \vec{E}}{\partial t}, \quad (6.6)$$

where $\Gamma_j = (1 - v_j^2/c^2)^{-1/2}$ is the Lorentz factor, c is the speed of light, γ_j , n_j , \vec{v}_j , T_j , m_j and q_j are, respectively, the adiabatic exponent, the number density, the fluid velocity, the temperature, the rest mass and the charge of particle species j (equals e for electrons and p for positrons). Here, $\rho = e(n_p - n_e)$ and $\vec{J} = e(n_p \vec{v}_p - n_e \vec{v}_e)$ are the charge and the current densities. Equations (6.2) and (6.3) are the charge conservation and relativistic momentum equations, respectively, whereas equation (6.4) is the Poisson's equation and equations (6.5) and (6.6) are the Maxwell's equations. We take $m_e = m_p = m_o$, $q_e = -q_p = -e$, where e is the magnitude of

the electron charge. The electric and magnetic fields are given by

$$\vec{E} = -\nabla\varphi - \frac{1}{c}\frac{\partial\vec{A}}{\partial t} \quad (6.7)$$

and

$$\vec{B} = \nabla \times \vec{A}, \quad (6.8)$$

where φ and \vec{A} are the scalar and vector potentials, respectively.

Inserting equations (6.7) and (6.8) into equation (6.6) we get

$$\nabla \times (\nabla \times \vec{A}) + \frac{1}{c^2} \frac{\partial^2 \vec{A}}{\partial t^2} = \frac{4\pi}{c} \vec{J} - \frac{1}{c} \frac{\partial \nabla \varphi}{\partial t}. \quad (6.9)$$

Using a standard vector identity, we write

$$\nabla(\nabla \cdot \vec{A}) - \nabla^2 \vec{A} + \frac{1}{c^2} \frac{\partial^2 \vec{A}}{\partial t^2} = \frac{4\pi}{c} \vec{J} - \frac{1}{c} \frac{\partial \nabla \varphi}{\partial t}. \quad (6.10)$$

Since we are interested in the propagation of electromagnetic waves in a plasma medium, we chose Coulomb gauge $\nabla \cdot \vec{A} = 0$. Therefore, we have

$$\left(\nabla^2 - \frac{1}{c^2} \frac{\partial^2}{\partial t^2} \right) \vec{A} = -\frac{4\pi}{c} \vec{J} + \frac{1}{c} \frac{\partial}{\partial t} (\nabla \varphi). \quad (6.11)$$

We now separate \vec{J} into a transverse component \vec{J}_t (associated with the EM wave) and a longitudinal component \vec{J}_l (associated with forced electrostatic perturbations). The longitudinal part of \vec{J} can be related to $\vec{E} = -\nabla\varphi$ with equations (6.2) and (6.4). By eliminating ρ between equations (6.2) and (6.4), we obtain

$$\nabla^2 \left(\frac{\partial \varphi}{\partial t} \right) = 4\pi \nabla \cdot \vec{J}. \quad (6.12)$$

since $\nabla \cdot \vec{J}_t = 0$, we obtain

$$\nabla \left(\frac{\partial \varphi}{\partial t} \right) = 4\pi \vec{J}_l. \quad (6.13)$$

Substituting equation (6.13) into equation (6.11) yields

$$\left(c^2 \nabla^2 - \frac{\partial^2}{\partial t^2}\right) \vec{A} = -4\pi c \vec{J}_t. \quad (6.14)$$

The total transverse current density is defined as

$$\vec{J}_t = e(n_p \vec{u}_p - n_e \vec{u}_e), \quad (6.15)$$

where \vec{u}_j is the transverse velocity of the species j in the presence of the electric field of the EM wave. We find \vec{u}_j from the equation of motion of a particle of species j in the electric field of the EM wave

$$m_o \frac{\partial}{\partial t} \left\{ (1 - u_j^2/c^2)^{-1/2} \vec{u}_j \right\} = q_j \vec{E}. \quad (6.16)$$

Using equation (6.7), we obtain from equation (6.16)

$$(1 - u_j^2/c^2)^{-1/2} \vec{u}_j = -\frac{q_j}{cm_o} \vec{A}. \quad (6.17)$$

Equation (6.17) gives

$$u_j^2 = \frac{q_j^2 A^2}{m_o^2 c^2} \left(1 + \frac{q_j^2 A^2}{m_o^2 c^4} \right)^{-1} \quad (6.18)$$

Substituting equation (6.18) into equation (6.17), we get

$$\begin{aligned} \vec{u}_j &= -\frac{q_j}{m_o c} \left(1 + \frac{q_j^2 A^2}{m_o^2 c^4} \right)^{-1/2} \vec{A}. \\ &\approx -\frac{q_j}{m_o c} \left(1 - \frac{1}{2} \frac{q_j^2 A^2}{m_o^2 c^4} \right) \vec{A}. \end{aligned} \quad (6.19)$$

Substituting equation (6.19) into equation (6.15), we get

$$\vec{J}_t = -\frac{e^2}{m_o c} (n_p + n_e) \left(1 - \frac{1}{2} \frac{e^2 A^2}{m_o^2 c^4} \right) \vec{A}. \quad (6.20)$$

We now suppose that

$$\vec{A}(\vec{r}, t) = \frac{1}{2} [\vec{A}_s(\vec{r}, t) e^{i(\vec{k}_o \cdot \vec{r} - \omega_o t)} + \vec{A}_s^*(\vec{r}, t) e^{-i(\vec{k}_o \cdot \vec{r} - \omega_o t)}], \quad (6.21)$$

where $\vec{A}_s(\vec{r}, t)$ is a slowly varying function of space and time, and $\vec{A}_s^*(\vec{r}, t)$ is its complex conjugate. Squaring equation (6.21) on both sides, we obtain $A^2 = (1/2)\vec{A}_s \cdot \vec{A}_s^*$, where we have neglected the higher frequency terms $2\omega_o$ as they are non-resonant.

Substituting the expressions for \vec{J}_t and $\vec{A}(\vec{r}, t)$ into equation (6.14) and equating the coefficients of $e^{i(\vec{k}_o \cdot \vec{r} - \omega_o t)}$ and $e^{-i(\vec{k}_o \cdot \vec{r} - \omega_o t)}$ on both sides, we obtain

$$\left[c^2 \nabla^2 + i2c^2 \vec{k}_o \cdot \nabla - c^2 k_o^2 - \frac{\partial^2}{\partial t^2} + i2\omega_o \frac{\partial}{\partial t} + \omega_o^2 \right] \vec{A}_s = \frac{4\pi e^2}{m_o} (n_e + n_p) \left\{ 1 - \frac{1}{4} \frac{e^2 (\vec{A}_s \cdot \vec{A}_s^*)}{m_o^2 c^4} \right\} \vec{A}_s, \quad (6.22)$$

and

$$\left[c^2 \nabla^2 - i2c^2 \vec{k}_o \cdot \nabla - c^2 k_o^2 - \frac{\partial^2}{\partial t^2} - i2\omega_o \frac{\partial}{\partial t} + \omega_o^2 \right] \vec{A}_s^* = \frac{4\pi e^2}{m_o} (n_e + n_p) \left\{ 1 - \frac{1}{4} \frac{e^2 (\vec{A}_s \cdot \vec{A}_s^*)}{m_o^2 c^4} \right\} \vec{A}_s^*. \quad (6.23)$$

Using $n_j(\vec{r}, t) = n_o + \delta n_j(\vec{r}, t)$ and $\vec{A}_s(\vec{r}, t) = \vec{A}_o + \delta \vec{A}(\vec{r}, t)$, linearizing equations (6.22) and (6.23), we have

$$\left[c^2 \nabla^2 + i2c^2 \vec{k}_o \cdot \nabla - \frac{\partial^2}{\partial t^2} + i2\omega_o \frac{\partial}{\partial t} + \omega_o^2 - c^2 k_o^2 - 2\omega_p^2 \left(1 - \frac{\epsilon^2}{4} \right) \right] (\vec{A}_o + \delta \vec{A}) = -\frac{\omega_p^2}{2} \frac{e^2}{m_o^2 c^4} (\delta \vec{A} \cdot \vec{A}_o^* + \vec{A}_o \cdot \delta \vec{A}^*) \vec{A}_o + \omega_p^2 \delta N \left(1 - \frac{\epsilon^2}{4} \right) \vec{A}_o, \quad (6.24)$$

and

$$\left[c^2 \nabla^2 - i2c^2 \vec{k}_o \cdot \nabla - \frac{\partial^2}{\partial t^2} - i2\omega_o \frac{\partial}{\partial t} + \omega_o^2 - c^2 k_o^2 - 2\omega_p^2 \left(1 - \frac{\epsilon^2}{4} \right) \right] (\vec{A}_o^* + \delta \vec{A}^*) = -\frac{\omega_p^2}{2} \frac{e^2}{m_o^2 c^4} (\delta \vec{A} \cdot \vec{A}_o^* + \vec{A}_o \cdot \delta \vec{A}^*) \vec{A}_o^* + \omega_p^2 \delta N \left(1 - \frac{\epsilon^2}{4} \right) \vec{A}_o^*. \quad (6.25)$$

where $\delta n_j(\vec{r}, t)$ and $\delta \vec{A}(\vec{r}, t)$ are the perturbations, $\omega_p^2 = 4\pi n_o e^2 / m_o$ is the plasma frequency, $\epsilon^2 = e^2 |A_o|^2 / m_o^2 c^4$ and $\delta N = (\delta n_e + \delta n_p) / n_o$.

The relation between ϵ^2 and luminosity of radiation L is given by

$$\epsilon^2 = \frac{e^2 |A_o|^2}{m_o^2 c^4} = \frac{2e^2}{m_o^2 c^3} \frac{1}{\omega_o^2} \frac{L}{r^2} = 2.1 \times 10^4 \frac{1}{\omega_o^2} \frac{L}{r^2}, \quad (6.26)$$

where r is the distance between the source of radiation and the plasma medium.

From the zeroth order terms in equations (6.24) and (6.25), we have

$$\omega_o^2 = 2\omega_p^2 \left(1 - \frac{\epsilon^2}{4}\right) + c^2 k_o^2. \quad (6.27)$$

This is the dispersion relation for an intense EM wave (\vec{k}_o, ω_o) propagating in an electron-positron plasma. It shows that the plasma frequency of the electron-positron plasma gets depleted by a factor of $\epsilon^2/4$.

From the first order terms in equations (6.24) and (6.25), we now find

$$\left[c^2 \nabla^2 + i2c^2 \vec{k}_o \cdot \nabla - \frac{\partial^2}{\partial t^2} + i2\omega_o \frac{\partial}{\partial t} + \omega_o^2 - c^2 k_o^2 - 2\omega_p^2 \left(1 - \frac{\epsilon^2}{4}\right) \right] \delta \vec{A} = -\frac{\omega_p^2}{2} \frac{e^2}{m_o^2 c^4} (\delta \vec{A} \cdot \vec{A}_o^* + \vec{A}_o \cdot \delta \vec{A}^*) \vec{A}_o + \omega_p^2 \delta N \left(1 - \frac{\epsilon^2}{4}\right) \vec{A}_o, \quad (6.28)$$

and

$$\left[c^2 \nabla^2 - i2c^2 \vec{k}_o \cdot \nabla - \frac{\partial^2}{\partial t^2} - i2\omega_o \frac{\partial}{\partial t} + \omega_o^2 - c^2 k_o^2 - 2\omega_p^2 \left(1 - \frac{\epsilon^2}{4}\right) \right] \delta \vec{A}^* = -\frac{\omega_p^2}{2} \frac{e^2}{m_o^2 c^4} (\delta \vec{A} \cdot \vec{A}_o^* + \vec{A}_o \cdot \delta \vec{A}^*) \vec{A}_o^* + \omega_p^2 \delta N \left(1 - \frac{\epsilon^2}{4}\right) \vec{A}_o^*, \quad (6.29)$$

where $\omega_o \gg \omega$ and ω is the frequency of the electrostatic wave. Fourier transformation of equations (6.28) and (6.29) with

$$\delta \vec{A}(\vec{k}, \omega) = \frac{1}{2\pi} \int_{-\infty}^{\infty} \int_{-\infty}^{\infty} \delta \vec{A}(\vec{r}, t) e^{-i(\vec{k} \cdot \vec{r} - \omega t)} d^3 r dt \quad (6.30)$$

and

$$\delta \vec{N}(\vec{k}, \omega) = \frac{1}{2\pi} \int_{-\infty}^{\infty} \int_{-\infty}^{\infty} \delta N(\vec{r}, t) e^{-i(\vec{k} \cdot \vec{r} - \omega t)} d^3 r dt, \quad (6.31)$$

gives

$$D_+ \delta \vec{A} = \frac{\omega_p^2}{2} \frac{e^2}{m_o^2 c^4} (\delta \vec{A} \cdot \vec{A}_o^* + \vec{A}_o \cdot \delta \vec{A}^*) \vec{A}_o - \omega_p^2 \delta \tilde{N} \left(1 - \frac{\epsilon^2}{4}\right) \vec{A}_o \quad (6.32)$$

and

$$D_- \delta \vec{A}^* = \frac{\omega_p^2}{2} \frac{e^2}{m_o^2 c^4} (\delta \vec{A} \cdot \vec{A}_o^* + \vec{A}_o \cdot \delta \vec{A}^*) \vec{A}_o^* - \omega_p^2 \delta \tilde{N} \left(1 - \frac{\epsilon^2}{4}\right) \vec{A}_o^*, \quad (6.33)$$

where $D_{\pm} = (\vec{k}_o \pm \vec{k})^2 c^2 - (\omega_o \pm \omega)^2 + 2\omega_p^2(1 - \epsilon^2/4)$ are the dispersion relations for the Stokes mode (\vec{k}_s, ω_s) and the anti-Stokes mode (\vec{k}_a, ω_a) when the following resonant conditions are satisfied:

$$\begin{aligned} \omega_o - \omega &= \omega_s, & \vec{k}_o - \vec{k} &= \vec{k}_s, \\ \omega_o + \omega &= \omega_a, & \vec{k}_o + \vec{k} &= \vec{k}_a. \end{aligned} \quad (6.34)$$

Combining equations (6.32) and (6.33), we obtain

$$\begin{aligned} \delta \vec{A} \cdot \vec{A}_o^* + \vec{A}_o \cdot \delta \vec{A}^* &= \left\{ -\omega_p^2 |A_o|^2 \left(1 - \frac{\epsilon^2}{4}\right) \delta \tilde{N} + \frac{\omega_p^2}{2} \epsilon^2 (\delta \vec{A} \cdot \vec{A}_o^* + \vec{A}_o \cdot \delta \vec{A}^*) \right\} \times \\ &\times \left[\frac{1}{D_-} + \frac{1}{D_+} \right]. \end{aligned} \quad (6.35)$$

We must now calculate the low-frequency electron and positron density fluctuations δn_e and δn_p produced by the radiation (ponderomotive) force $\vec{F}_\omega = -\nabla \psi_\omega$, where ψ_ω is the ponderomotive potential, which corresponds physically to radiation pressure. The ponderomotive force depends quadratically on the amplitude and produces slowly varying longitudinal field, which leads to slow longitudinal motion and modifies the density. The ponderomotive potential is given by

$$\psi_\omega = \frac{e^2 n_o}{2m_o c^2} \langle A^2 \rangle_\omega = \frac{e^2 n_o}{m_o c^2} \langle \vec{A}_s \cdot \vec{A}_s^* \rangle_\omega, \quad (6.36)$$

where the angular bracket $\langle \rangle_\omega$ represents the ω frequency component of an average over the fast time-scale $\omega_o \gg \omega$. In the presence of the ponderomotive force, the slow motion of the plasma is governed by the following linearized equations:

$$\frac{\partial \delta n_j}{\partial t} + n_o \nabla \cdot \vec{\delta v}_j = 0, \quad (6.37)$$

$$\frac{\partial \delta \vec{v}_j}{\partial t} = -\frac{q_j}{m_o} \nabla \varphi - \frac{1}{2} \frac{e^2}{m_o^2 c^2} \nabla (\delta \vec{A} \cdot \vec{A}_o^* + \vec{A}_o \cdot \delta \vec{A}^*) - \gamma_j v_{tj}^2 \nabla \left(\frac{\delta n_j}{n_o} \right), \quad (6.38)$$

and

$$\nabla^2 \varphi = -4\pi \sum_{j=e,p} q_j \delta n_j, \quad (6.39)$$

where, φ is the scalar potential associated with electrostatic perturbations, $v_{tj} = (k_B T_j / m_j)^{1/2}$ is the thermal velocity of the particle species j , and k_B is the Boltzmann constant.

When the continuity and momentum equations for the electron fluid are combined with equation (6.39), we obtain

$$\left(\frac{\partial^2}{\partial t^2} - \gamma_e v_{te}^2 \nabla^2 + \omega_p^2 \right) \delta n_e = \omega_p^2 \delta n_p + S, \quad (6.40)$$

where the source term is defined as $S = (n_o e^2 / 2 m_o^2 c^2) \nabla^2 (\delta \vec{A} \cdot \vec{A}_o^* + \vec{A}_o \cdot \delta \vec{A}^*)$.

Similarly, for the positron fluid, we have

$$\left(\frac{\partial^2}{\partial t^2} - \gamma_p v_{tp}^2 \nabla^2 + \omega_p^2 \right) \delta n_p = \omega_p^2 \delta n_e + S. \quad (6.41)$$

Fourier-transforming equations (6.40) and (6.41), we obtain

$$(\omega^2 - \gamma_e k^2 v_{te}^2 - \omega_p^2) \delta \tilde{n}_e = -\omega_p^2 \delta \tilde{n}_p + \tilde{S}, \quad (6.42)$$

and

$$(\omega^2 - \gamma_p k^2 v_{tp}^2 - \omega_p^2) \delta \tilde{n}_p = -\omega_p^2 \delta \tilde{n}_e + \tilde{S}. \quad (6.43)$$

In the absence of the EM wave, we obtain from equations (6.42) and (6.43)

$$1 - \sum_{j=e,p} \frac{\omega_p^2}{(\omega^2 - \gamma_j k^2 v_{tj}^2)} = 0, \quad (6.44)$$

which is the dispersion relation for electrostatic plasma oscillations in a warm electron-positron plasma. By summing equations (6.42) and (6.43) and assuming $\gamma_e = \gamma_p = \gamma$ and $T_e = T_p = T$, we obtain

$$(\omega^2 - \gamma k^2 v_t^2) \delta \tilde{N} = \frac{e^2}{m_o^2 c^2} k^2 (\delta \vec{A} \cdot \vec{A}_o^* + \vec{A}_o \cdot \delta \vec{A}^*), \quad (6.45)$$

where $v_t = (k_B T / m_o)^{1/2}$.

Substituting the expression for $\delta\tilde{N}$ from equation (6.45) into equation (6.35), we obtain

$$\left[1 - \frac{\omega_p^2}{2} \varepsilon^2 \left(\frac{1}{D_-} + \frac{1}{D_+}\right)\right] (\omega^2 - \gamma k^2 v_t^2) = -\omega_p^2 k^2 c^2 \varepsilon^2 \left\{1 - \frac{\varepsilon^2}{4}\right\} \left(\frac{1}{D_-} + \frac{1}{D_+}\right). \quad (6.46)$$

This is the dispersion relation for the modulational instability of an EM wave propagating in an electron-positron plasma. Note that equation (6.46) is general and can be applied to the circularly polarized radiation also.

Since $\omega \ll \omega_o$, we have $D_{\pm} \approx k^2 c^2 \pm 2\vec{k} \cdot \vec{k}_o c^2 \mp 2\omega\omega_o$. For a cold plasma (i.e. $\omega^2 \gg \gamma_j k^2 v_{tj}^2$), equation (6.46) can be written as

$$(\omega - \vec{k} \cdot \vec{v}_g)^2 = \frac{1}{2} \frac{k^2 c^2}{\omega_o} \left[\frac{1}{2} \frac{k^2 c^2}{\omega_o} - \frac{1}{2} \frac{\omega_p^2 \varepsilon^2}{\omega_o} \left\{1 - 2 \frac{k^2 c^2}{\omega^2} \left(1 - \frac{\varepsilon^2}{4}\right)\right\} \right], \quad (6.47)$$

where the group velocity of the EM wave is denoted by $\vec{v}_g = \vec{k}_o c^2 / \omega_o$. The last two-terms on the right-hand side of (6.47) are the contribution of the radiation pressure driven finite-frequency density perturbations.

In a special case, for $k = \varepsilon\omega_p/c$, the solution to equation (6.47) is given by

$$\omega = \frac{1}{2} \vec{k} \cdot \vec{v}_g \pm \frac{1}{2} \sqrt{(\vec{k} \cdot \vec{v}_g)^2 \pm 2k^2 c^2 \frac{\omega_p}{\omega_o} \varepsilon \left\{2 \left(1 - \frac{\varepsilon^2}{4}\right)\right\}^{1/2}} \quad (6.48)$$

Equation (6.48) predicts an oscillatory instability for

$$\varepsilon \left\{2 \left(1 - \frac{\varepsilon^2}{4}\right)\right\}^{1/2} > \frac{\omega_o (\vec{k} \cdot \vec{v}_g)^2}{2\omega_p k^2 c^2},$$

with the growth rate:

$$\Gamma_m \approx \left(\frac{2\omega_p^3}{\omega_o}\right)^{1/2} \varepsilon^{3/2} \left\{2 \left(1 - \frac{\varepsilon^2}{4}\right)\right\}^{1/4} \quad (6.49)$$

It follows that the growth rate of the modulational instability for the case $k = \epsilon\omega_p/c$ is proportional to $\epsilon^{3/2}[2(1-\epsilon^2/4)]^{1/4}$, in contrast to the growth rate of the relativistic modulational instability (Chain and Kennel 1983), which is proportional to ϵ^2 .

Since $\omega \ll \omega_o$, the ω^4 and ω^3 terms in (6.46) can be dropped, and for $\epsilon/\beta \ll v_t \ll c$, $\Phi \approx 90^\circ$, $v_g \approx c$ and $k \ll k_o$, we have the expressions for quasi-period of the modulation

$$P = \frac{2\pi}{\omega_r} = \frac{2\pi}{\omega_o \cos \Phi} \frac{1}{y} \quad (6.50)$$

and for the e-folding time

$$t_e = \frac{1}{\Gamma} = \frac{6v_t}{\omega_o c} \left\{ 36 \frac{v_t^2}{c^2} \cos^2 \Phi - 12 \frac{\epsilon^2}{\beta^2} \right\}^{-1/2} \frac{1}{y}, \quad (6.51)$$

where $y = k/k_o$, $\beta = \omega_o/\omega_p$, Γ is the growth rate of the modulational instability, ω_r is the frequency of the electrostatic density perturbation and Φ is the angle between \vec{k}_o and \vec{k} .

6.3 LARGE-AMPLITUDE EM WAVES IN AGN AND PULSARS AND THE EFFECT OF THEIR INCOHERENCE ON THE MODULATIONAL INSTABILITY

Above results have been derived assuming the incident field to be monochromatic. In reality, however, some amount of incoherence is always present. It has been shown by Tamour (1973) and Thomson et al. (1974) that the effect of the finite bandwidth $\Delta\omega_o$ of the incident field on the instability can be taken care of by replacing the damping rate of the sidebands Γ_L by $(\Gamma_L + 2\xi) \approx (\Gamma_L + \Delta\omega_o)$, where ξ is the number of phase jumps per unit time. This replacement is possible because Γ_L is a measure of the length of time an electron is allowed to oscillate with the driving field before being knocked out of phase by a collision. The same effect results when the driving field suffers a phase shift, and the two effects are additive. Thus replacing Γ_L by $\Gamma_L + \Delta\omega_o$ certainly raises the threshold for the instability.

Another source of incoherence of the EM radiation is the lack of definite polarization. In an unpolarized beam, the tip of the electric field vector undergoes random changes of direction. Thus an electron in such a field undergoes changes in its direction of motion at the same rate. This essentially increases the effective collision frequency of the electrons and thus raises the threshold for the modulation instability. In the case of quasars, 1–10 per cent of the radiation is known to be polarized.

If Γ is the growth rate due to a monochromatic pump at ω_o , then the actual growth rate Γ' due to the broad pump with a spectral width $\Delta\omega_o \gg \Gamma$ is given by

$$\Gamma' = \frac{1}{\Delta\omega_o} \Gamma^2, \quad (6.52)$$

(Kruer 1988; see section F in appendix). Thus the reduction in the growth rate due to the finite bandwidth may be compensated to some extent by the high-luminosity radiation believed to be generated by coherent emission processes.

Several coherent processes, such as (i) emission from bunches of relativistic electron beams (Ruderman and Sutherland 1975), (ii) curvature radiation (Asséo, Pellat and Sol 1980; Gil and Snakowski 1990a, 1990b) and (iii) the parallel acceleration mechanism (Melrose 1978), have been proposed for the radio emission from pulsars. On the other hand, the role of the coherent emission processes in the generation of continuum emission from AGN was emphasized long ago (Burbidge and Burbidge 1967) and has now begun to receive the attention it deserves (Baker et al. 1988; Krishan and Wiita 1990; Weatherall and Benford 1991; Gangadhara and Krishan 1992; Gangadhara, Krishan and Shukla 1992; Lesch and Pohl 1992). Thus the presence of incoherence, due to finite bandwidth and lack of polarization in the radiation field, effectively increases the damping rate and therefore the threshold (in the kinetic treatment) and reduces the growth rate (t_e increases) of the modulational instability. Here, since we use a fluid treatment of treated the modulational instability, there is no damping of the side band modes, and therefore there are no

thresholds. However, due to a smaller pump luminosity being available (say 1-10 per cent) at a frequency ω_o , the growth rate Γ and frequency ω_r are reduced, with an attendant increase in the e-folding time t_e and the period P .

6.4 DISCUSSION

In this paper, we have shown that low-frequency electrostatic density perturbations can be non-linearly excited due to the interaction of a large amplitude linearly polarized EM wave with an electron-positron plasma. The superposition of low-frequency oscillations (\vec{k}, ω) over the high-frequency waves (\vec{k}_o, ω_o) produces an amplitude-modulated wave:

$$A(\vec{r}, t) = A_o \left[1 + \frac{\delta A}{A_o} e^{t/t_e} \cos(\vec{k} \cdot \vec{r} - t/P) \right] \cos(\vec{k}_o \cdot \vec{r} - \omega_o t), \quad (6.53)$$

(from equation 6.21). Initially, δA is infinitesimally small, but it grows exponentially with time and reaches saturation due to some non-linear processes. Since here the nodulational instability has been investigated in the linear regime, we can not find the depth of modulation. For the sake of illustration, with $\delta A/A_o = 0.5$, $t_e = 200$ s and $P = 23$ minutes, we have plotted the amplitude modulated vector potential as a function of time in Fig. 6.1. In the beginning i.e. for $0 \leq t < 92$ minutes, δA is small and starts to grow exponentially. For $0 \leq t < 92$ minutes, the incident radiation therefore remains unchanged; but for $t \geq 92$ minutes, δA grows and the radiation is modulated.

For the case of BL Lac object OJ 287, we derive a value of $\delta A/A_o = 0.02$ from the observations of Carrasco, Dultzin-Hacyan and Cruz-Gonzalez (1985). For the plasma parameters assumed in section 4.1 for an AGN, we obtain a period of 23 minutes. This object has the redshift $z = 0.306$, the mag $m_v = 12$ and modulated luminosity $L = 4 \times 10^{45}$ erg s^{-1} . Using $H_o = 50$ km s^{-1} Mpc $^{-1}$, the value of A_o corresponding to this luminosity is given by 6.86×10^{-16} gauss cm. For $t_e = 200$ s the Fig. 6.2 shows the modulated flux $f = \omega_o^2 |A(t)|^2 / (8\pi c)$ as a function of time.

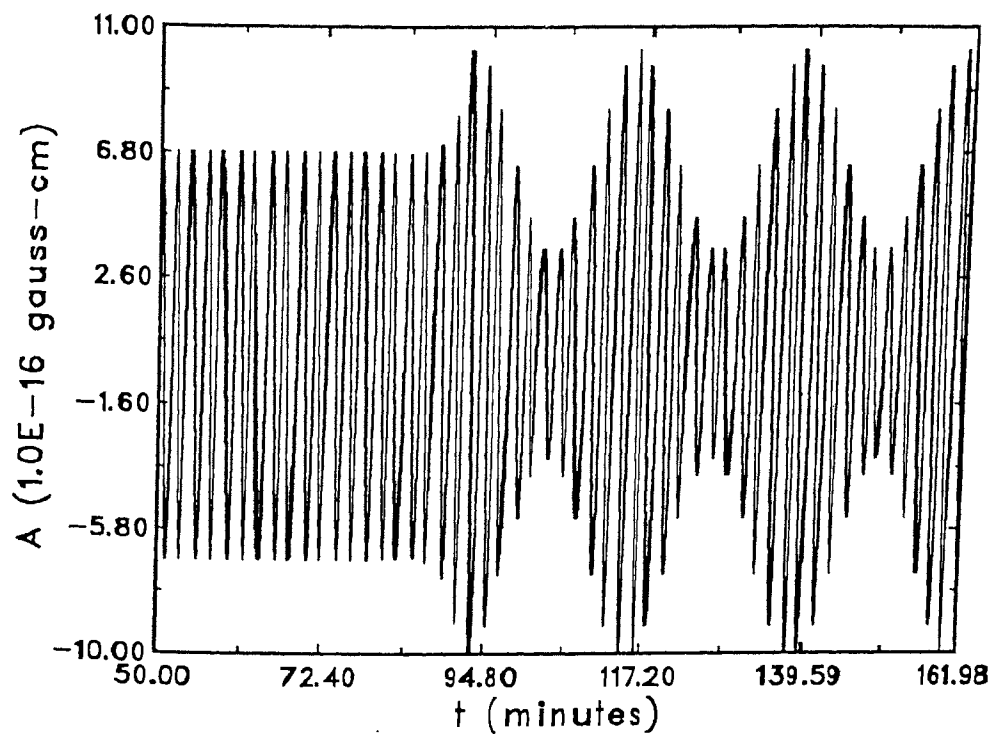


Fig. 6.1 The modulated vector potential of EM wave versus time t .

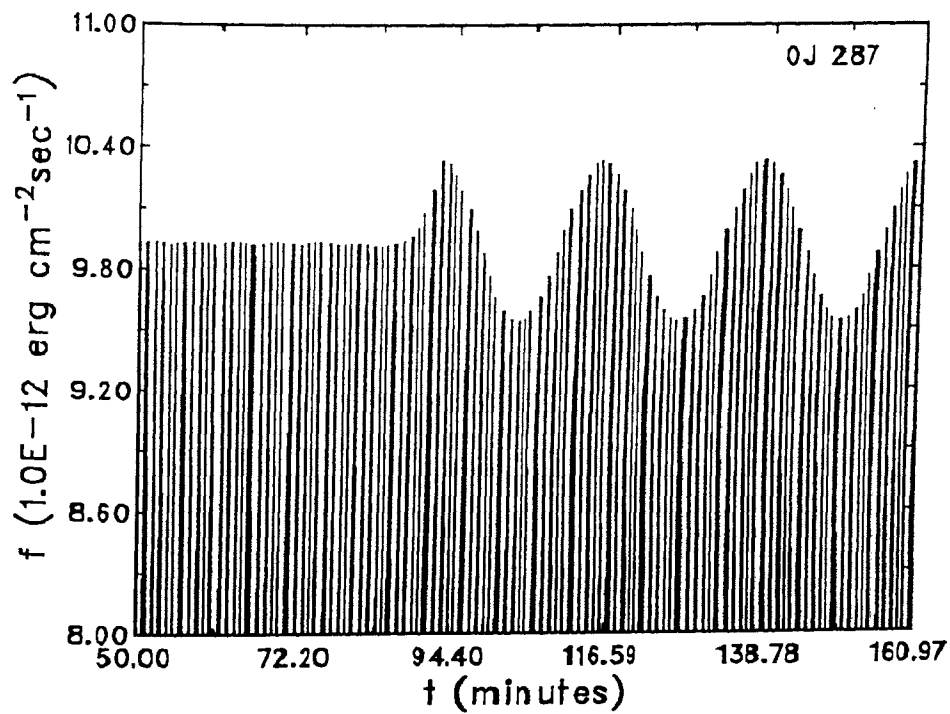


Fig. 6.2 The theoretical light curve of BL Lac object OJ 287 showing the modulated emission of radiation.

We solve equation (6.46) numerically, using conditions typical to an AGN and a pulsar, to find $\omega = \omega_r + i\Gamma = 2\pi/P + i1/t_e$.

6.4.1 In an AGN

The typical values of the plasma and radiation parameters at a distance $r = r_{15} \times 10^{15}$ cm from the central engine of an AGN are (Lightman and Zdziarski 1987; Krishan and Wiita 1990; Gangadhara and Krishan 1992) pair density $n_j = n_9 \times 10^9$ cm $^{-3}$, temperature $T_j = T_4 \times 10^4$ K and luminosity in the radio band $L = L_{42} \times 10^{42}$ erg s $^{-1}$. For $\Phi = 90^\circ$ instability is purely growing and non-periodic, but for $\Phi = 0^\circ$ the instability is purely oscillatory.

Fig. 6.3 shows the period $P = 2\pi/\omega_r$ of the modulational instability of radio wave of frequency $\nu_o = 10^9$ Hz as a function of the wavenumber $y = k/k_o$ of the

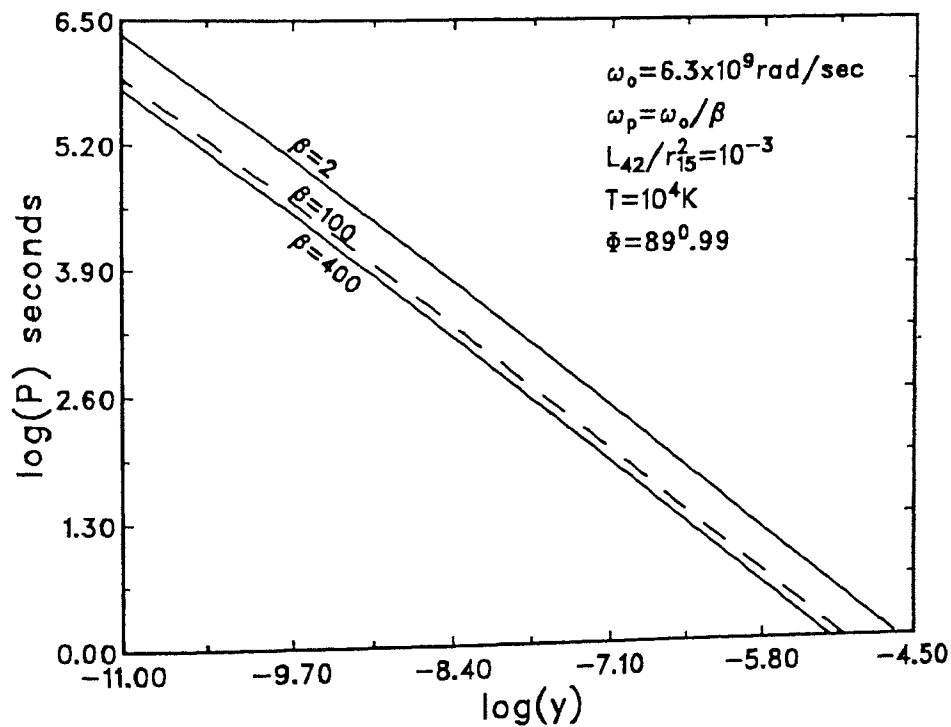


Fig. 6.3 The period of modulation $P = 2\pi/\omega_r$ versus the wave number $y = k/k_o$ of electrostatic density perturbations at three plasma frequencies, $\omega_p = \omega_o/2$, $\omega_o/100$ and $\omega_o/400$.

density perturbations at three plasma densities corresponding to $\beta = \omega_o/\omega_p = 2, 100$ and 400 . The figure shows that P is inversely proportional to y , as expected from equation (6.50). When $y \ll 1$, P can be as large as a few days. The e-folding time t_e i.e. the reciprocal of the growth rate of the modulational instability, is plotted as a function of y in Fig. 6.4. For $y \ll 1$, t_e is inversely proportional to y , as expected from equation (6.51).

Fig. 6.5 shows the period P as a function of L_{42}/r_{15}^2 for $\beta = 2, 100$ and 400 , and $y = 10^{-9}$. This figure shows that the period P of the modulation is nearly independent of the value of L_{42}/r_{15}^2 . The e-folding time t_e is plotted in Fig. 6.6 as a function of L_{42}/r_{15}^2 . If we include the effect of incoherence in the incident radiation, then t_e will increase.

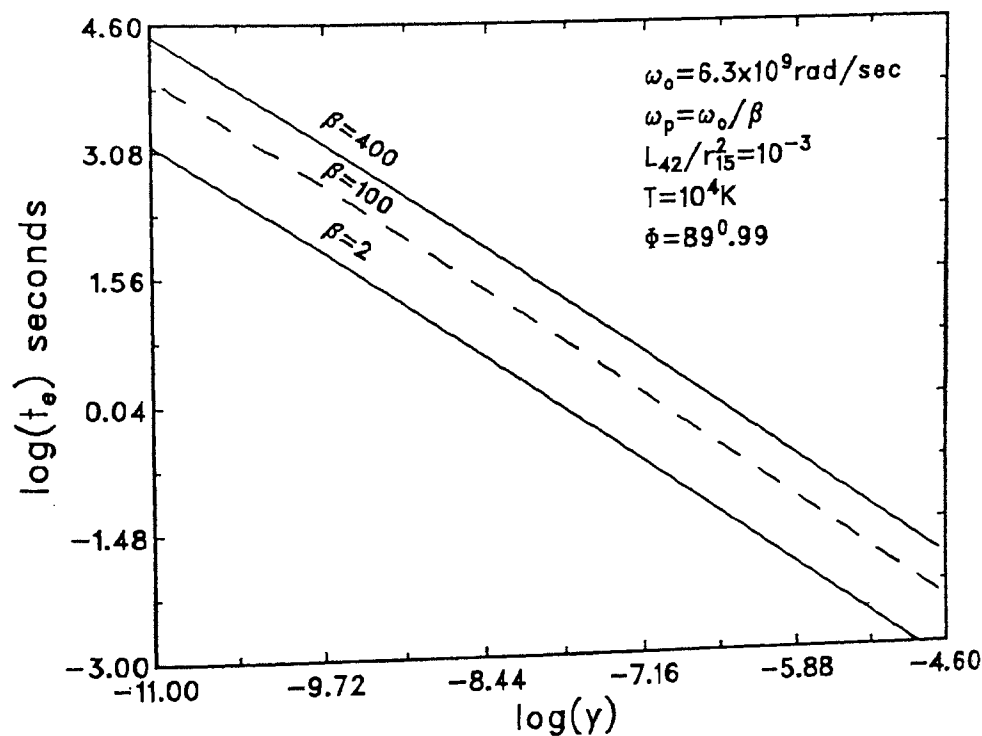


Fig. 6.4 The e-folding time $t_e = 1/\Gamma$ versus $y = k/k_o$ at three plasma frequencies, $\omega_p = \omega_o/2, \omega_o/100$ and $\omega_o/400$.

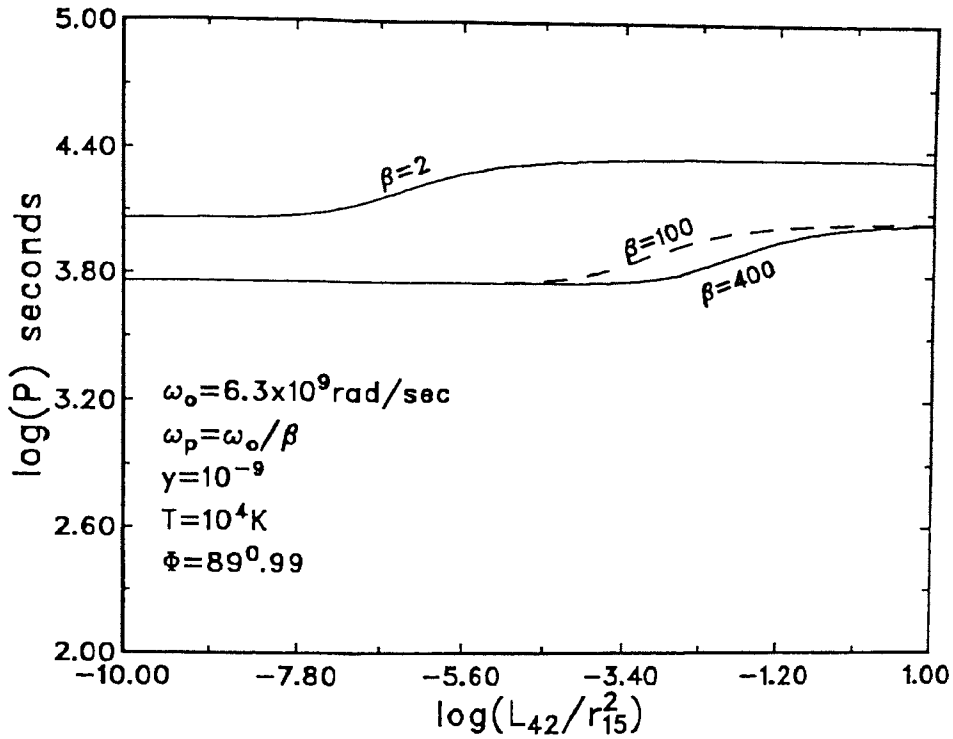


Fig. 6.5 The period of modulation P versus the L_{42}/r_{15}^2 at $\omega_p = \omega_o/2$, $\omega_o/100$ and $\omega_o/400$.

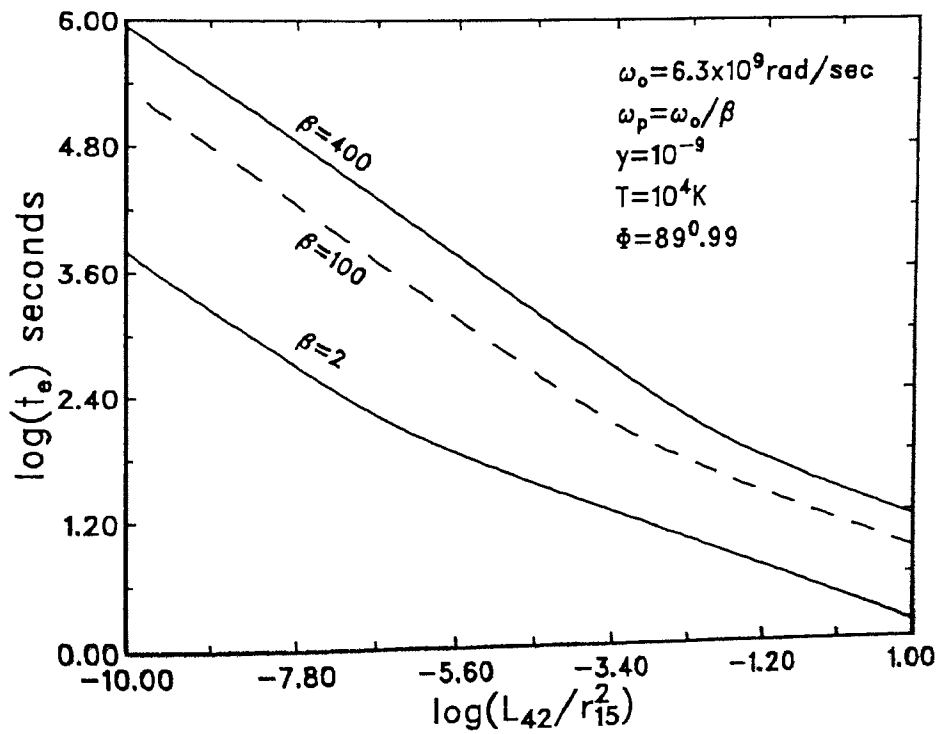


Fig. 6.6 The e-folding time t_e versus the L_{42}/r_{15}^2 at $\omega_p = \omega_o/2$, $\omega_o/100$ and $\omega_o/400$.

The period of modulation P is a strong function of the angle Φ (see Fig. 6.7). At frequencies close to the plasma frequency ($\omega_o = 2\omega_p$), the instability occurs over a large range of Φ ($87^\circ.5 \leq \Phi \leq 92^\circ.5$). If the radiation frequency is much above the plasma frequency, then the instability is confined to a narrow range of Φ around 90° . The large-period ($P > 1$ h) pulses are produced when Φ is close to 90° .

Fig. 6.8 shows t_e as a function of Φ : when $\Phi \approx 90^\circ$, t_e is small and the density perturbations grow very fast in time. The instability therefore becomes very strong near $\Phi \approx 90^\circ$.

Figs. 1–8 describe the modulational instability of a radio wave with frequency $\omega_o = 6.3 \times 10^9 \text{ rad s}^{-1}$ for plasma parameters typical of an AGN.

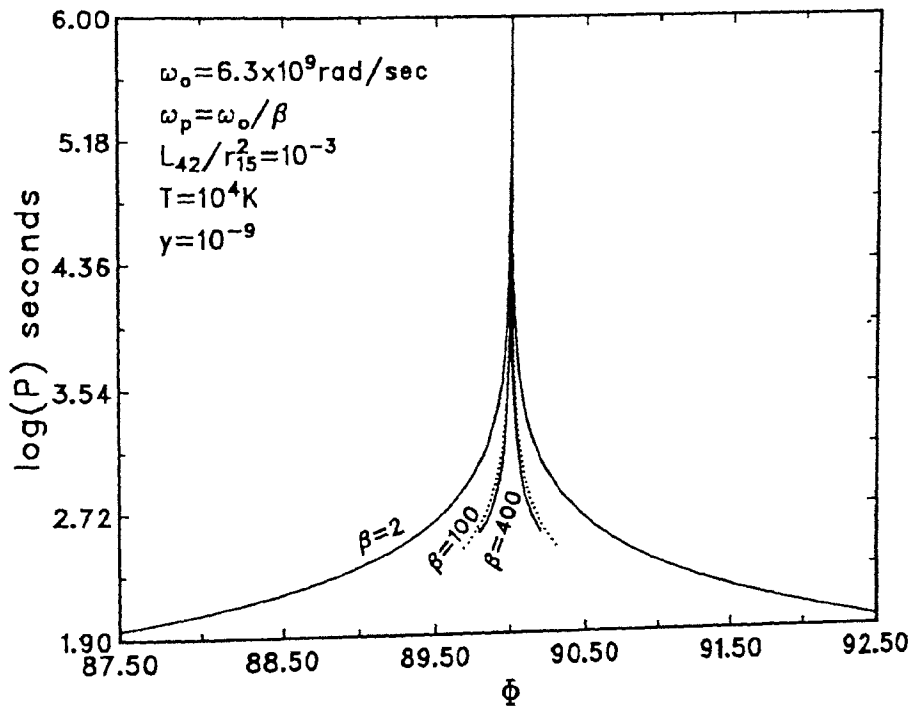


Fig. 6.7 The period of modulation P versus $\Phi = \cos^{-1}(\hat{k} \cdot \hat{k}_o)$ at $\omega_p = \omega_o/2$, $\omega_o/100$ and $\omega_o/400$.

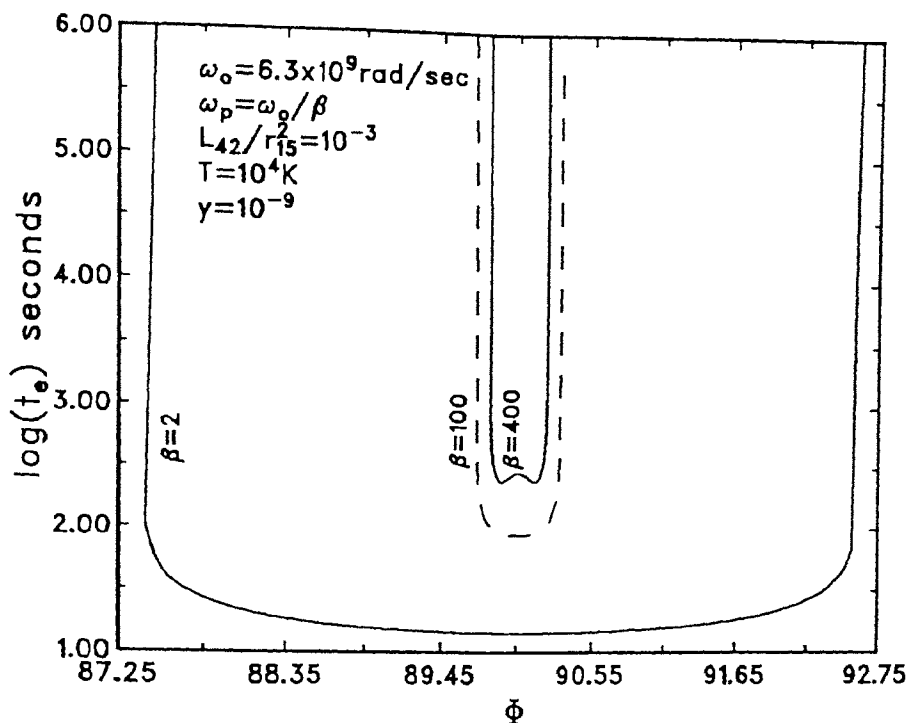


Fig. 6.8 The e-folding time t_e versus $\Phi = \cos^{-1}(\hat{k} \cdot \hat{k}_o)$ at $\omega_p = \omega_o/2$, $\omega_o/100$ and $\omega_o/400$.

Consider now the modulation of optical radiation ($\omega_o = 4 \times 10^{15}$) Hz in the electron-positron plasma. The period $P = 2\pi/\omega_r$ versus $y = k/k_o$ is plotted in Fig. 6.9. For $\beta > 1000$, the period is independent of β . The value of the period of modulation P lies in the observed range of time-scales (10–50 minutes) of variations in the optical flux (Frolich 1973; Visvanathan and Elliot 1973; Kiplinger 1974; Folsom et al. 1976; Carrasco, Dultzin-Hacyan and Cruz-Gonzalez 1985; Smith et al. 1985). The figure shows that, at smaller wave numbers $y < 10^{-10}$, pulses of $P > 1$ day are produced. Fig. 6.10 shows t_e as a function of y at three values of $\beta = 1000$, 2000 and 3000.: t_e is inversely proportional to y for $y < 10^{-7.5}$. At $y = 10^{-7.5}$, growth rate is maximum. The modulational instability of X-ray radiation at $\beta \approx 10^5$ exhibits variations similar to those in the optical case.

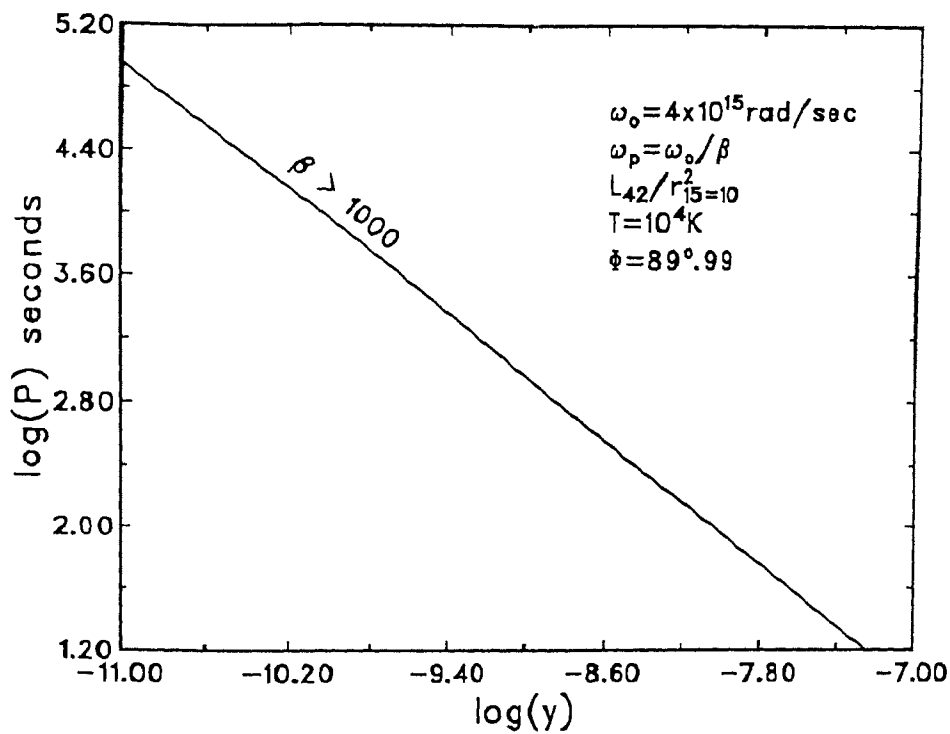


Fig. 6.9 The period of modulation P of optical radiation versus y for $\beta > 1000$.

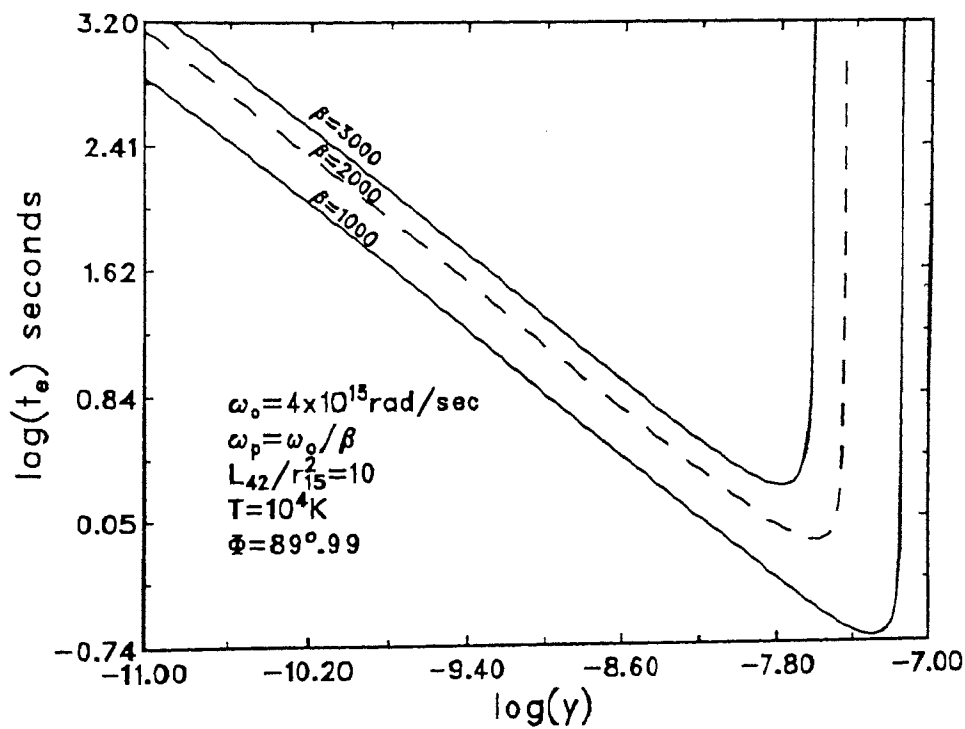


Fig. 6.10 The e-folding time t_e versus y at $\beta = 1000, 2000$ & 3000 .

The period of modulation P is independent of L_{42}/r_{15}^2 in the optical range (see Fig. 6.11). The values of $y = 5 \times 10^{-8}$, 2.5×10^{-8} and 1.7×10^{-8} adopted here are those values for which growth rate is maximum in Fig. 6.10. At $y = 10^{-10}$ growth is not maximum but P is large. Fig. 6.12 shows t_e as a function of L_{42}/r_{15}^2 , at different values of β and y .

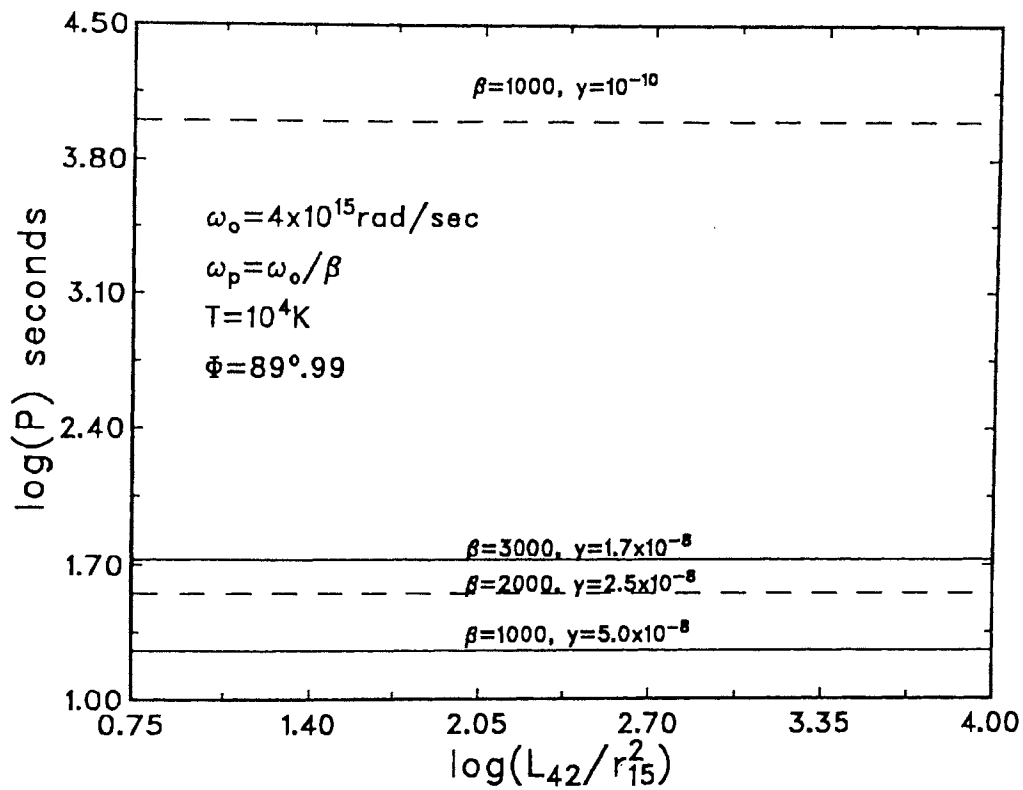


Fig. 6.11 The period of modulation P of optical radiation versus L_{42}/r_{15}^2 at $\beta = 1000, 10^{-10}$; $\beta = 1000, 1.7 \times 10^{-8}$; $\beta = 2000, 2.5 \times 10^{-8}$ and $\beta = 3000, y = 5 \times 10^{-8}$.

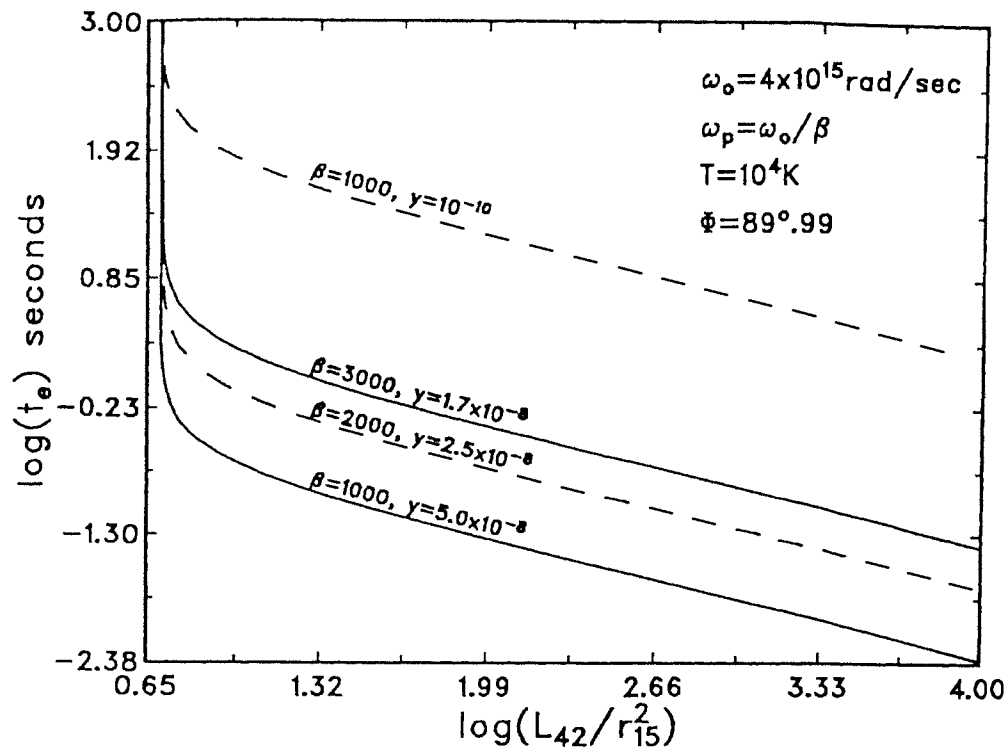


Fig. 6.12 The e-folding time t_e versus L_{42}/r_{15}^2 at β and γ as for Fig.11.

6.4.2 In a Pulsar

Typical values of the plasma and radiation parameters at a distance $r = 100R_{NS} = 10^8$ cm, (Neutron star radius $R_{NS} \approx 10$ km) for the pulsar PSR 1133+16 are pair density $n_j = n_9 \times 10^9 \text{ cm}^{-3}$, temperature $T_j = T_6 \times 10^6$ K and luminosity, in the band $\Delta\nu < \nu = 600$ MHz, $L = L_{30} \times 10^{30} \text{ erg s}^{-1}$ (Cordes and Hankins 1977; Cordes 1983). The micropulses of duration $1\mu\text{s}$ to a few ms at 600 MHz have been observed. Fig. 6.13 shows P as a function of y . The period P is found to lie in the observed range. Fig. 6.14 shows the e-folding time t_e as a function of y . The growth rate is maximum at $y \approx 0.2$.

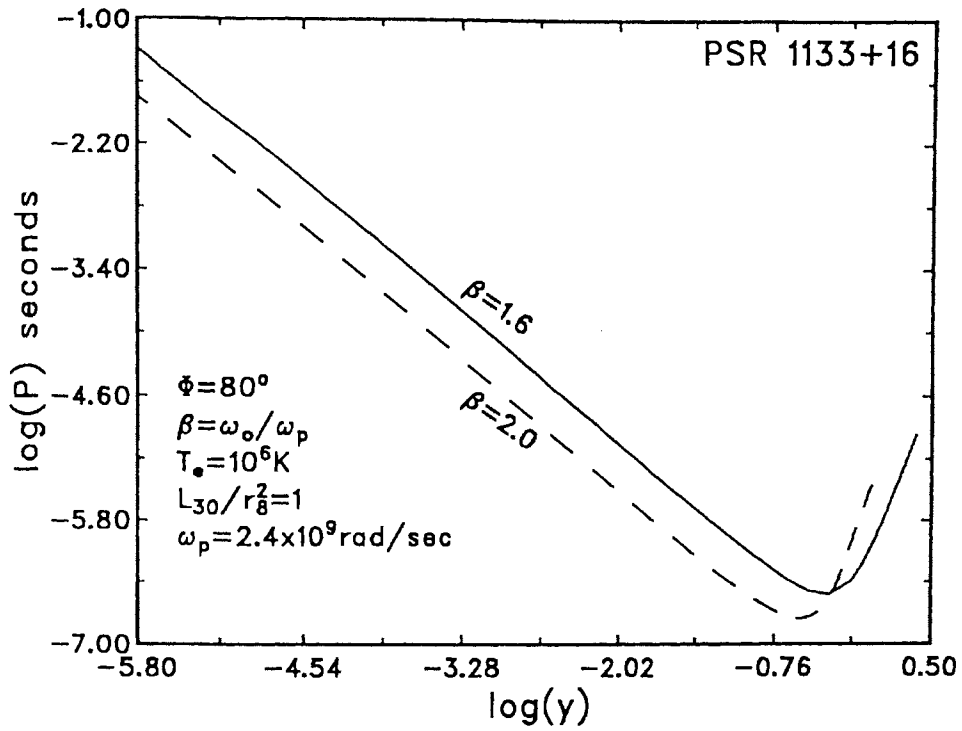


Fig. 6.13 The period of modulation P versus y at $\beta = 1.6$ & 2 for PSR 1133+16.

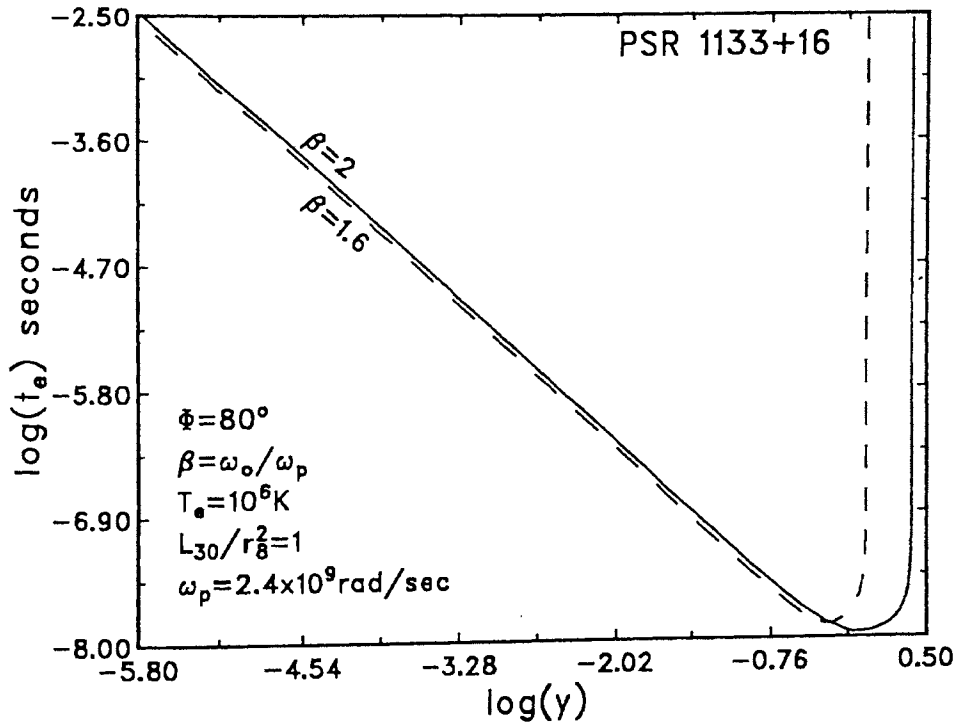


Fig. 6.14 The e-folding time t_e versus y at $\beta = 1.6$ & 2 for PSR 1133+16.

6.5 CONCLUSION

In our model, we have taken an electron–positron plasma with uniform and isotropic distributions of temperature and density. We have also assumed that the plasma is at rest with respect to the source of radiation. If the plasma is moving with relativistic velocities, then the relativistic effects must be taken into account. Tajima and Tanuti (1990) investigated the non-linear interaction of EM wave and acoustic modes in an electron–positron plasma, invoking the assumption of quasi-neutrality in the dynamics of plasma slow motion and ignoring relativistic mass variations of charged particles. Here we have investigated the non-linear interaction of the EM wave with electrostatic density fluctuations in an electron–positron plasma including the relativistic mass variation. The relativistic mass variation of electrons and positrons produces the non-linear wave equations (6.22 and 6.23) for an EM wave propagating in the electron–positron plasma. The ponderomotive force of the EM wave leads to the excitation of low-frequency density perturbations. The modulational instability of an EM wave produces localized EM pulses. This is an intrinsic process since it occurs in the source itself. The growth rate of the instability is proportional to $\epsilon^{3/2}[2(1 - \epsilon^2/4)]^{1/4}$. The electron–positron plasma is modulationally unstable for either linear or circular polarization. A strong magnetic field can also affect the process: we intend to study this in detail in later work.

We believe that plasma processes such as modulational instability are potential mechanisms for the rapid variability and the production of micropulses in AGN and pulsars. Most of the mechanisms proposed previously, require very specific environmental conditions; microlensing, for example, requires the nuclei of AGN to be large and transverse velocities to be of the order of 40 c, and refractive interstellar scintillation requires very small scatterers close to the Sun (≤ 100 pc) and unusual filaments associated with the galactic loop III. Since the conditions for modulational instability exist naturally in the source region, modulation of the EM radiation may take place through this process.

References

- Angione, R., 1969, *Pub. A. S. P.*, **80**, 339.
- Arons, J. & Scharlemann, E., 1979, *Astrophys. J.* **231**, 854.
- Assó, E., Pellat, R. & Sol, H., 1980, *Pulsars, IAU Symp. No. 95*, eds. Sieber, W. & Wielebinski, R., Reidel, Dordrecht, p 111.
- Baker, D. N., Borovsky, J. E., Benford, G. & Eilek, J. A., 1988 *Astrophys. J.* **326**, 110.
- Beal, J. H., 1990, in *Physical Processes in Hot Cosmic Plasmas*, eds Brinkmann, W., Fabian, A.C. & Giovannelli, F., Kluwer, Dordrecht, p 341.
- Benford, G., 1992, *Astrophys. J.*, **391**, L 59.
- Bertaud, Ch., Wlerick, G., Veron, P., DuMortier, B., Bigay, J., Paturel, G., Dupuy, M. & deSaevsky, P., 1973, *Astron. and Astrophys.*, **24**, 357.
- Burbidge, G. R. & Burbidge, E. M., 1967, *Quasi-Stellar-Objects*, (Freeman, San Francisco).
- Carrasco, L., Dultzin-Hacyan, D. & Cruz-Gonzalez, I., 1985, *Nature*, **314**, 146.
- Chain, A. C. -L. & Kennel, C. F., 1983, *Astrophys. Space Sci.*, **97**, 9.
- Cordes, J. M., 1983, *AIP Conference No.101, on Positron—Electron pairs in Astrophysics*, eds. M. L. Burns, A. K. Harding, & R. Ramaty, p 98.
- Cordes, J. M. & Hankins, T. H., 1977, *Astrophys. J.*, **218**, 484.
- Eachus, A. D. & Liller, W., 1975, *Astrophys. J. (Letters)*, **200**, L-61.
- Folsom, G. H., Miller, H. R., Wingert, D. W. & Williammon, R. M., 1976, *Astron. J.*, **81**, 145.
- Frolich, A., 1973, *IAU Circ. No. 2525*.
- Gangadhara, R. T. & Krishan, V., 1990, *J. Astrophys. Astr.*, **11**, 515.
- Gangadhara, R. T. & Krishan, V. 1992, *Mon. Not. R. astr. S.*, **256**, 111.
- Gangadhara, R. T. Krishan, V. & Shukla, P. K. 1992, **Modulation of radiation in an Electron—Positron plasma**, *Mon. Not. R. astr. S.*, in press.
- Gedalin, M. E., Lominadze, J. G. & Stenflo, L., 1985, *Astrophys. Space Sci.* **108**, 393.

- Gil, J., 1986, *Astrophys. J.*, **308**, 691.
- Gil, J. A. & Snakowski, J. K., 1990a, *Astron. and Astrophys.*, **234**, 237.
- Gil, J. A. & Snakowski, J. K., 1990b, *Astron. and Astrophys.*, **234**, 269.
- Goldreich, P. & Julian, W. H., 1969, *Astrophys. J.*, **157**, 869.
- Heeschen, D. S., Krichbaum, T., Schalinski, C. J. & Witzel, A., 1987, *Astron. J.*, **94**, 1493.
- Kates, R. E. & Kaup, D. J., 1989, *J. Plasma Phys.*, **42**, 507.
- Kiplinger, A. L., 1974, *Astrophys. J. (Letters)*, **191**, L 109.
- Krishan, V., 1988, *Mon. Not. R. astr. Soc.*, **230**, 183.
- Krishan, V. & Wiita, P. J., 1986, *Quasars, IAU Symp. No. 199*, eds. Swarup, G. & Kapahi, V. K., Reidel, Dordrecht, p 419.
- Krishan, V. & Wiita, P. J., 1990, *Mon. Not. R. astr. Soc.*, **2467**, 597.
- Kruer, W. L., 1988, in *The Physics of Laser-Plasma Interactions*, ed. Allan M. Wylde, Addison-Wesley, New York, p 70.
- Lesch, H. & Pohl, M., 1992, *Astron. and Astrophys.*, **254**, 29.
- Lightman, A. P., 1983, *AIP Conference No.101, on Positron—Electron pairs in Astrophysics*, eds. M. L. Burns, A. K. Harding, & R. Ramaty, p 359.
- Lightman, A. P. & Zdziarski, A. A., 1987, *Astrophys. J.*, **319**, 643.
- Liller, W. & Liller, M., 1975, *Astrophys. J. (Letters)*, **199**, L 133.
- Lominadze, J. G., Machabelli, C. Z. & Usov, V. V., 1983, *Astrophys. Space Sci.*, **90**, 19.
- Melrose, D. B., 1978, *Astrophys. J.*, **225**, 557.
- Miller, H. R., 1975, *Astrophys. J. (Letters)*, **201**, L 109.
- Miller, H. R., 1977, *Astrophys. J.*, **212**, 153.
- Miller, H. R. & Wiita, P. J., 1987, *Active Galactic Nuclei*, Springer-verlag, Berlin.
- Mofiz, U. A., de Angelis, U. & Forlani, A., 1985, *Phy. Rev. A*, **31**, 951.
- Oke, J. B., 1967, *Astrophys. J.*, **147**, 901.
- Quirrenbach, A., 1990, in *Meeting on Variability of Active Galactic Nuclei*, eds. Miller, H.R. & Wiita, P.J., Cambridge Uni. Press, p 165.

- Racine, R., 1970, *Astrophys. J.*, **159**, L 99.
- Rees, M. J., 1983, in *The Very Early Universe*, ed. G. W. Gibbons, S. W. Hawking, & S. Siklos, Cambridge University Press.
- Rickett, B., 1975, *Astrophys. J.*, **197**, 185.
- Ruderman, M. & Sutherland, P., 1975, *Astrophys. J.*, **196**, 51.
- Shen, B. S. P. & Usher, P., 1970, *Nature*, **228**, 1070.
- Shukla, P. K., 1985, *Astrophys. Space Sci.*, **114**, 381.
- Shukla, P. K., Rao, N. N., Yu, M. Y. & Tsintsadze, N. L., 1986 *Phys. Rep.*, **138**, 1.
- Smith, H. E. & Hoffleit, D., 1963, *Nature*, **198**, 650.
- Smith, P. S., Balonek, T. J., Heckert, P. A., Elston, R. & Schmidt, G. D., 1985, *Astron. J.*, **90**, 1184.
- Smirnova, T. V., 1988, *Soviet Astron. Lett.*, **14**, 20.
- Smirnova, T. V., Solasnov, V. A., Popov, M. V. & Novikov, A. Yu., 1986, *Soviet Astron.*, **30**, 51.
- Tajima, T. & Taniuti, T., 1990, *Phys. Rev. A*, **42**, 3587.
- Tamour, S., 1973, *Phys. Fluids*, **16**, 1169.
- Thomson, J. J., Kruer, W. L., Bodner, S. E. & DeGroot J., 1974, *Phys. Fluids*, **17**, 849.
- Visvanathan, N. & Elliot, J. L., 1973, *Astrophys. J.*, **179**, 721.
- Voronov, S. A., Gal'per, A. M., Kirilov-Ugryumov, V. G., Koldashov, S. V. & Popov, A. V., 1986, *JETP Lett.*, **43**, 307.
- Weatherall, J. C. & Benford, G., 1991, *Astrophys. J.*, **378**, 543.
- Webb, J. R., Smith, A. G., Leacock, R. J., Fitzgibbons, G. L., Gombola, P. P. & Shepard, D. W., 1988, *Astron. J.*, **95**, 374.
- Wiita, P. J., 1985, *Phys. Rep.*, **123**, 117.

Chapter 7

SUMMARY

In this final and concluding chapter, we would like to summarize the important results presented in the previous chapters and discuss the scope of future work on the mechanisms under study.

In this Thesis, we have explained the results of analytical as well as numerical investigations of radiation-plasma interaction instabilities in astrophysical plasmas. We investigated the role of collective plasma phenomena in the (1) generation of non-thermal power-law spectrum of quasars, (2) radio frequency heating, (3) polarization variability and (4) rapid flux variability in BL Lacs and quasars and the production of micropulses in pulsars.

The non-thermal continuum of quasars is believed to be produced through the combined action of synchrotron and inverse Compton processes, which are essentially single-particle processes. Collective plasma processes can *duplicate* all features of ordinary single-particle synchrotron emission, while greatly enhancing the emissivity. Astrophysicists have long been assumed synchrotron emission as the *default* choice, since no one could make a case for other, more powerful mechanisms.

Collective processes such as SRS and SCS of electromagnetic waves from relativistic electron beams, can amplify both the frequency as well as the flux. We find SRS is much faster than SCS and hence relativistic electron beam decelerates much faster due to SRS. The power-law spectrum of the quasar 3C 273 can be reproduced from a relativistic electron beam. We believe the change of scattering

process from SRS to SCS or vice versa, can be the reason for blue bump in the spectrum of 3C 273. Slight variations in the density or temperature of electron beam shifts bump to other frequencies.

Radiation with frequency close to the plasma frequency can be anomalously absorbed in a plasma, due to parametric decay instability (PDI). This instability causes anomalous absorption of intense electromagnetic radiation under specific conditions of energy and momentum conservation and thus cause anomalous heating of the plasma. The rise in plasma temperature is determined by luminosity of the radio radiation and plasma parameters. It is believed that this process may be taking place in many astrophysical objects. For example, the conditions in the sources 3C 273, 3C 48 and Crab Nebula are shown to be conducive to the excitation of parametric decay instability. This process can also contribute towards the absorption of 21-cm radiation, which is otherwise mostly attributed to neutral hydrogen regions. With this phenomenon one can explain the strong radio frequency heating in BL Lacs and quasars. Decay instability may be the mechanism for the formation of hot lower density corona adjoining each photoionized dense region. The dip in the spectrum of 3C 273 at 5.0×10^9 Hz (Cowsik and Lee, 1982; Wiita 1985) may be due to the anomalous absorption of radio waves through PDI. Since the growth rate of parametric decay instability is much higher than collisional damping rate of electromagnetic wave, this dip can not be due to collisional damping alone. Compared to all other heating processes reviewed by Davidson and Netzer (1979), PDI is a faster process. Since PDI is fast and efficient process, it must be included while accounting for the observed value of the radio luminosity which is less than that obtained by extrapolation from the high frequency part of the spectrum.

Usually, when one talks about polarization change, one is referring to the same wave. SRS however brings about change of frequency but when the frequency of the incident wave is much higher than the plasma frequency, the scattered wave frequency differs very little from the incident wave frequency. Similar to the frequency and wave number matching conditions (see equation 5.13) we found conditions between the phases δ_i , δ_{\pm} and δ_e (see equation 5.16) in the process of three-wave interaction. Through SRS the clockwise polarized radiation can change into counterclockwise polarized radiation and vice versa. In addition, circularly polarized wave can change into a linearly polarized, a circularly polarized or an elliptically polarized wave or vice versa. The SRS also mimics Faraday rotation but at a tremendously enhanced rate.

A direct measurement of the growth rate cannot be done by a remote observer. The e-folding time represents a characteristic time during which a significant change in the degree of polarization, sense and rotation of plane of polarization takes place. Therefore, the observed variability time should be of the order of or a few times the e-folding time.

The features like a large change in rotation of polarization plane, sense reversal and extremely rapid temporal changes would help to explain many observations, for which, the existing mechanisms prove to be inadequate. Because of the very strong dependence of rotation angle on plasma parameters via the growth rate, in an inhomogeneous plasma medium the depolarization is a natural outcome. We believe that the plasma process such as the SRS may be a potential mechanism for the polarization variability in pulsars and quasars.

We have investigated the modulational instability of an EM wave with electro-

static density fluctuations in an electron–positron plasma including the relativistic mass variation. Tajima and Taniuti (1990) investigated the non-linear interaction of EM wave and acoustic modes in an electron–positron plasma, invoking the assumption of quasi-neutrality in the dynamics of plasma slow motion and ignoring relativistic mass variations of charged particles. The relativistic mass variation of electrons and positrons produce the non-linear wave equations (6.22 and 6.23) for an EM wave propagating in the electron–positron plasma. The ponderomotive force of the EM wave leads to the excitation of low-frequency density perturbations. The modulational instability of an EM wave produces localized EM pulses. This is an intrinsic process since it occurs in the source itself. The electron–positron plasma is modulationally unstable for either linear or circular polarization. We believe that a plasma process such as modulational instability is a potential mechanism for the rapid variability and the production of micropulses in AGN and pulsars.

A strong magnetic field can also affect the collective processes. So it has to be taken into account in future work with more realistic plasma and radiation parameters.

COLLECTIVE PLASMA PROCESSES MUST BE INCLUDED IN THE
SCHEME OF UNDERSTANDING ASTROPHYSICAL PLASMAS.

References

- Cowsik, R. & Lee, Y. C., 1982, *Proc. R. Soc. London Ser. A* **383**, 409.
 Davidson, K. & Netzer, H., 1979, *Rev. Mod. Phys.*, **51**, 715.
 Tajima, T. & Taniuti, T., 1990, *Phys. Rev. A*, **42**, 3587.
 Wiita, P. J., 1985, *Phys. Repts*, **123**, 117.

APPENDIX

A. PLASMA WAVES

A plasma supports electrostatic as well as electromagnetic waves due to long range electromagnetic forces. The electrostatic waves are associated with charge density fluctuations at characteristic frequencies determined by the electrons and ions plasma parameters. In the absence of an external magnetic field, there are two types of such plasma waves, one is of high-frequency known as (1) electron plasma wave and other one is of low-frequency known as (2) ion plasma wave.

(1) The Electron Plasma Wave

This wave is associated with an high frequency charge density fluctuations due to the motion of the electrons. Since this is a high frequency oscillation, we can treat the massive ions as an immobile ($\chi_i = 0$) and uniform neutralizing background with density n_0 . In the kinetic treatment and in the absence of external pump ($\vec{E}_o = 0$), we obtain from the equation (2.46), the dispersion relation for an electron plasma wave:

$$1 + \chi_e = 0. \quad (a.1)$$

When the thermal velocity of the electrons (v_e) is much smaller than the phase velocity ($v = \omega/k$) the electron plasma wave is undamped. Therefore, when $\omega \gg kv_e$, using the asymptotic form for χ_e , (see equation 2.36), we obtain from equation (a.1)

$$\omega^2 - \omega_{pe}^2 \left(1 + \frac{3}{2} \frac{k^2 v_e^2}{\omega^2} \right) + i \frac{\sqrt{\pi}}{(k\lambda_{De})^2} \frac{\omega_{pe}^3}{kv_e} \left(\frac{\omega}{\omega_{pe}} \right)^3 \exp \left[- \frac{\omega^2}{(kv_e)^2} \right] = 0. \quad (a.2)$$

Here, we make an approximation that $\omega_{pe}/\omega \approx 1$. Therefore, we have

$$\omega^2 - \omega_{pe}^2 - \frac{3}{2} k^2 v_e^2 + i \frac{\sqrt{\pi}}{(k\lambda_{De})^2} \frac{\omega_{pe}^3}{kv_e} \exp \left[- \frac{\omega^2}{(kv_e)^2} \right] = 0. \quad (a.3)$$

To find the frequency and damping rate of electron plasma wave, we set $\omega = \omega_e - i\Gamma_e$, where ω_e is the frequency and $\Gamma_e \ll \omega_e$ is the damping rate. From equation (a.3), we obtain

$$\omega_e^2 - i2\Gamma_e\omega_e - \omega_{pe}^2 - \frac{3}{2}k^2v_e^2 + i\frac{\sqrt{\pi}}{(k\lambda_{De})^2}\frac{\omega_{pe}^3}{kv_e}\exp\left[-\frac{\omega^2}{(kv_e)^2}\right] = 0. \quad (a.4)$$

Separating real and imaginary parts, we have

$$\omega_e^2 = \omega_{pe}^2 + \frac{3}{2}k^2v_e^2 \quad (a.5)$$

$$\Gamma_e = \frac{\sqrt{\pi}}{2(k\lambda_{De})^2}\frac{\omega_{pe}^2}{kv_e}\exp\left[-\frac{\omega_e^2}{(kv_e)^2}\right]. \quad (a.6)$$

Note that, the frequency (ω_e) of electron plasma wave is essentially ω_{pe} , the electron plasma frequency, with a small thermal correction dependent on the wave number k .

Substituting equation (a.5) into equation (a.6), we get

$$\begin{aligned} \Gamma_e &= \frac{\sqrt{\pi}}{2(k\lambda_{De})^2}\frac{\omega_{pe}^2}{kv_e}\exp\left[-\frac{\omega_{pe}^2}{(kv_e)^2} - \frac{3}{2}\right] \\ &= \sqrt{\frac{\pi}{8}}\frac{\omega_{pe}}{(k\lambda_{De})^3}\exp\left[-\frac{1}{2(k\lambda_{De})^2} - \frac{3}{2}\right], \end{aligned} \quad (a.7)$$

where $\lambda_{De} = v_e/\sqrt{2}\omega_{pe}$ is the Debye length of the electron plasma. Here, Γ_e is known as the Landau damping and it is significant when $k\lambda_{De} \geq 0.4$, (see section B).

(2) The Ion Plasma Wave

A plasma can support charge density oscillations at much lower frequency determined by the ion inertia. To derive the dispersion relation for these oscillations, we have to consider the motion of both electrons and ions.

In the absence of the incident (pump) wave ($\vec{E}_o = 0$) from equation (2.46), we obtain

$$1 + \chi_e + \chi_i = 0. \quad (a.8)$$

When $kv_i \ll \omega \ll kv_e$, the ion plasma wave is weakly damped and well excited. Therefore, using asymptotic forms for χ_e and χ_i , we obtain

$$\omega^2 + \frac{\omega^2}{(k\lambda_{De})^2} \left(1 + i\sqrt{\pi} \frac{\omega}{kv_e}\right) - \omega_{pi}^2 + i \frac{\sqrt{\pi}}{(k\lambda_{De})^2} \left(\frac{T_e}{T_i}\right) \frac{\omega^3}{kvi} \exp\left[-\frac{\omega^2}{(kv_i)^2}\right] = 0. \quad (a.9)$$

Now, for $\omega = \omega_i - i\Gamma_i$, we have

$$\omega_i^2 - i2\omega_i\Gamma_i + \frac{\omega_i^2}{(k\lambda_{De})^2} - \omega_{pi}^2 + i \frac{\sqrt{\pi}}{(k\lambda_{De})^2} \left\{ \left(\frac{\omega_{pi}}{kv_e}\right) \omega_i^2 + \left(\frac{T_e}{T_i}\right) \frac{\omega_i^3}{kvi} \exp\left[-\frac{\omega_i^2}{(kv_i)^2}\right] \right\} \approx 0. \quad (a.10)$$

Separating the real and the imaginary parts, we get, the frequency

$$\omega_i = \omega_{pi} \left\{ 1 + \frac{1}{(k\lambda_{De})^2} \right\}^{-1/2} \quad (a.11)$$

and the Landau damping rate

$$\Gamma_i = \frac{\sqrt{\pi}}{2} \frac{\omega_i}{(k\lambda_{De})^2} \left[\frac{\omega_{pi}}{kv_e} + \frac{T_e}{T_i} \frac{\omega_i}{kvi} \exp\left\{-\frac{\omega_i^2}{(kv_i)^2}\right\} \right]. \quad (a.12)$$

of the ion plasma wave.

The spectrum of ion plasma oscillations extend from a maximum of the ion plasma oscillation frequency ω_{pi} to zero. When $k\lambda_{De} \gg 1$, or for short wave-lengths $\lambda \ll 2\pi\lambda_{De}$, where $\lambda = 2\pi/k$, the frequency approaches a limiting value of $\omega_i \approx \omega_{pi}$, which is analogous to the frequency of the electron plasma wave oscillations. Most of the considerations applicable to electron plasma oscillations apply to these short-wave ion oscillations. However, if λ is considerably larger than $2\pi\lambda_{De}$ i.e., $\lambda \gg 2\pi\lambda_{De}$ then the ion oscillations lose their similarity to the electron oscillations and change over to ion-acoustic waves with dispersion relation

$$\omega_i = kc_s, \quad (a.13)$$

where $c_s = \sqrt{k_B T_e / M}$ is the ion-sound speed.

B. The Landau Damping

In a collisionless plasma, the Landau damping is a natural phenomenon by which waves and particles exchange energy among themselves. It has applications in other fields also. For example, in the kinetic treatment of a galaxy formation, stars can be considered as atoms of a plasma interacting via gravitational forces. Instabilities of the gas of stars can cause spiral arms to form, but this process is limited by Landau damping.

To see what is responsible for Landau damping, we find the frequency ω of the electrostatic wave, in the absence of external pump ($\psi_{e\omega} = 0$), from equation (2.33):

$$\omega = \omega_{pe} \left(1 + i \frac{\pi}{2} \frac{\omega_{pe}^2}{k^2} \left[\frac{\partial f_o}{\partial v} \right]_{v=v_p} \right), \quad (b.1)$$

where $v_p = \omega/k$ is the phase velocity of the electrostatic wave. The $\text{Im}(\omega) = \Gamma_e$ (see equation a.7) arises from the pole at $v = v_p$ in equation (2.33). This effect is concerned with only those particles which have a velocity nearly equal to the phase velocity of the wave. These particles travel along with the wave and do not see a rapidly fluctuating electric field. Therefore, they can exchange energy with the wave efficiently. Particles with velocity much lower than the phase velocity of the wave merely move back and forth as the wave goes by and do not gain any energy on the average. Similarly, particles moving much faster than the wave cannot exchange energy with the wave. However, if the particles have almost the same velocity as the wave, they can be caught and pushed along by the wave. In that case, particles gain energy at the cost of wave energy. In a plasma there are electrons both faster and slower than the wave. A Maxwellian distribution, however, has more slow electrons than fast ones (see Fig. b.1). Therefore, there are more particles taking energy from the wave than vice versa, and the wave is damped. As particles with $v \approx v_p$ are trapped in the wave, $f(v)$ is flattened near the phase velocity. As seen in Fig. b.2,

the perturbed distribution function contains the same number of the particles but has gained total energy (at the expense of the wave energy).

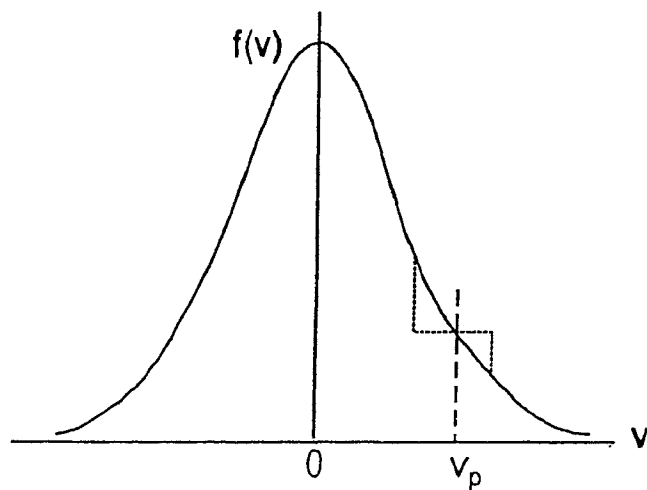


Fig. b.1 Distortion of a Maxwellian distribution in the region $v \approx v_p$ can be caused by Landau damping.

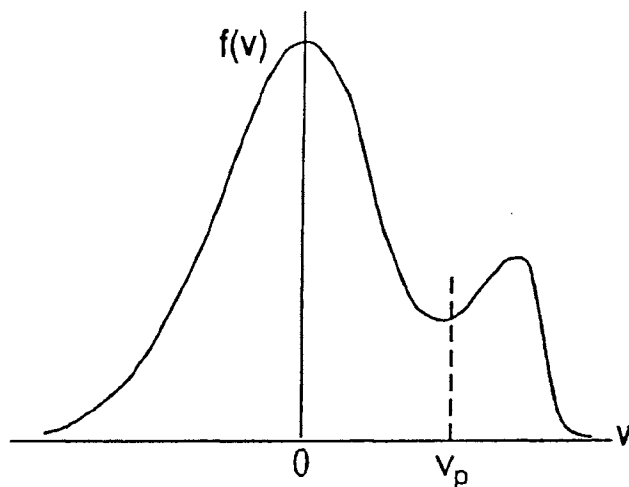


Fig. b.2 A double-humped distribution and the region where instabilities will develop.

One can conclude that if $f(v)$ contained more fast particles than slow particles, a wave can be excited. Equation (b.1) shows that for $\partial f_0 / \partial v$ positive, $\text{Im}(\omega)$ is positive at $v = v_p$ and such a distribution is shown in Fig. b.2. A wave can gain energy and hence become unstable at the expense of the particles energy when its

phase velocity is in the region of positive slope of the distribution function.

There are actually two kinds of Landau damping: the *linear* Landau damping and the *non-linear* Landau damping. Both kinds are independent of dissipative collisional mechanisms. Particles can be trapped in a potential well of the wave. But linear theory can not explain the trapping phenomena. This can be seen from the equation of motion

$$m_e \frac{d^2 x}{dt^2} = -eE(x). \quad (b.2)$$

This is a non-linear equation, because to solve this exactly one has to find the value of $E(x)$ at the instantaneous position of the particle. Linear theory uses for x the unperturbed orbit; i.e., $x = x_o + v_o t$. But when a particle is trapped in the potential well of a wave this approximation may not be valid. When a particle encounters a potential hill large enough to reflect it, its velocity and position are, of course, greatly affected by the wave. In fluid theory, the equation of motion of an electron plasma is

$$m_e \left[\frac{\partial \vec{v}}{\partial t} + (\vec{v} \cdot \nabla) \vec{v} \right] = -e\vec{E}(x). \quad (b.3)$$

Here the $(\vec{v} \cdot \nabla) \vec{v}$ term is non-linear. In linear theory one neglects $(\delta \vec{v} \cdot \nabla) \delta \vec{v}$ term which amounts to using the unperturbed orbits. When particles are trapped, they reverse their direction of travel relative to the wave, so the distribution function $f(v)$ is greatly disturbed near $v_p = \omega/k$. This means that $\partial \delta f / \partial v$ is comparable to $\partial f_o / \partial v$, and the term $(\delta \vec{v} \cdot \nabla) \delta \vec{v}$ is not negligible. Hence, the trapping can not be explained with the linear theory.

Collisionless damping and trapping of particles can take place when the wave grows in amplitude and becomes non-linear. Once the wave reaches this stage its amplitude fluctuates as the trapped particles bounce back and forth in the potential wells. This is a non-linear Landau damping.

C. The Ponderomotive Force

Intense electromagnetic waves in a plasma can couple with plasma waves via charge density fluctuations. When a strong electromagnetic wave impinges on a plasma, the plasma particles experience a non-linear Lorentz force since the electric and magnetic fields are to be determined at the positions of the particles, which move under the action of these fields. Using the concept of ponderomotive force we can explain many non-linear effects in a plasma. To derive this non-linear force we shall follow the method by Chen (1974), i.e., the single particle method.

Let \vec{E} and \vec{B} be the electric and magnetic fields of the electromagnetic radiation. The motion of the electron in the presence of these fields is governed by

$$m_e \frac{d\vec{v}}{dt} = -e[\vec{E}(\vec{r}) + \frac{1}{c}\vec{v} \times \vec{B}(\vec{r})]. \quad (\text{c.1})$$

This equation is non-linear and it is exact only when we evaluate \vec{E} and \vec{B} at the instantaneous position of the particle. The non-linearity comes from the $\vec{v} \times \vec{B}$ term and which is of second order. The other part of non-linearity, as we shall see, comes from evaluating \vec{E} at the actual position of the particle rather than at its initial position.

We can expand the position vector and the velocity of the particle as

$$\vec{r} = \vec{r}_o + \vec{r}_1 + \vec{r}_2 + \dots, \quad (\text{c.2})$$

$$\vec{v} = \vec{v}_o + \vec{v}_1 + \vec{v}_2 + \dots \quad (\text{c.3})$$

Let $\vec{E} = \vec{E}_s(\vec{r}) \cos(\omega t)$ be the electric field of the electromagnetic wave. Using first order terms in equation (c.1), we evaluate \vec{E} at the initial position \vec{r}_o

$$m_e \frac{d\vec{v}_1}{dt} = -e\vec{E}(\vec{r}_o). \quad (\text{c.4})$$

Integrating equation (c.4), we get

$$\vec{v}_1 = -\frac{e}{m_e \omega} \vec{E}_s(\vec{r}_o) \sin(\omega t). \quad (\text{c.5})$$

Integrating again we find

$$\vec{r}_1 = \frac{e}{m_e \omega^2} \vec{E}_s(\vec{r}_o) \cos(\omega t). \quad (\text{c.6})$$

Before we consider second order terms, we must expand $\vec{E}(\vec{r})$ about \vec{r}_o , i.e.,

$$\vec{E}(\vec{r}) = \vec{E}(\vec{r}_o) + [(\vec{r}_1 \cdot \nabla) \vec{E}_s(\vec{r}_o)]_{r=\vec{r}_o} + \dots \quad (\text{c.7})$$

From the second order terms in equation (c.1), we find

$$m_e \frac{d\vec{v}_2}{dt} = -e[(\delta\vec{r}_1 \cdot \nabla) \vec{E}_s(\vec{r}_o) + \frac{1}{c} \vec{v}_1 \times \vec{B}_s(\vec{r}_o)]. \quad (\text{c.8})$$

Using a Maxwell's equation

$$\nabla \times \vec{E}_s = -\frac{1}{c} \frac{d\vec{B}_s}{dt}, \quad (\text{c.9})$$

we find

$$\vec{B}_s(\vec{r}_o) = -\frac{c}{\omega} \nabla \times \vec{E}_s(\vec{r}_o) \sin(\omega t). \quad (\text{c.10})$$

Inserting equations (c.5), (c.6) and (c.10) into equation (c.8) and averaging over time $t = 2\pi/\omega$, we get

$$m_e \left\langle \frac{d\vec{v}_2}{dt} \right\rangle = -\frac{e^2}{2m_e \omega^2} [(\vec{E}_s(\vec{r}_o) \cdot \nabla) \vec{E}_s(\vec{r}_o) + \vec{E}_s(\vec{r}_o) \times (\nabla \times \vec{E}_s(\vec{r}_o))] = \vec{f}_{NL}. \quad (\text{c.11})$$

Here, we have used $\langle \cos^2(\omega t) \rangle = \langle \sin^2(\omega t) \rangle = 1/2$.

Using a standard vector identity, we obtain from equation (c.11)

$$\vec{f}_{NL} = -\frac{e^2}{4m_e \omega^2} \nabla E_s^2 \equiv -\frac{1}{16\pi n_o} \frac{\omega_{pe}^2}{\omega^2} \nabla E_s^2(\vec{r}_o). \quad (\text{c.12})$$

The force per cm^3 is given by

$$\begin{aligned} \vec{F}_{NL} &= n_o \vec{f}_{NL} \\ &= -\frac{\omega_{pe}^2}{8\pi \omega^2} \nabla \langle E^2(\vec{r}_o) \rangle, \end{aligned} \quad (\text{c.13})$$

where we have used $E_s^2(\vec{r}_o) = 2\langle E^2(\vec{r}_o) \rangle$ and n_o is the equilibrium electron density. The ponderomotive pressure P_{pond} can be defined as

$$P_{pond} = (\epsilon - 1) \frac{\langle E^2(\vec{r}_o) \rangle}{8\pi}. \quad (c.14)$$

Here, ϵ is the dielectric function of the plasma, given by

$$\epsilon = 1 - \frac{4\pi n e^2}{m_e \omega^2}. \quad (c.15)$$

A very important effect arises from \vec{F}_{NL} is the electrostriction. The density of the plasma no longer remains constant, but varies under the influence of the electromagnetic field pressure. Ponderomotive force is a mean force acting on each particle caused by the wave pressure equal to $-\nabla\psi_{pond}$, with

$$\psi_{pond} = \frac{e^2}{4m_e\omega^2} |\vec{E}(\vec{r}, t)|^2. \quad (c.16)$$

The electron density in the presence of this mean force is given by

$$\begin{aligned} n &= n_o \exp[-\psi_{pond}/k_B(T_e + T_i)] \\ &= n_o \exp(-|E|^2/\beta), \end{aligned} \quad (c.17)$$

where

$$\beta = \frac{4m_e\omega^2 k_B(T_e + T_i)}{e^2}.$$

To first order in $|E|^2$, we obtain from equation (c.17),

$$n = n_o \left(1 - \frac{|E|^2}{\beta} \right). \quad (c.18)$$

Substituting this expression for n into equation (c.15), we obtain

$$\begin{aligned} \epsilon &= \left(1 - \frac{4\pi n_o e^2}{m_e \omega^2} \right) + \frac{4\pi n_o e^2}{m_e \omega^2} \frac{|E|^2}{\beta} \\ &= \epsilon_{linear} + \epsilon_{NL} |E|^2 \\ &= \epsilon_o + \epsilon_1 |E|^2. \end{aligned} \quad (c.19)$$

The relation between the refractive index $\eta(\omega)$ of the plasma and dielectric function ϵ is

$$\begin{aligned}\eta(\omega) &= \sqrt{\epsilon} \\ &\approx \sqrt{\epsilon_o(\omega)} + \delta\eta_{NL}(\omega),\end{aligned}\tag{c.20}$$

where

$$\delta\eta_{NL}(\omega) = \frac{\pi n_o e^4}{2\epsilon_o m_e^2 \omega^4 k_B (T_e + T_i)} |E|^2\tag{c.21}$$

is the non-linear part of the refractive index. Equation (c.20) shows that the non-linear part of the refractive index is a positive term and

$$\frac{\partial\eta}{\partial|E|^2} > 0.$$

The non-linear force, thus drives away the charged particles from the region of high electric field to a region of low electric field (see Fig. c.1). A direct effect of \vec{F}_{NL} is the self-focusing of radiation in a plasma.

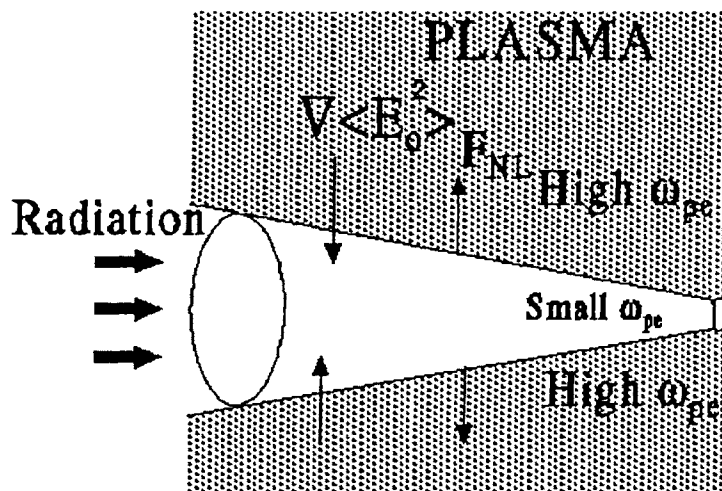


Fig. c.1 Focusing of radiation beam in a plasma is caused by the ponderomotive force.

D. Collision Frequency

In a fully ionized plasma, collisions occur between like particles (ion–ion or electron–electron) and unlike particles (ion–electron or electron–ion). Generally, the collisions between unlike particles are important because they are inelastic in nature, whereas the collisions between like particles are almost elastic. Hence, we consider a case in which an electron collides with an ion (see Fig. d.1) with charge ze , where z is the atomic number.

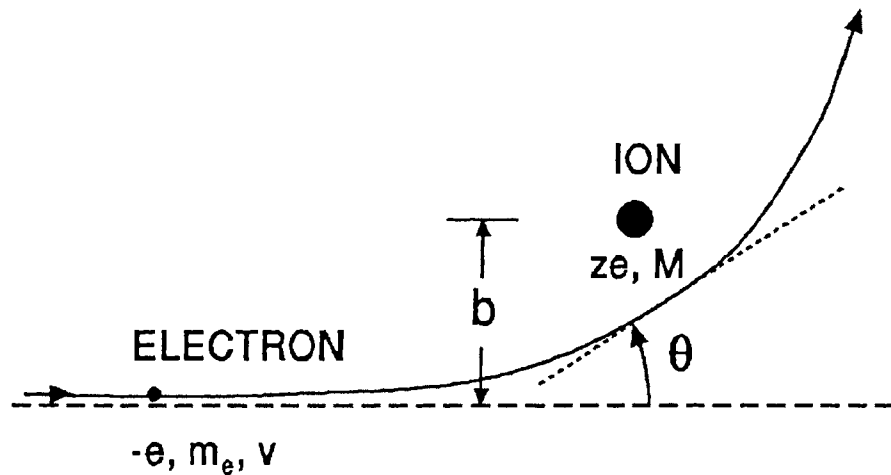


Fig. d.1 Propagation of electron in the ion field.

Assume that an electron with velocity \vec{v} undergoes deflection in the electric field of an ion, which is at rest. Let b be the impact parameter and θ be the deflection angle. The Coulomb force between the electron and the ion is given by

$$\vec{F} = -\frac{ze \cdot e}{r^3} \vec{r}. \quad (d.1)$$

The time duration during which the electron experiences the Coulomb force of ion

is

$$t \approx \frac{b}{v}. \quad (d.2)$$

Change in the electron momentum ($p = m_e v$) in this encounter is approximately given by

$$\Delta p \approx Ft = \frac{e^2 r_o}{r^2 v} \approx \frac{e^2}{r_o v}. \quad (d.3)$$

The angle θ of scattering is related to the impact parameter via

$$\cot(\theta/2) = \frac{b m_e v^2}{|z e^2|}. \quad (d.4)$$

The differential cross-section $d\sigma$ for scattering into an infinitesimal solid angle $d\Omega$ is given by the famous Rutherford formula

$$\frac{d\sigma}{d\Omega} = \left[\frac{z e^2}{2 m_e v^2 \sin(\theta/2)} \right]^2. \quad (d.5)$$

The cross-section σ_m for the momentum transfer can then be calculated by integrating equation (d.5) over the solid angle with a weighting function $(1 - \cos \theta)$ which represents the fractional change of momentum on scattering. Choosing θ_{min} as the lower limit of θ and using $d\Omega = 2\pi \sin \theta d\theta$ integrating equation (d.5), we have

$$\begin{aligned} \sigma_m &= \int_{\theta_{min}}^{\pi} (1 - \cos \theta) \left[\frac{z e^2}{2 m_e v^2 \sin^2(\theta/2)} \right]^2 2\pi \sin \theta d\theta \\ &= 4\pi \left(\frac{z e^2}{m_e v^2} \right)^2 \ln \left[\frac{1}{\sin(\theta_{min}/2)} \right]. \end{aligned} \quad (d.6)$$

For $\theta_{min} \ll 1$, we have

$$\sigma_m \approx 4\pi \left(\frac{z e^2}{m_e v^2} \right)^2 \ln \left(\frac{2}{\theta_{min}} \right). \quad (d.7)$$

Let b_{min} be the minimum value of the impact parameter corresponding to θ_{min} .

Then from equation (d.4), we get

$$\theta_{min} \approx 2 \frac{|z e^2|}{b_{min} m_e v^2}. \quad (d.8)$$

Using this expression, we get

$$\sigma_m \approx 4\pi \left(\frac{ze^2}{m_e v^2} \right)^2 \ln \left(\frac{b_{max} m_e v^2}{|ze^2|} \right). \quad (d.9)$$

The logarithmic factor, in equation (d.9) is called Coulomb logarithm. The cross section is seen to diverge logarithmically as θ_{min} approaches zero. The origin of the logarithmic divergence can be traced to those scattering acts which take place with large impact parameters and thus with small scattering angles. In a plasma medium the impact parameter is indefinite therefore Debye length is used as its upper limit. The collision frequency is defined as

$$\nu_{ei} = n_o \sigma_m v = \frac{4\pi n_o e^4}{m_e^2 v^3} \ln \Lambda, \quad (d.10)$$

where n_o is the density of electrons. Substituting $v = (k_B T_e / m_e)^{1/2}$, we get

$$\nu_{ei} = \omega_{pe} \left(\frac{r_c}{\lambda_{De}} \right) \ln \Lambda. \quad (d.11)$$

For most plasmas of interest, $5 < \ln \Lambda < 20$. Usually, it is taken to be 10, regardless of the type of the plasma. If $\nu_{ei} / \omega_{pe} < 1$, then the plasma oscillations which arise due to collective interactions of the charged particles can not be destroyed by large-angle binary collisions between individual particles. In electron plasma waves, electrons oscillate in the field of ions and hence wave energy gets transferred to ions or it can be emitted as non-thermal bremsstrahlung radiation at the rate of ν_{ei} .

Similar to electrostatic waves, electromagnetic waves also experience collisional damping in a plasma medium. If ν_o is the collisional damping rate of electromagnetic wave, then rate of energy loss from the electromagnetic wave ($\nu_o E_o^2 / 8\pi$) must balance the rate at which the oscillatory energy of electrons is randomized by the electron-ion scattering, i.e., $(\nu_o E_o^2 / 8\pi) = (\nu_{ei} m_e v_o^2 / 2)$. Since $v_o = e E_o / m_o \omega_o$, this power balance gives

$$\nu_o = \left(\frac{\omega_{pe}}{\omega_o} \right)^2 \nu_{ei}. \quad (d.12)$$

E. Propagation of Electromagnetic waves in an Inhomogeneous Plasma

In a plasma with mobile electrons and a stationary ionic background, an electromagnetic wave satisfies the following wave equation:

$$\nabla^2 \vec{E} + \frac{\omega^2}{c^2} \epsilon \vec{E} = 0 \quad (e.1)$$

where \vec{E} is the electric field oscillating with frequency ω and ϵ is the dielectric function which for an unmagnetized plasma is given by: $\epsilon = 1 - \omega_{pe}^2/\omega^2$. Thus, $\omega_{pe} = \omega$ defines the maximum plasma density to which an electromagnetic wave of frequency ω can penetrate.

Let us consider wave propagation in an inhomogeneous plasma, where the spatial variations are all in the vertical z direction along which the wave propagates. In the cartesian coordinates, the wave equation (e.1) becomes:

$$\frac{d^2 E_x}{dz^2} + \frac{\omega^2}{c^2} \epsilon(\omega, z) E_x = 0 \quad (e.2)$$

and

$$\epsilon(\omega, z) = 1 - \frac{n(z)}{n_{cr}}, \quad (e.3)$$

where $\omega^2 = 4\pi n_{cr} e^2/m$. Assuming that the electron density varies linearly with z , i.e.,

$$n = n_{cr} \frac{z}{L},$$

where L is the scale length. One obtains:

$$\frac{d^2 E_x}{dz^2} + \frac{\omega^2}{c^2} \left(1 - \frac{z}{L}\right) E_x = 0$$

or

$$\frac{d^2 E_x}{d\eta^2} - \eta E_x = 0, \quad (e.4)$$

where

$$\eta = \left(\frac{\omega^2}{c^2 L} \right)^{1/3} (z - L).$$

The solution of equation (e.4) can be expressed in terms of the Airy functions as (Kruer 1988):

$$E_x(\eta) = \alpha A_i(\eta) \quad (e.5)$$

For $\omega L/c \gg 1$ and the asymptotic representation

$$A_i(-\eta) = \frac{1}{\sqrt{\pi} \eta^{1/4}} \cos \left(\frac{2}{3} \eta^{3/2} - \pi/4 \right) \quad (e.6)$$

we find

$$E_x(z = 0) = E_{in} \left[1 + \exp \left\{ -i \left(\frac{4\omega L}{3c} - \frac{\pi}{2} \right) \right\} \right] \quad (e.7)$$

where $\alpha = 2\sqrt{\pi}(\omega L/c)^{1/6} E_{in} e^{i\varphi}$ and E_{in} is the free space value of the incident electric field and φ is a phase factor. Therefore,

$$E(\eta) = 2\sqrt{\pi} \left(\frac{\omega L}{c} \right)^{1/6} E_{in} e^{i\varphi} A_i(\eta) \quad (e.8)$$

and reaches a maximum value.

$$\left(\frac{E_{max}}{E_{in}} \right)^2 \approx 3.6 \left(\frac{\omega L}{c} \right)^{1/3} \quad (e.9)$$

The swelling of E occurs due to the standing wave formation [eq. (e.7)] and the reduction in the group velocity as the dielectric function decreases. Also since $k = \epsilon\omega/c$, the wavelength becomes longer.

F. Effect of incoherence in the pump wave on instability.

Presence of temporal incoherence in the pump wave reduces the growth rate of the instability. Consider a ion-acoustic wave driven by the incoherent pump with frequency near ω_{pe} .

Let pump be of the form

$$\vec{E}_o = E_o \alpha(t) \cos(\omega t) \hat{e}_o, \quad (f.1)$$

where \vec{E}_o is the electric field and $\alpha(t)$ is a stochastic variable with a zero mean and a variance of unity. When the growth rate is much less than the ion-acoustic frequency, the amplitude (\tilde{f}) of an unstable wave can be represented by terms of the form

$$\tilde{f} = \beta \exp[\gamma_o \int_0^t \alpha(t') dt']. \quad (f.2)$$

Here γ_o is the growth rate due to a coherent pump and β is a constant determined by the initial conditions. If we assume that $\alpha(t)$ is Gaussian,

$$\langle \tilde{f} \rangle = \beta \exp \left[\frac{\gamma_o^2}{2} \int_0^t dt' \int_0^t dt'' \langle \alpha(t') \alpha(t'') \rangle \right], \quad (f.3)$$

where $\langle \rangle$ denote an average. The effective band-width $\delta\omega$ is defined via the auto-correlation function

$$\frac{1}{\delta\omega} = \int_0^\infty d\tau \langle \alpha(t) \alpha(t+\tau) \rangle.$$

If $\delta\omega \gg \gamma_o$, then equation (f.2) gives

$$\langle \tilde{f} \rangle = \beta \exp \left(\frac{\gamma_o^2 t}{\delta\omega} \right), \quad (f.4)$$

Therefore the growth rate due to the incoherent pump is

$$\gamma' = \frac{\gamma_o^2}{\delta\omega}. \quad (f.5)$$

Hence the growth rate is reduced by the ratio $\gamma_o/\delta\omega$.

Intensity of the pump can be distributed over the band-width $\delta\omega$ but the resonance width of the instability is the growth rate. Hence when $\delta\omega \gg \gamma_o$, only some fraction of the pump wave resonantly couples to any two given unstable waves.

References

- Chen, F. F., 1977, *Introduction to Plasma Physics*, Plenum Press, New York, p 213
- Kruer, W. L., 1988, *The Physics of Laser-Plasma interactions*, Addison-Wesley, New York, p70

LIST OF SYMBOLS

c	:	velocity of light.
k_B	:	Boltzmann constant.
m_e	:	electron mass.
m_i	:	ion mass.
m_o	:	rest mass of electron or positron.
$-e$:	electron charge.
e	:	ion or positron charge.
n_e	:	electron density.
n_i	:	ion density.
n_p	:	positron density.
T_e	:	electron temperature.
T_i	:	ion temperature.
v_e	:	electron thermal velocity.
v_i	:	ion thermal velocity.
c_s	:	ion-acoustic velocity.
ω_{pe}	:	electron plasma frequency.
ω_p	:	electron or positron plasma frequency.
ω_{pi}	:	ion plasma frequency.
λ_{De}	:	Debye length of electron plasma.
λ_D	:	Debye length of electron or positron plasma.
λ_{Di}	:	Debye length of ion plasma.
\vec{v}_b	:	relativistic electron beam velocity.

\vec{v}_g	:	group velocity of electromagnetic wave.
ω	:	angular frequency.
\vec{k}	:	wavenumber.
ω_e	:	electron plasma wave frequency.
\vec{k}_e	:	electron plasma wave wavenumber.
χ_e	:	electron susceptibility function.
χ_i	:	ion susceptibility function.
\vec{S}	:	poynting flux vector.
ν_{ei}	:	electron-ion collision frequency.
Γ_e	:	damping rate of electron plasma wave.
Γ_i	:	damping rate of ion plasma wave.
OTS	:	Oscillating Two-Stream instability.
PDI	:	Parametric Decay Instability.
SCS	:	Stimulated Compton Scattering.
SRS	:	Stimulated Raman Scattering.